GCA-TR-68-1-N

STRUCTURE AND VARIABILITY OF EARTH'S ATMOSPHERE

R. A. Minzner
P. Morgenstern

GCA CORPORATION
GCA TECHNOLOGY DIVISION
Bedford, Massachusetts

FINAL REPORT

Contract No. NASW-1463

February 1968

Prepared for

NATIONAL AERONAUTICS AND SPACE ADMINISTRATION
Headquarters
Washington, D. C.

TABLE OF CONTENTS

STRUCTURE AND VARIABILITY OF EARTH'S ATMOSPHERE

By R. A. Minzner* and P. Morgenstern
GCA Corporation, GCA Technology Division
Bedford, Massachusetts

SUMMARY

Density-altitude profiles obtained from 437 rocket soundings for various portions of the altitude interval 30 to 200 km have been statistically studied for variations associated with solar flux variations. The soundings have been sorted into homogeneous cells of a three-dimensional array defined by specific diurnal, seasonal and latitudinal categories. Six diurnal categories are defined in terms of solar zenith angles and earth shadow heights rather than in terms of standard or Greenwich time. Eight seasonal categories are defined in terms astronomical as well as continental climatological considerations. Six latitude bands are defined in 15-degree increments with seasonal inversions to permit combining of southern and northern latitude regions.

The quasi-homogeneous stratification of data has permitted the examination of the influence of 10.7-cm solar flux radiation independent of the influence of each of the three variables mentioned above. The results of these various computations are presented as a portfolio of 92 altitude profiles of the coefficient of correlation between density and 10.7-cm solar flux.

INTRODUCTION

This report presents the results from a program of research on density variation in the upper atmosphere conducted for NASA Headquarters under Contract NASW-1463. The principal motivation for this study is the work reported by Jacchia [1]** which indicates a strong positive correlation between atmospheric density and solar activity in the region above 200 km. On the premise that similar effects may be present at lower altitudes, the current investigation was initiated to explore this possibility.

The model proposed by Jacchia [2] states that atmospheric density in the region above 200 km is a function both of the solar flux density and of the interaction between solar flux density and the "diurnal" bulge effect of the atmosphere. Jacchia notes, however, that the "diurnal" bulge effect is small below 200 km and thus , it was neglected

*Now with National Aeronautics and Space Administration, Electronics Research Center, Cambridge, Massachusetts.

**Numbers in [ ] represent reference numbers.

in the current study. Also in the present work it has been assumed that the dependence of density on solar flux is a linear one although the basic model allows for a power law dependence. This assumption was based on the evaluations of the power law exponent made by Jacchia [2] from satellite acceleration data which yield two cases with a value of 1.0 and one case with a value of 0.7.

The analysis procedure used in the study consisted of calculating the coefficient of correlation (linear) between atmospheric density and the 10.7-cm solar flux density. The 10.7-cm solar flux density was used rather than the 20-cm solar flux density because longer records were available for the former quantity. These correlations were calculated for both the solar flux measured on the same day as the density observation and for the solar flux measured on the preceding day. The objective here was to explore the possibility of a lag relationship between solar activity and atmospheric density variations. An attempt was made to minimize the influence of latitude, season and time of day by stratifying the data into quasi-homogeneous cells. This system of stratification is described in detail in subsequent sections of the report.

The data used for the study were obtained from reported rocket soundings or rocket instrument releases in the height region 30 to 200 km. Thermodynamic data from approximately 437 soundings have been collected from 17 fixed launch sites and a few shipboard launch sites. These high-altitude data consist of profiles of one or more of three properties: density, ρ; temperature, T; and pressure, p. The knowledge of any two of these quantitites for any time and any point in the atmosphere permits determination of the third by means of the equation of state.

$$p = \frac{R}{M} \rho T \qquad (1)$$

where M is the mean molecular weight of air and R is the universal gas constant.

The set of calculations described above are given in the Appendix as a portfolio of graphs showing the coefficient of correlation versus altitude. The curves shown in these graphs have been smoothed by a running average extending over a 5 km height interval to remove some of the variability due to sampling fluctuations.

MEASUREMENT TECHNIQUES

In the altitude region 30 to 200 km, atmospheric data have been obtained primarily by vertical sounding rockets, although vertical light probes have also been used. In many instances only one of the three basic thermodynamic properties is determined at any time-space point. If this property is determined over an extended altitude region at essentially the same time, as in a near-vertical rocket-probe flight, this altitude profile of a single property leads to altitude profiles of the other two thermodynamic properties. If the basic data are for pressure versus altitude, the temperature-versus-height profiles may be deduced in principle from the slope of the semi-log graph of pressure versus altitude, that is,

$$T(h) = \frac{GM}{R} \frac{1}{\frac{d\ \ell n\ p(h)}{dh}} \qquad (2)$$

where G is a constant numerically equal to the sea-level value of the acceleration of gravity at about 45° latitude with dimensions depending on those of geopotential [3], and h is geopotential altitude. Thus, with p(h) and T(h) determined, $\rho(h)$ is determined from Equation (1). Actually, the temperature determined is the mean temperature for the altitude interval between successive pressure measurements. Unfortunately, for practical pressure gauges, the temperature uncertainty becomes very large when the altitude interval is decreased to values less than 5 km, and this method has not been used extensively in the reduction of rocket sounding data.

If the primary data are values of density versus altitude of a specified accuracy without an independent knowledge of temperature at the top of the density-altitude profile, one may determine a temperature-altitude profile for all but the upper 10 to 15 km of the altitude region of the density data [4]. This is done using a numerical integration form of the expression

$$T_2 = T_1 \frac{\rho_1}{\rho_2} + \frac{GM}{R\rho_2} \int_{h_2}^{h_1} \rho(h)\ dh \qquad (3)$$

where h_1 is the geopotential of the greatest height for which a density value exists, i.e., ρ_1, and h_2 is the geopotential associated with successive values of densities ρ at successively lower heights, for which heights of the successive values of T_2 is determined. When h_2 is sufficiently below h_1 so that the value $T_1(\rho_1/\rho_2)$ becomes small compared with T_2 for some reasonable value for T_1, T_2 is determined essentially by the integral term of Equation (3). Thus, for altitudes of 10 to 15 km below h_1 down to the lowest altitude of density data, temperature-altitude profile may be determined from density-altitude

data alone. The percentage uncertainty in T_2 is comparable with the percentage uncertainty of ρ_2.

If the observed data consist of an altitude profile of temperature, an additional piece of information consisting of a reference-level value of pressure or of density is required to develop a related pressure-altitude profile or a density-altitude profile. When this additional piece of information is a pressure-height value, p_o at h_o, a complete pressure-altitude profile may be determined.

If the temperature-altitude profile consists of a series of discrete temperature-altitude values so that the segments between these successive values may be taken as linear, the following equations may be used.

$$p = p_o \left[\frac{T_o}{T_o + (h - h_o)L} \right]^{\frac{GM}{RL}}, \quad \text{for } L = \frac{dt}{dh} \neq 0 \qquad (4)$$

and

$$p = p_o \exp \left[- \frac{GM}{R} \frac{(h - h_o)}{T_o} \right], \text{ for } \frac{dt}{dh} = 0 \quad . \qquad (5)$$

These are the equations which were employed in the calculation of various standard and model atmospheres, Diehl [5]; Minzner and Ripley [3]; Minzner et al. [6]; Minzner et al. [7]; U.S. Standard Atmosphere [8]. Other suitable series-expansion equations of the type discussed by Minzner [9] are not limited to zero or nonzero values of temperature-altitude gradients, and are far more desirable when values of L may approach zero yet are not equal to zero.

The pressure equation of this latter type is

$$P = P_o \exp \left\{ - \left[\frac{GM}{R} \frac{(h - h_o)}{(1/2)(T + T_o)} \right] \left[\left(\frac{T - T_o}{T + T_o} \right) + \frac{1}{3} \left(\frac{T - T_o}{T + T_o} \right) + \frac{1}{5} \left(\frac{T - T_o}{T + T_o} \right) \right] \right\} \qquad (6)$$

When the additional piece of information is a density-height value, ρ_o at h_o, the appropriate equations commonly used for a linearly segmented temperature-altitude profile are:

$$\rho = \rho_o \left[\frac{T_o}{T_o + (h - h_o)L} \right]^{1 + \frac{GM}{RL}}, \quad \text{for } L = \frac{dt}{dh} \neq 0 \qquad (7)$$

and

$$\rho = \rho_o \exp\left[-\frac{GM}{R}\frac{(h - h_o)}{T_o}\right], \quad \text{for } \frac{dt}{dh} = 0 \quad . \tag{8}$$

In the case of digital data, where dt/dh may be any realistic value, including values near zero as well as zero, Minzner [20] has shown that the following rapidly converging series expansion is very convenient:

$$\rho = \rho_o \exp\left\{-\left[\frac{GM\,(h - h_o)}{1/2\,(T - T_o)R} + 1\right]\left[\left(\frac{T - T_o}{T + T_o}\right) + \frac{1}{3}\left(\frac{T - T_o}{T + T_o}\right)^3 + \frac{1}{5}\left(\frac{T - T_o}{T + T_o}\right)^5 + \ldots\right]\right\} \tag{9}$$

Both Equations (6) and (9) are related to equations derived earlier by Nicolet [11].

Following the use of Equations (4), (5), or (6) in conjunction with the single pressure-altitude point, the density-altitude profile may be determined from Equation (1), or from combinations of Equation (1) and one of Equations (7), (8), or (9). If Equation (7), (8), or (9) are first used in conjunction with an initial density-altitude point, the related pressure-altitude profile may be deduced using Equation (1) or a combination of Equation (1), (4), (5), and (6).

In the above methods, altitude was observed along with pressure, temperature, or density. Altitude need not be one of the fundamental observations, however; it may be inferred. A corresponding pair of values of pressure p_2 and temperature T_2 at unknown altitude h_2, where the altitude increment $h_2 - h_1$ is small relative to some initially known reference altitude h_1, leads to the determination of the value of h_2 the altitude of these observations:

$$h_2 = h_1 + \frac{R\bar{T}}{GM}\left[\ell n\, p_1 - \ell n\, p_2\right] \tag{10}$$

where $\bar{T}$ is the mean value of temperature between T_1 and T_2. Successive pairs of values of p_2 and T_2 thus lead to altitude profiles of pressure and temperature provided the altitude of the first observation is known.

The various high-altitude rocketborne experiments measure parameters which lead to one or the other of the thermodynamic properties, and rarely are these measured "directly" as with a thermometer, thermocouple system, or thermistor system for temperature determination, or as with an aneroid or mercurial barometer in the case of pressure or by some inertial device in the case of density. On the contrary they are all measured indirectly. Thus, for these observations it is meaningless to consider which is the independent and which is the dependent observation. Typical examples of the types of upper atmosphere observation follow.

In the grenade experiment, the mean velocity of sound is determined for a series of successive atmospheric layers. This is accomplished by a ground-based microphone array which measures the phase velocity of the wave system generated by each of a series of grenade bursts. These observations lead to values of mean temperatures for the altitude layers between successive grenade bursts.

In the falling-sphere experiment, the drag acceleration a_d experienced by the falling sphere is measured, either directly by an accelerometer or indirectly from radar tracking data. These same radar data or the results of single and double integration of the net acceleration (gravity minus drag) lead to velocity v and altitude h. These values of a_d and v when combined with the appropriate value of drag coefficient c_d and the area-to-mass ratio lead to density at altitude h. While the only thermodynamic property measured is density, this measurement can hardly be considered a direct or independent one.

In the pitot-tube experiment, ratios of impact pressures to cone-wall pressures or to ambient pressures are measured, sometimes with aneroid type pressure gauges, but more likely by some form of ionization gauge which actually measures particle number density. These pressure ratios lead to Mach numbers as well as to ambient pressure. The Mach number along with rocket velocity from some form of radar observation leads to sound speed and then to temperature.

In various ionization gauges experiments, measurements lead to the number density, mass density, or pressure depending upon calibration of the location of the gauge on the rocket, the rocket altitude and wall-temperature considerations.

In none of the above methods may the temperatures, densities or pressures be considered directly independent observations. While some of the measurement techniques have smaller errors than others, for various reasons, there appears to be no other inherent advantage to having measured one or another of the thermodynamic properties at various altitudes. With each method, altitude profiles of p, T, and ρ may be obtained ultimately for each of the individual soundings considered provided the correct initial conditions are met.

The investigators involved in the various atmospheric sounding experiments do not always derive all three of the thermodynamic properties p, T, and ρ from their observed data, and in some instances, the methods employed by one investigator may lead to greater uncertainties than that used by another. The study being herein reported used only the results of those soundings for which there existed a published set of density-altitude values, and only these data were used regardless of what other data may also have been published. Thus, in one sense, density-altitude data may be considered as the independent data in this study. The related temperatures for each sounding is used in this study were determined in all cases by a numerical integration form of Equation (3) and the pressures were then determined using Equation (1).

DATA SOURCES AND PRELIMINARY STEPS

A total of 437 soundings covering the period 1947 to early 1965 were assembled for analysis. This basic data was collected from 45 different sources including journal articles, institutional reports and private communications. Table 1 gives an inventory of the soundings showing the number available from each of 25 different launch sites. With the exception of three flights, data published in the reports of the Meteorological Rocket Network (MRN) [12] were not taken as the basic source of data in this study. MRN reports do, however, contain the same or revised forms of data for a considerable number of soundings used by us. The originally published forms of the soundings used had the common feature of density-altitude profiles $\rho(Z)$ in one of a number of systems of units. Temperatures or pressures were frequently not published with the basic density data in the original sources, and when published, were arrived at by a variety of methods. Consequently, to obtain uniformity, all temperature-altitude data used in this study were recomputed by us from the density-altitude data for each sounding using Equation (3); i.e., the principle of downward integration of the density-altitude data. The perfect integral of Equation (3) was replaced by a numerical-integration procedure using a semi-logarithmic trapezoidal rule described by Minzner and Sauermann [13]. The resultingtemperatures, the original densities, and the Gas Law were then used to calculate the pressure-altitude profile. These data were compiled and published in a separate scientific technical report by Minzner, Morgenstern and Mello [14].

Checking and Editing

The calculated temperatures served as a basis for checking the quality of the density data and for verifying the key-punching accuracy. The computed temperatures were compared with interpolated values of the temperatures of the U.S. Standard Atmosphere [8] and with the originally published temperatures when these were available. The machine listings of the resulting temperature differences were then reviewed noting any large temperature differences or any abrupt change in differences from one level to the next. Such situations result from abnormal increments in the value of $\Delta \ell n \rho/\Delta Z$ versus altitude, and suggested key-punch errors or other difficulties in the basic data cards. The related data cards and the basic data were then checked and corrected when necessary. In at least two instances, this test indicated errors in the basic publication from which our data had been taken. Corrections of the basic data were made in these instances. At least six cases were found where one investigator in each of four different reports in the same year, had smoothed one or more extreme temperature values within a sounding without smoothing the density values which generated them.

TABLE 1

INVENTORY OF ATMOSPHERIC DATA BY SITE

SITE NAME	CODE	LAT.	LONG.	LST HRS.	NUMBER OF SOUNDINGS
ALBUQUERQUE, N. MEXICO	AQ	35.05N	106.40W	GMT-07.0	26
ASCENSION I., ATL. O.	AI	07.98S	014.42W	GMT-00.0	44
BARKING SANDS, HAWAII	BS	22.05N	159.78W	GMT-10.0	6
CARNARVON, W. AUSTRALIA	CA	24.82S	113.87E	GMT+08.0	9
EGLIN AF BACE, FLORIDA	EG	30.38N	086.70W	GMT-06.0	74
FT. CHURCHILL, MANITOBA	FC	58.73N	093.82W	GMT-06.0	49
GUAM, MARINA I., PAC. O.	GM	13.62N	144.85E	GMT+10.0	7
HEISS I., FRANZ JOS. L.	HI	80.62N	058.13E	GMT+05.0	25
HOLLOMAN AFB, N. MEXICO	HA	32.85N	106.10W	GMT-07.0	6
KAPUSTIN YAR, EUR. USSR	KY	48.6 N	045.8 E	GMT+04.0	2
KWAJALEIN, MARSHAL I., P.	KW	08.73N	167.73E	GMT+12.0	23
MCMURDO SOUND, ANTARCTICA	MC	77.88S	166.73E	GMT+11.0	20
POINT MUGU, CALIFORNIA	PM	34.12N	119.12W	GMT-08.0	3
SHIP A, EQ. PACIFIC OCEAN	SA	00.18N	161.42W	GMT-11.0	1
SHIP B N. ATLANTIC OCEAN	SB	62.06N	063.92W	GMT-04.0	1
SHIP C LANCASTER SND.	SC	74.57N	094.48W	GMT-06.0	1
SHIP D N. ATLANTIC OCEAN	SD	54.0 N	053.33W	GMT-04.0	2
SHIP E N. ATLANTIC OCEAN	SE	58.43N	055.06W	GMT-04.0	2
SHIP F N. ATLANTIC OCEAN	SF	49.0 N	048.4 W	GMT-03.0	2
SHIP G N. ATLANTIC OCEAN	SG	57.8 N	046.7 W	GMT-03.0	2
SHIP H N. ATLANTIC OCEAN	SH	65.6 N	058. W	GMT-04.0	2
THULE, GREENLAND	TH	76.55N	068.82W	GMT-04.0	5
WALLOPS I., VIRGINIA	WI	37.83N	075.48W	GMT-05.0	59
WHITE SANDS, NEW MEXICO	WS	32.38N	106.48W	GMT-07.0	25
WOOMERA S. AUSTRALIA	WO	31.11S	136.97E	GMT+09.5	41

Some observed density data were shown by this test to have a very erratic behavior, which most likely was not real but which probably represented the uncertainty in some phase of the measurement. Where such erratic observations resulted in density inversions; i.e., density increasing with increasing altitude, the data were either eliminated or smoothed in one of two ways: (1) in a selective smoothing process, individual data points were adjusted to eliminate isolated density inversions, and (2) in a number of other instances where many inversions existed within a sounding, a third order root-mean-square fit was made of the entire sounding. Soundings containing identical densities for two successive levels yielded impossible temperatures at the lowest of these levels, and these cases were eliminated by selective adjustment of density-data pairs. The pressure-altitude profiles, which in some instances were published in the original data source, were universally disregarded in the checking and editing procedures.

Soundings of which the data have been adjusted in one of several ways have been given appropriate code designations in the separate data report. In spite of the very large effort expended in editing the density-altitude data, at least four soundings containing uncorrected density inversions have been found since the publication of this data [14].

Normalizing the Data to Integer Altitudes

The values of density temperature and pressure published in the data report are given for the same altitudes cited in the basic source of the data. In the current statistical study, however, the data for the various soundings must all be normalized to a common set of altitudes. The set chosen is the series of successive integer geometric kilometer altitudes between the greatest and lowest altitude of the sounding. (It has since been determined that integer geopotential kilometer altitudes would have been preferable.) The adjustment of the data to this common set of altitudes were performed by a series of steps, the first of which was a semilogarithmic interpolation of the density-altitude data. The interpolated densities then served as the basis for a calculation of a temperature-altitude profile at the integer altitudes using the same method previously described. This temperature calculation, as in the case of that used for the data report, accounted for the variation of the acceleration of gravity with latitude of the site, as well as with altitude over the site. The temperature calculation also effectively accounted for possible diffusive separation (or change in molecular weight of air) at high altitudes by yielding a result which is commonly called molecular scale temperature [3]. This refinement, accounting for variations in molecular weight, is insignificant for data below 110 or 120 km altitude, but its influence at higher altitudes can be considerable. The molecular scale temperature was then used in the Gas Law equation with the related density values and with the appropriate constants to yield rigorously correct pressures at the integer altitudes.

The corresponding values of density, temperature and pressure at successive integer altitudes for each of 437 soundings, comprises the set of data hereinafter designated as the interpolated data. These data have an internal consistency and homogeneity in basic editing and method of generation which we believe adds considerably to the validity of the statistical results of this study. These data have not been separately published, but exist as a set of 17,000 IBM cards. In addition to the values of the three altitude-dependent parameters, density, temperature, and pressure, each card also contains a number of other pieces of information which are fixed for any particular sounding. This other information includes the following: (1) the date and time of the sounding in Greenwich or universal time, (2) the site of the launching, (3) the solar flux for the day preceeding and for the day of the launching, and (4) three sets of codes designating seasonal groupings, diurnal groupings, and a latitude grouping. The Greenwich time was assigned to each sounding on the basis of local standard time, plus or minus a time-zone correction. The solar flux was taken from the recordings of the 10.7-cm radiation at Ottawa, Canada [15,16]. The seasonal, diurnal and latitudinal codes were assigned in a manner described in the following sections.

STRATIFICATION OF THE DATA

Seasonal, Diurnal and Latitudinal Coding of the Data

The four basic types of seasonal divisions and one special seasonal division are determined and coded. These divisions are based on various numbers of days relative to the vernal equinox as shown in Table 2. They include a 16-season division, an 8-season division, a 4-season division, a 2-season division, and an extreme-season division.

Two kinds of diurnal divisions have been coded; a six-period division and a three-period division. These are based on the following criteria: (1) subsolar angle or zenith angle of the sun during daylight hours, (2) local apparent noon and midnight, and (3) height of earth's shadow during nighttime periods. These divisions are shown in Table 3 and in Figure 1.

Only one kind of latitude-belt division was coded, that shown in Table 4. This division allows for 7 latitude belts in a single hemisphere, each belt being 15 degrees wide with the exception of the tropical and polar belts which are only 7.5 degrees in one hemisphere. Data from a particular latitude belt in the southern hemisphere are combined with data in the corresponding latitude belt in the northern hemisphere after the southern hemisphere data have had a 183-day phase shift applied prior to the seasonal designation. A second type of latitude-belt division was considered. In this one, adjacent pairs of those belts designated in Table 4 would have been combined. Thus belts 0 plus 1, 2 plus 3, and 4 plus 5 form three wider belts. No coding was developed specifically for this division, although some initial calculations were made on the basis of such a division.

Four-Season Stratification of the Data

The four types of seasonal divisions, two types of diurnal divisions and two types of latitudinal division lead to 16 possible types of stratifications of the data in regard to the three variables; season, diurnal period, and latitude band. The system of codes greatly facilitated the process of trying various combinations of divisions and of sorting the data into homogeneous stratifications. Several different sortings were made to study the variation of sample size for different degrees of space and time resolution. For the number of soundings available (437) the maximum usable resolution of the three variables was judged after several trials to be four seasons, three diurnal periods (daytime, nighttime and diurnal transition), and six latitude belts. This leads to 72 possible basic cells. The distribution of maximum sample size (maximum number of soundings per cell) for such resolution is shown in Figure 2.

TABLE 2

DEFINING CONDITIONS OF SEASONAL CODING FOR NON-LEAP YEARS

DATE	DAY OF YEAR	DAYS IN SEASON	SIXTEEN SEASON CODE	EIGHT-SEASON CODE	FOUR-SEASON CODE	TWO-SEASON CODE	EXTREME-SEASON CODE
FEB 26	57		---	---	---		
		23	16		S		
MAR 21	80		---	7	P		
		23	1		R		
APR 13	103		---	---	I 1	---	
		23	2		N		
MAY 06	126		---	0	G		
		23	3			S	
MAY 29	149		---	---	---	U	
		23	4		S	M	
JUN 21	172		---	1	U	M	---
		23	5		M	E	S
JUL 14	195		---	---	M 2	R 2	U 8
		23	6		E		X
AUG 06	218		---	2	R	H	---
		23	7			A	
AUG 29	241		---	---	---	L	
		23	8		A	F	
SEP 21	264		---	3	U		
		23	9		T		
OCT 14	287		---	---	U 3	---	
		23	10		M		
NOV 06	310		---	4	N		
		22	11			W	
NOV 28	332		---	---	---	I	
		23	12		W	N	
DEC 21	355		---	5	I	T	---
		22	13		N	E	W
JAN 12	12		---	---	T 4	R 1	I 9
		23	14		E		X
FEB 04	35		---	6	R	H	---
		22	15			A	
FEB 26	57		---	---	---	L	
		23	16			F	
MAR 21	80		---	7			
		23	1				
APR 13	103		---	---		---	

TABLE 2 CONTINUED

FOR SOUTHERN-HEMISPHERE SITES THE SEASONS ARE INVERTED BY SUBTRACTING 183 FROM THE NUMBER OF THE DAY OF THE YEAR WHEN THAT NUMBER IS EQUAL TO OR GREATER THAN 183, OR BY ADDING 183 WHEN THAT NUMBER IS LESS THAN 183.

FOR LEAP YEARS, ONE DAY IS ADDED TO THE DAY OF THE YEAR FOR MONTHS MARCH THROUGH DECEMBER. CORRESPONDINGLY NO CORRECTION IS MADE FOR THE ACCUMULATED QUARTER-DAY ERRORS IN SUCCESSIVE MEMBERS OF THE REMAINDER OF THE FOUR YEAR CYCLE, IN SO FAR AS THE SEASONAL DIVISION IS CONCERNED.

ABBREVIATIONS LEGEND
SUX = SUMMER EXTREME
WIX = WINTER EXTREME

TABLE 3

DIURNAL CODING
AS RELATED TO RANGES OF
LOCAL APPARENT TIME, SUBSOLAR ANGLE, AND SHADOW HEIGHT

SHADOW HEIGHT	SUBSOLAR ANGLE	LOCAL APPARENT TIME	DIURNAL CLASSES 6-PERIOD 6-CLASS CODE	DIURNAL CLASSES 3-PERIOD 3-CLASS CODE
≥ 300 KM	>60 DEG	----------	-------	2 NIGHTTIME
			6	
-------			-------	----------
		<12.00 HRS	1	0 TRANSITION
	---------		-------	----------
			2	
<300 KM	≤ 60 DEG	----------	-------	1 DAYTIME
			3	
	---------		-------	----------
		≥ 12.00 HRS	4	0 TRANSITION
-------			-------	----------
			5	
≥ 300 KM	>60 DEG	----------	-------	2 NIGHTTIME

MIDNIGHT IS NEVER DESIGNATED AS 24.00 HOURS OF THE JUST-ENDING DAY, RATHER IT IS DESIGNATED AS 00.00 HOURS OF THE JUST-BEGINNING DAY.

TABLE 4

LATITUDE CODING

RANGE OF LATITUDE INCREMENTS	LATITUDE CODE	NAME OF BAND OF LATITUDE	SITES INCLUDED
DEGREES			
0.00 TO +07.50	0	EQUITORIAL	SA
0.00 TO -07.50	0	EQUITORIAL	
+7.51 TO +22.50	1	TROPICAL	BS,GM,KW
-7.51 TO -22.50	1	TROPICAL	AI
-22.51 TO -37.50	2	SUBTROPICAL	CA,WO
+22.51 TO +37.50	2	SUBTROPICAL	AQ,EG,HA,PM,WS
+37.51 TO +52.50	3	MIDLATITUDE	KY,SF,WI
-37.51 TO -52.50	3	MIDLATITUDE	
+52.51 TO +67.50	4	SUBARCTIC	FC,SB,SD,SE,SG,SH
-52.51 TO -67.50	4	SUBARCTIC	
+67.51 TO +82.50	5	ARCTIC	HI,SC,TH
-67.51 TO -82.50	5	ARCTIC	MS
+82.51 TO +90.00	6	POLAR	
-82.51 TO -90.00	6	POLAR	

LATITUDES IN THE NORTHERN HEMISPHERE ARE DESIGNATED POSITIVE
LATITUDES IN THE SOUTHERN HEMISPHERE ARE DESIGNATED NEGATIVE.

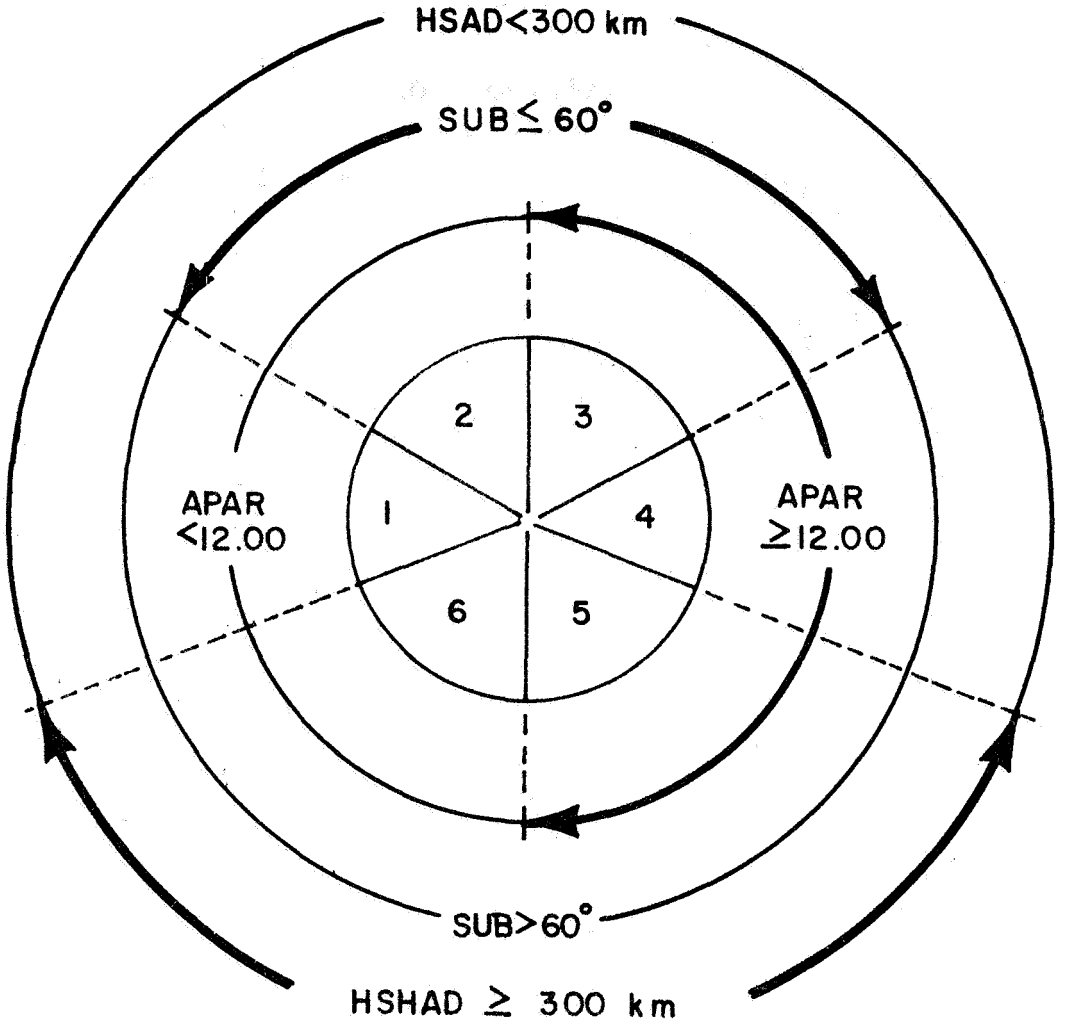

DEFINITIONS OF SYMBOLS AS USED IN THE COMPUTER CODING PROGRAM

SUB	-	sub-solar angle
APAR	-	local apparent time
HAHAD	-	height of the earth's shadow
1	-	morning-transition period
2	-	early-day period
3	-	late-day period
4	-	evening-transition period
5	-	early-night period
6	-	late-night period

Figure 1. Definitions of symbols as used in the computer coding program.

	DIURNAL TYPE			
	NIGHT	TRANSITION	DAY	TOTAL
SPRING	–	–	1	1
SUMMER	–	–	–	–
AUTUMN	–	–	–	–
WINTER	–	–	–	–
TOTAL	–	–	1	

EQUITORIAL, BELT 0

	DIURNAL TYPE			
	NIGHT	TRANSITION	DAY	TOTAL
SPRING	13	3	5	21
SUMMER	8	10	2	20
AUTUMN	4	19	6	29
WINTER	6	1	3	10
TOTAL	31	33	16	

TROPICAL, BELT 1

	DIURNAL TYPE			
	NIGHT	TRANSITION	DAY	TOTAL
SPRING	17	6	22	45
SUMMER	12	15	14	41
AUTUMN	9	37	29	75
WINTER	13	2	8	23
TOTAL	51	60	73	

SUBTROPICAL, BELT 2

	DIURNAL TYPE			
	NIGHT	TRANSITION	DAY	TOTAL
SPRING	2	2	10	14
SUMMER	5	3	13	21
AUTUMN	1	3	9	13
WINTER	–	7	8	15
TOTAL	8	15	40	

MIDLATITUDE, BELT 3

	DIURNAL TYPE			
	NIGHT	TRANSITION	DAY	TOTAL
SPRING	1	–	6	7
SUMMER	8	–	8	16
AUTUMN	–	2	14	16
WINTER	–	9	10	19
TOTAL	9	11	38	

SUBARCTIC, BELT 4

	DIURNAL TYPE			
	NIGHT	TRANSITION	DAY	TOTAL
SPRING	1	–	11	12
SUMMER	3	–	14	17
AUTUMN	–	1	7	8
WINTER	–	6	8	14
TOTAL	4	7	40	

ARCTIC, BELT 5

FIGURE 2. DISTRIBUTION OF SOUNDINGS INTO A THREE-DIMENSIONAL ARRAY OF CELLS DISTINGUISHING THREE DIURNAL PERIODS, FOUR SEASONS, AND SIX LATITUDE BELTS, WHEN THE INDICATED LAYERS ARE STACKED NORMAL TO THE PLANE OF THE PAPER IN ASCENDING ORDER OF BELT NUMBER

Figure 2 represents a partial disection of a six-layer, three-dimensional array of cells in which each layer is shown as a separate part of the figure. Each layer is associated with a particular latitude belt and represents a two-dimensional array of 12 cells stemming from four seasonal units and three diurnal-period units.

A comparison of statistical results associated with any horizontal row of three cells (left to right in the plane of the paper) should indicate any influence of diurnal variability within a particular season and latitude belt. A comparison of results associated with any column of three cells, top to bottom in the plane of the paper should indicate any influence of seasonal variability within a particular diurnal period and latitude belt. A comparison of results associated with any column of six cells normal to the plane of the paper in the three-dimensional view (i.e., cells of corresponding season and diurnal period, one from each of the six latitude belts) should indicate any influence of latitudinal variability within a particular season or diurnal period.

The numbers within the 72 different cells represent the numbers of soundings (from our data set) which are associated with the particular cells. The most populous latitude belt is the subtropical belt with 184 soundings. This number accounts for over 40 percent of the total sample. The remainder of the data are distributed somewhat uniformly across the other latitude belts, with the exception of the equitorial belt for which there is but a single sounding in our sample.

Little reliance could be placed upon any atmospheric variability between latitude bands 0 and 1 which might be demonstrated by the data of the single sounding in belt 0 when compared with the data of the 80 soundings in belt 1. Consequently, for this study, the data from the single belt-0 sounding were combined with the data in the corresponding cell of latitude belt 1, thereby eliminating latitude belt 0, and reducing the number of basic cells under consideration to 60. (Therefore all subsequent discussion of Figure 2 will refer to only latitude belts 1 through 5.)

The four totals in the right-hand column of each of the two-dimensional arrays of cells in Figure 2 represent the sums of soundings in each of the associated four seasons disregarding diurnal periods. Each of these sums is associated with what we call a compressed cell, wherein the number of soundings is increased at the expense of losing the opportunity of discerning the influence of one of the variables, in

this instance the diurnal period. The stacked three-dimensional array of cells of Figure 2, when viewed from the right, shows a set of 20 first-compression cells in the latitude-season plane as presented in Figure 3. A comparison of statistical results associated with any horizontal row of 4 cells in Figure 3 should indicate any influence of seasonal variability within a given latitude belt, provided it is not masked by the unresolved diurnal variability. Similarly, a comparison of results associated with any vertical column should indicate any influence of a latitudinal variability within a given season, without regard to diurnal period.

The three totals in the bottom row of each of the five latitude sections in Figure 2 represent the sums of the number of soundings in the four seasons for any one diurnal period. These numbers are associated with a set of 15 first-compression cells within which the number of soundings is increased at the expense of losing the seasonal resolution. As viewed from the front of the stacked array of Figure 2, this set of first-compression cells lies in the plane defined by latitude and diurnal periods as shown in Figure 4. A comparison of statistical results associated with any horizontal row of these cells permits the examination of diurnal variability at a fixed latitude, without regard for season. Similarly, a comparison of results of any vertical column of these cells permits the examination of latitudinal variability for a fixed diurnal period, provided that the unresolved seasonal variability does not obscure the results.

The first four totals in the bottom row of the array of Figure 3 represent the totals of the corresponding columns. Each of these numbers is associated with one member of a set of four second-compression cells within which neither diurnal period nor latitude belt is resolved. These cells constitute a one-dimensional array in which only the season is resolved. The first five totals in the right-hand column of the array of Figure 3 are each associated with a corresponding member of a set of five second-compression cells. In this instance, neither the four seasons nor the three-diurnal periods are resolved. Hence, these five cells constitute a one-dimensional array in which latitude belt is the only resolved variable.

Similarly, the three totals in the bottom row of the array of Figure 4 are each associated with corresponding members of a set of three second-compression cells. In this instance, however, it is the four seasons and six latitude belts which are not resolved. Thus, these cells constitute a one-dimensional array in which only diurnal period is resolved.

The number on the lower right-hand corner of the array of Figure 3 is the identical sum of the corresponding column and row. This number is

		WINTER	AUTUMN	SUMMER	SPRING	TOTAL
ARCTIC,	BELT 5	14	8	17	12	51
SUBARCTIC,	BELT 4	19	16	16	7	58
MIDLATITUDE,	BELT 3	15	13	21	14	63
SUBTROPICAL,	BELT 2	23	75	41	45	184
TROPICAL,	BELT 1	10	29	20	22	81
	TOTAL	81	141	115	100	437

FIGURE 3. DISTRIBUTION OF SOUNDINGS INTO FOUR DISTINCT SETS OF CELLS,-- ONE FIRST-COMPRESSION SET, TWO DIFFERENT SECOND-COMPRESSION SETS, AND ONE THIRD-COMPRESSION SET,-- WHERE THE FOUR SETS OF CELLS DISTINGUISH RESPECTIVELY THE FOLLOWING SEASONAL AND LATITUDINAL DIVISIONS. FOUR SEASONAL PERIODS AND FIVE LATITUDE BELTS,- FOUR SEASONAL PERIODS ONLY,- FIVE LATITUDE BELTS ONLY,- AND NEITHER SEASONAL PERIODS NOR LATITUDE BELTS

		NIGHT		
		DAY		
ARCTIC,	BELT 5	4	7	50
SUBARCTIC,	BELT 4	9	11	38
MIDLATITUDE,	BELT 3	8	15	40
SUBTROPICAL,	BELT 2	51	60	73
TROPICAL,	BELT 1	31	23	17
	TOTAL	103	126	208

FIGURE 4. DISTRIBUTION OF SOUNDINGS INTO TWO DISTINCT SETS OF CELLS,-- ONE FIRST-COMPRESSION SET, AND ONE SECOND-COMPRESSION SET,-- WHERE THE TWO SETS OF CELLS DISTINGUISH RESPECTIVELY THE FOLLOWING DIURNAL AND LATITUDINAL DIVISIONS. THREE DIURNAL PERIODS AND FIVE LATITUDE BELTS,- AND THREE DIURNAL PERIODS ONLY

associated with a single third-compression cell in which none of the three variables, season, diurnal period, or latitude belt is resolved. The number in this cell is, of course, the size of the total sample. The total number of cells defined in the four-season classifications described above is 108.

Extreme-Season Stratification

In addition to the four-season classification scheme shown in Figures 2, 3, and 4, the data were also stratified according to a two extreme-season classification. One of these extreme seasons consists of a summer extreme which is half the length of the previously defined summer season, and covers the 46-day period following the summer solstice. The second extreme season consists of a winter extreme which covers the 46-day period following the winter solstice. These two subsets were designed to aid in the detection of extremes of any statistical model which depends upon the annual heating and cooling cycle.

As in the four-season classification, the sounding data in the summer-extreme and winter-extreme classes were further stratified into three times-of-day periods, and five latitude belts. This stratification leads to 30 basic cells for which the sample sizes are shown in the basic portions of the five layers of the three-dimensional array in Figure 5. Each horizontal row of these basic cells was compressed across diurnal periods yielding first-compression cells with numbers of soundings shown in the columns entitled total in each section of Figure 5. These ten, first-compression, extreme-season cells are shown grouped in the season-latitude plane in Figure 6. Here the results of a second compression, this one across latitude belts, is shown as two cells with sounding numbers given in the totals of Figure 6. Figure 6 bears the same relationship to Figure 5 as Figure 3 bears to Figure 2.

No second-compression, extreme-season cells were obtained by compressing across seasons. This is because the annual mean value so obtained would not be as valid as one obtained from the four, quarter-year periods. There is, therefore, no extreme-season, second-compression diagram comparable to the basic second-compression diagram of Figure 4. There are also no corresponding data cells for analysis.

In the extreme-season category, a total of 12 compressed cells and 30 basic cells yield a sum of 42 extreme-season cells. These cells added to the 60 basic cells and the 48 compressed cells in the four-season category yield a total of 90 basic cells and 60 compressed cells or a grand total of 150 defined data cells.

Sample-Size Distribution Within the Data Cells

A review of the 150 possible data cells shows that a wide range of sample size exists particularly in the 90 basic cells; i.e., 0 to 37

TROPICAL, BELT 1

	NIGHT	DAY	TOTAL
SUMMER EXTREME	-	3	5
	2		
WINTER EXTREME	1	1	3
	1		

SUBTROPICAL, BELT 2

	NIGHT	DAY	TOTAL
SUMMER EXTREME	2	8	16
	6		
WINTER EXTREME	7	1	9
	1		

MIDLATITUDE, BELT 3

	NIGHT	DAY	TOTAL
SUMMER EXTREME	5	1	8
	2		
WINTER EXTREME	-	2	3
	1		

SUBARCTIC, BELT 4

	NIGHT	DAY	TOTAL
SUMMER EXTREME	5	-	8
	3		
WINTER EXTREME	-	2	8
	6		

ARCTIC, BELT 5

	NIGHT	DAY	TOTAL
SUMMER EXTREME	3	-	8
	5		
WINTER EXTREME	-	-	4
	4		

FIGURE 5. DISTRIBUTION OF SOUNDINGS INTO A THREE-DIMENSIONAL ARRAY OF CELLS DISTINGUISHING THREE DIURNAL PERIODS, TWO EXTREME-SEASON PERIODS, AND FIVE LATITUDE BELTS, WHEN THE INDICATED LAYERS ARE STACKED NORMAL TO THE PLANE OF THE PAPER IN ASCENDING ORDER OF THE BELT NUMBER

		WINTER EXTREME-SEASON FIRST-COMPRESSION CELLS	SUMMER EXTREME-SEASON SECOND-COMPRESSION CELLS
ARCTIC,	BELT 5	4	8
SUBARCTIC,	BELT 4	8	8
MIDLATITUDE,	BELT 3	3	8
SUBTROPICAL,	BELT 2	9	16
TROPICAL,	BELT 1	3	5
	TOTAL	23	33

FIGURE 6. DISTRIBUTION OF SOUNDINGS INTO TWO DISTINCT SETS OF CELLS,-- ONE FIRST-COMPRESSION SET, AND ONE SECOND-COMPRESSION SET,-- WHERE THE TWO SETS OF CELLS DISTINGUISH RESPECTIVELY THE FOLLOWING DIURNAL AND LATITUDINAL DIVISIONS. TWO EXTREME-SEASON PERIODS AND FIVE LATITUDE BELTS,- AND TWO EXTREME-SEASON PERIODS ONLY

soundings. Sixteen basic cells contain no soundings from our sample, 14 contain soundings such that there is one and only one data point at any altitude, while 10 additional cells contain soundings such that the greatest concentration of data points at any particular altitude is two. Since our programs made statistical analyses only for sample sizes of 3 or more, no computations were made for 40 of the basic cells. Hence, results exist for only 110 data cells.

There are at least four general factors which contribute to the disproportionate distribution of the sample size; these factors involve geographical, sociological, psychological and astronomical considerations. Of these, only the latter can be specifically defined, but some subjective comments appear to be applicable to the others. The more remote areas, and hence the subarctic and arctic belts, have fewer soundings merely because of the logistical problems involved. The first half of the winter-extreme period between December 21 and mid-January have very few soundings in any latitude belt largely because of the holidays. Arctic and subarctic regions are most uncomfortable during the winter, and field parties tend to avoid discomfort by avoiding extreme conditions. These reasons are largely responsible for the fact that only 37 percent of all extreme-season soundings occurred during the winter-extreme period.

In retrospect it is apparent that defined astronomical conditions for day and night divisions in our study are responsible for a large amount of the disproportionate distribution of sample size, particularly in latitude belts 4 and 5, although these reasons also apply to a lesser degree to latitude belt 3. Our definition of daytime required the local elevation angle of the sun to be greater than 30 degrees. It may be demonstrated, therefore, that no winter or winter-extreme daytime conditions are possible in latitude belts 4 and 5 and that only a few hours of such daytime conditions exist in latitude belt 3. In particular, on the day of the winter solstice no such daytime conditions exist at latitudes greater than 36.56° and even at the summer solstice, the northern boundary of the arctic belt is just within the latitude which satisfies the condition. Similarly, autumn daytime conditions are almost non-existent in the arctic belt with the total number of daytime hours per autumn season gradually increasing as the latitude decreases.

Our definition of nighttime required an earth's shadow height of 300 km. It may be shown that this condition is met at local midnight when the sum of the latitude and the declination angle is equal to or less than 71.43 degrees (atmospheric refraction being considered). Taking the value of the sun's declination angle for those dates which serve as boundaries to the several seasons as defined by us, one may readily estimate the periods when no nighttime conditions exists at the various latitudes. One sees that there is no summer night in the arctic and almost none in the subarctic. Even at the more northerly portions of latitude belt 3, summer nighttime as defined by us does not exist for some

days around the summer solstice. Spring and autumn nighttimes are severly curtailed in the arctic and partly curtailed in the subarctic and mid-latitudes by our definition.

High-Resolution Stratifications

A finer resolution of the three variables, season, diurnal period and latitude was also considered during the early part of this study. This resolution involved eight seasons, six diurnal periods and five latitude bands. It leads consequently to a total of 240 basic cells without considering any compression cells. The basic three-dimensional array of cells for this resolution, with the number of sounding of our basic data in each cell is given in Figure 7. The many cells in such an array which have fewer than three soundings make it obvious that our basic data set is too small for such resolution.

Special Stratifications

In addition to the uniform sequence of data stratifications described above, several special data groupings were used. The objective here was to obtain increased sample sizes by selectively grouping some of the higher resolution cells. The three special stratifications were:

(1) Division of the annual cycle into winter half and summer half seasons (see Table 2). This grouping was made only for the data in the tropical and arctic latitude belts.

(2) All data from the subtropical and mid-latitude belts were combined into a single 30^{o} latitude belt class.

EQUATORIAL, BELT 0

SEASONS	DIURNAL PERIODS 1	2	3	4	5	6	TOTAL
0				1			1
S 1							
E 2							
A 3							
S 4							
O 5							
N 6							
S 7							
TOTAL				1			1

TROPICAL, BELT 1

SEASONS	DIURNAL PERIODS 1	2	3	4	5	6	TOTAL
0			5	1	3		9
S 1			8	2	3	2	15
E 2						5	5
A 3	1			3	2	1	7
S 4			4	2	7	9	22
O 5			2			1	3
N 6	3	1	3				7
S 7	2		8	2			12
TOTAL	6	1	30	10	15	18	80

SUBTROPICAL, BELT 2

SEASONS	DIURNAL PERIODS 1	2	3	4	5	6	TOTAL
0	4	2	11	12	3	3	35
S 1	3	2	2	4	6	1	18
E 2	6	4	4	1	4	4	23
A 3	1	2	5	12	19	3	42
S 4	4	2		12	8	7	33
O 5	1		3	4	1		9
N 6		4	6	3	1		14
S 7	3	1	3	3			10
TOTAL	22	17	34	51	42	18	184

MIDLATITUDE, BELT 3

SEASONS	DIURNAL PERIODS 1	2	3	4	5	6	TOTAL
0	1	1	1	2	1		6
S 1	1		4	8	1		14
E 2	1	1		3	2		7
A 3				1		1	2
S 4	1		1	7	1	1	11
O 5	3			2		1	6
N 6	1			2	6		9
S 7	2			5	1		8
TOTAL	10	2	6	30	12	3	63

SUBARCTIC, BELT 4

SEASONS	DIURNAL PERIODS 1	2	3	4	5	6	TOTAL
0				1			1
S 1							
E 2	1	1	7	7			16
A 3				1			1
S 4	5			8	1	1	15
O 5				1	2	1	4
N 6				9	4	2	15
S 7		1		5			6
TOTAL	6	2	7	32	7	4	58

ARCTIC, BELT 5

SEASONS	DIURNAL PERIODS 1	2	3	4	5	6	TOTAL
0	2		1				3
S 1	1		2	2			5
E 2	4		1	7			12
A 3	1						1
S 4	4			2	1		7
O 5				3	1	3	7
N 6	2			3		2	7
S 7	3			6			9
TOTAL	17		4	23	2	5	51

FIGURE 7. DISTRIBUTION OF SOUNDINGS ACCORDING TO SIX DIURNAL PERIODS, EIGHT SEASONS, AND SIX LATITUDE BELTS

COMPUTATION PROCEDURES

The coefficient of correlation (linear) between atmospheric density (ρ) and 10.7-cm solar flux (SF) may be stated as

$$r\{\rho, SF\} = \frac{\text{cov}\ \{\rho,\ SF\}}{\sigma\{\rho\}\ \ \sigma\{SF\}} \tag{11}$$

where

$\text{cov}\ \{\rho,\ SF\}$ is the covariance between ρ and SF
$\sigma\{\rho\}$ is the standard deviation of ρ
$\sigma\{SF\}$ is the standard deviation of SF.

For computation purposes, it is more convenient, however, to express Equation (11) in the form

$$r\{\rho,\ SF\} = \frac{n \Sigma\ \rho \cdot SF - \Sigma\rho\ \Sigma SF}{\sqrt{[n \Sigma\ \rho^2 - (\Sigma\rho)^2]\ [n \Sigma\ SF^2 - (\Sigma SF)^2]}} \tag{12}$$

where n is the sample size and the summations extend over all n. Either of these forms may be more properly referred to as the product-moment coefficient of correlation.

The computation procedure used to develop the graphs in Appendix A consisted of calculating the vertical profile of the coefficient of correlation for each of the data stratifications discussed in the previous sections. More specifically, for a given stratification cell the sample data at each altitude was used to calculate $r\{\rho, SF\}$ by means of Equation (12). Furthermore, the calculations were conducted for both the value of 10.7-cm solar flux recorded on the day of the density sounding and for the solar flux value observed on the preceding day. The computer program developed for the IBM 1620 data processing system to perform these calcualtions is listed in Appendix B. This program uses the instruction set from the 1620 PDQ FORTRAN code. A second computer program was written for the IBM 1620 AUTOPLOTTER system to machine plot the results of these calculations on an IBM 870 document writing system.

Because of scattering due to sampling fluctuations, the individual correlations calculated by Equation (12) were smoothed across altitude as part of the plotting operation. The particular smoothing operator used was

$$\tilde{r}_h = \alpha\ r_h + (1 - \alpha)\ \tilde{r}_{h-1} \tag{13}$$

where r_h is the unsmoothed value of the correlation coefficient at height h, $\tilde{r}_h$ is the smoothed correlation coefficient at height h, $\tilde{r}_{h-1}$ is the smoothed value at a unit height interval below h, and α is the smoothing coefficient. The process defined by Equation (13) is called exponential smoothing [17] since maximum weight is assigned to the value at height (h) with the weights at other altitudes decreasing exponentially as a function of the separation distance. The response of this smoothing operator to changes in the profile is governed by the value of α selected. In the current application, maximum response was desired so that small scale changes in the profile would be retained. Accordingly, a value of $\alpha = 0.5$ was used which is equivalent, in terms of the average height, to a three-point moving average. The graphs given in Appendix A represent a plot of these smoothed values as a function of height.

SIGNIFICANCE OF THE CORRELATION PROFILES

As noted earlier, Jacchia [18-22] has shown that the 10.7-cm solar flux and the density in the atmosphere above 200 km have a high degree of correlation. This is a positive correlation so that at times of high solar flux the atmospheric density is also high, while at times of low solar flux, the atmospheric density above 200 km is relatively lower. This 10.7-cm solar flux is undoubtedly not the radiation which is directly responsible for the variation in density. Rather, it is hypothesized that this radiation is most probably an indicator of some other radiation which does influence the atmosphere; i.e., radiation which is absorbed by some thin layer of the atmosphere below 200 km in greater or lesser amounts as the 10.7-cm flux increases or decreases. An alternative hypothesis is that there may be a variation of mass influx into the upper atmosphere of gaseous material directly related to variations in solar activity; i.e., directly related to variations in the 10.7-cm flux which causes the atmospheric density at altitudes of 300 to 500 km to vary accordingly. If the former hypothesis is correct, we should find at least one region of negative correlation below 200 km. If the latter hypothesis alone is correct there should be no correlation between ρ and solar flux below 200 km.

If a related radiation is the primary cause of the correlation, this radiation must be absorbed in some lower layer of the atmosphere, such that the atmosphere there is heated in a proportionate amount with an accompanying inverse relationship in the value of the local density, and a directly related variation in density at higher altitudes. For example, a high value of 10.7-cm flux implies increased radiation which in turn produces a high local value of temperature in the layer in which it was absorbed. This results in a decreased local density, a lifting of the atmosphere above this layer and correspondingly higher densities at altitudes above the absorbing layer. Thus, if there is but a single layer absorbing significant amounts of radiation, a negative correlation between solar flux and density should be observed at the altitude of this layer. At greater altitudes, a positive correlation should be observed.

It is well known that in the regions between 100 and 150 km, a considerable amount of radiation absorption does occur. If this radiation primarily in the Shumann-Runge continuum (at wavelengths shorter than 1760Å) is associated with the variability of the solar flux, then it is reasonable to believe that density changes occur in this region in such a way that they are negatively correlated with solar flux. The corresponding lifting and falling of the atmosphere above this absorption layer would then be influenced in the opposite way to give positive correlations.

A similar situation might be expected to exist in the upper regions of the ozone layer extending from about 60 km down to 20 km or below. While the maximum ozone concentration occurs perhaps as low as 25 to 27 km, the ultraviolet radiation from the Herzberg continuum (for wavelengths of 2420Å and shorter) is nearly entirely absorbed by the very small concentration of ozone in the upper regions of this layer, namely from about 60 km down to 45 km. If the Herzberg-continuum portion of the ultraviolet spectrum is keyed to the 10.7-cm radiation, then we might expect to find an increase of heating in the top of the ultraviolet layer with increases in the 10.7-cm flux and correspondingly decreases in heating during periods of low solar flux. If this situation exists, then we would expect to find negative correlations between solar flux and atmospheric density in these regions (45 to 60 km) with a corresponding region of positive correlation some kilometers above, say, in the 70 to 90 km region.

If the 10.7-cm flux is keyed to the visible or infrared portion of the solar spectrum, then we might expect to find an increase of local heating at the surface of the earth and in the lower boundary layers of the atmosphere with a resultant negative correlation near the surface and again more positive correlations at some altitudes above this level.

Thus it appears that there may be as many as three layers: 140-km layer, the 50-km layer, and the surface layer, each of which might conceivably be influenced by variations in radiation associated with variation in the 10.7-cm flux. For each of these three layers, we would expect to find a degree of negative correlation, whereas the regions in between would tend towards positive correlations. In each instance, however, the influence of the lifting of the atmosphere from the lowest layer would tend to confuse the simple picture and would be added onto the influences of radiation absorption in the successively higher layers. Only in the regions above the highest region of significant energy absorption that is above the 120-km layer, would one expect to find a consistent positive correlation.

Interpretation of the profiles given in Appendix A to evaluate the extent to which they tend to support this theory requires establishing the statistical significance of the calculated correlation values. In the absence of a priori knowledge for the population correlation coefficient, we may test the null hypothesis of no significant difference from a population correlation of zero. Any significant departure from this hypothesis may be indicative of a relation between solar flux and atmospheric density.

The exact distribution of the correlation coefficient for small samples originally derived by R. A. Fisher has been tabulated by David [23]. Based on these tables an empirical function was derived to aid in calculating fiducial limits for the correlation coefficient as a function of sample size. For the 5 percent and 95 percent confidence belt to test significance of the sample correlation coefficient with an assumed population of zero, these limits are given by

$$R = \pm 1.89\ n^{(-0.535)}$$

where R is taken as the upper or lower limit depending upon the sign and n is the sample size. This function, then, was used to interpret the significance of the correlation coefficient profiles.

The procedure consisted of testing the significance of the calculated value for the correlation coefficient (unsmoothed) at each 1-km altitude interval of the profile. The test was, however, limited to correlations obtained from data consisting of more than three sample points. If the calculated value of the correlation coefficient exceeded the confidence limit value, then the null hypothesis of no significant difference from a population correlation of zero must be rejected. All altitudes for which the null hypothesis was rejected were noted and tabulated.

Examination of the results from this analysis tend to give some preliminary support to the proposed model for the effects of solar flux anomalies on atmospheric density variations below 200 km. This result is most clearly evident from analysis of the combined hemispherical data shown in Figure 8. The bars in this graph show the height intervals over which the correlation coefficient was found to be significantly different from zero (either positive or negative). Figure 8(A) for example, illustrates that when all data from the study are grouped into a single profile; i.e., seasonal mean diurnal mean, and hemispherical mean, the correlation is negative at lower altitudes (40-83 km) and positive at higher altitudes (93-104 km). The exact boundary over which these intervals apply is somewhat arbitrary since they are determined by the confidence levels used in the statistical test. However, even when 1 percent confidence limits are applied to this profile, the key result of a significant negative correlation centered at approximately 60 km and a significant positive correlation centered at 100 km remains clearly evident.

A more detailed analysis showing the seasonal variation is shown in Figure 8(B). Both the spring, autumn and winter seasons show the characteristic low altitude negative correlations and higher altitude positive correlations. The summer season, though, presents an anomaly to this pattern by indicating positive correlation at all altitudes. Figure 8(C) shows the difference is observed even when the finer resolution summer and winter extreme season results are compared.

The diurnal variation is shown in Figure 8(D) of this graph. In this case both the nighttime and diurnal transition periods indicate negative correlations at lower altitudes with positive correlations at higher altitudes. The daytime cases, however, show only a positive correlation of density with solar flux.

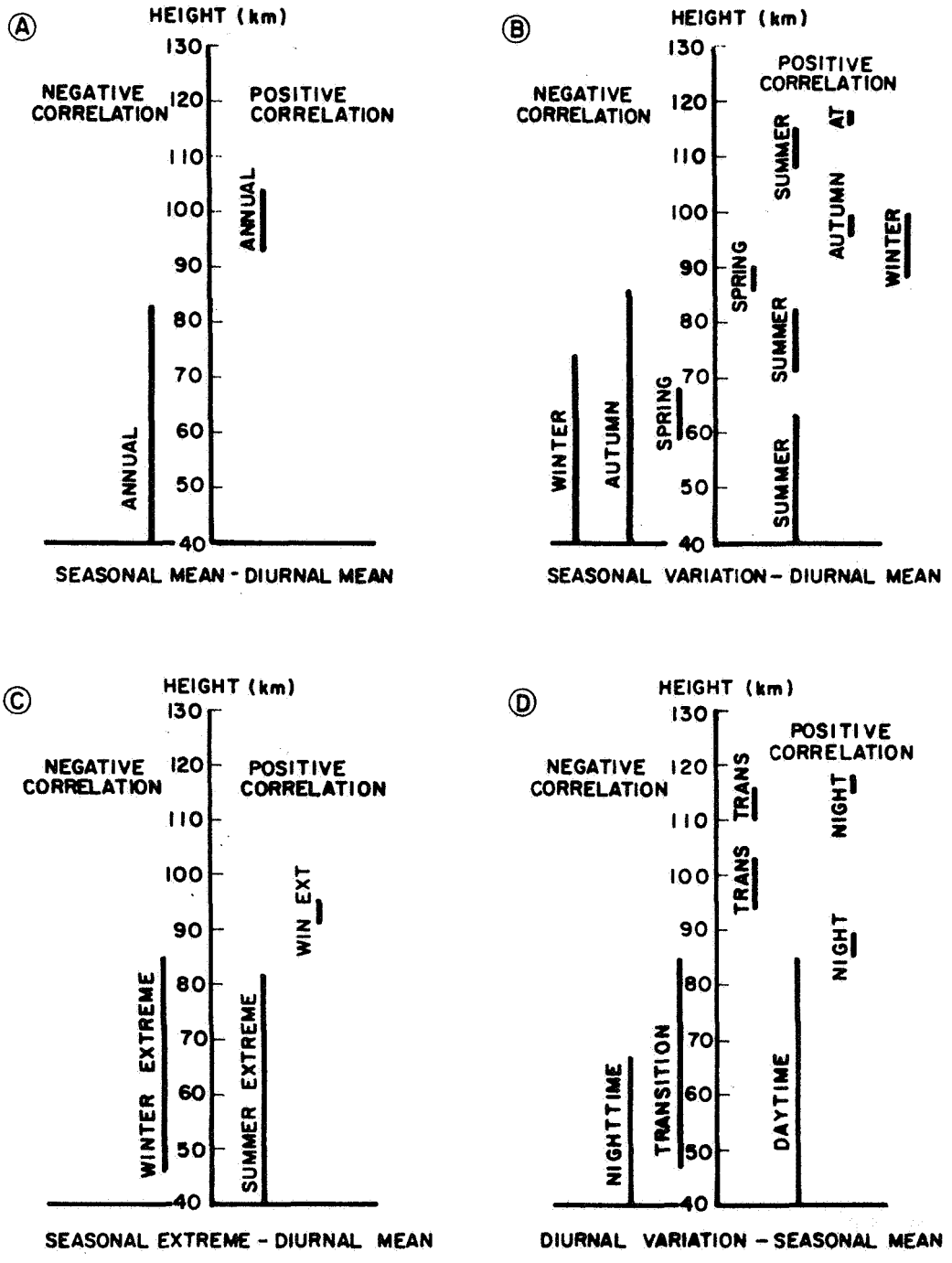

Figure 8. Altitudes of significant correlation coefficient for combined hemispherical data.

All of the graphs in Figure 8 show the variation for a given single stratification while averaging over the other factors. A further analysis was conducted on a more homogeneous set of data in an attempt to minimize any interaction effects of latitude, season, and time of day. Significant results were obtained here in only a limited number of cases because of the small sample sizes available when the data are highly stratified. From the cases which did yield significant results, the data indicated that season was the stronger factor in determining whether the correlation was positive or negative than was the time of day. No similar evaluation was possible as to the relative influence of latitude on this result.

Finally, a review of the difference in the correlations between those for the solar flux of current day and those for the solar flux from the preceding day shows in general that the profiles are very similar. Only in a single case do the two profiles show a significantly different result (see Figure 24 in Appendix A). In this instance, the two profiles are similar up to about 100 km but above this height they diverge. Because the sample size in this upper region is very small, the reliability of this particular result is extremely limited. Hence, no important lag relationship has been observed by the current set of calculations.

VARIABILITY OF ATMOSPHERIC DENSITY

The density data accumulated for study of its relation to solar flux also served as the basis for a separate investigation of the latitudinal, seasonal, and diurnal variability of atmospheric density alone. By means of the division of the data into the cells of various resolutions, the correlation studies were performed in such a manner so as to eliminate the effects of latitude, season, and time of day. The studies of the variation of density with latitude, season, and time of day, however, had no provisions for normalizing the solar flux influences. The variations of density at each altitude with variations of latitude, season, and time of day, were determined by comparing the differences between average values of density for a particular altitude in each of the various cells with a common reference density value for that altitude.

The reference values used consisted of the hemispheric, seasonal mean, diurnal mean, density-altitude profile calculated from the 437 soundings making up the data set. This will henceforth be called the hemispheric mean. This hemispheric mean density-altitude profile is compared with the 1962 U.S. Standard Atmosphere [8] in Figure 9. The several considerable departures of the calculated hemispheric mean density-altitude profile from the U.S. Standard Atmosphere suggest that the U.S. Standard Atmosphere is not a good mean atmosphere particularly near 95 km where the density of the hemispheric mean atmosphere is 26 percent greater than that of the U. S. Standard.

The percentage of deviation from the hemispheric mean of the mean density-altitude profiles for each member of two selected sets of cells was calculated and plotted.

The first of these sets consisted of the summer diurnal mean, and the winter diurnal mean cells for each of five latitude bands. The second of these sets consisted of the annual mean day and annual mean night cells for each of five latitude bands. The graphs for each of the two sets of cells are presented as composites in Figures 10 and 11.

The winter to summer variations for the various latitudes are shown in the first of these figures. While the percentage of departures were not calculated for altitudes below 30 km, the slope of the winter and summer arctic graphs strongly suggest the existence of the first isopycnic layer perhaps near 10-km altitude. The second isopycnic layer [24] near 90 km is dramatically evident in the case of the subarctic and mid-latitude pairs of curves with distinct crossings occurring at 87 and 90 km respectively. The arctic data do not extend to a sufficient altitude to substantiate this isopycnic layer. The winter to summer variation as shown by the subtropical pair of curves is so small that the second isopycnic layer is not sharply defined by these data. The winter to summer tropical variations are even smaller and were omitted from this composite

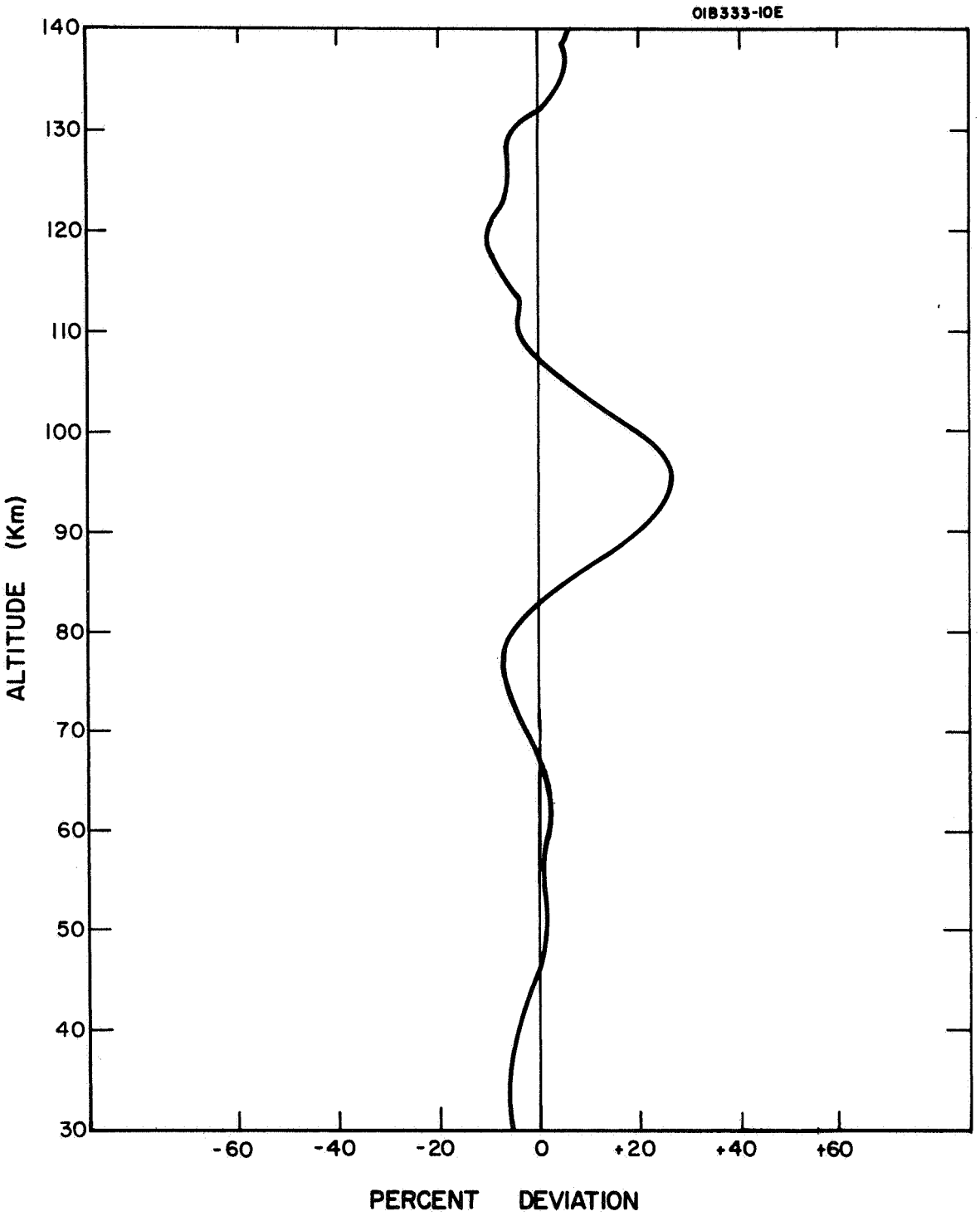

Figure 9. Percent deviation of the hemispherical, seasonal, diurnal mean density-altitude profile from that of the 1962 U.S. Standard Atmosphere.

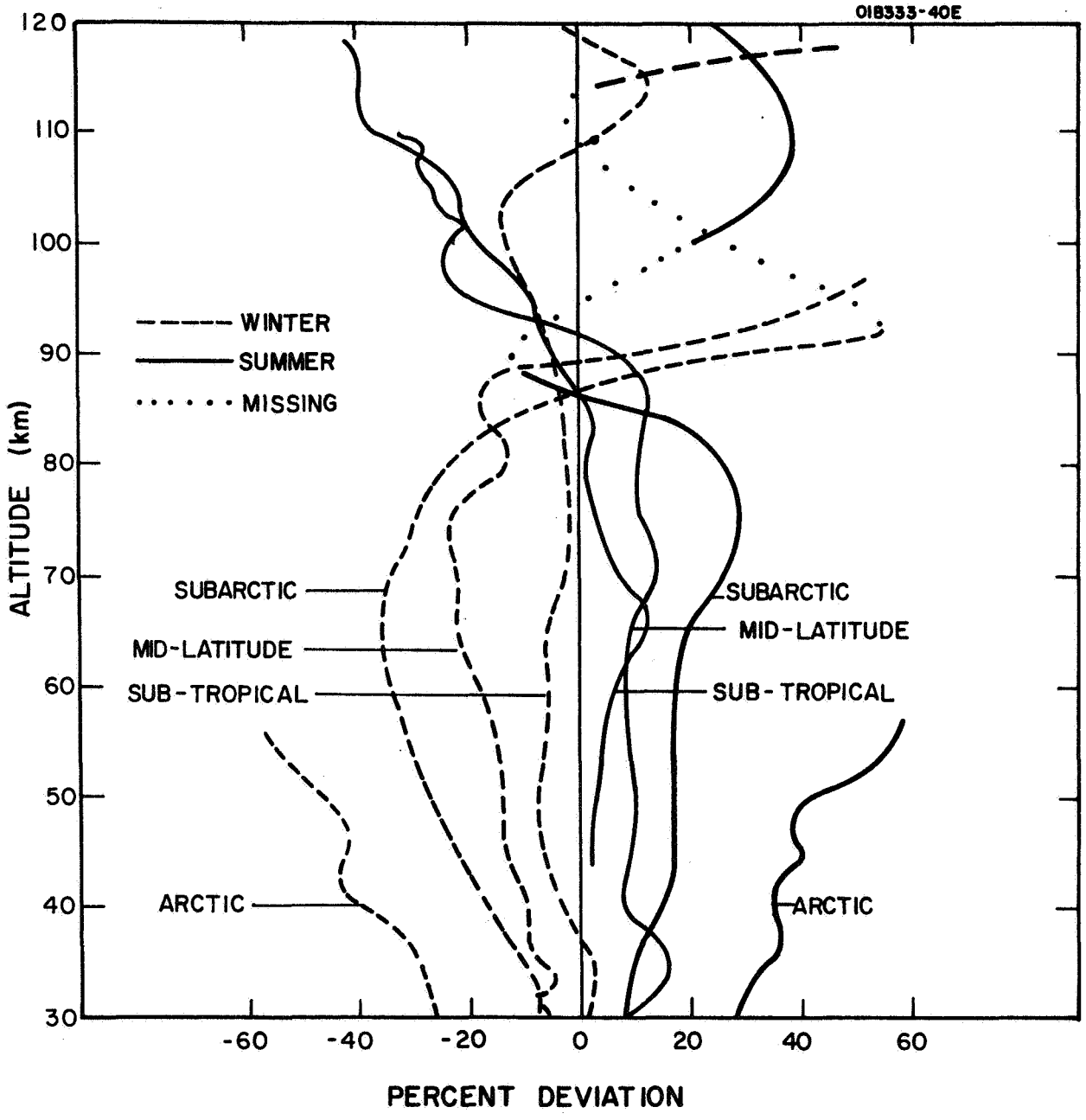

Figure 10. Winter diurnal mean to summer diurnal mean variability of density-altitude profiles for various latitudes shown as percent deviations of such profiles (for various combinations of season and latitude) from that of the mean atmosphere.

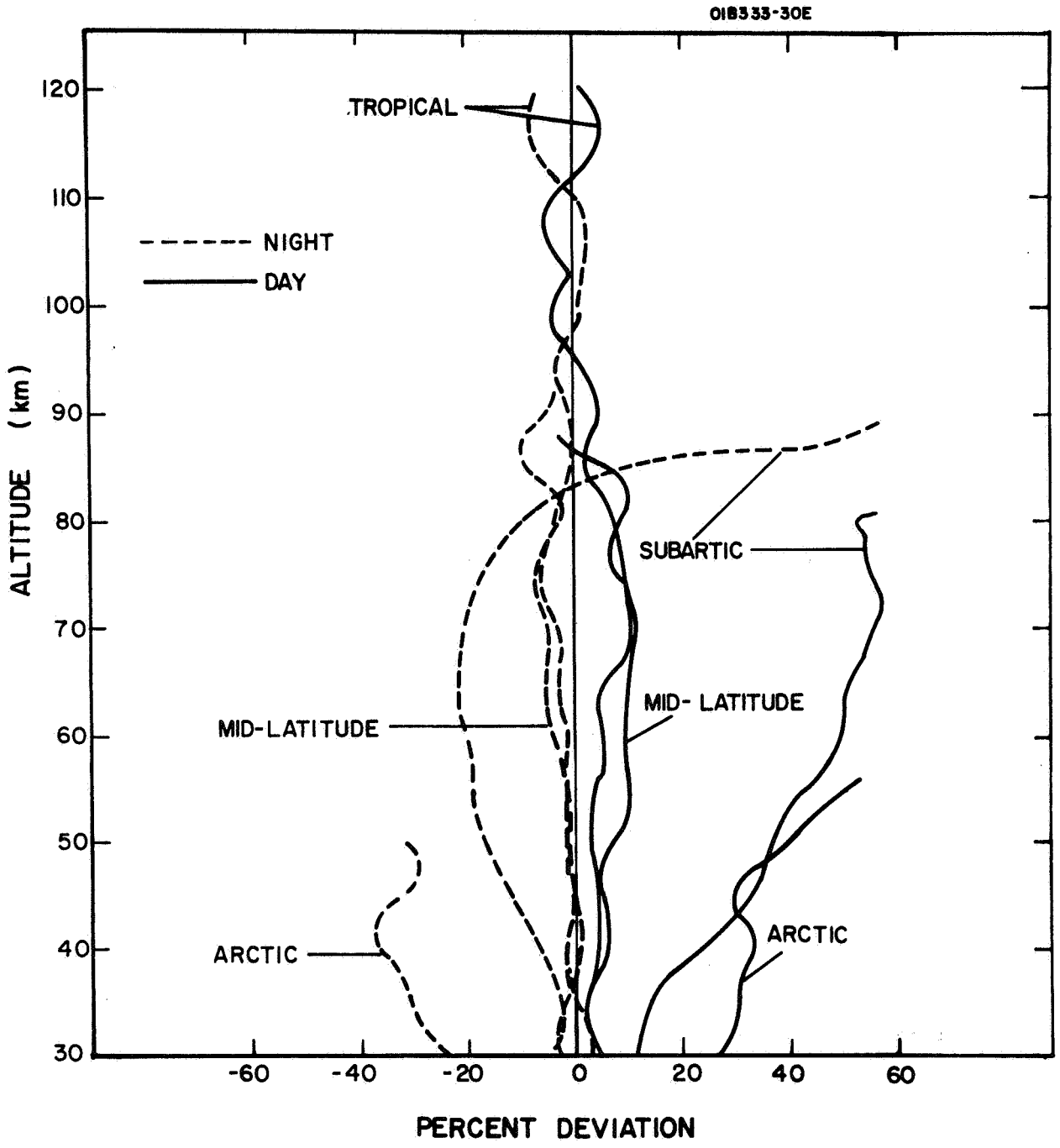

Figure 11. Annual mean day to annual mean night variability of density-altitude profiles for various latitudes shwon as percent deviations of such profiles (for various combinations of time of day and season) from that of the mean atmosphere.

graph to reduce the confusion. This graph also shows the seasonal dependence of the mesospheric density to vary strongly with latitude with variations of at least ±60 percent from the mean for the arctic decreasing to about ±5 percent from the mean for the subtropic. Above the mesopause the picture is confused, with subarctic winter and summer graphs crossing at 102 and at 117 km. The simple tulip-shaped seasonal-latitudinal model suggested in the 1966 U.S. Supplement to the Standard Atmosphere [25] is not substantiated by these curves.

It should be noted that while each of the curves of this figure represent data from any time of day and hence comprise a kind of diurnal mean sample, the arctic curves are far from representing such a mean. In accordance with the definitions of day, night, and transition period used in this study, almost no summer nighttime data exist for the arctic. Similarly almost no winter daytime data exist for the arctic, thus the two arctic curves really show the difference essentially between winter nighttime and summer daytime data.

The second composite figure depicts the variation between annual mean daytime and annual mean nighttime density altitude profiles for various latitudes. A first isopycnic layer near 10 km altitude is strongly suggested by a downward extension of the two arctic curves. Again the mesospheric density variability is greatest for the arctic region and becomes smaller with decreasing latitude to the mid-latitude region at which point no further decrease in variation is seen. A minimum variation of about ±7 percent from the mean is observed for the tropics. In this figure the subtropical curves were omitted to reduce the confusion.

The large diurnal variations shown for subarctic and arctic curves are somewhat misleading for reasons discussed above. While these curves in principle represent annual mean data, the arctic night data are almost entirely for summer. This situation also prevails but to a lesser extent for the subarctic data. Thus while the small diurnal variations of density shown for the lower latitudes are truly a diurnal effect, the larger values at higher latitudes are based with a seasonal influence.

The two composite figures would undoubtedly show improved results with larger sample size, a normalization for the influence solar flux, and an improved smoothing function.

REFERENCES

1. Jacchia, L.G., 1963: "Solar Effects on the Acceleration of Artificial Satellites", Smithsonian Contributions to Astrophysics, Research in Space Science, 6.

2. Jacchia, L.G., 1960: "A Variable Atmospheric Density Model from Satellite Accelerations", Smithsonian Astrophys. Obs., Special Report 39.

3. Minzner, R.A., and W.S. Ripley, 1956: "The ARDC Model Atmosphere, 1956", Air Force Surveys in Geophysics No. 86, AFCRC IN-56-204.

4. Minzner, R.A., G.O. Sauermann, and G.A. Faucher, 1965: "Low Mesopause Temperatures over Eglin Test Range Deduced from Density Data," GCA Tech. Rpt. 65-1-N, Contract NASW-976. Also J. Geophys. Res., 70(3), 739-742 (1965).

5. Diehl, W.S., 1925: "Standard Atmosphere Tables and Data," NACA Rpt. 218 (Reprinted 1948).

6. Minzner, R.A., W. S. Ripley, and T.P. Condron, 1958: "U.S. Extension to the ICAO Standard Atmosphere," U.S. Government Printing Office, Washington, D.C.

7. Minzner, R.A., K.S. Champion, and H.L. Pond, 1959: "The ARDC Model Atmosphere, 1959," Air Force Surveys in Geophys., No. 115, AFCRC-TR-59-267.

8. "U.S. Standard Atmosphere, 1962", National Aeronautics and Space Administration, U.S. Air Force, and U.S. Weather Bureau, Government Printing Office, Washington, D.C..

9. Minzner, R.A., 1964: "Pressure and Density Scale Heights Defining Atmospheric Models," GCA Tech. Rpt. 64-6-A, AFCRL 64-450, Sci. Rpt. No. 5, Contract AF19(628)-1633.

10. Minzner, R.A., 1965: "Critical Examination of Equations for Atmospheric Number-Density Calculations - Computed Values Compared with Observations." GCA Tech Rpt. 65-27-N, Contract NASW-1225(Submitted to J. Geophys. Res.).

11. Nicolet, M., 1963: "Density of the Heterosphere Related to Temperature," Smithsonian Astrophys. Obs., Spec. Rpt. 75, 30pp., Republished in Smithsonian Contributions to Astrophys., Vol. 6, 175-187.

12. Meteorological Rocket Network Committee, Editors, 1962-1966:"Data Report of the Meteorological Rocket Network Firings"Document 109-62.

REFERENCES (Cont.)

13. Minzner, R.A., and G.O. Sauermann, 1966: "Temperature Determination of Planetary Atmospheres - Optimum Boundary Conditions for Both Low and High Solar Activity - Equation Analysis and Error Analysis,"GCA Tech. Rpt. 66-6-N, Contract NASW-1225.

14. Minzner, R.A., P. Morgenstern, and S. Mello, 1967: "Tabulations of Atmospheric Density, Temperature, and Pressure for 437 Rocket and Optical-Probe Soundings During the Period 1947 to Early 1965,"GCA Corp., Bedford, Mass., GCA-TR-67-10-N, Contracts NASW-1463 and NASW-1225.

15. Smith, R.S., 1965: Private Communication.

16. Smithsonian Astrophys. Observatory, "Listing of 10.7 Cm Solar Flux."

17. Brown, R. G., Smoothing, Forecasting and Predicting of Discrete Time Series, Prentice-Hall, 1963.

18. Jacchia, L. G., Slowey, J. W., and Campbell, I. G., "Semiannual Density Variations in the Upper Atmosphere, 1958 to 1966," Smithsonian Astrophysical Observatory Special Report 265, 15 Jan. 1968.

19. Jacchia, Luigi G., 1966: "Density Variations in the Heterosphere," Extrait des Annales de Geophysique tome 22, No. 1.

20. Jacchia, Luigi G., 1965: "Static Diffusion Models of the Upper Atmosphere with Empirical Temperature Profiles," Smithsonian Contributions to Astrophysics, Vol. 8 No. 9, pp 215-257.

21. Jacchia, Luigi G., 1964: "The Temperature Above the Thermopause," Smithsonian Astrophysical Observatory Special Report No. 150.

22. Jacchia, L. G., 1964: "The Temperature Above the Thermopause," Space Research V, Ed. P. Muller, North-Holland Publishing Company, Amsterdam, pp. 1152-1174.

23. David, F. M., 1954: Tables of the Correlation Coefficient, Issued by the Biomitrika Office, University College, London.

24. Cole, A. E., 1961: "Suggestion of a Second Isopycnic Level at 80 to 90 Kilometers over Churchill, Canada," J. Geophys. Res. 66, 2773-2778.

25. U. S. Standard Atmosphere Supplement 1966, Environmental Science Service Administration, National Aeronautics and Space Administration and U. S. Air Force, U. S. Government Printing Office, Washington, D.C.

APPENDIX A

ALTITUDE PROFILES OF THE CORRELATION COEFFICIENT BETWEEN SOLAR FLUX AND ATMOSPHERIC DENSITY

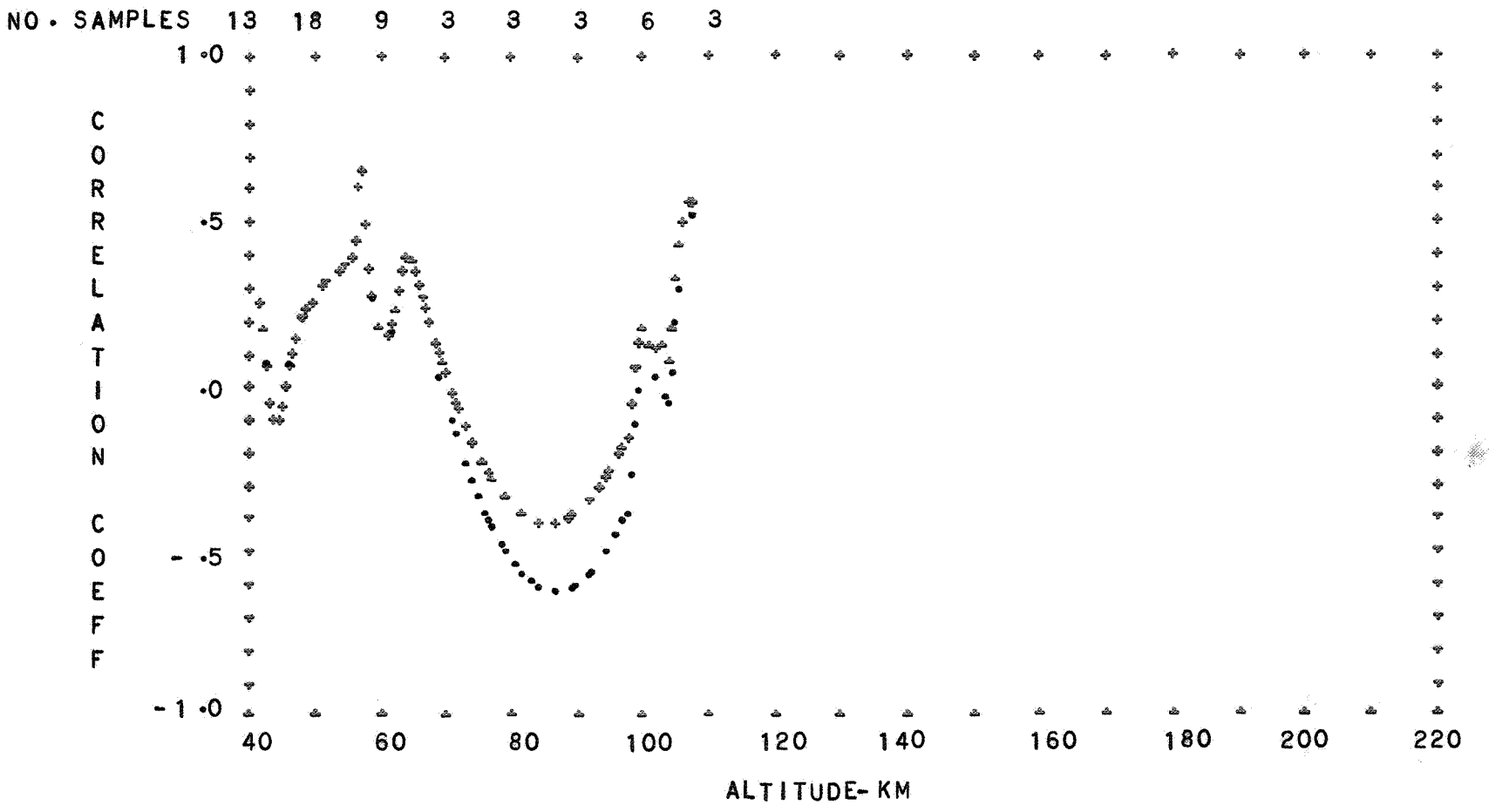

FIG. 1 CORRELATION OF DENSITY WITH SOLAR FLUX

TROPICAL SPRING DIURNAL MEAN

SAME DAY--CROSSES PRECEEDING DAY--DOTS

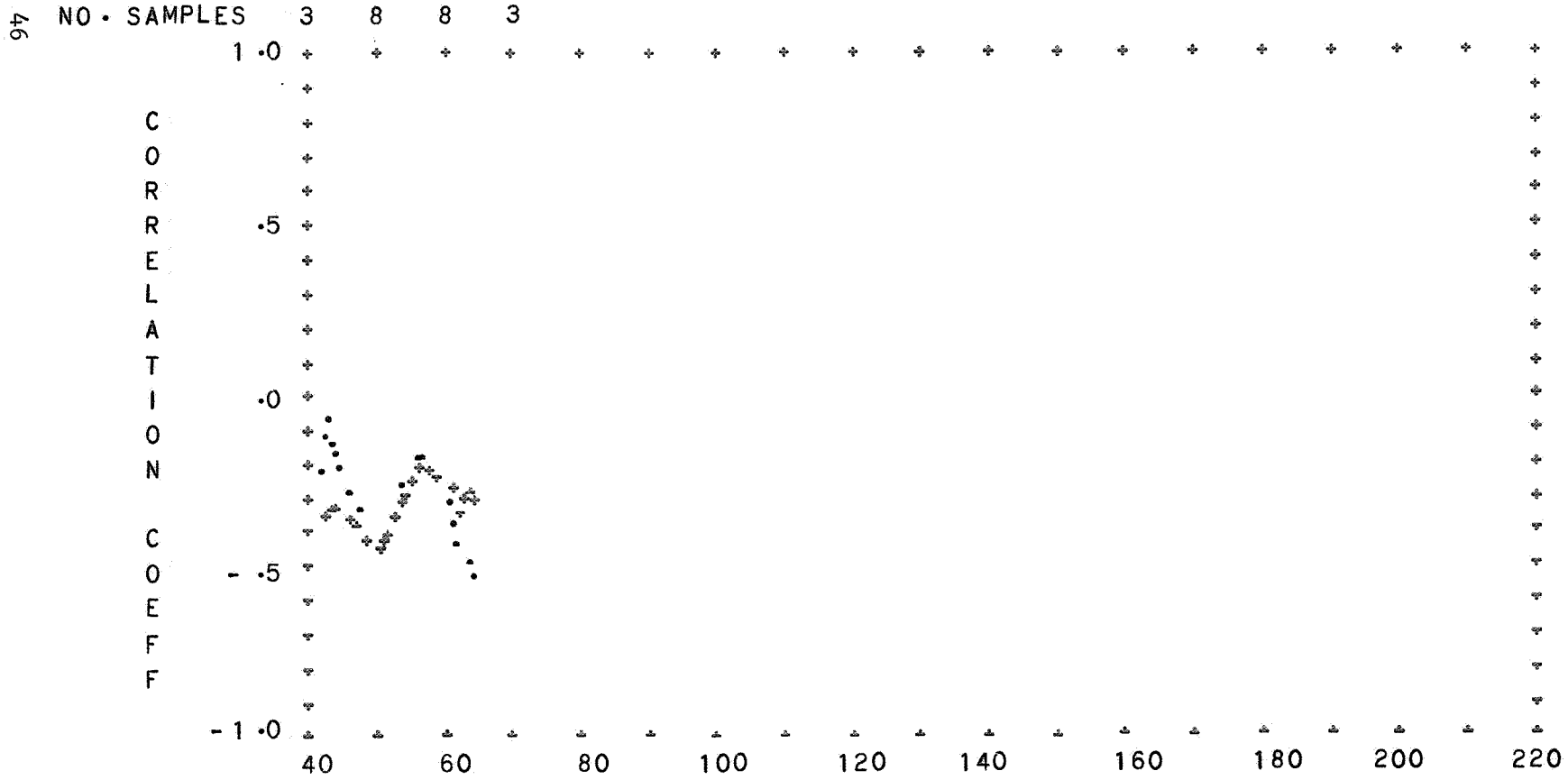

FIG. 2 CORRELATION OF DENSITY WITH SOLAR FLUX

TROPICAL WINTER HALF DIURNAL TRANSITION

SAME DAY--CROSSES PRECEEDING DAY--DOTS

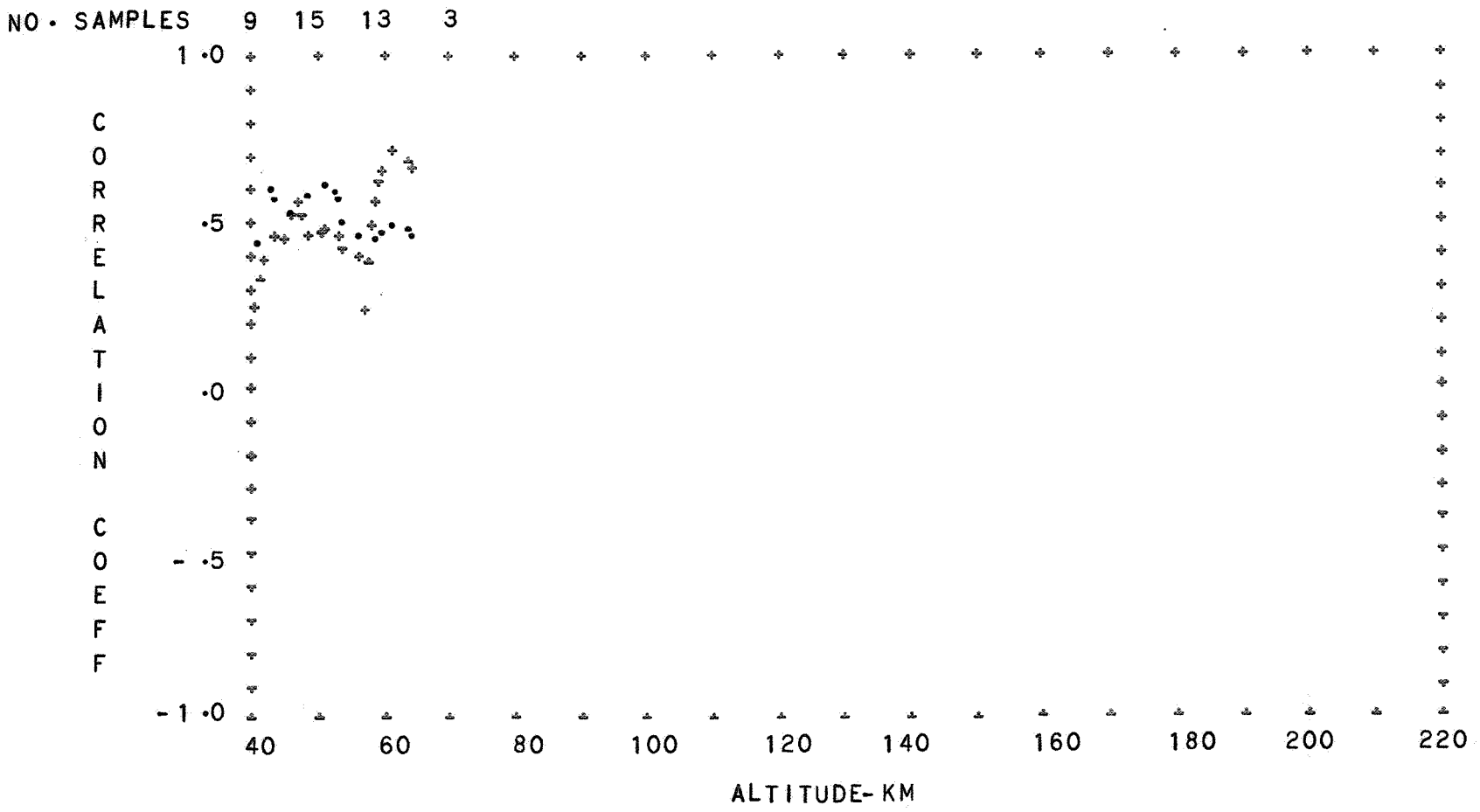

FIG. 3 CORRELATION OF DENSITY WITH SOLAR FLUX

TROPICAL WINTER HALF DAYTIME

SAME DAY--CROSSES PRECEEDING DAY--DOTS

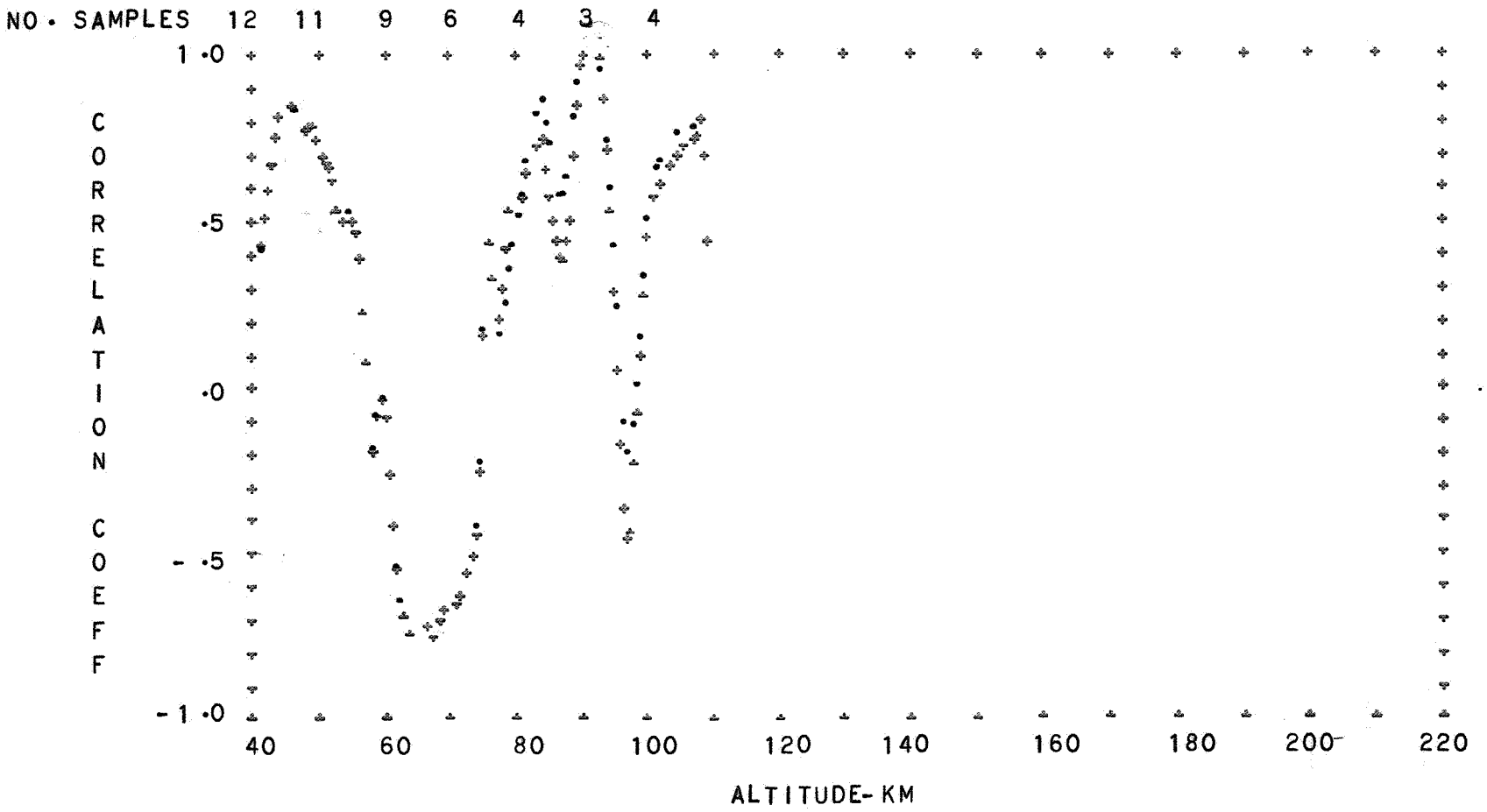

FIG. 4 CORRELATION OF DENSITY WITH SOLAR FLUX

TROPICAL WINTER HALF NIGHTTIME

SAME DAY--CROSSES PRECEEDING DAY--DOTS

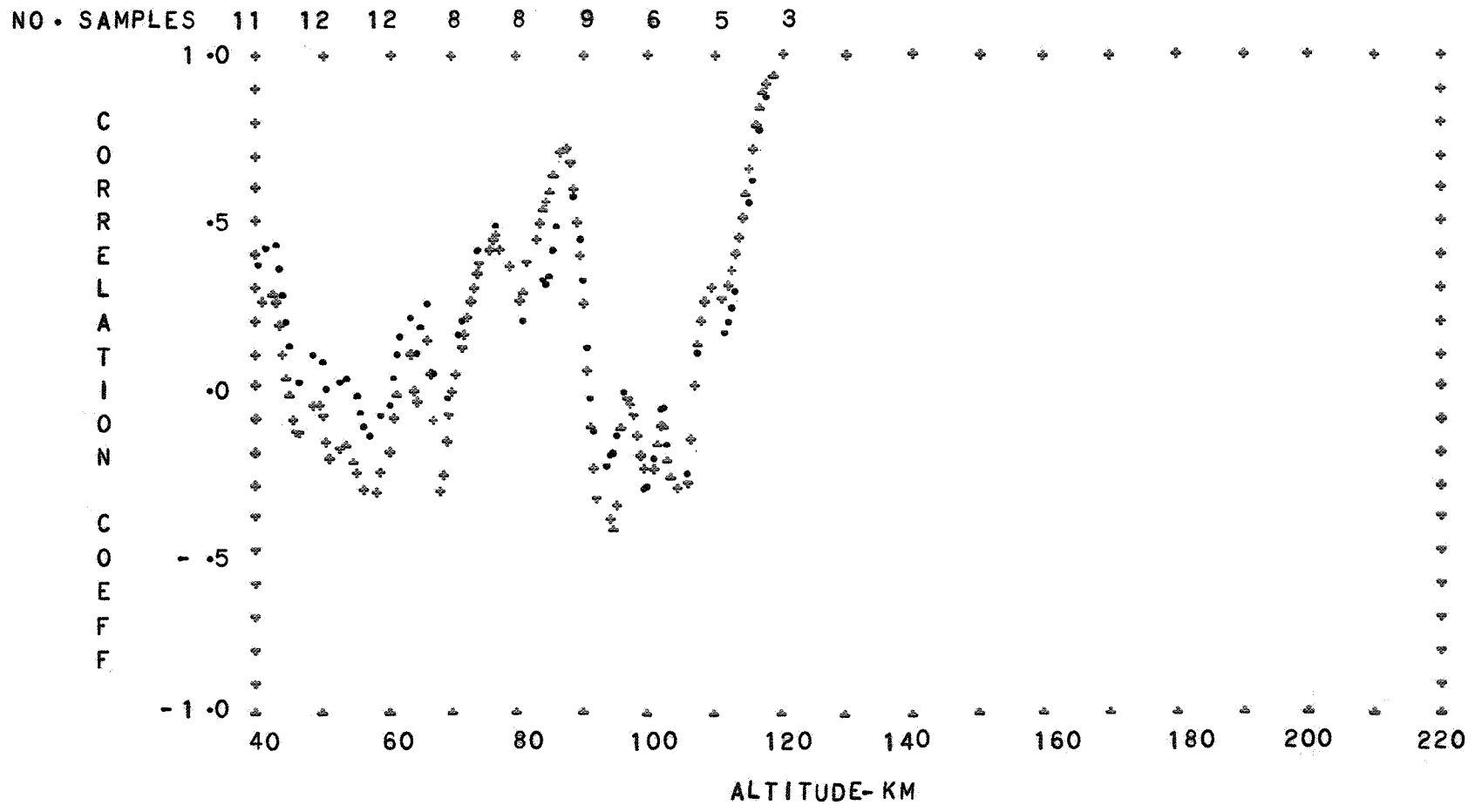

FIG. 5 CORRELATION OF DENSITY WITH SOLAR FLUX

TROPICAL SUMMER DIURNAL MEAN

SAME DAY--CROSSES PRECEEDING DAY--DOTS

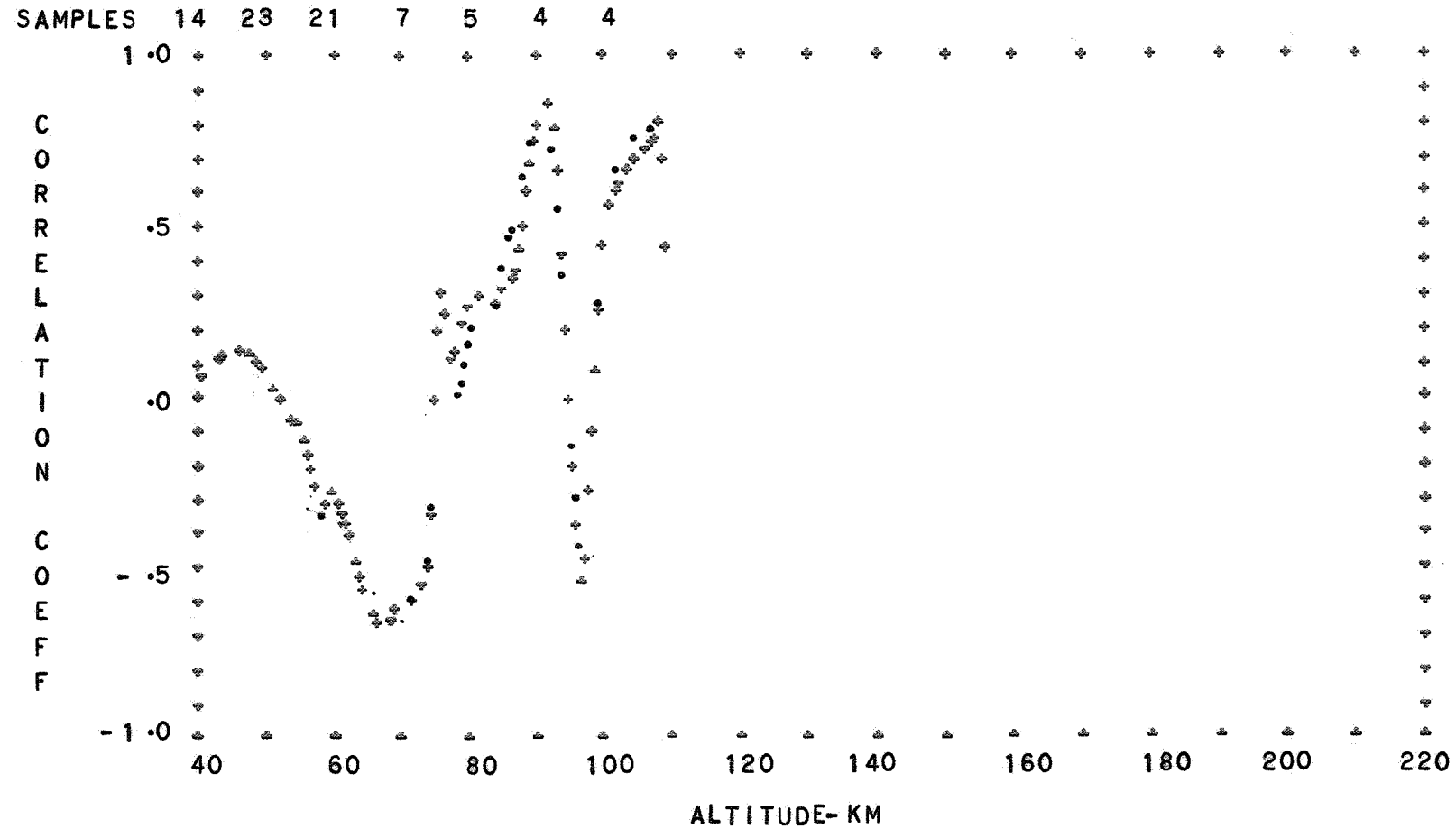

FIG. 6 CORRELATION OF DENSITY WITH SOLAR FLUX

TROPICAL AUTUMN DIURNAL MEAN

SAME DAY--CROSSES PRECEEDING DAY--DOTS

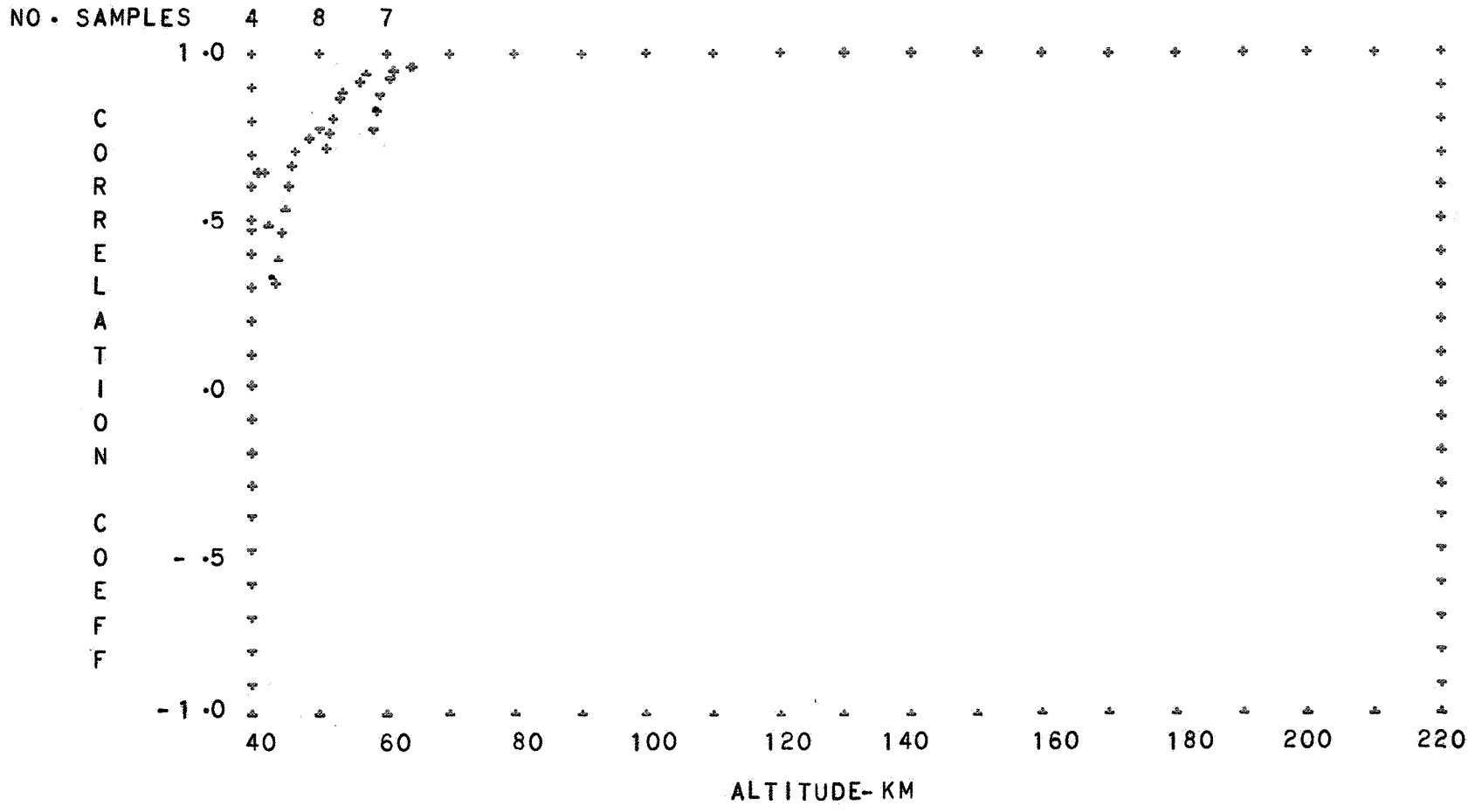

FIG. 7 CORRELATION OF DENSITY WITH SOLAR FLUX

TROPICAL SUMMER HALF DIURNAL TRANSITION

SAME DAY--CROSSES PRECEEDING DAY--DOTS

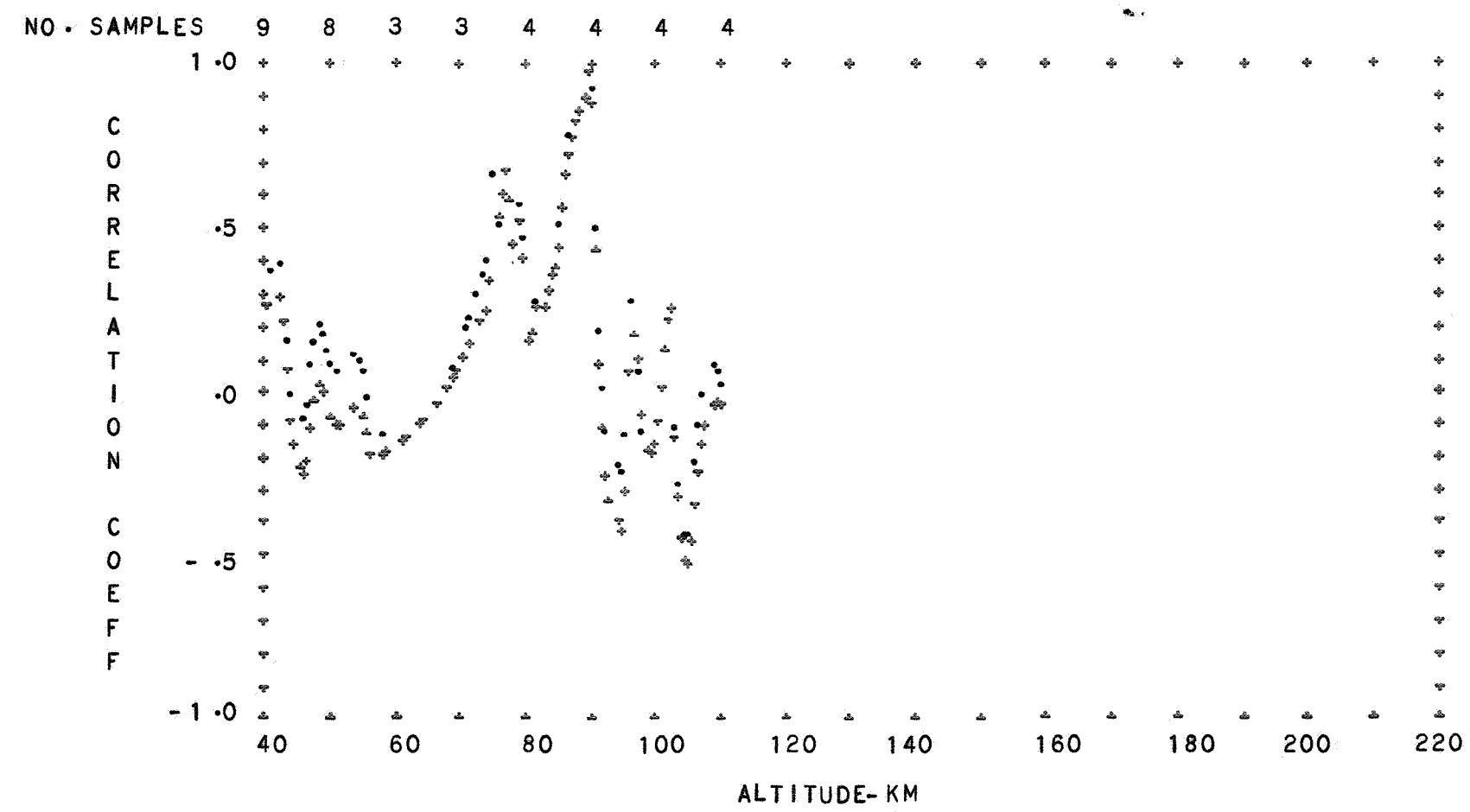

FIG. 8 CORRELATION OF DENSITY WITH SOLAR FLUX

TROPICAL SUMMER HALF DAYTIME

SAME DAY--CROSSES PRECEEDING DAY--DOTS

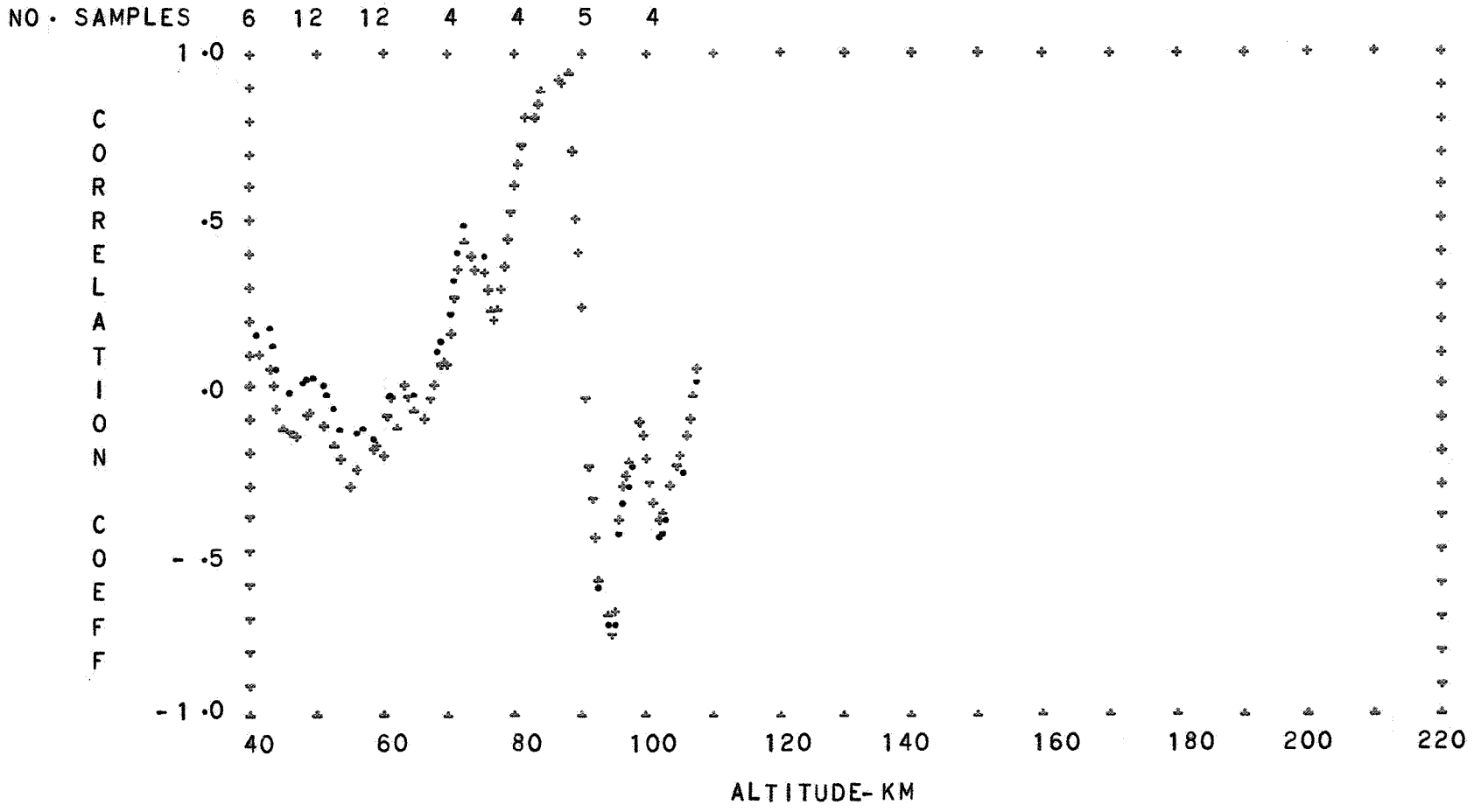

FIG. 9 CORRELATION OF DENSITY WITH SOLAR FLUX

TROPICAL SUMMER HALF NIGHTTIME

SAME DAY--CROSSES PRECEEDING DAY--DOTS

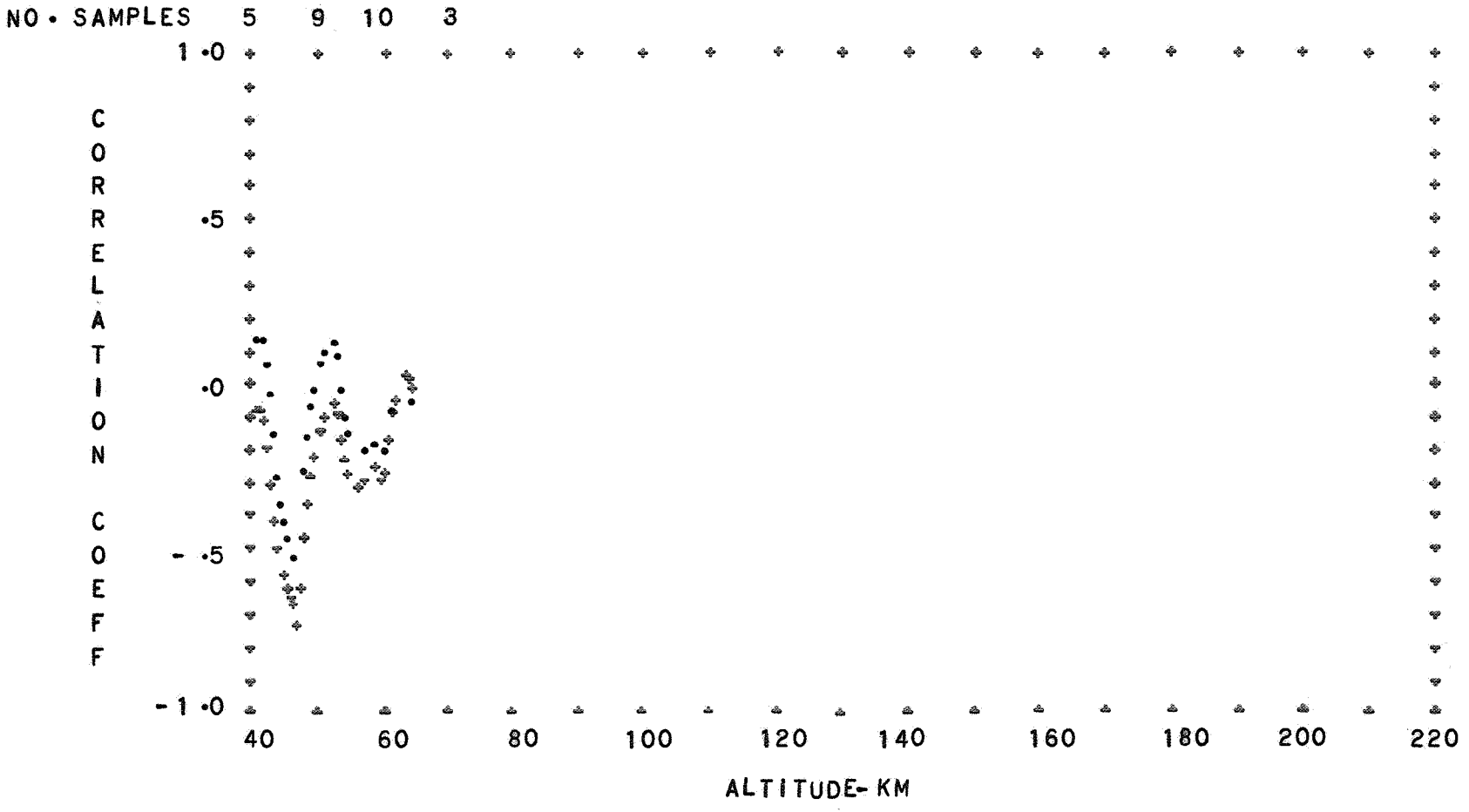

FIG. 10 CORRELATION OF DENSITY WITH SOLAR FLUX

TROPICAL WINTER DIURNAL MEAN

SAME DAY--CROSSES PRECEEDING DAY--DOTS

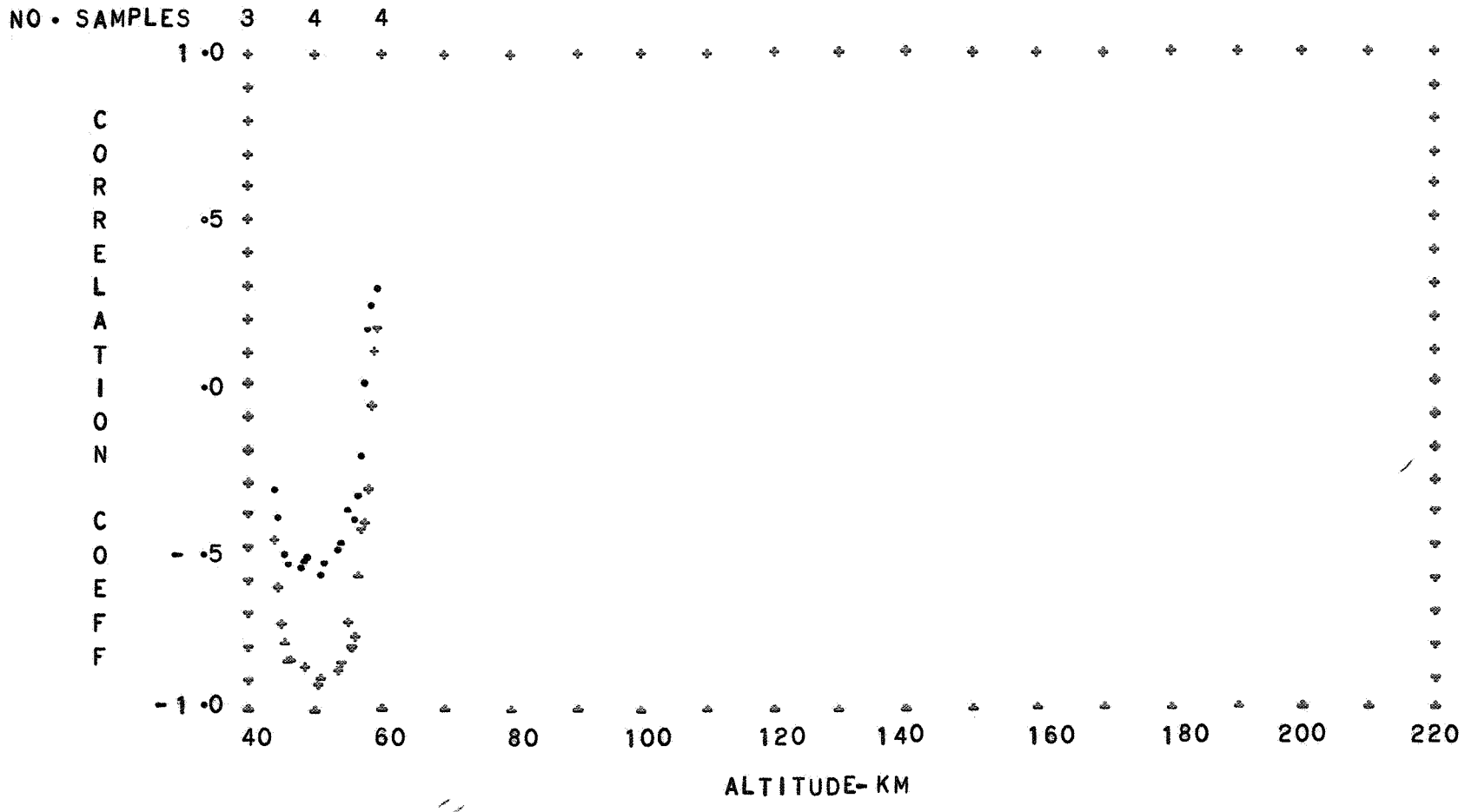

FIG. 11 CORRELATION OF DENSITY WITH SOLAR FLUX

TROPICAL SUMMER EXTREME DIURNAL MEAN

SAME DAY--CROSSES PRECEEDING DAY--DOTS

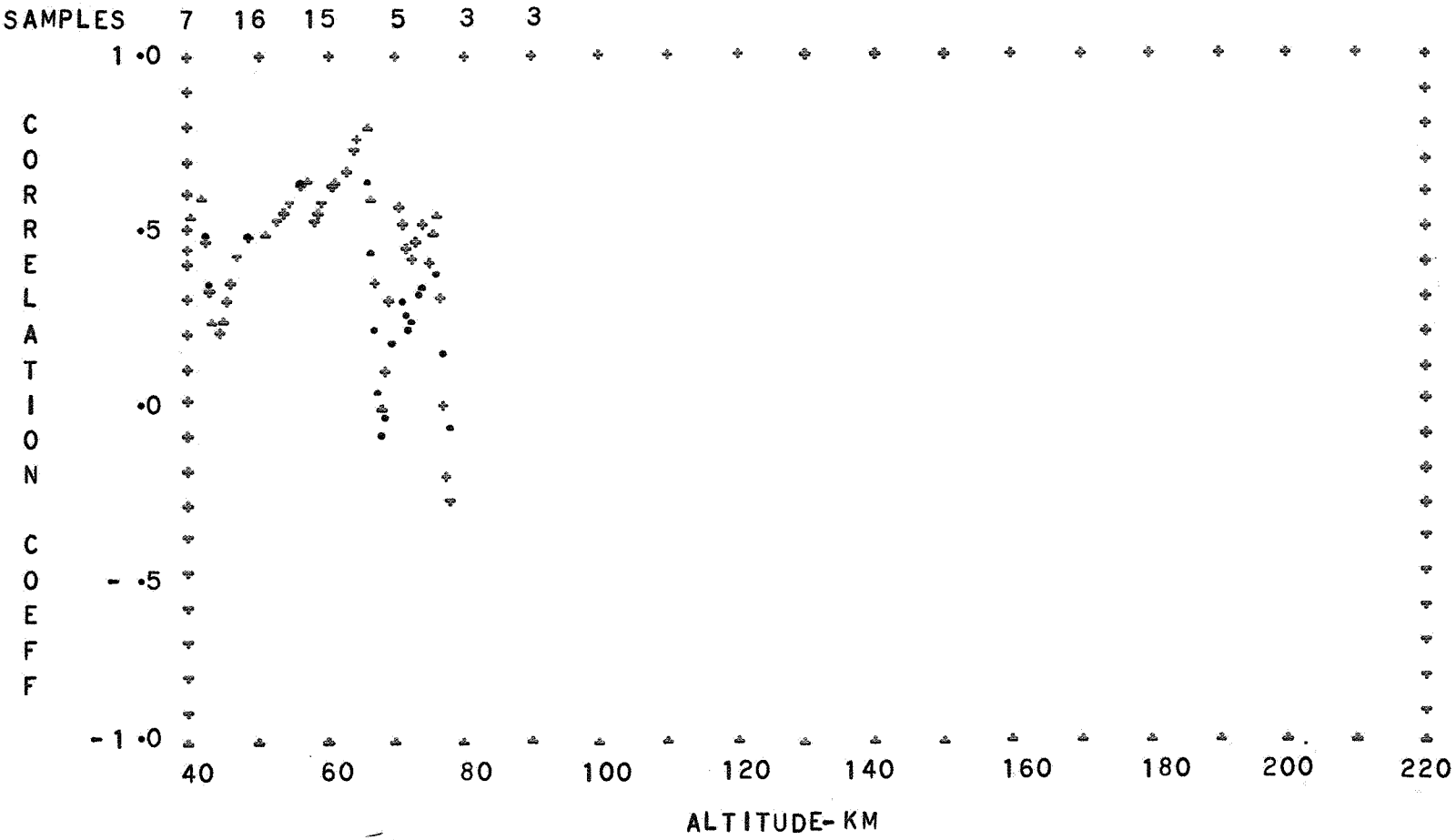

FIG. 12 CORRELATION OF DENSITY WITH SOLAR FLUX

TROPICAL ANNUAL MEAN DIURNAL TRANSITION

SAME DAY--CROSSES PRECEEDING DAY--DOTS

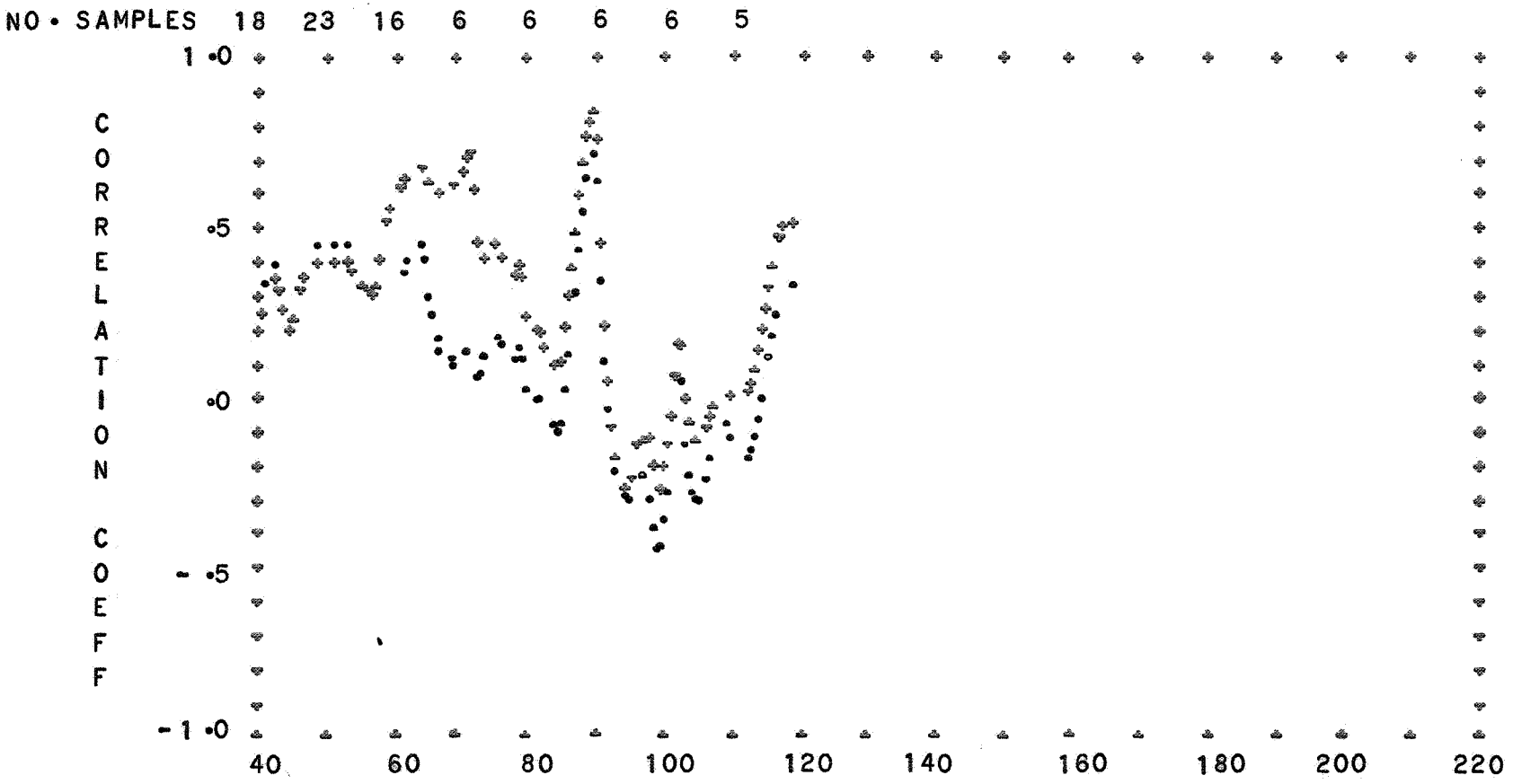

FIG. 13 CORRELATION OF DENSITY WITH SOLAR FLUX

TROPICAL ANNUAL MEAN DAYTIME

SAME DAY--CROSSES PRECEEDING DAY--DOTS

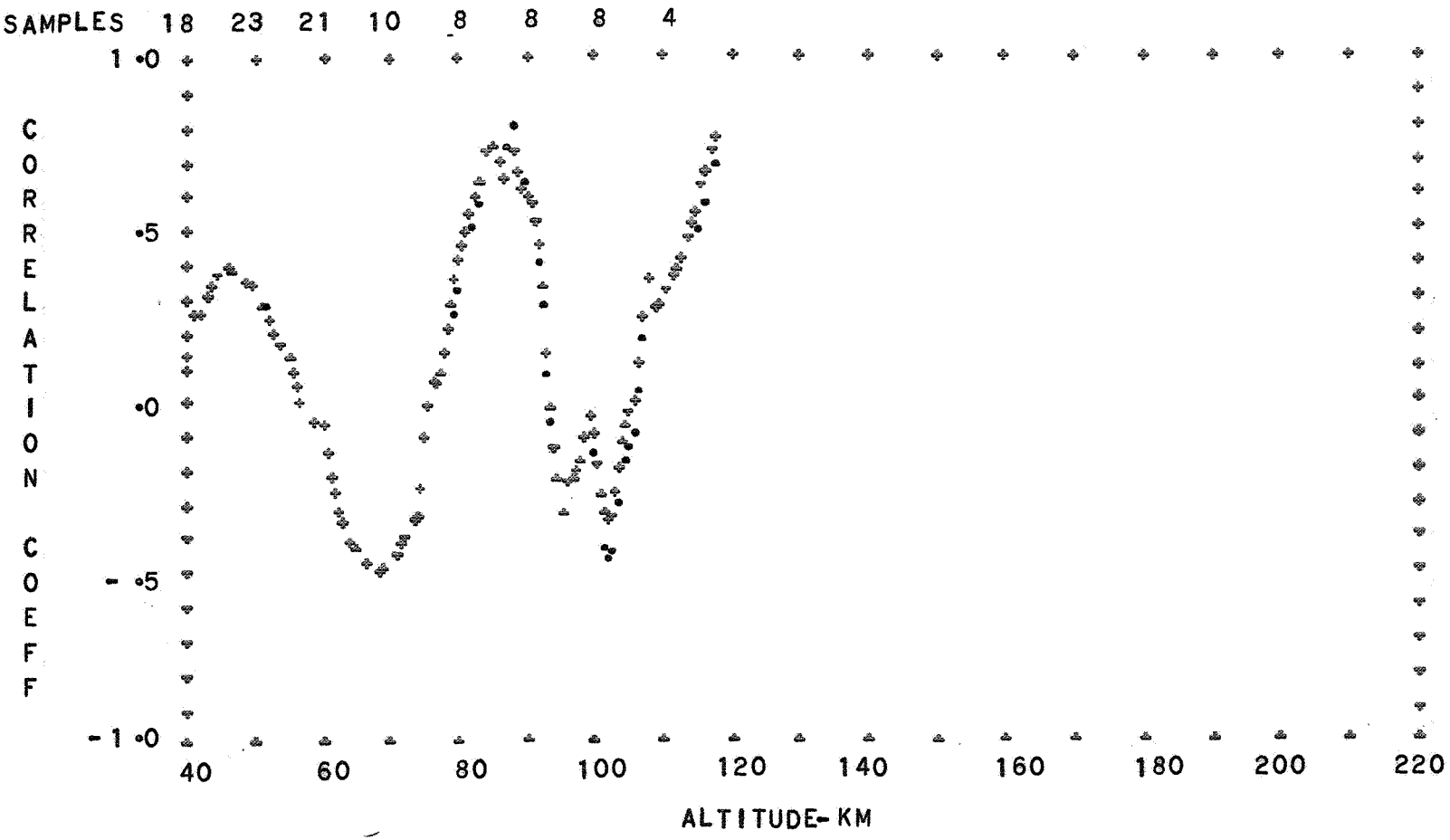

FIG. 14 CORRELATION OF DENSITY WITH SOLAR FLUX

TROPICAL ANNUAL MEAN NIGHTTIME

SAME DAY--CROSSES PRECEEDING DAY--DOTS

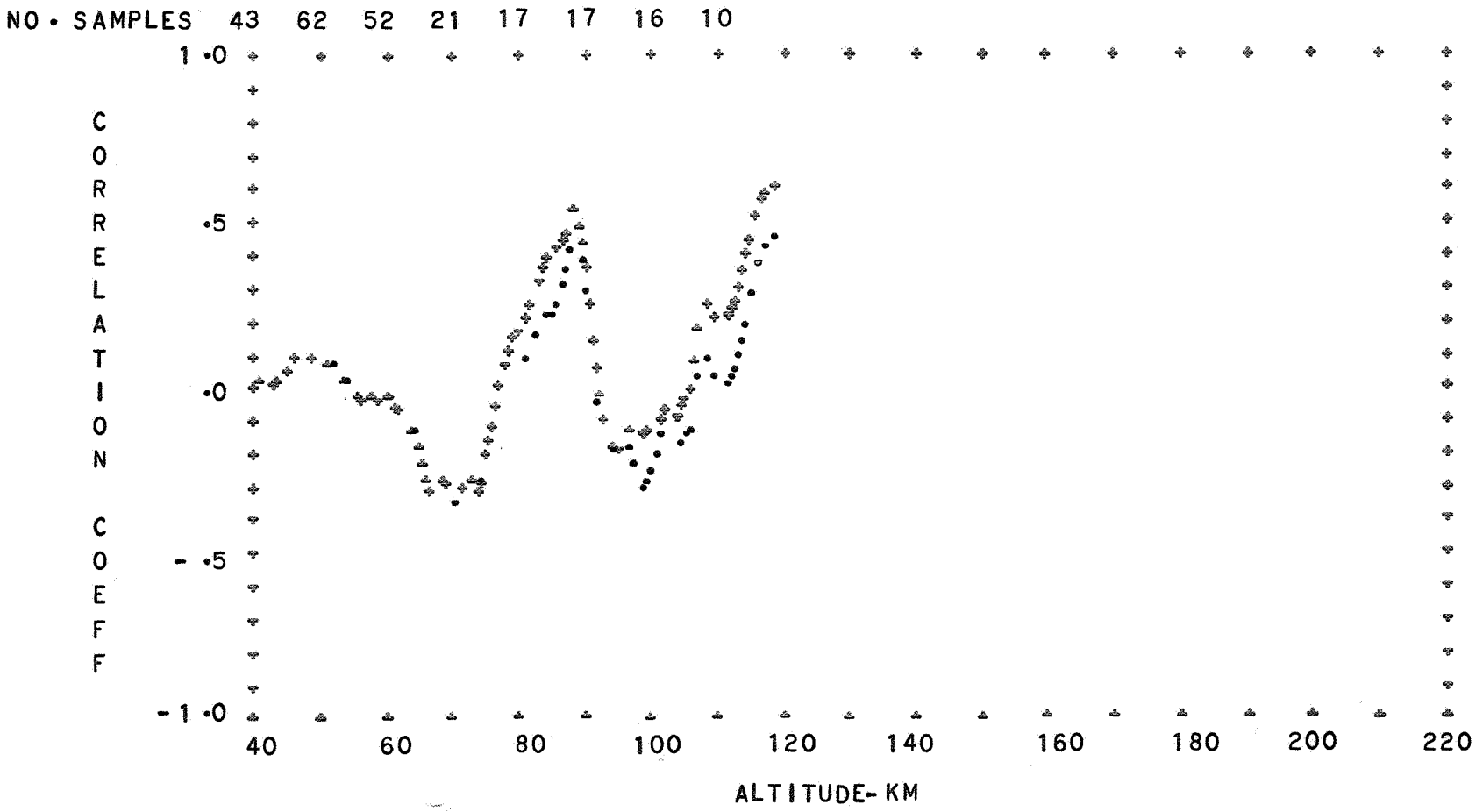

FIG. 15. CORRELATION OF DENSITY WITH SOLAR FLUX

TROPICAL ANNUAL MEAN DIURNAL MEAN

SAME DAY--CROSSES PRECEEDING DAY--DOTS

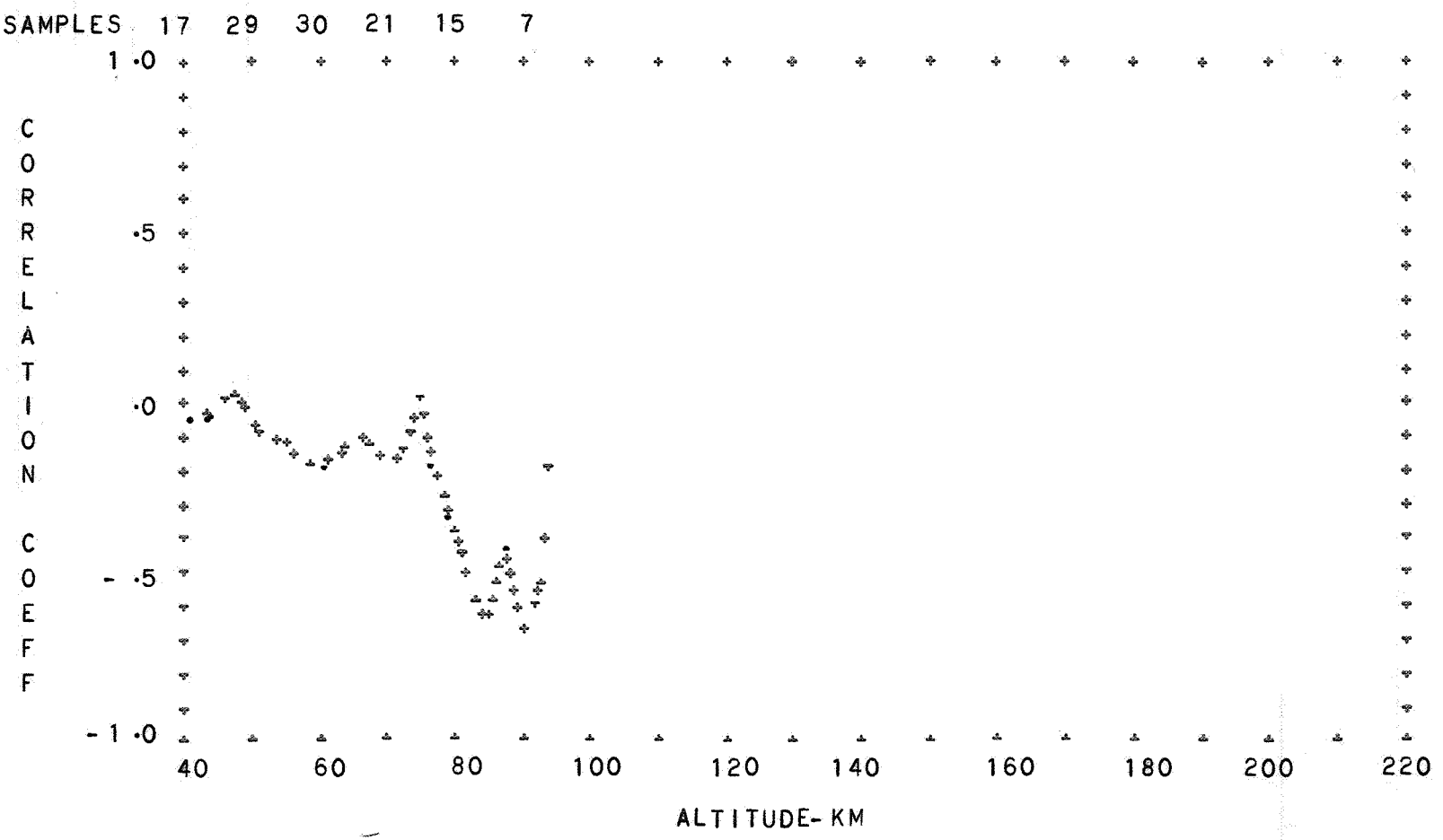

FIG. 16 CORRELATION OF DENSITY WITH SOLAR FLUX

SUBTROPICAL-MIDLATITUDE SPRING DIURNAL TRANSITION

SAME DAY--CROSSES PRECEEDING DAY--DOTS

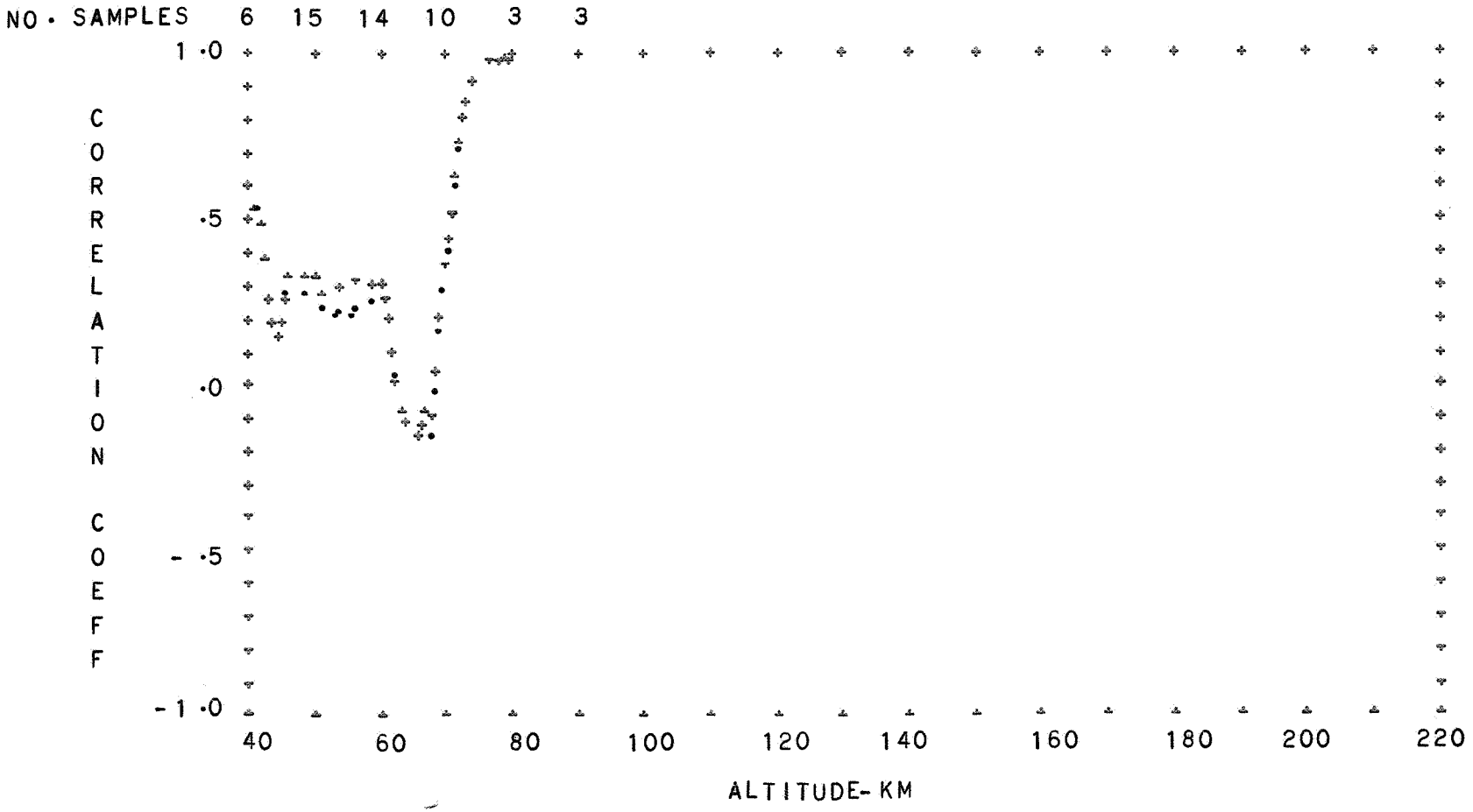

FIG. 17. CORRELATION OF DENSITY WITH SOLAR FLUX

SUBTROPICAL-MIDLATITUDE SPRING DAYTIME

SAME DAY--CROSSES PRECEEDING DAY--DOTS

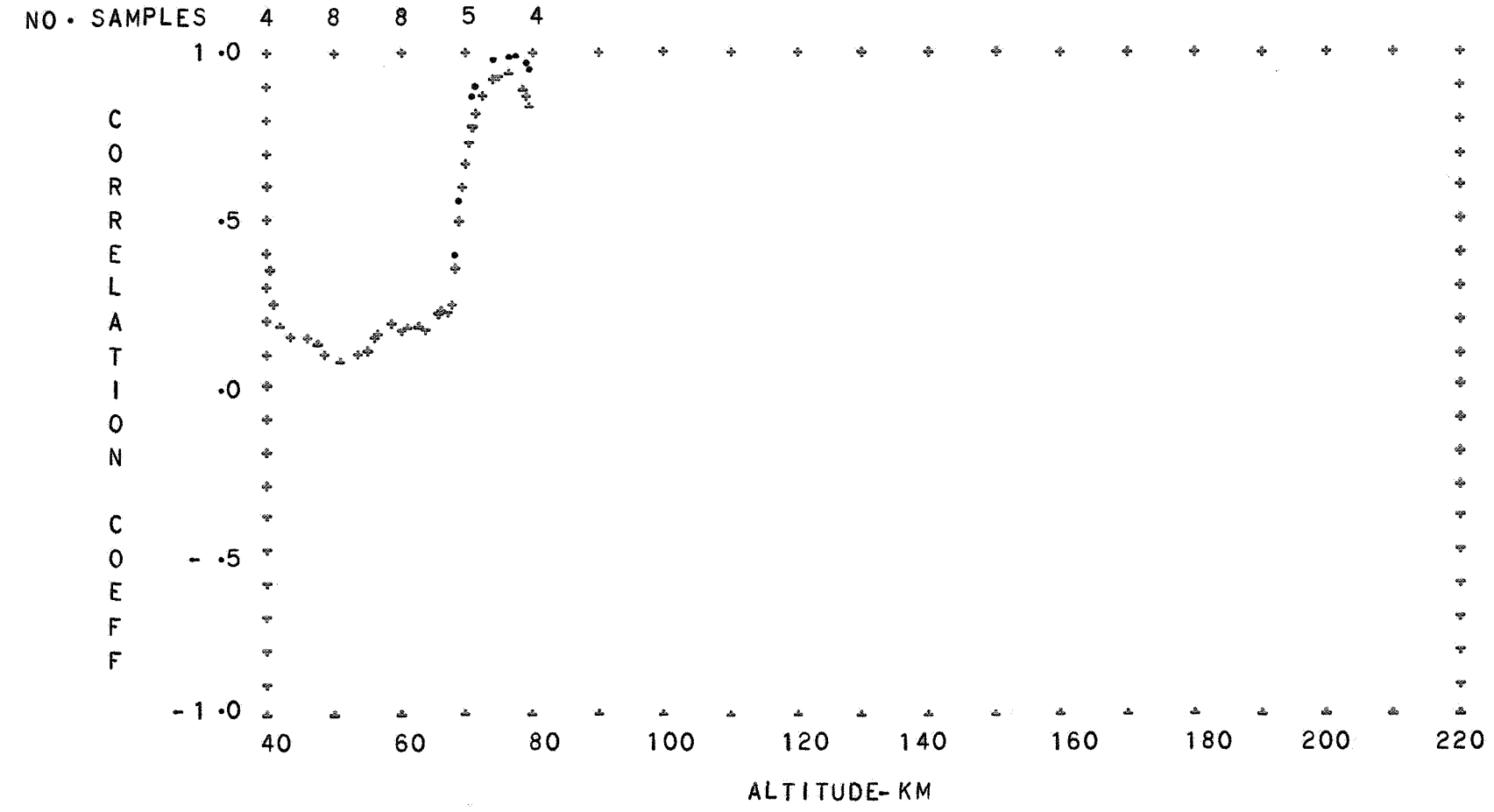

FIG. 18. CORRELATION OF DENSITY WITH SOLAR FLUX

SUBTROPICAL-MIDLATITUDE SPRING NIGHTTIME

SAME DAY--CROSSES PRECEEDING DAY--DOTS

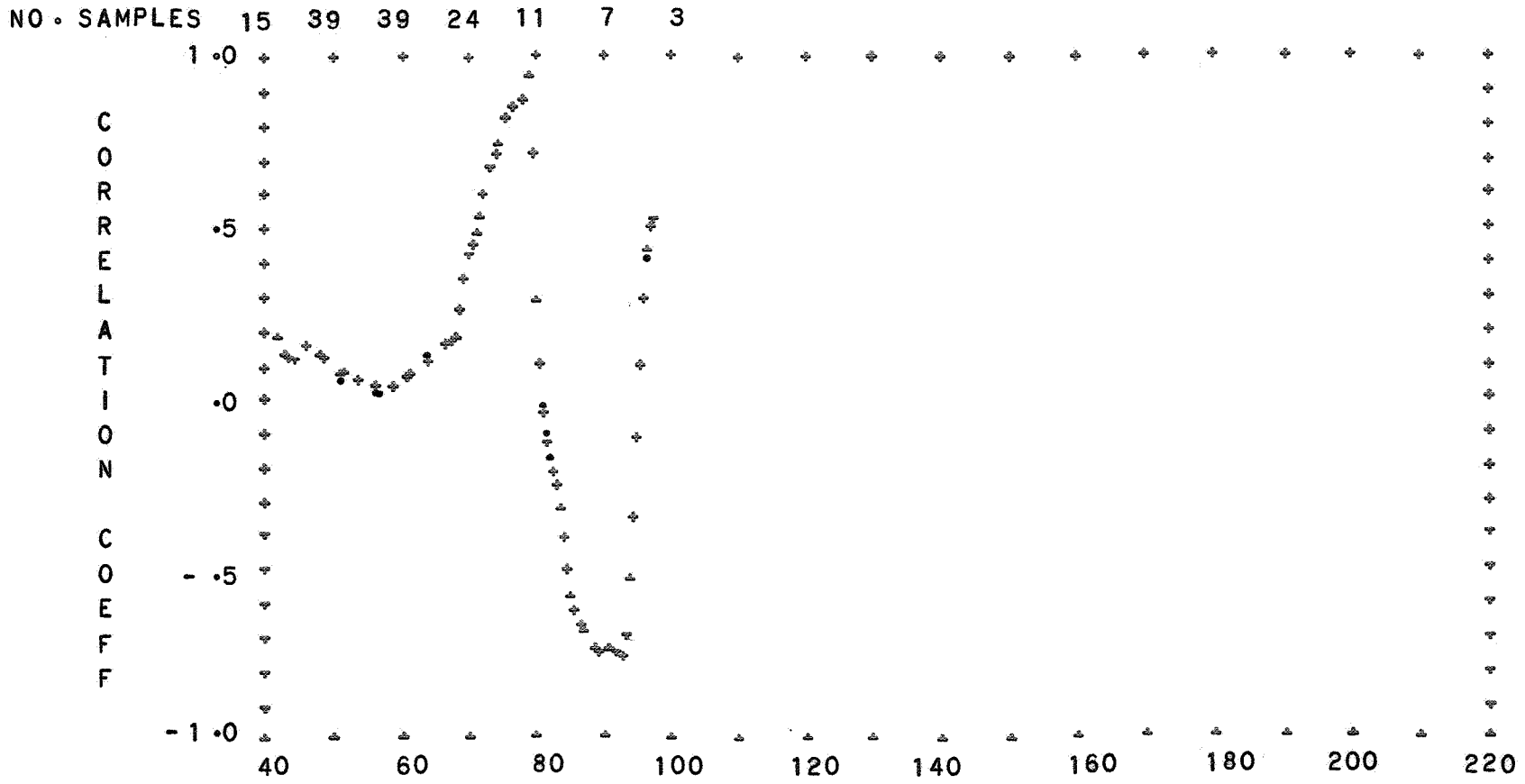

FIG. 19 CORRELATION OF DENSITY WITH SOLAR FLUX

SUBTROPICAL SPRING DIURNAL MEAN

SAME DAY--CROSSES PRECEEDING DAY--DOTS

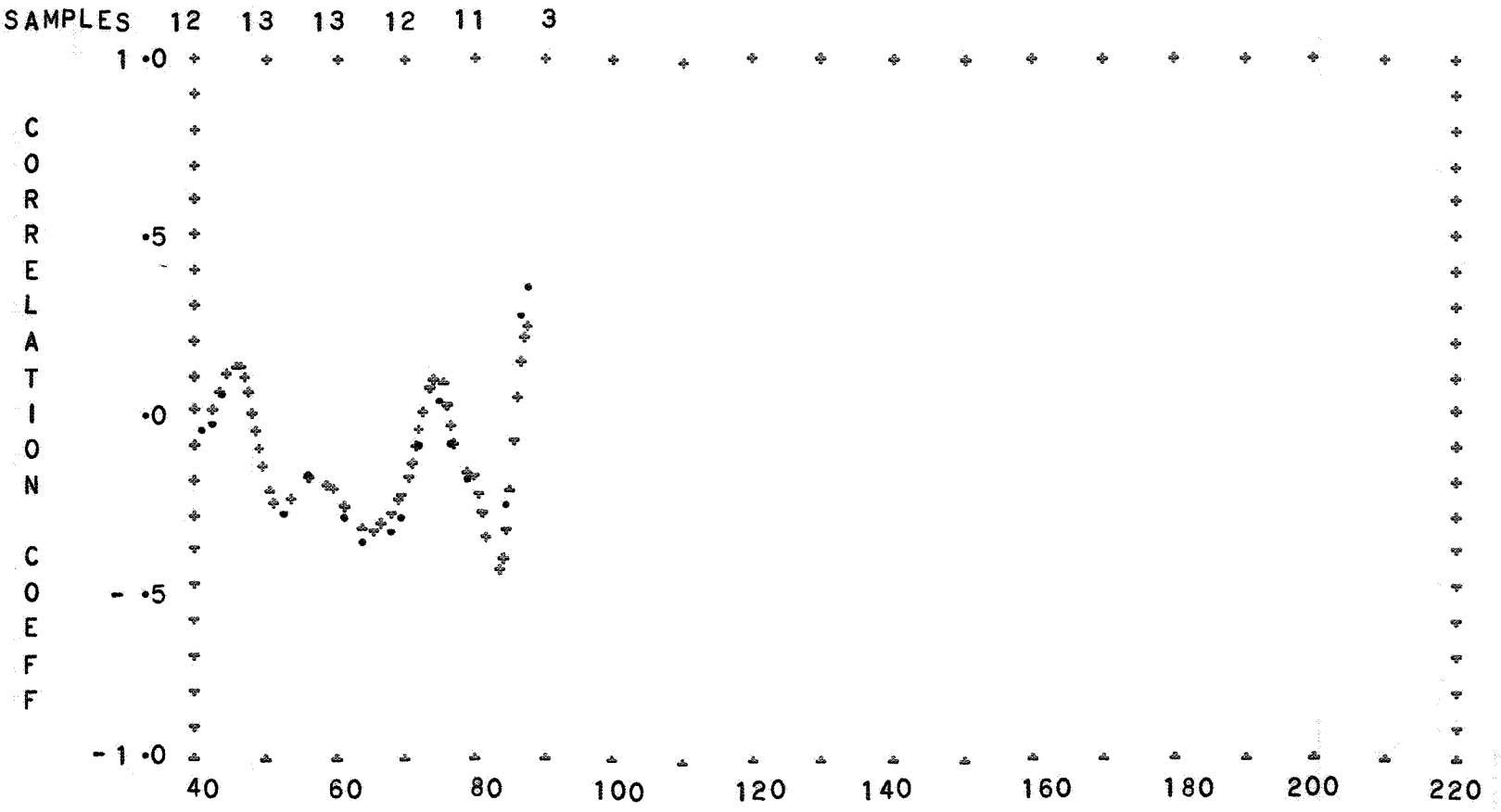

FIG. 20 CORRELATION OF DENSITY WITH SOLAR FLUX

MIDLATITUDE SPRING DIURNAL MEAN

SAME DAY--CROSSES PRECEEDING DAY--DOTS

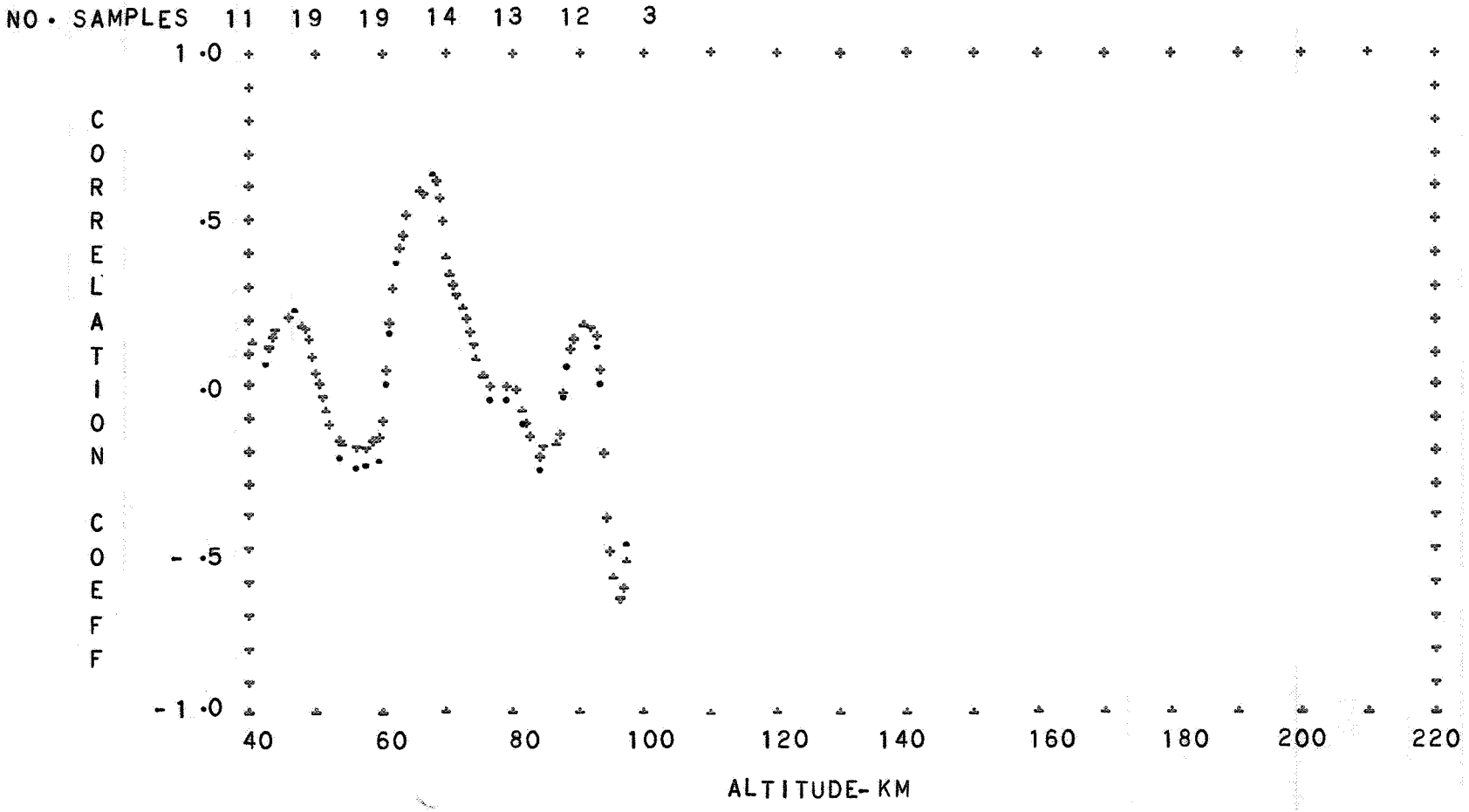

FIG. 21. CORRELATION OF DENSITY WITH SOLAR FLUX

SUBTROPICAL-MIDLATITUDE SUMMER DIURNAL TRANSITION

SAME DAY--CROSSES PRECEEDING DAY--DOTS

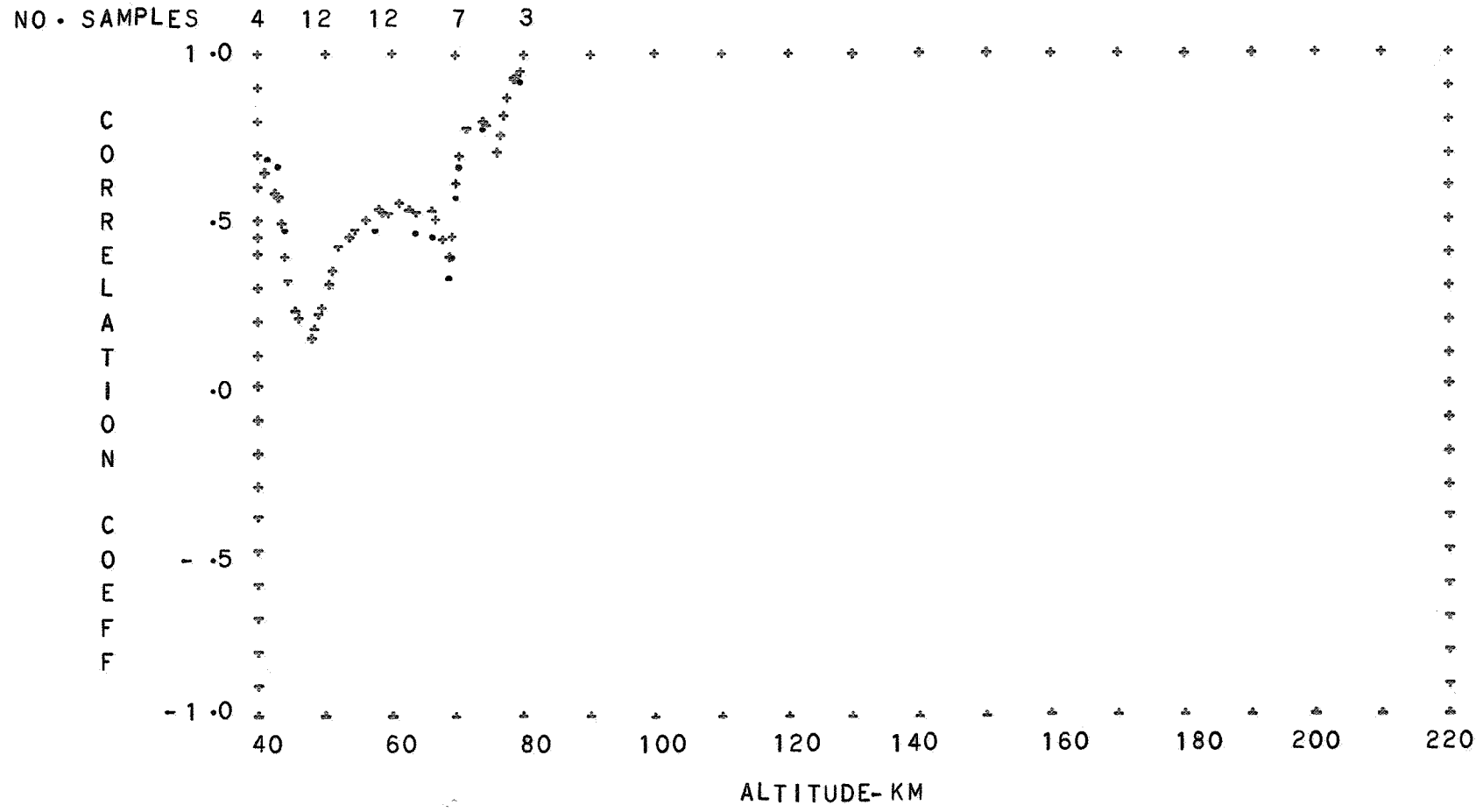

FIG. 22. CORRELATION OF DENSITY WITH SOLAR FLUX

SUBTROPICAL-MIDLATITUDE SUMMER DAYTIME

SAME DAY--CROSSES PRECEEDING DAY--DOTS

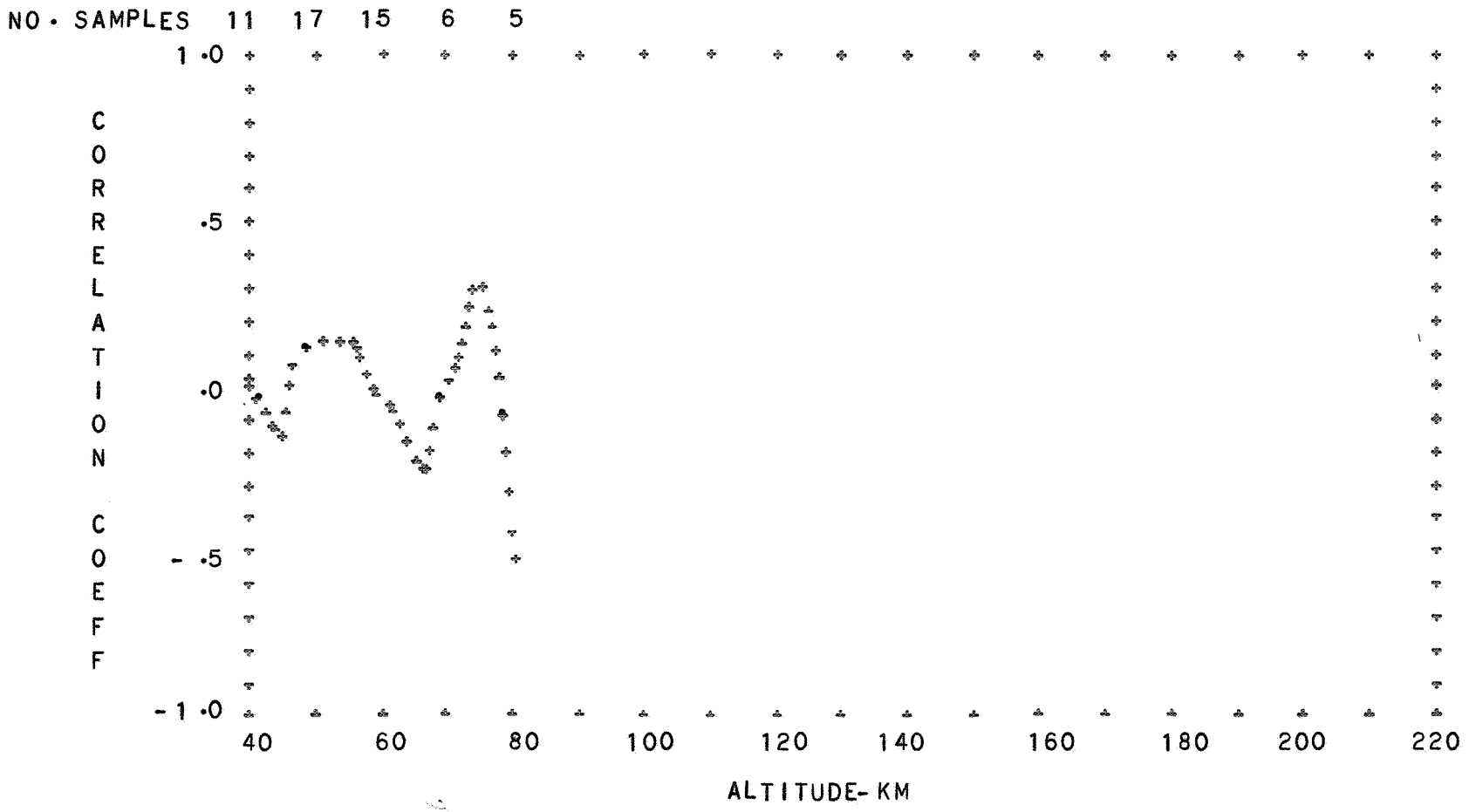

FIG. 23. CORRELATION OF DENSITY WITH SOLAR FLUX

SUBTROPICAL-MIDLATITUDE SUMMER NIGHTTIME

SAME DAY--CROSSES PRECEEDING DAY--DOTS

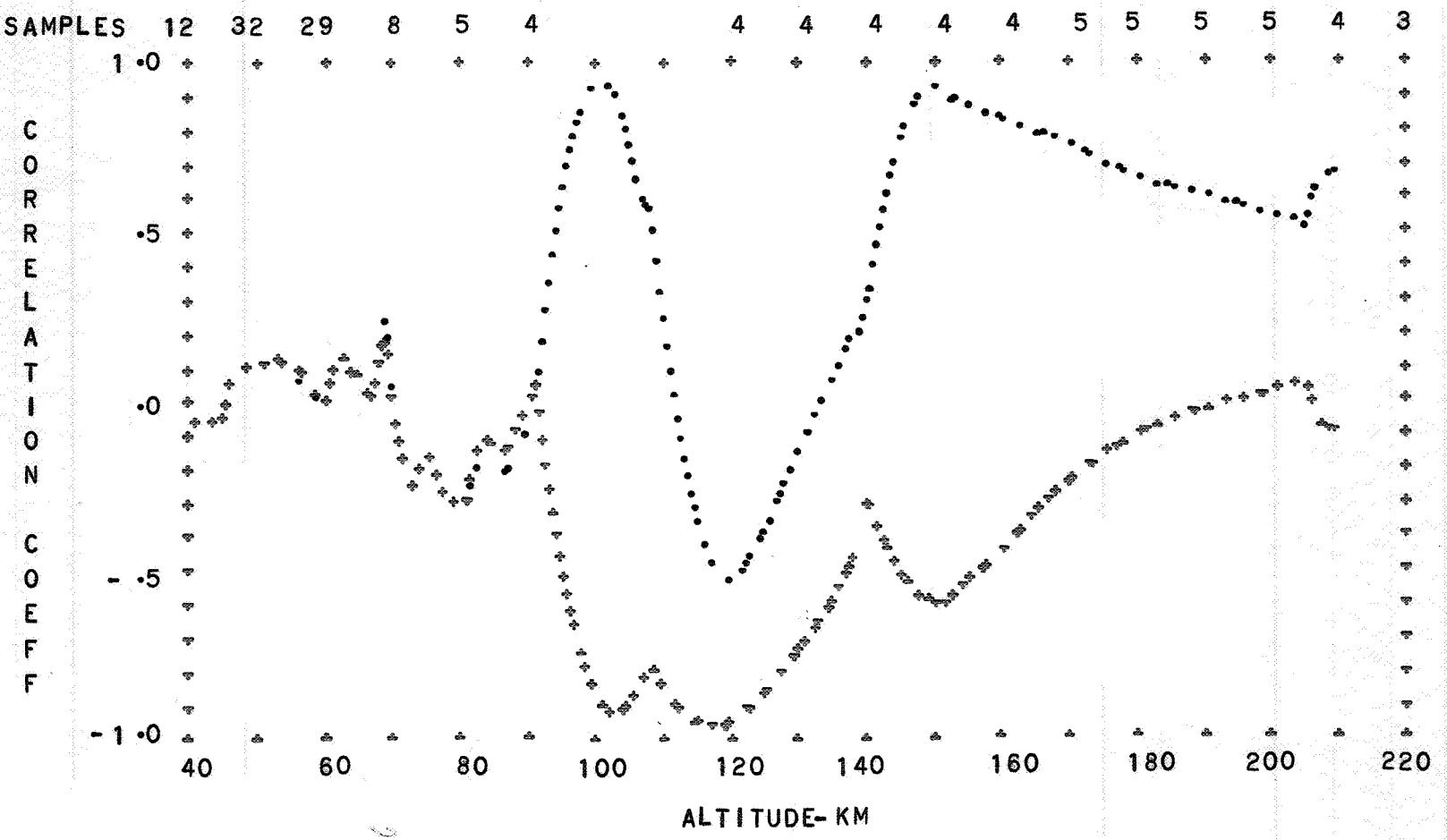

FIG. 24. CORRELATION OF DENSITY WITH SOLAR FLUX

SUBTROPICAL SUMMER DIURNAL MEAN

SAME DAY--CROSSES PRECEEDING DAY--DOTS

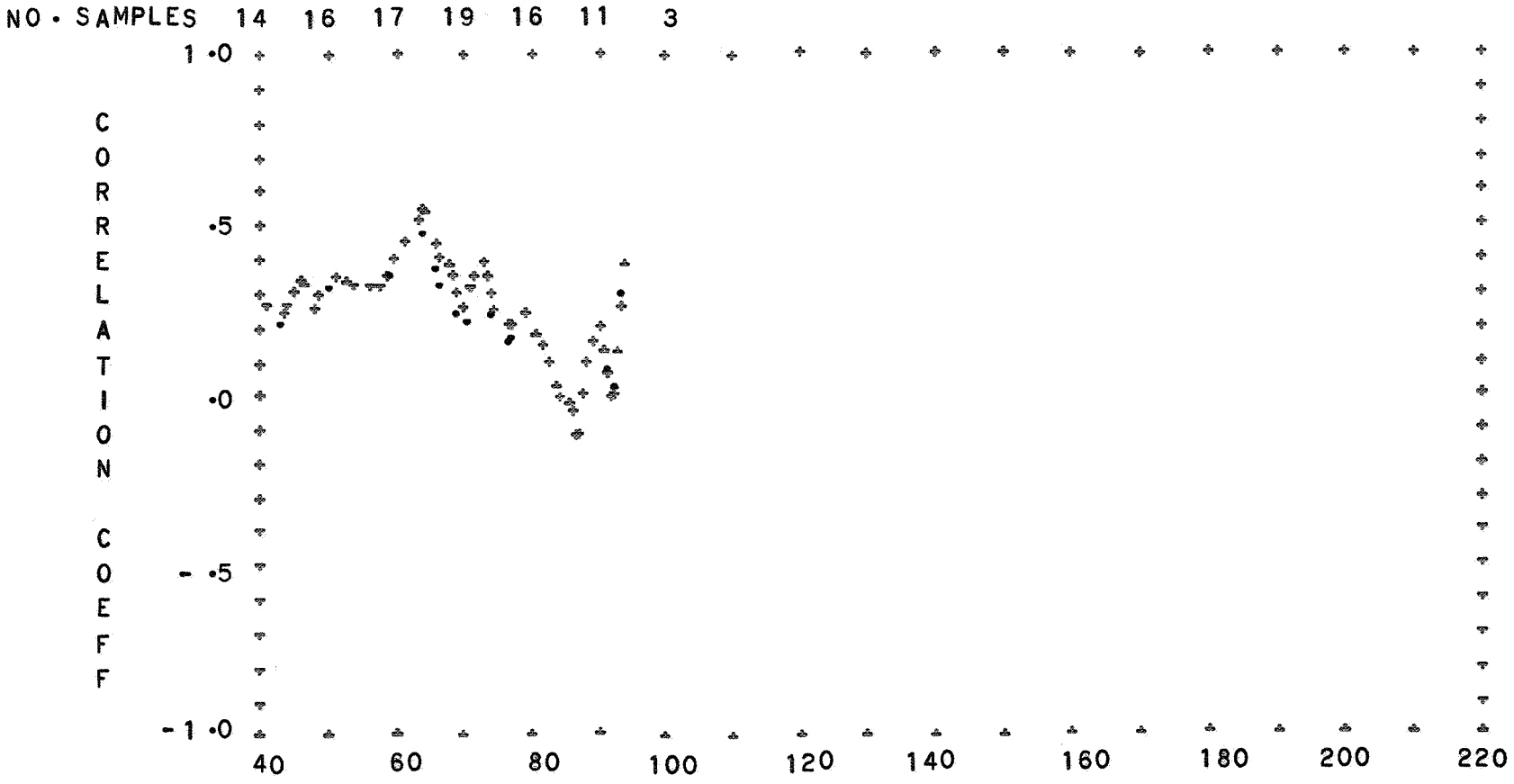

FIG. 25 CORRELATION OF DENSITY WITH SOLAR FLUX

MIDLATITUDE SUMMER DIURNAL MEAN

SAME DAY--CROSSES PRECEEDING DAY--DOTS

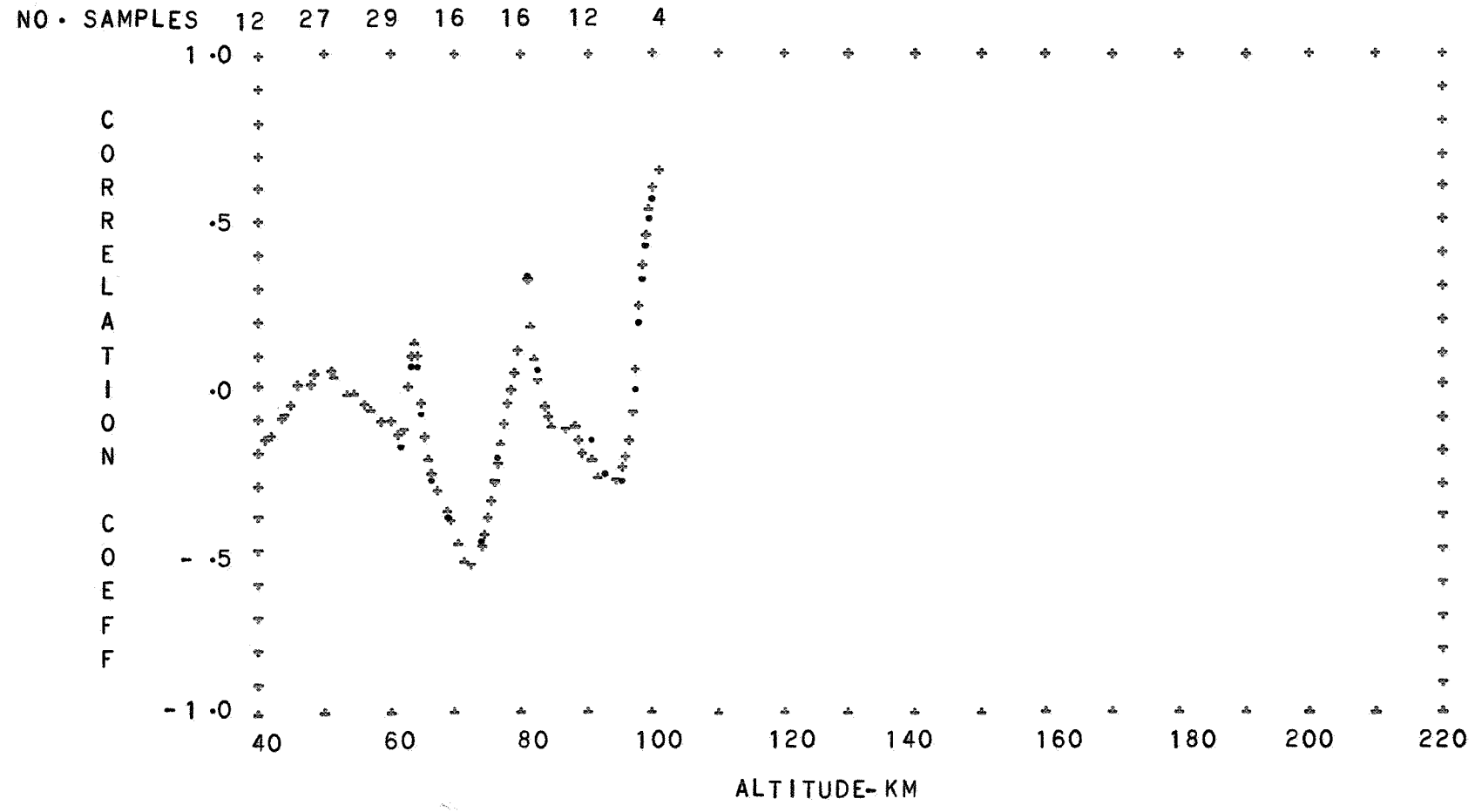

FIG. 26 CORRELATION OF DENSITY WITH SOLAR FLUX

SUBTROPICAL-MIDLATITUDE AUTUMN DIURNAL TRANSITION

SAME DAY--CROSSES PRECEEDING DAY--DOTS

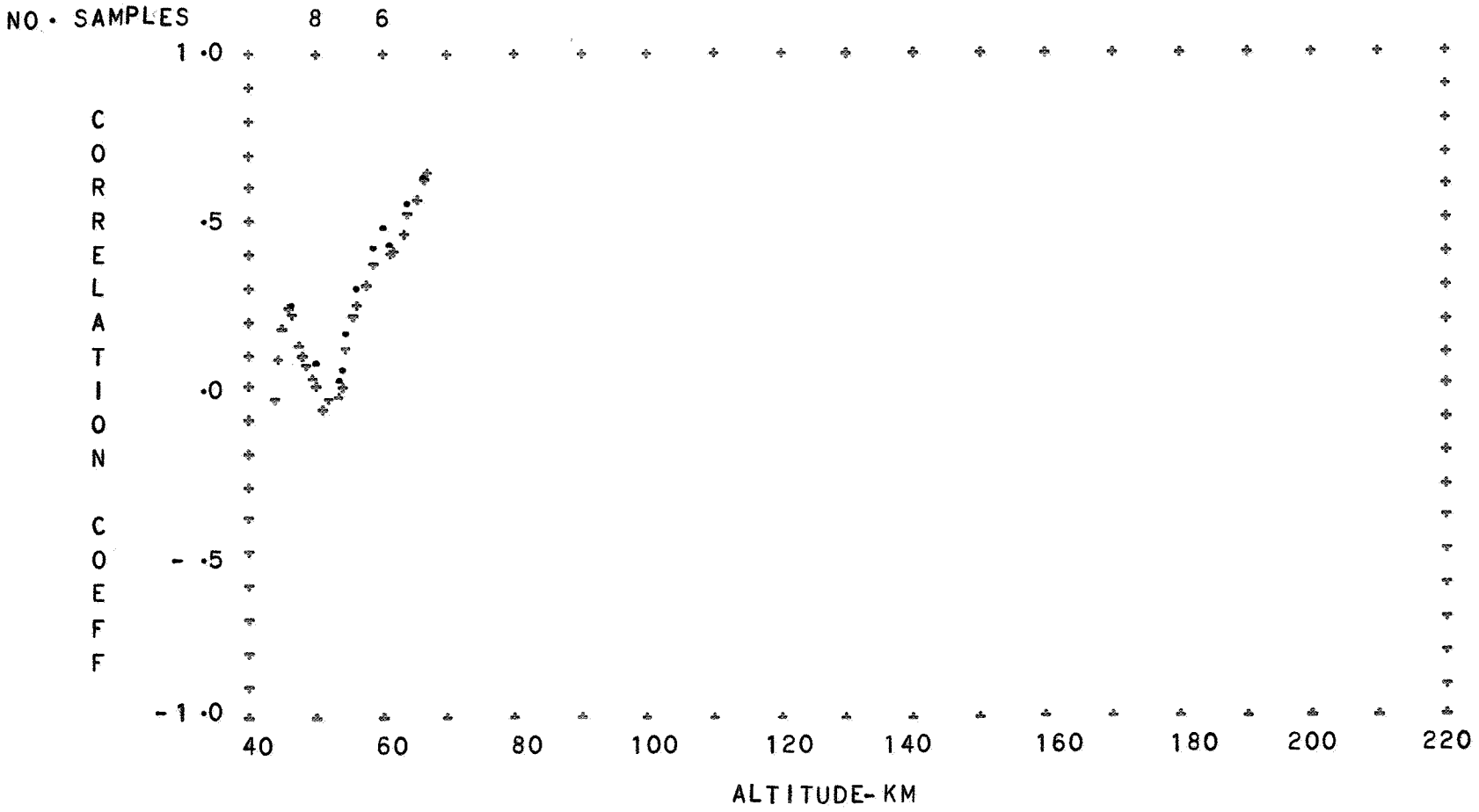

FIG. 27. CORRELATION OF DENSITY WITH SOLAR FLUX

SUBTROPICAL-MIDLATITUDE AUTUMN DAYTIME

SAME DAY--CROSSES PRECEEDING DAY--DOTS

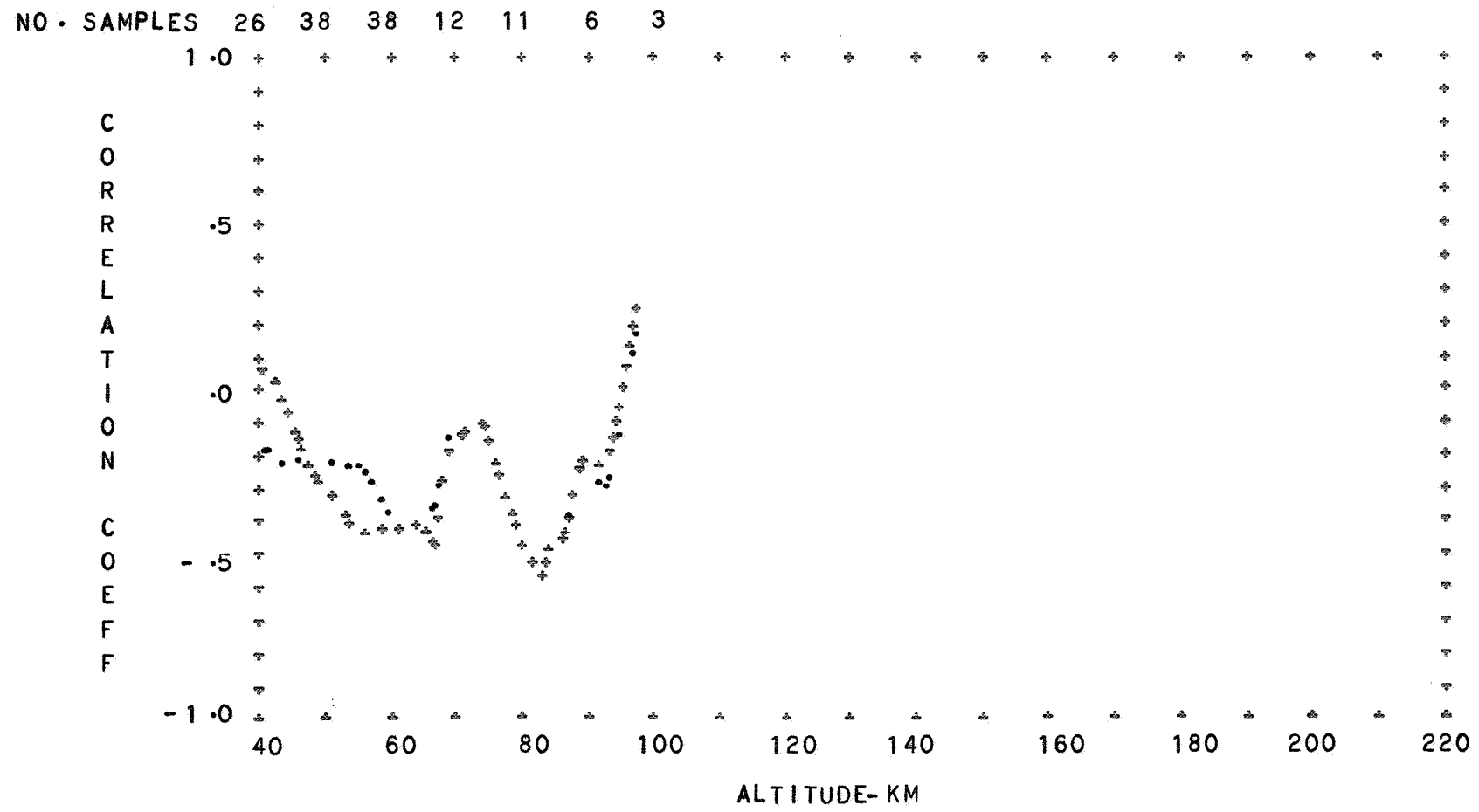

FIG. 28. CORRELATION OF DENSITY WITH SOLAR FLUX

SUBTROPICAL-MIDLATITUDE AUTUMN NIGHTTIME

SAME DAY--CROSSES PRECEEDING DAY--DOTS

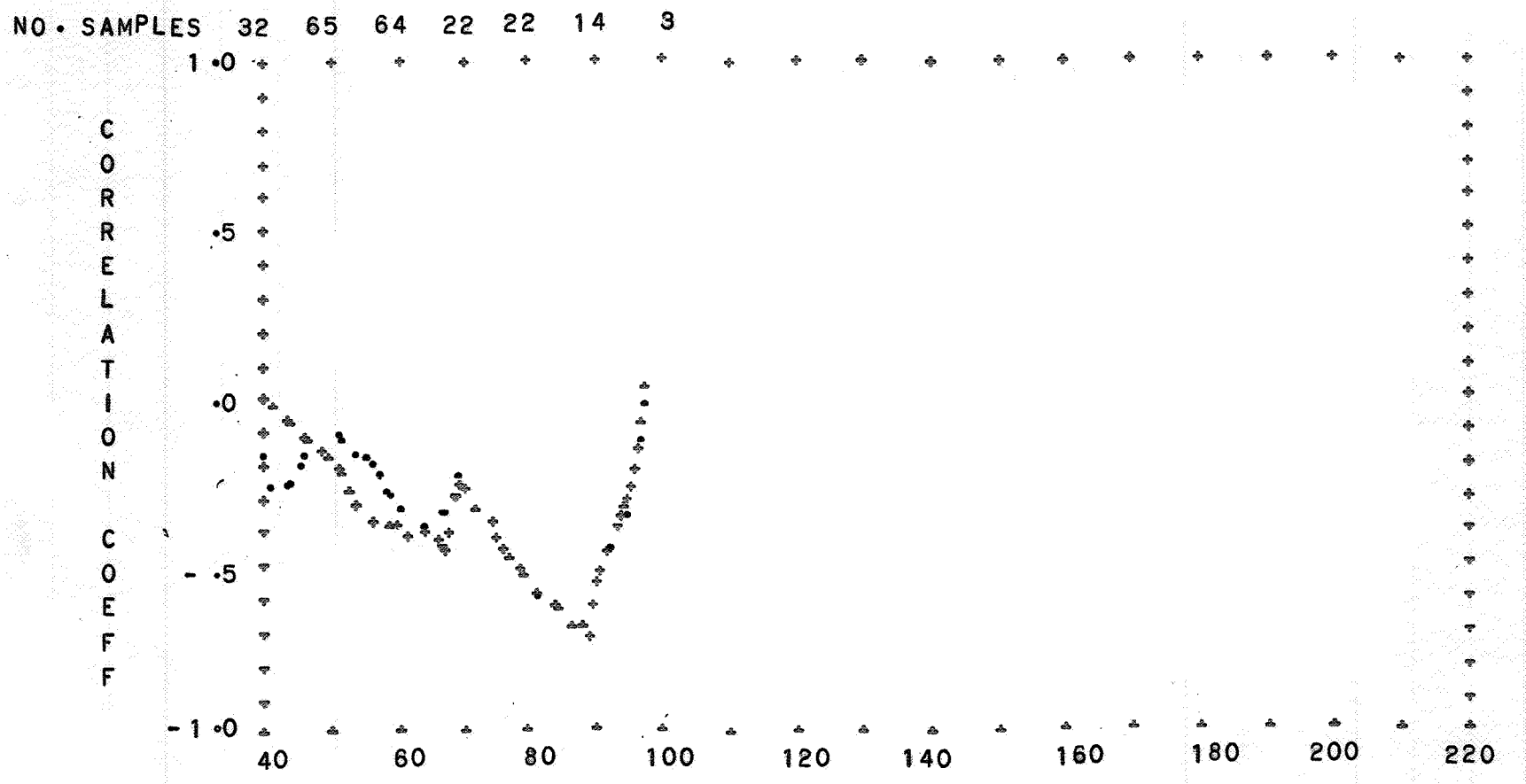

FIG. 29. CORRELATION OF DENSITY WITH SOLAR FLUX

SUBTROPICAL AUTUMN DIURNAL MEAN

SAME DAY— CROSSES PRECEEDING DAY-- DOTS

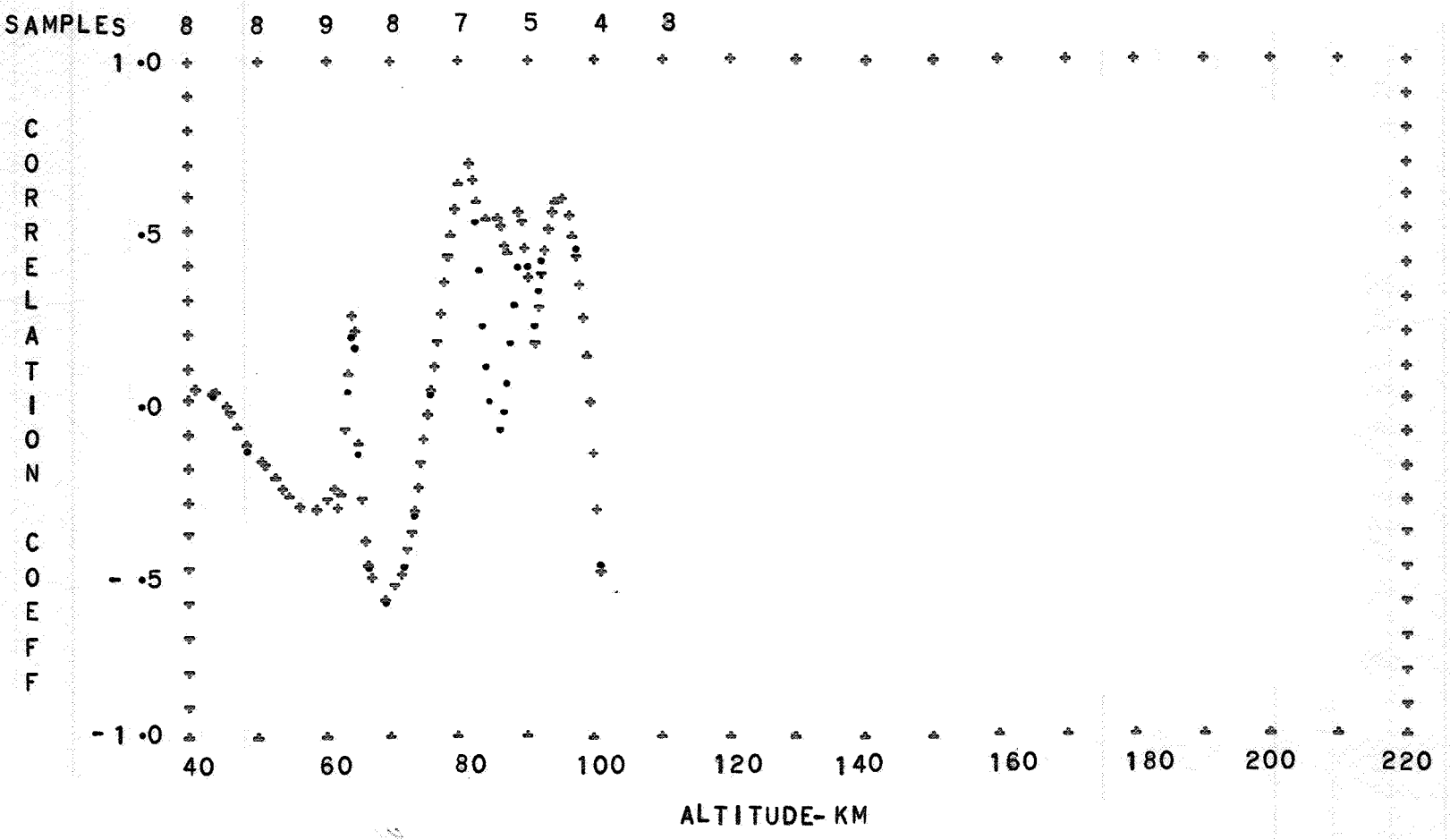

FIG. 30. CORRELATION OF DENSITY WITH SOLAR FLUX

MIDLATITUDE AUTUMN DIURNAL MEAN

SAME DAY--CROSSES PRECEEDING DAY--DOTS

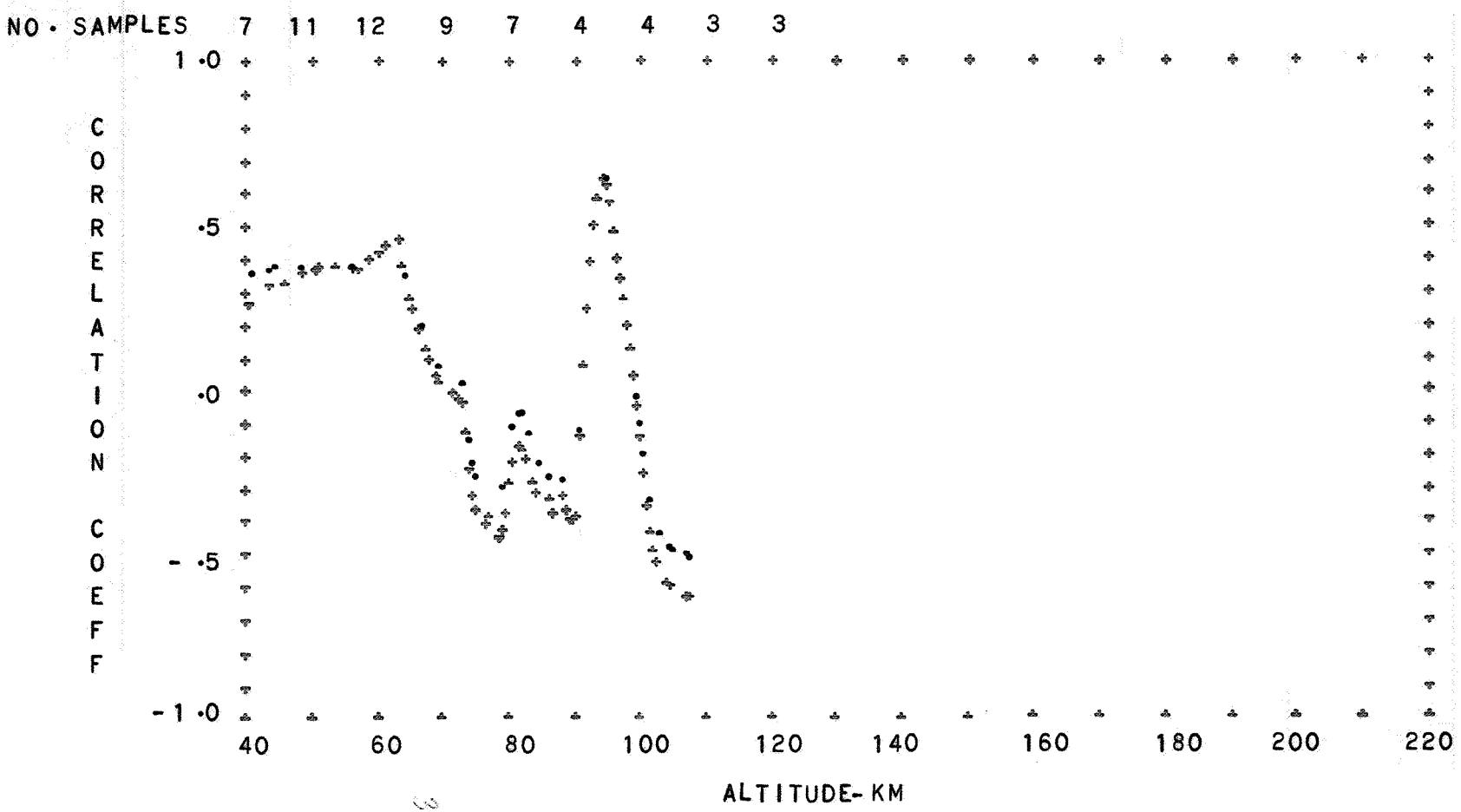

FIG. 31. CORRELATION OF DENSITY WITH SOLAR FLUX

SUBTROPICAL-MIDLATITUDE WINTER DIURNAL TRANSITION

SAME DAY--CROSSES PRECEEDING DAY--DOTS

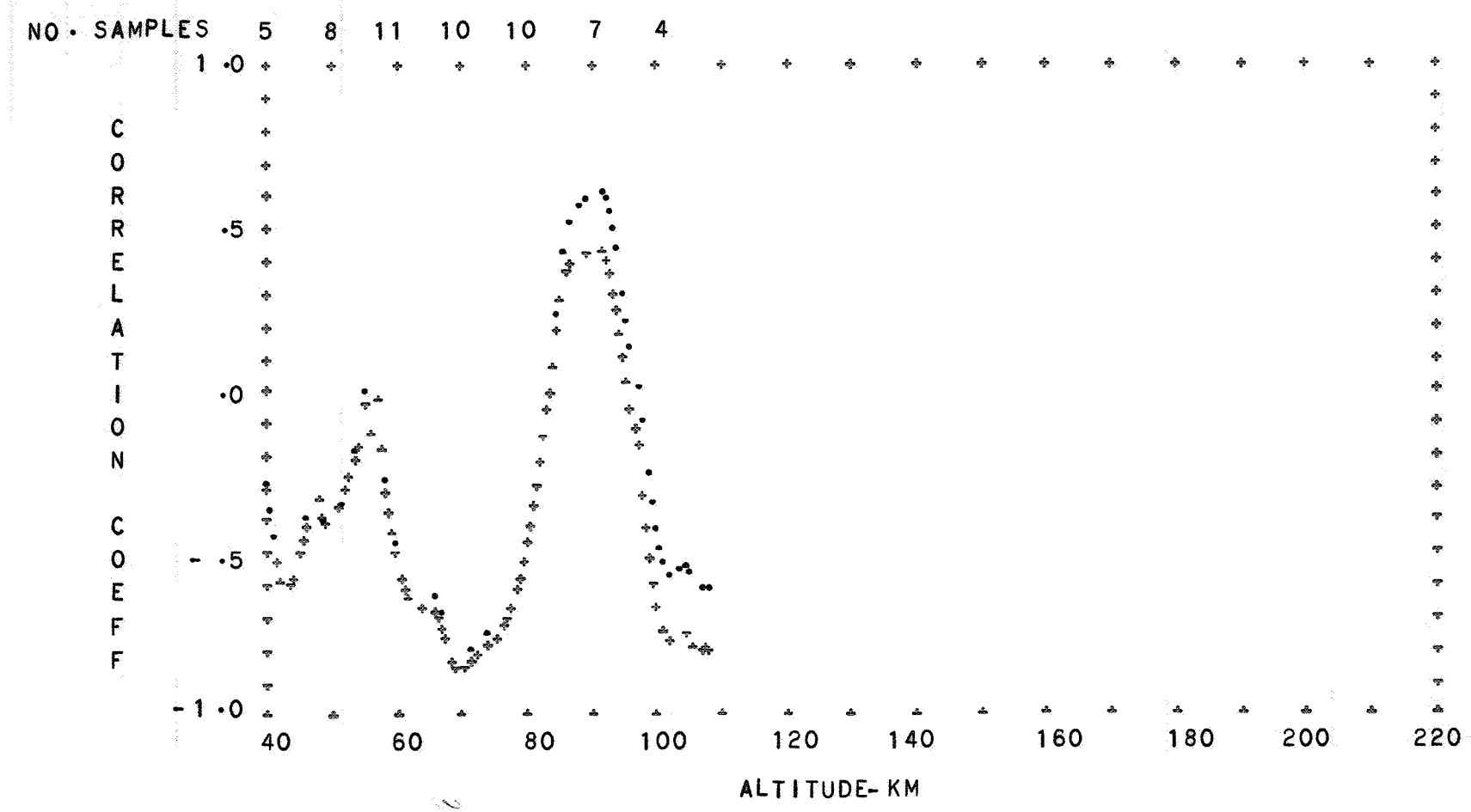

FIG. 32 CORRELATION OF DENSITY WITH SOLAR FLUX

SUBTROPICAL-MIDLATITUDE WINTER DAYTIME

SAME DAY--CROSSES PRECEEDING DAY--DOTS

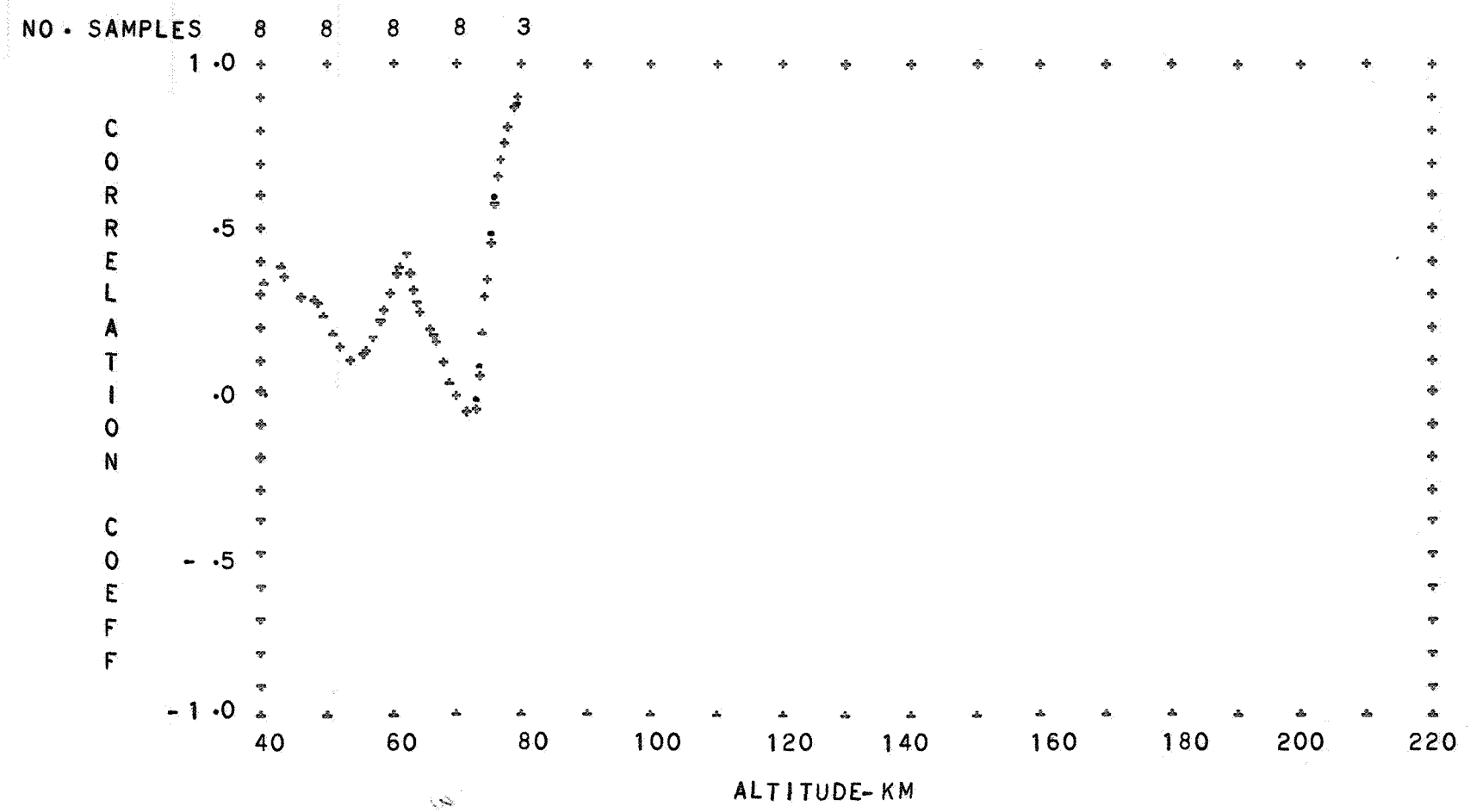

FIG. 33 CORRELATION OF DENSITY WITH SOLAR FLUX

SUBTROPICAL-MIDLATITUDE WINTER NIGHTTIME

SAME DAY--CROSSES PRECEEDING DAY--DOTS

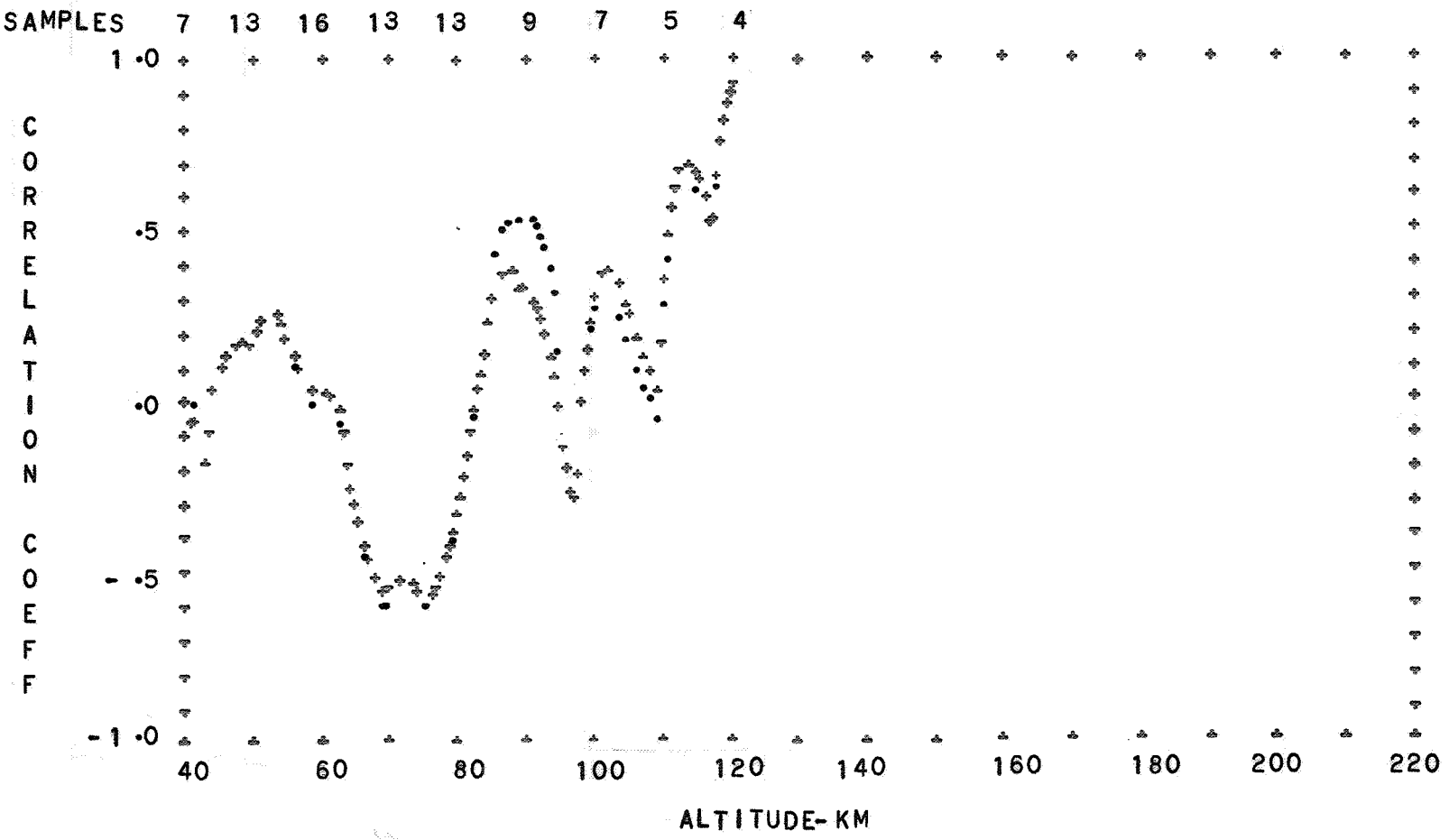

FIG. 34. CORRELATION OF DENSITY WITH SOLAR FLUX

SUBTROPICAL WINTER DIURNAL MEAN

SAME DAY--CROSSES PRECEEDING DAY--DOTS

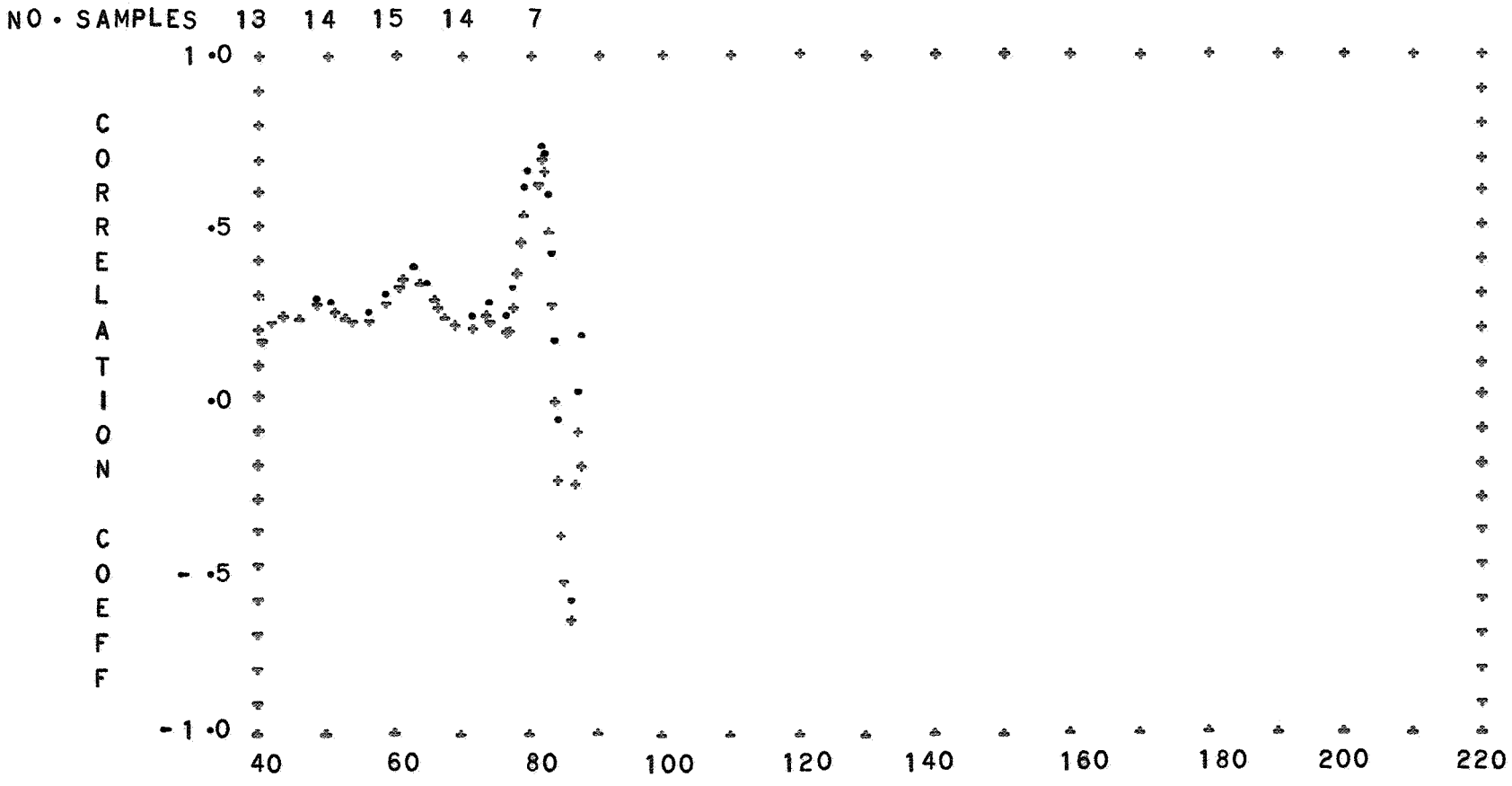

FIG. 35 CORRELATION OF DENSITY WITH SOLAR FLUX

MIDLATITUDE WINTER DIURNAL MEAN

SAME DAY--CROSSES PRECEEDING DAY--DOTS

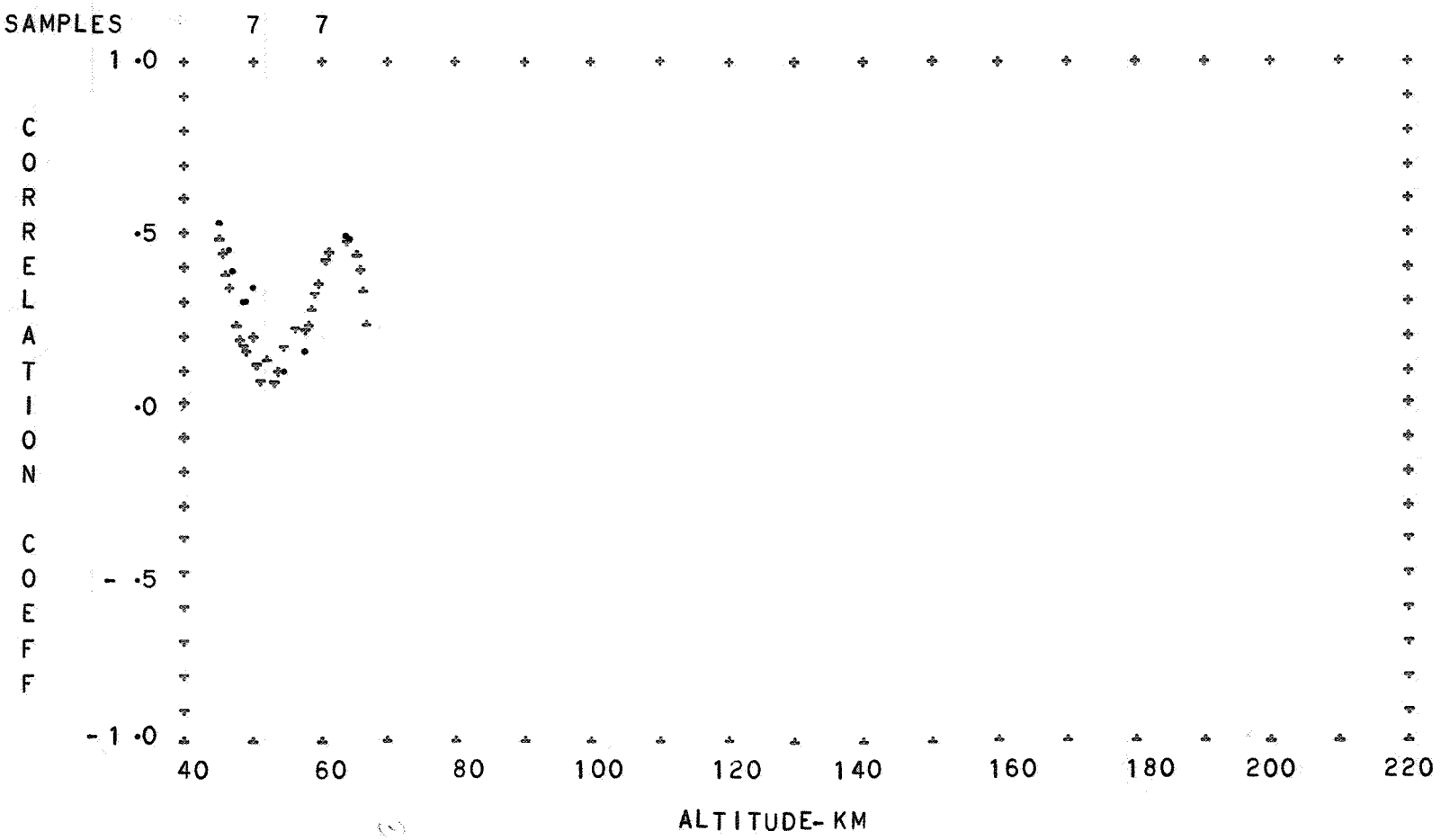

FIG. 36. CORRELATION OF DENSITY WITH SOLAR FLUX

SUBTROPICAL-MIDLATITUDE SUMMER EXTREME DIURNAL TRANSITION

SAME DAY--CROSSES PRECEEDING DAY--DOTS

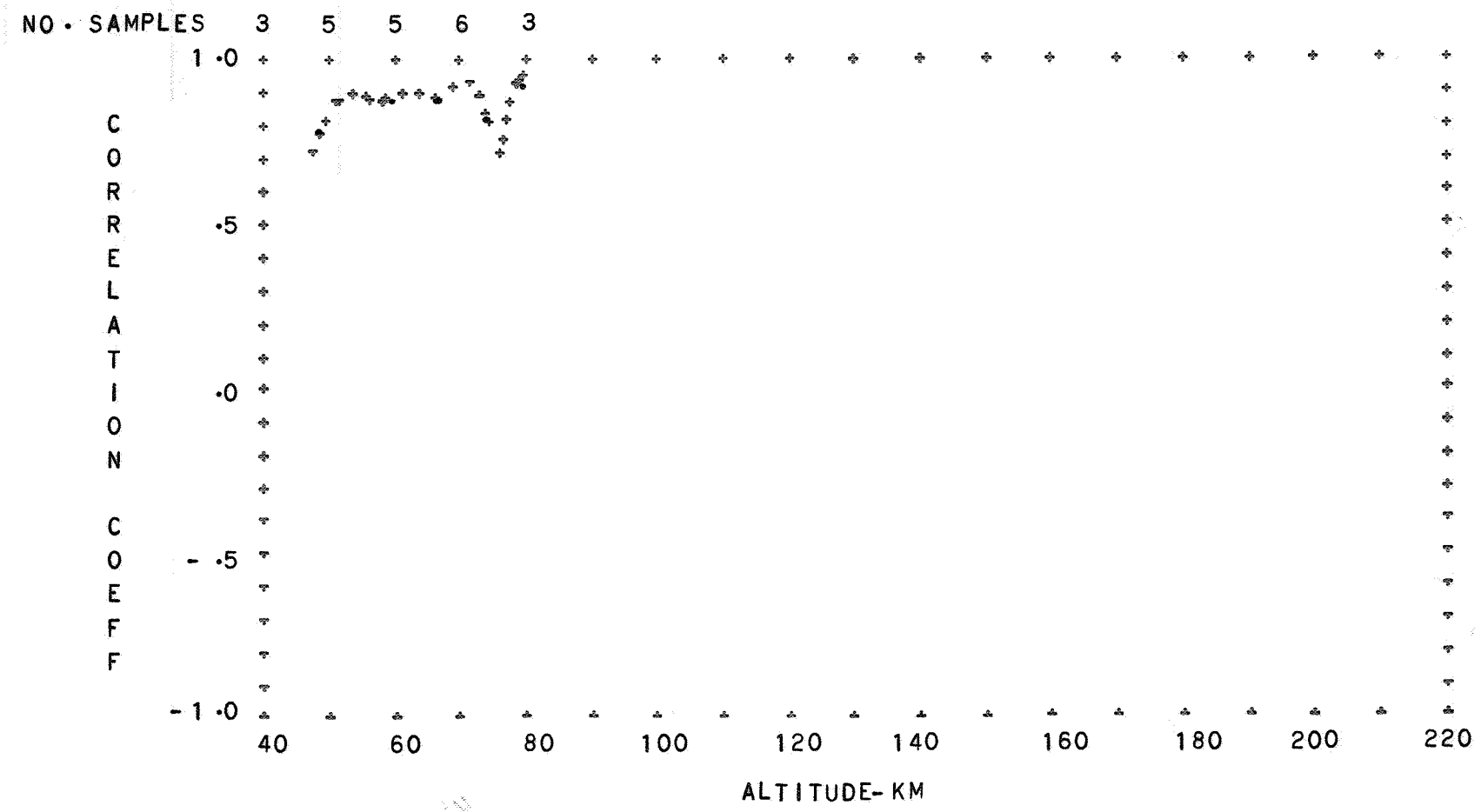

FIG. 37. CORRELATION OF DENSITY WITH SOLAR FLUX

SUBTROPICAL-MIDLATITUDE SUMMER EXTREME DAYTIME

SAME DAY--CROSSES PRECEEDING DAY--DOTS

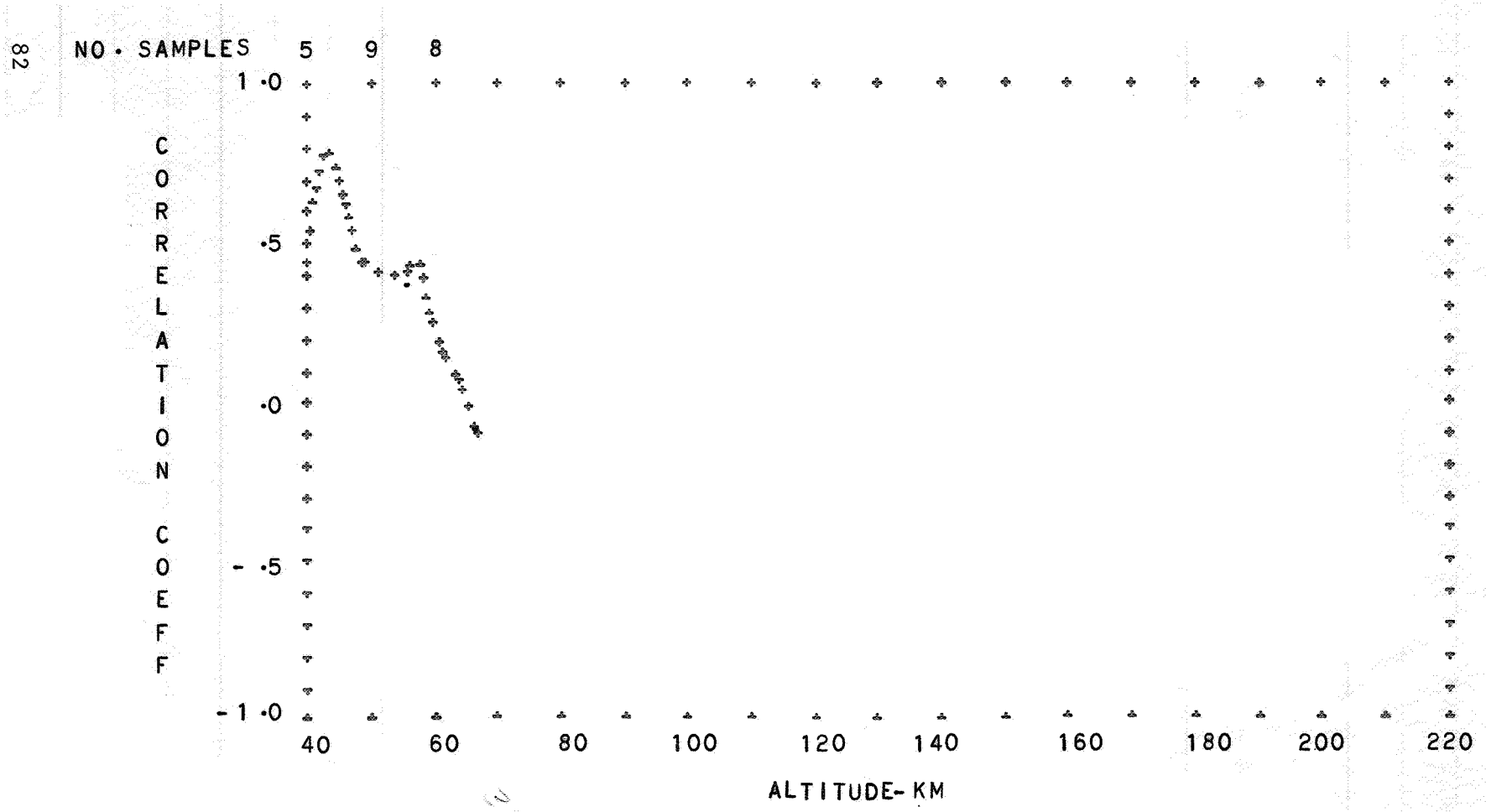

FIG. 38 CORRELATION OF DENSITY WITH SOLAR FLUX

SUBTROPICAL-MIDLATITUDE SUMMER EXTREME NIGHTTIME

SAME DAY--CROSSES PRECEEDING DAY--DOTS

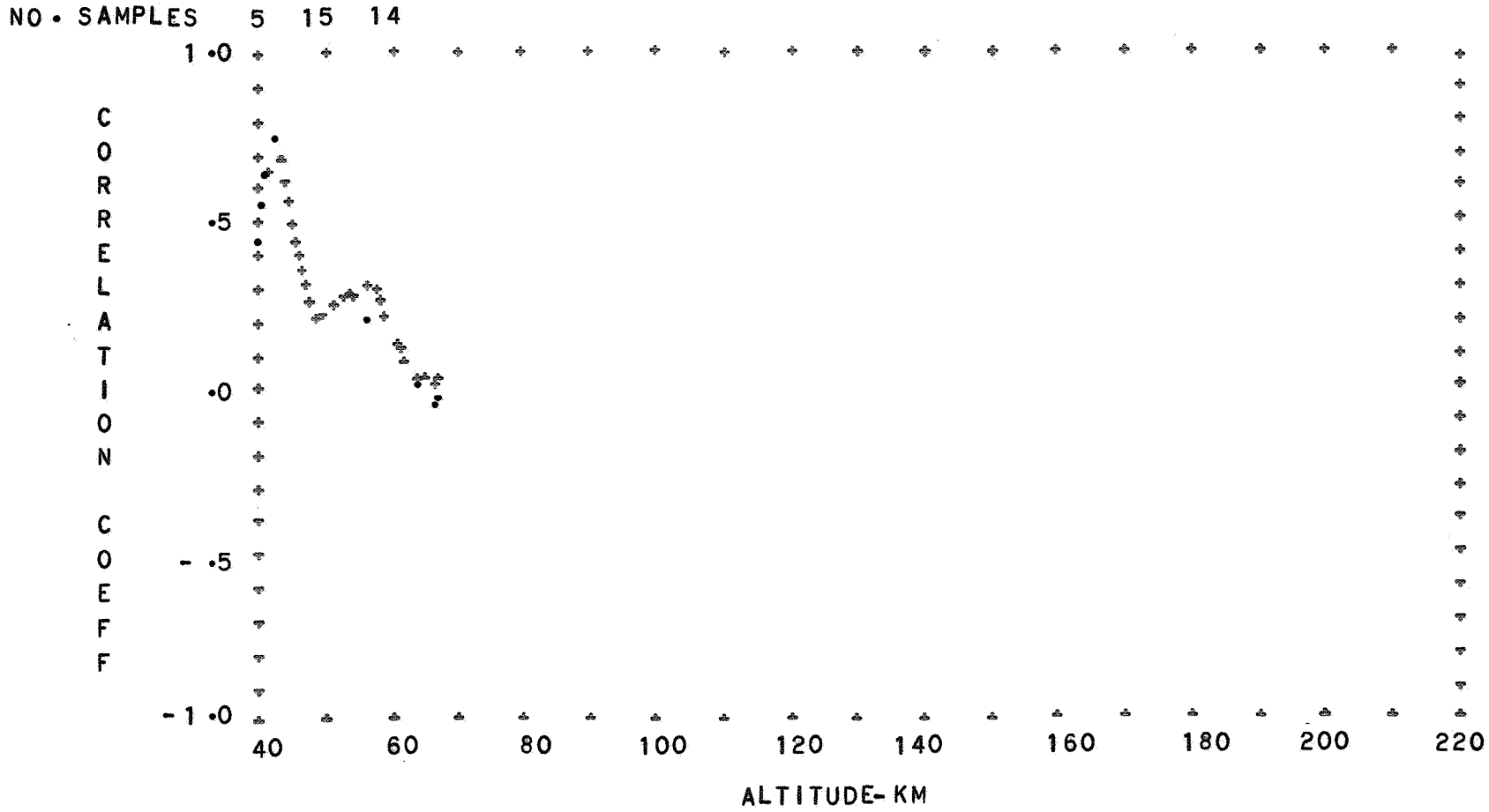

FIG. 39 CORRELATION OF DENSITY WITH SOLAR FLUX

SUBTROPICAL SUMMER EXTREME DIURNAL MEAN

SAME DAY--CROSSES PRECEEDING DAY--DOTS

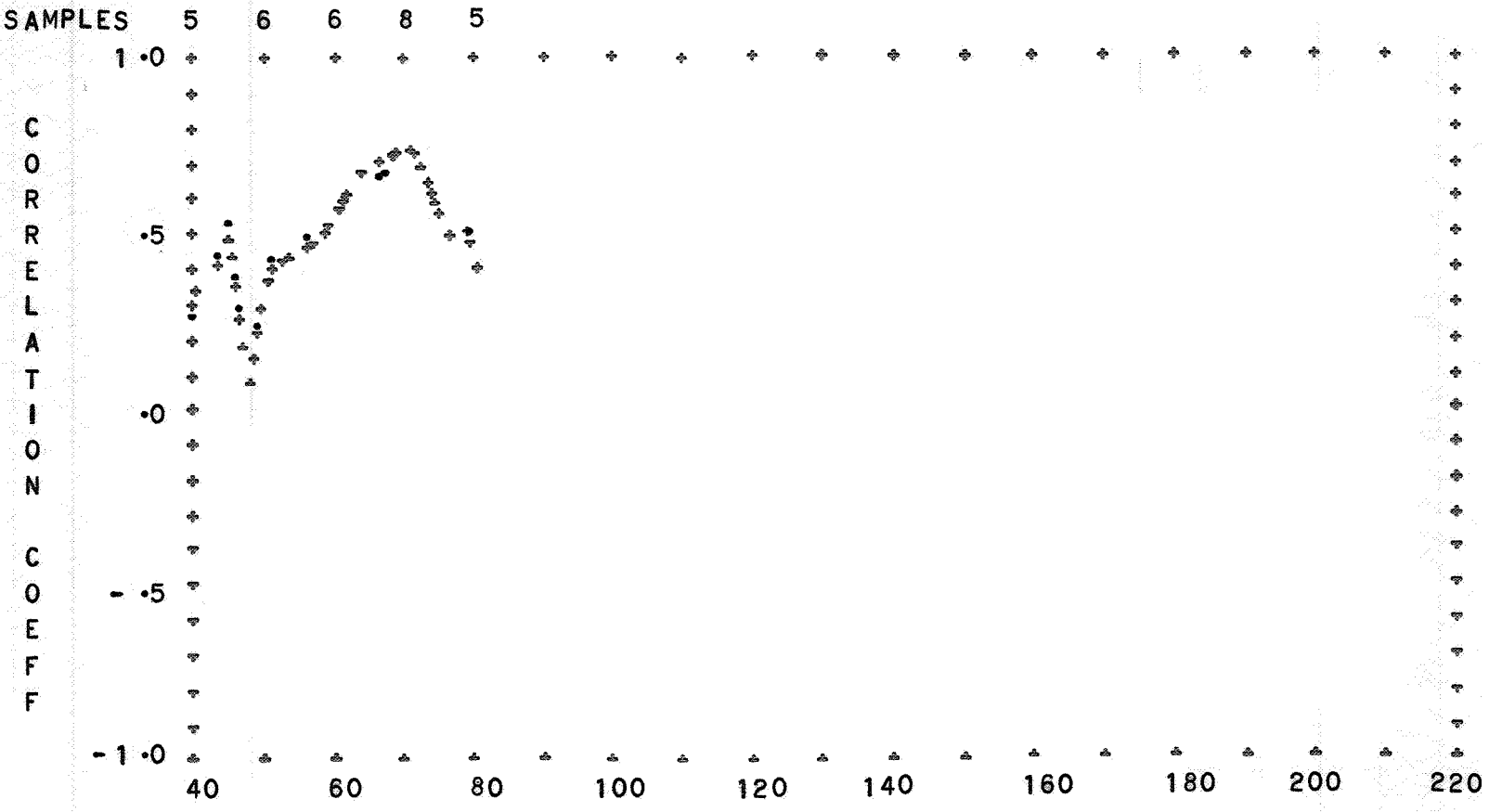

FIG. 40. CORRELATION OF DENSITY WITH SOLAR FLUX

MIDLATITUDE SUMMER EXTREME DIURNAL MEAN

SAME DAY--CROSSES PRECEEDING DAY--DOTS

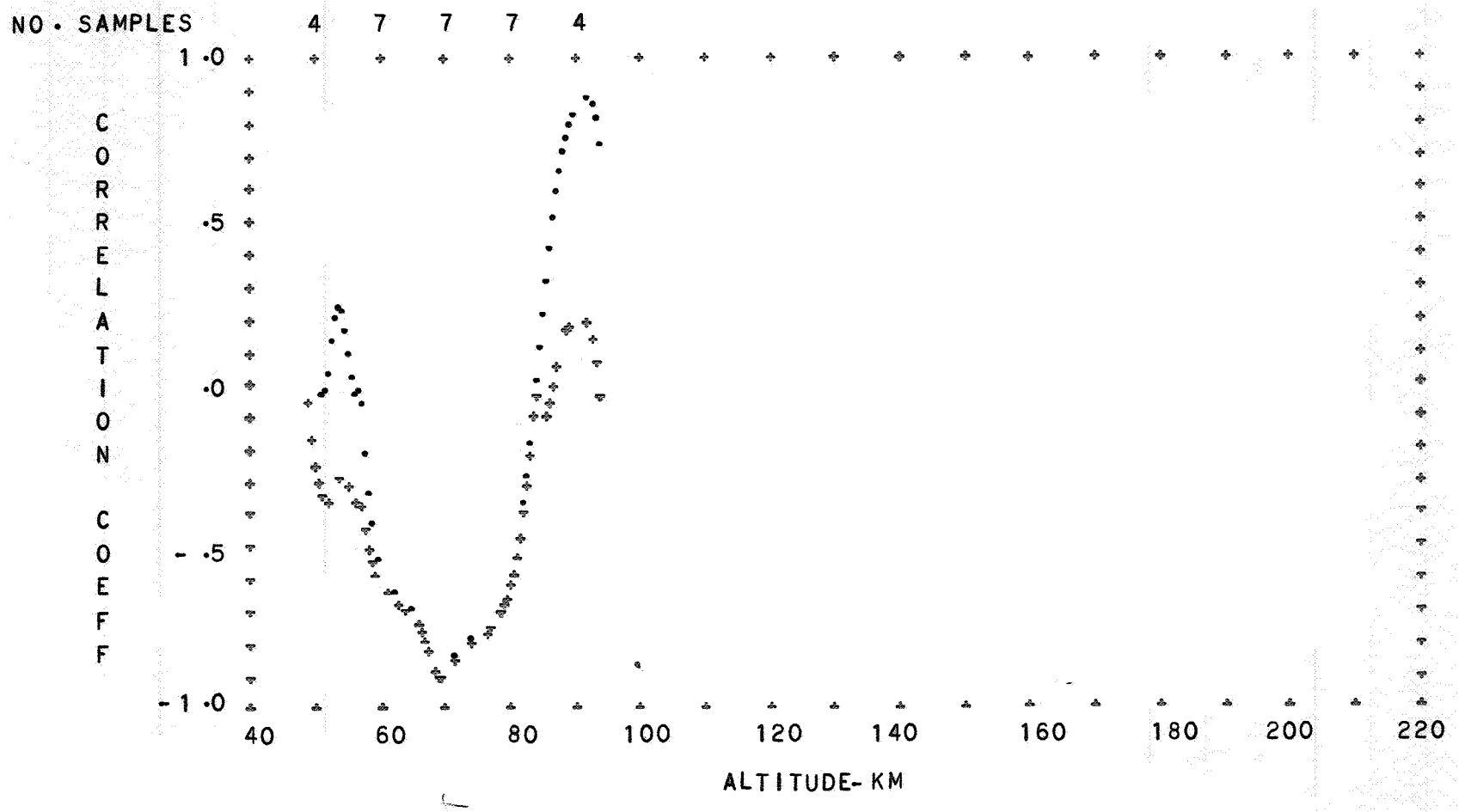

FIG. 41. CORRELATION OF DENSITY WITH SOLAR FLUX

SUBTROPICAL-MIDLATITUDE WINTER EXTREME DAYTIME

SAME DAY--CROSSES PRECEEDING DAY--DOTS

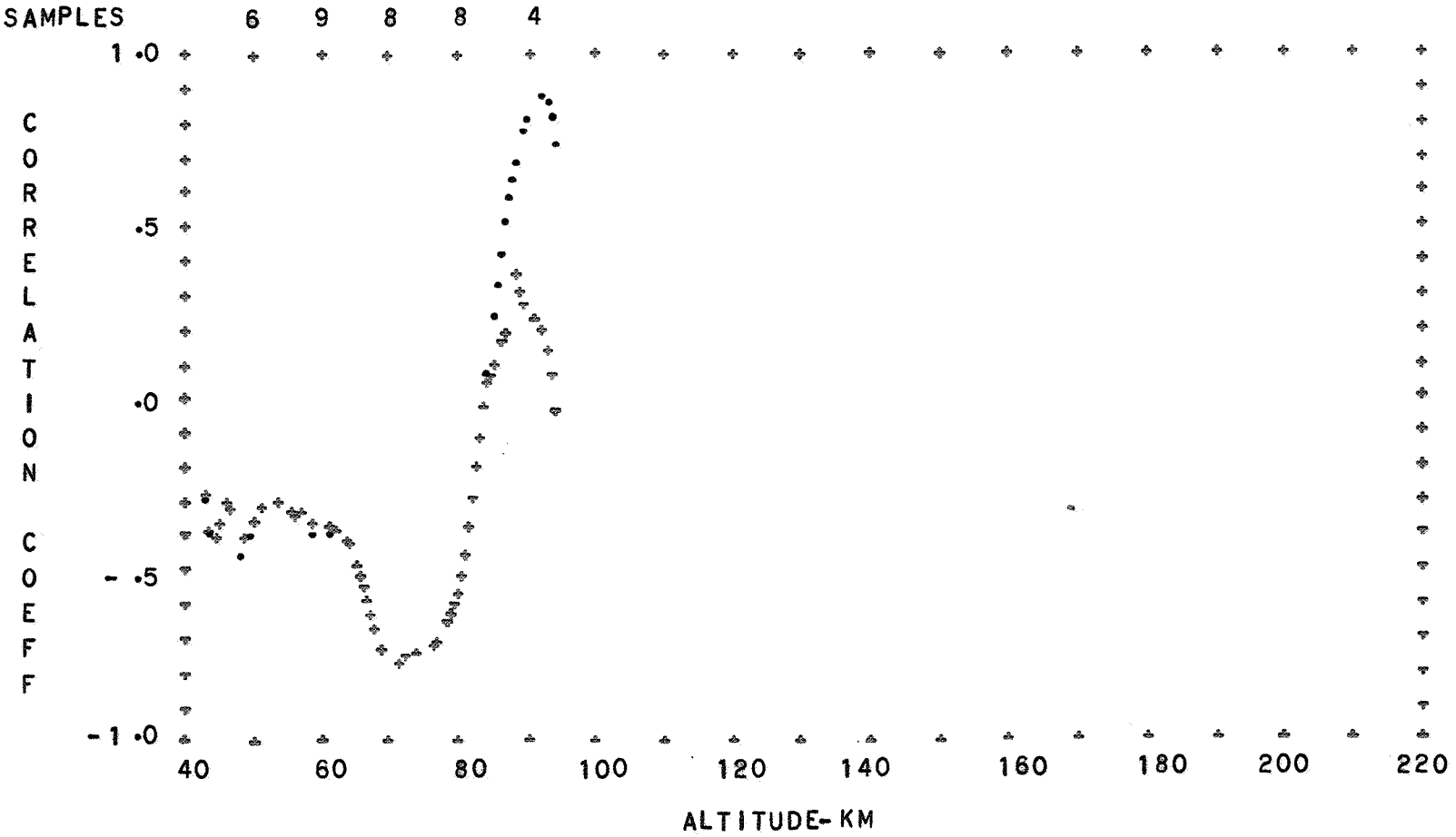

FIG. 42 CORRELATION OF DENSITY WITH SOLAR FLUX

SUBTROPICAL WINTER EXTREME DIURNAL MEAN

SAME DAY--CROSSES PRECEEDING DAY--DOTS

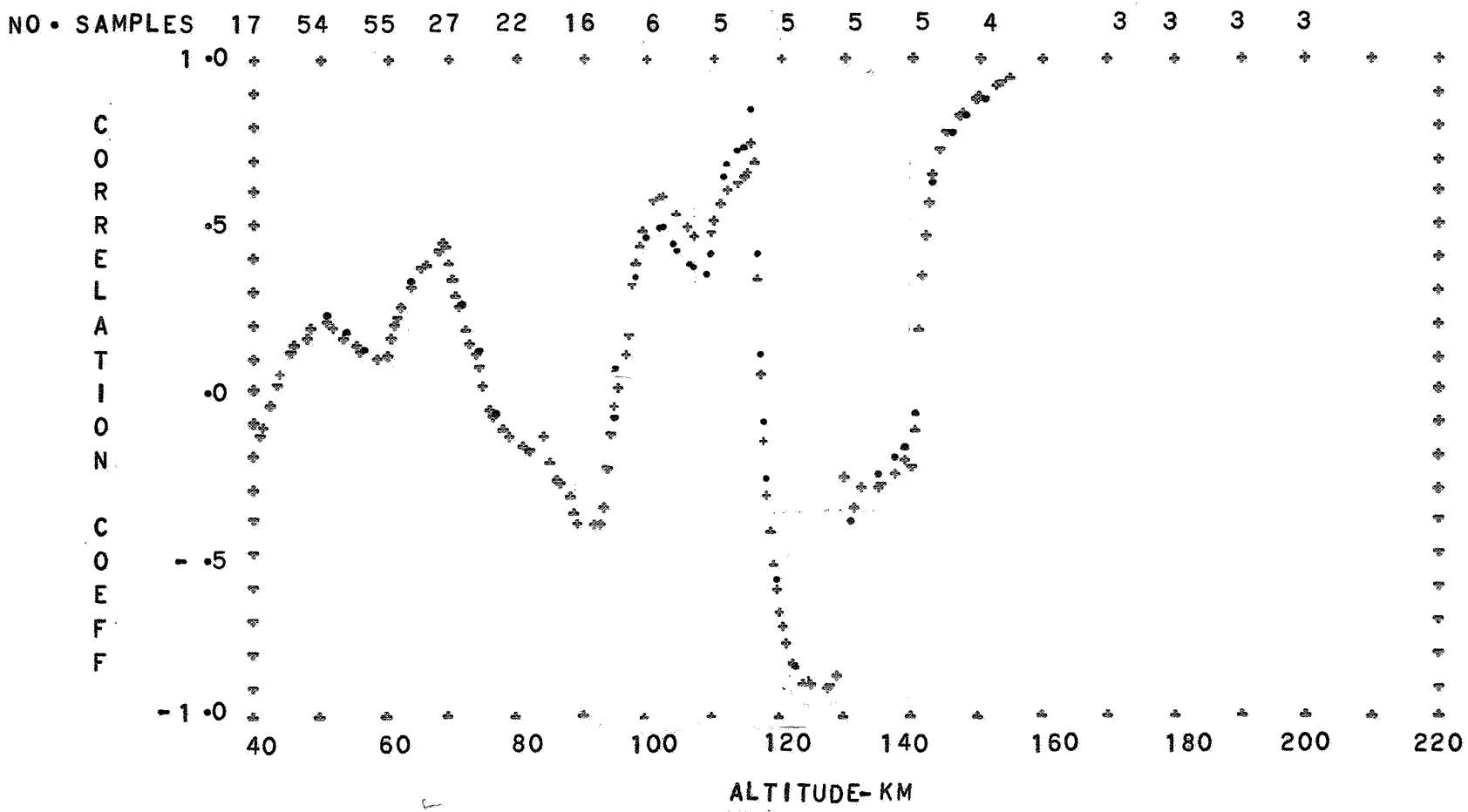

FIG. 43. CORRELATION OF DENSITY WITH SOLAR FLUX

SUBTROPICAL ANNUAL MEAN DIURNAL TRANSITION

SAME DAY--CROSSES PRECEEDING DAY--DOTS

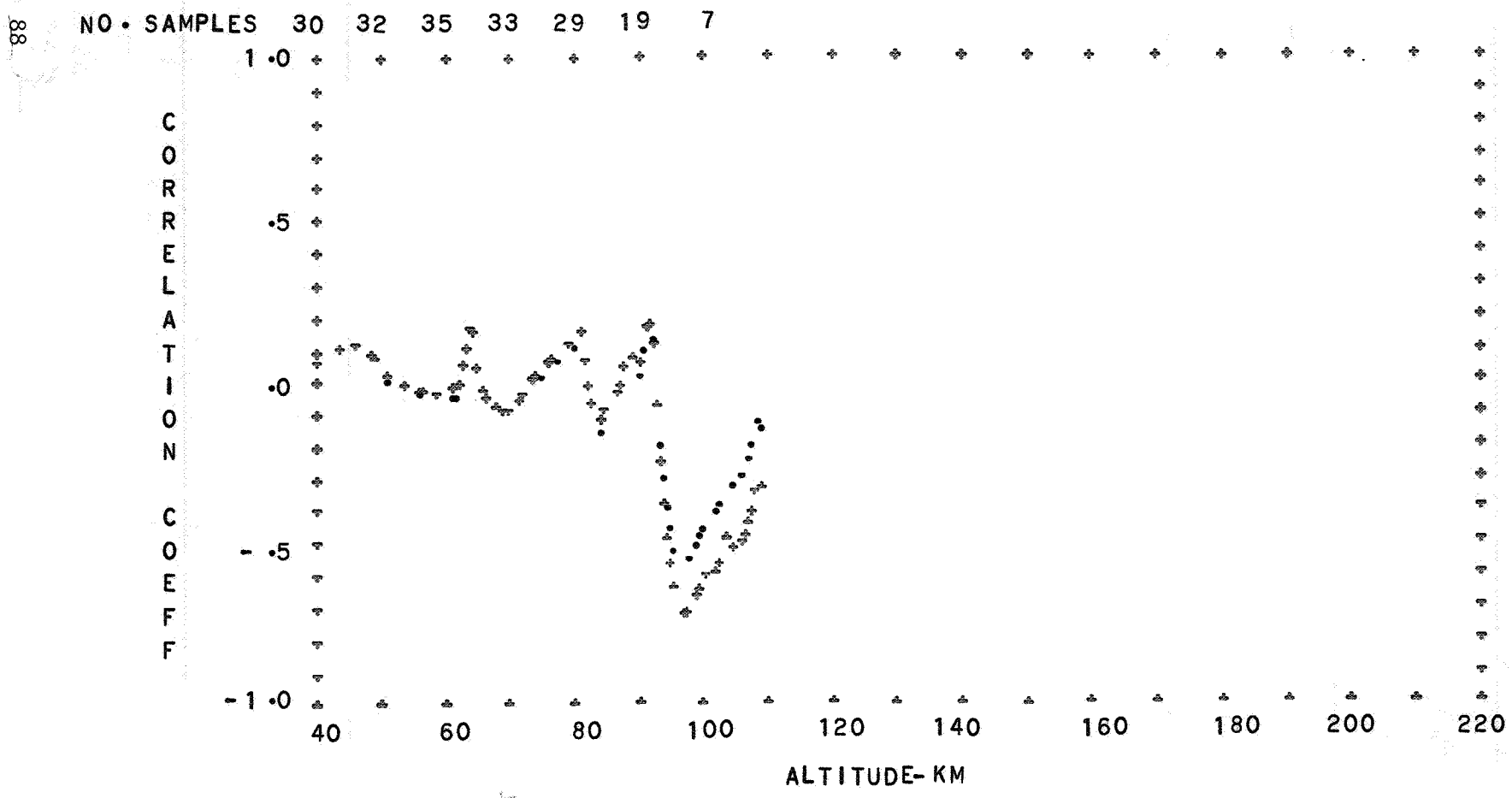

FIG. 44. CORRELATION OF DENSITY WITH SOLAR FLUX

MIDLATITUDE ANNUAL MEAN DIURNAL TRANSITION

SAME DAY--CROSSES PRECEEDING DAY--DOTS

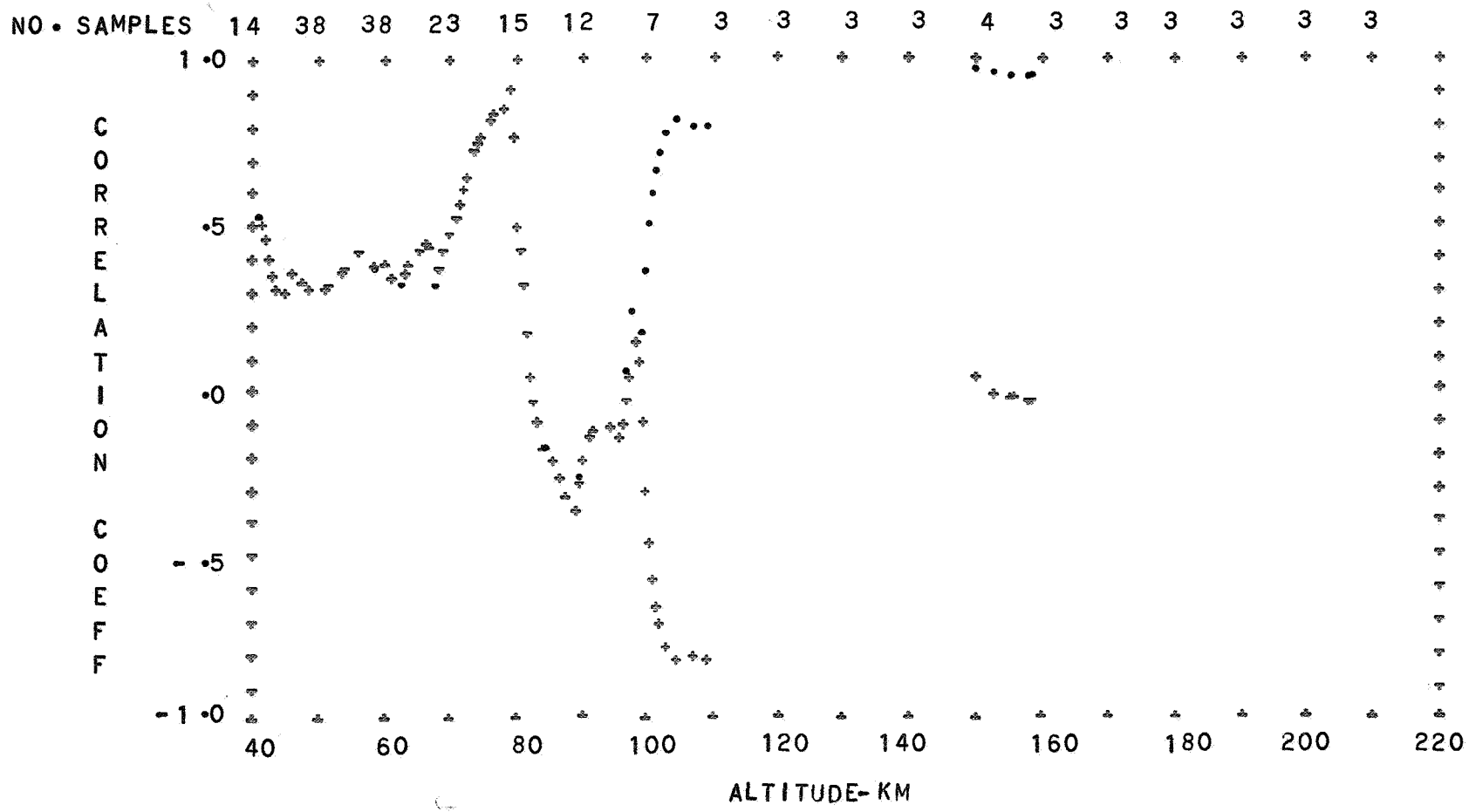

FIG. 45. CORRELATION OF DENSITY WITH SOLAR FLUX

SUBTROPICAL ANNUAL MEAN DAYTIME

SAME DAY--CROSSES PRECEEDING DAY--DOTS

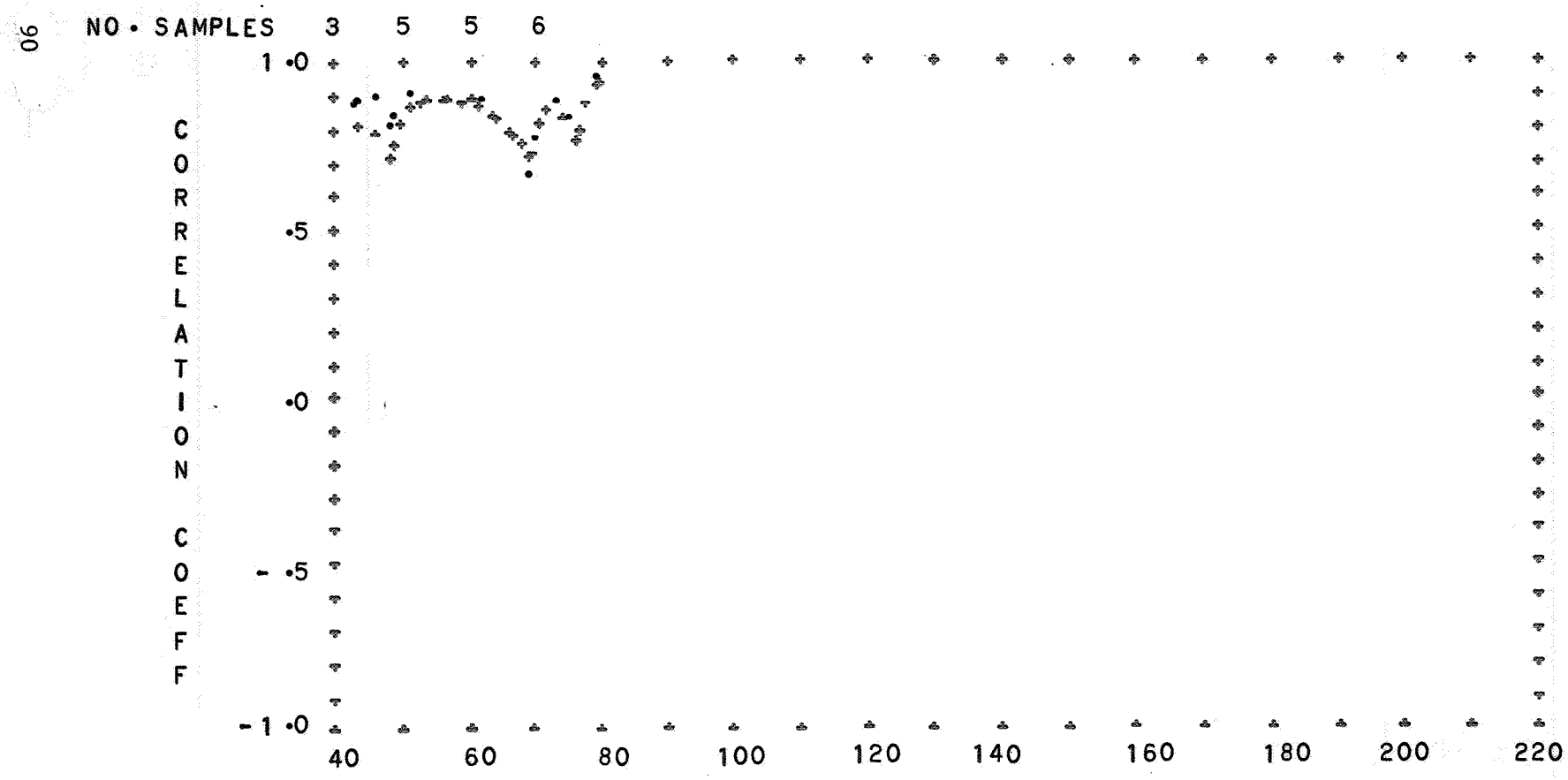

FIG. 46. CORRELATION OF DENSITY WITH SOLAR FLUX

MIDLATITUDE ANNUAL MEAN DAYTIME

SAME DAY--CROSSES PRECEEDING DAY--DOTS

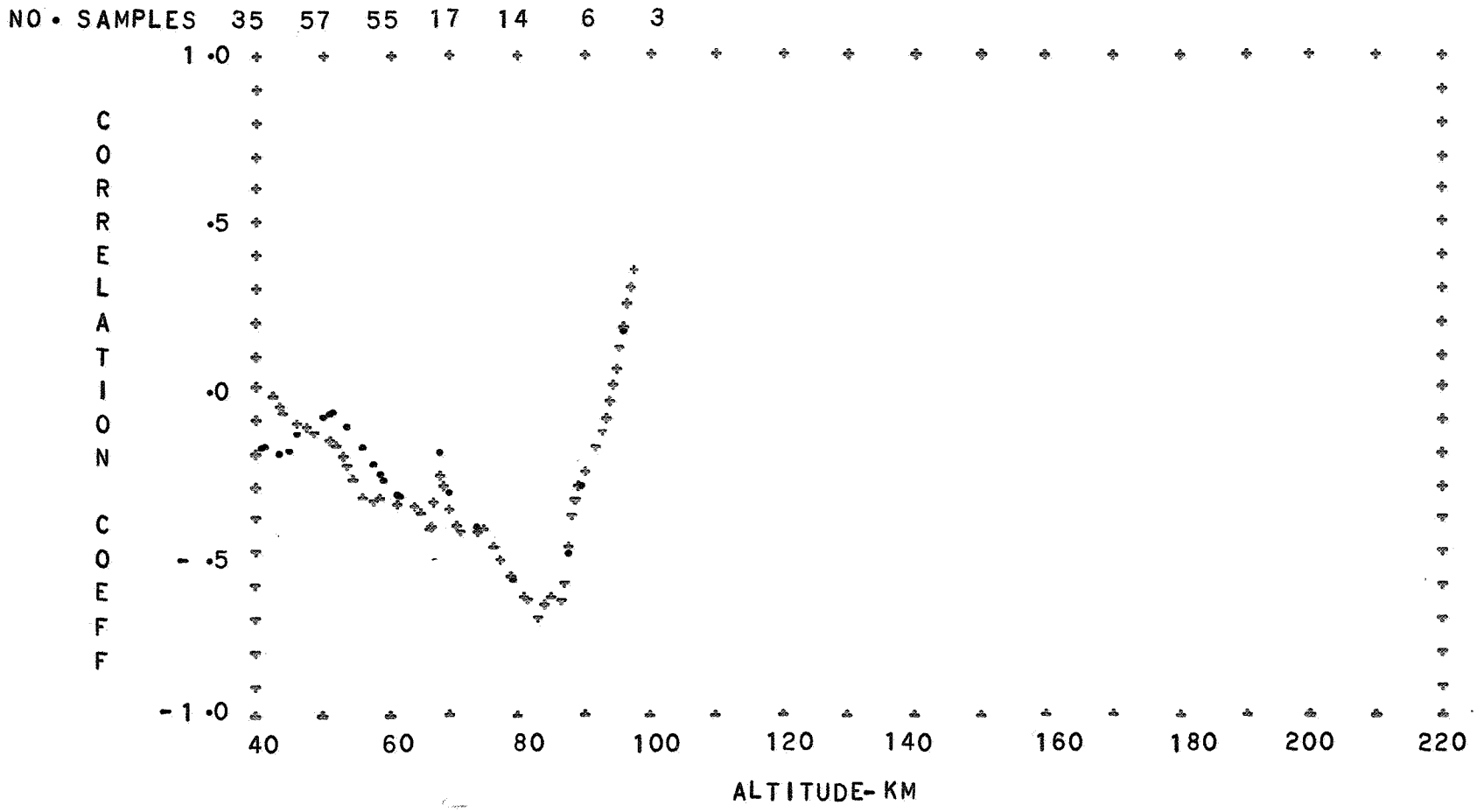

FIG. 47. CORRELATION OF DENSITY WITH SOLAR FLUX

SUBTROPICAL ANNUAL MEAN NIGHTTIME

SAME DAY--CROSSES PRECEEDING DAY--DOTS

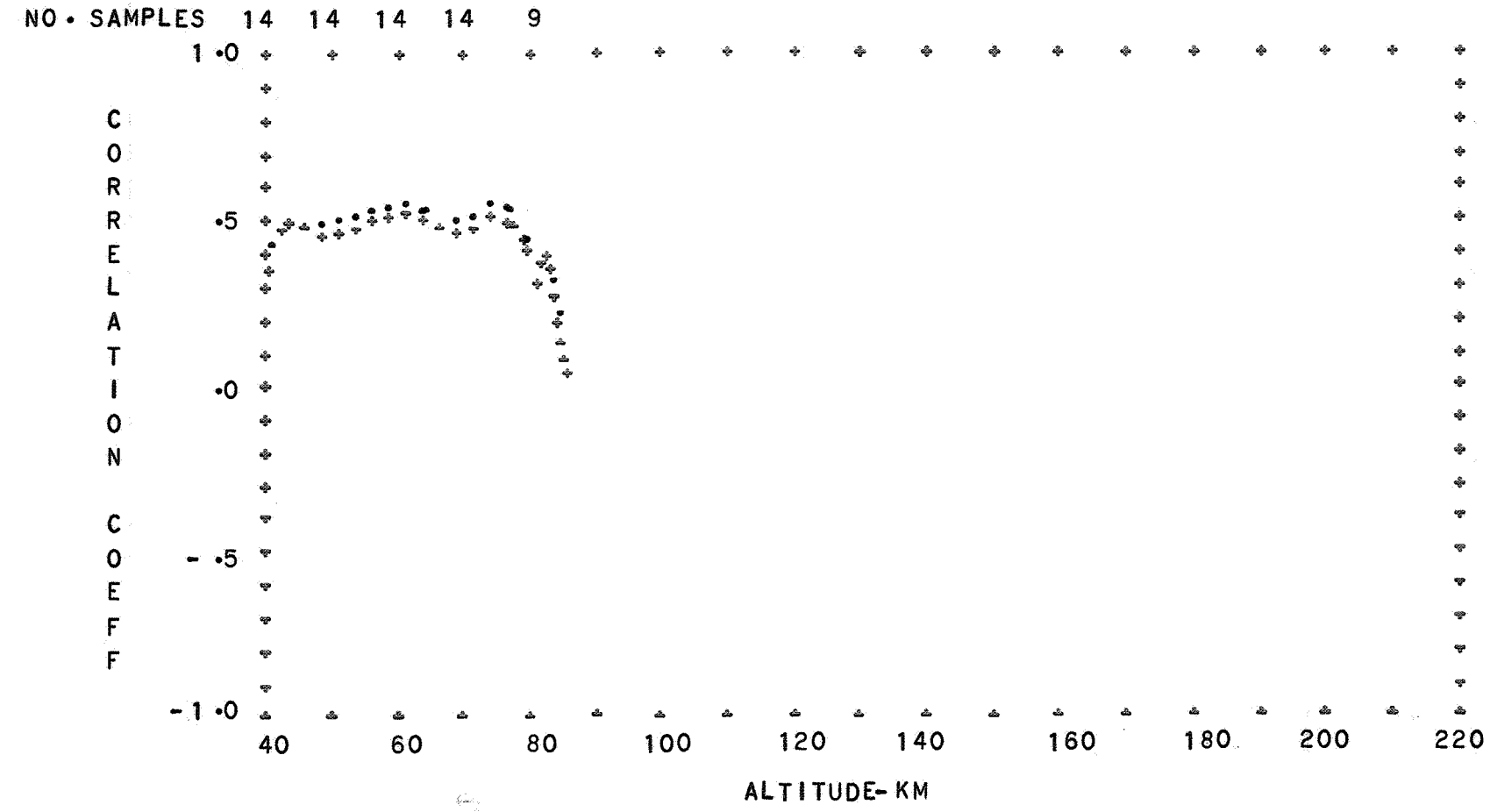

FIG. 48. CORRELATION OF DENSITY WITH SOLAR FLUX

MIDLATITUDE ANNUAL MEAN NIGHTTIME

SAME DAY--CROSSES PRECEEDING DAY--DOTS

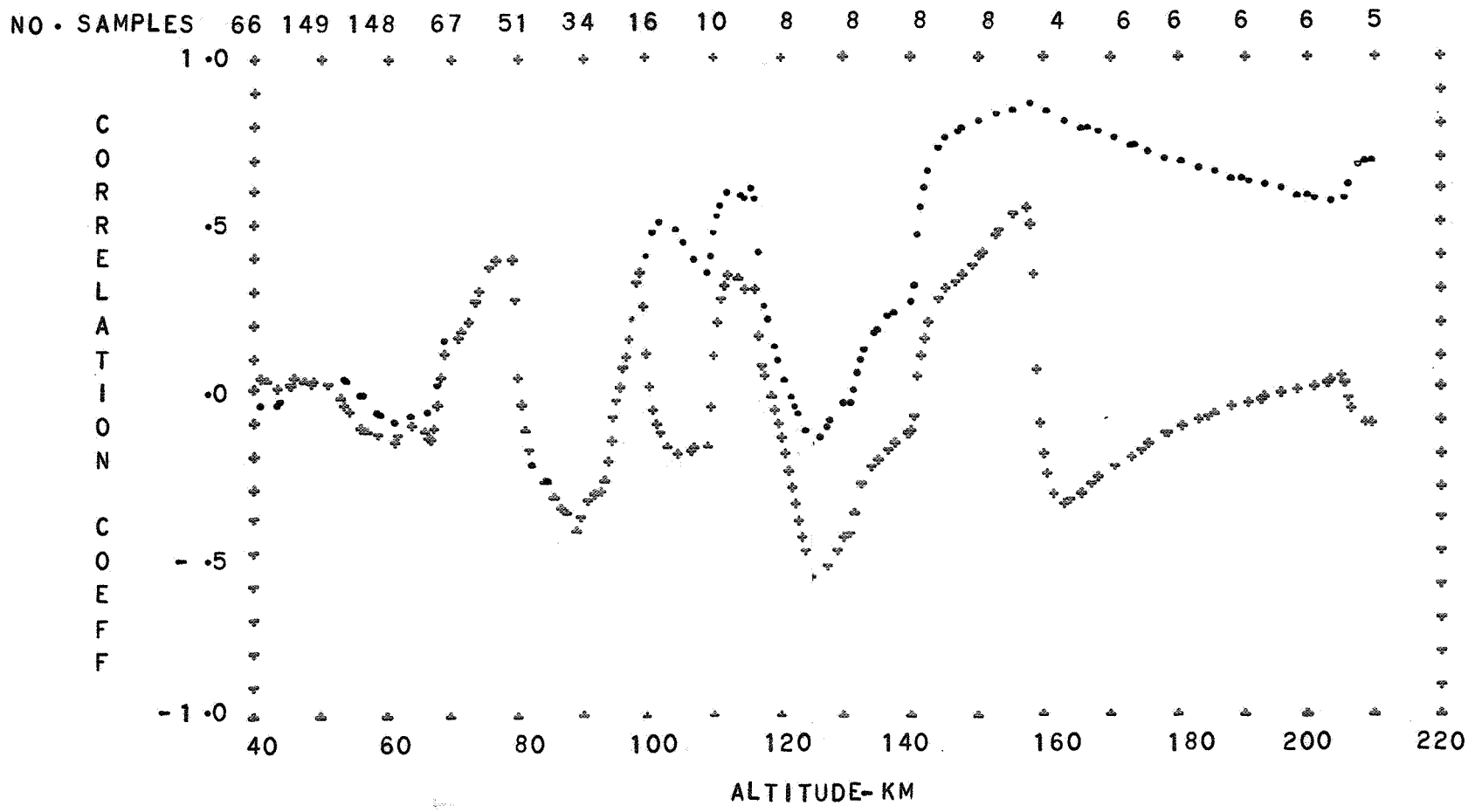

FIG. 49. CORRELATION OF DENSITY WITH SOLAR FLUX

SUBTROPICAL ANNUAL MEAN DIURNAL MEAN

SAME DAY--CROSSES PRECEEDING DAY--DOTS

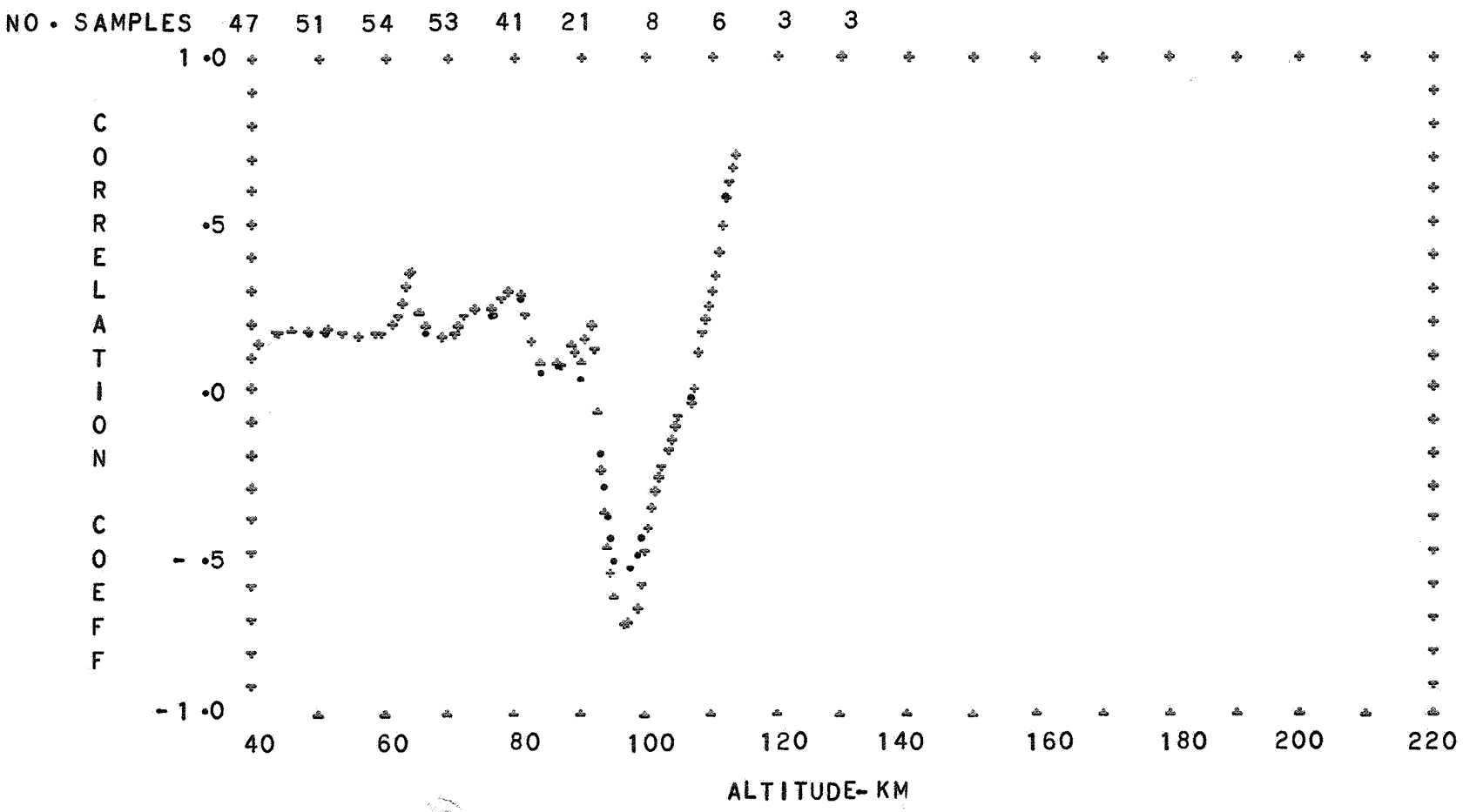

FIG. 50 CORRELATION OF DENSITY WITH SOLAR FLUX

MIDLATITUDE ANNUAL MEAN DIURNAL MEAN

SAME DAY--CROSSES PRECEEDING DAY--DOTS

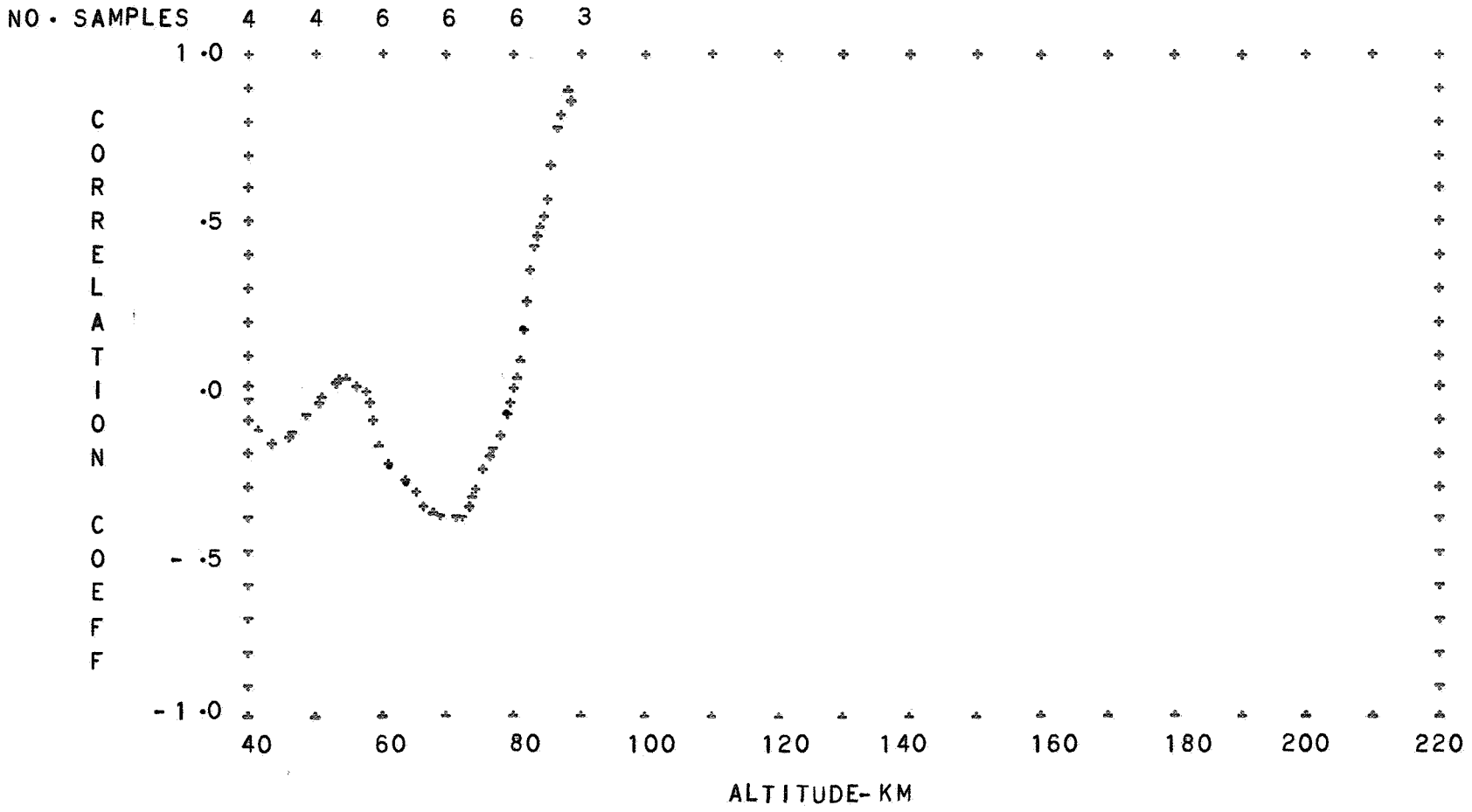

FIG. 51. CORRELATION OF DENSITY WITH SOLAR FLUX

SUBARCTIC SPRING DIURNAL TRANSITION

SAME DAY--CROSSES PRECEEDING DAY--DOTS

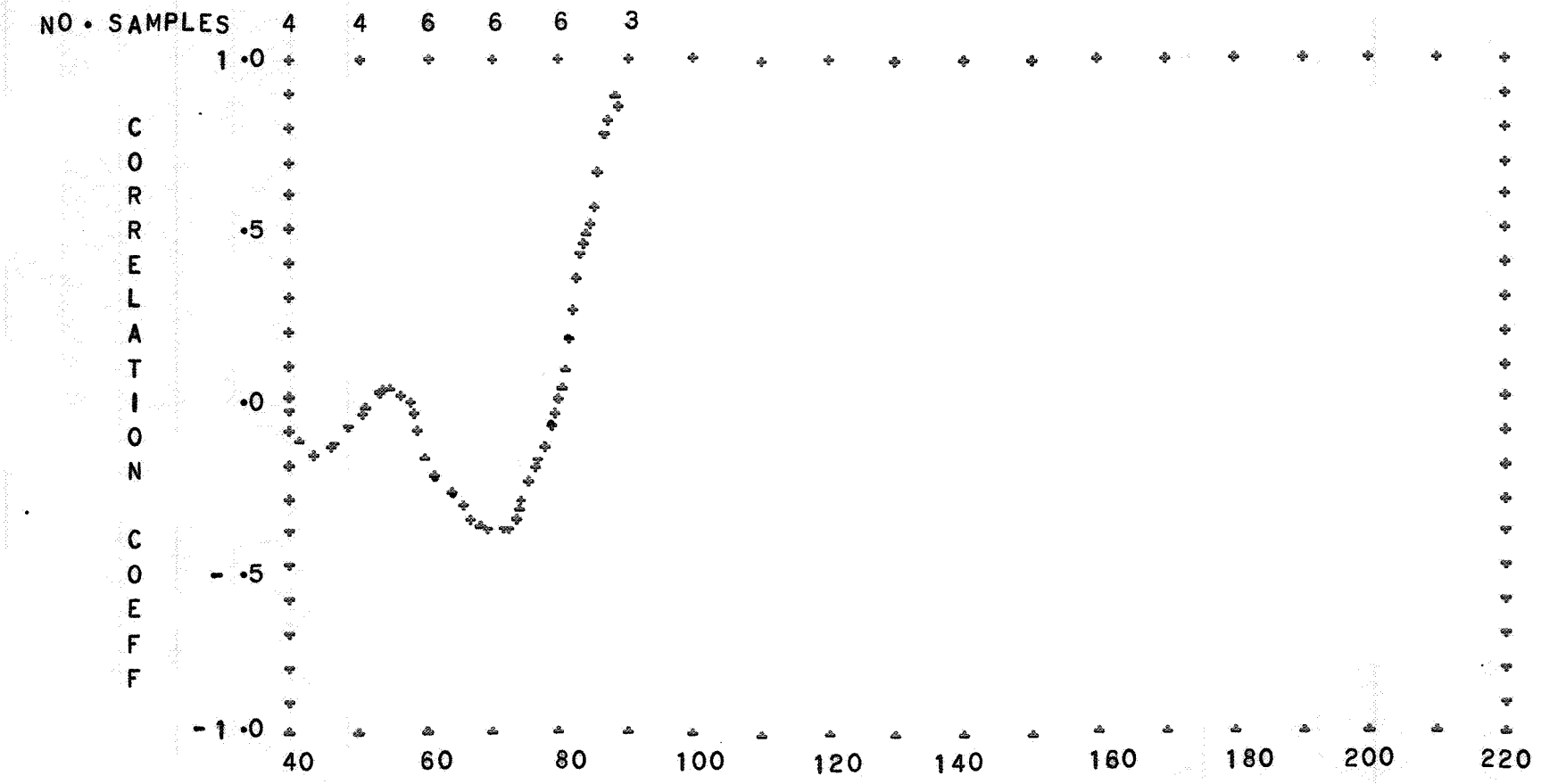

FIG. 52 CORRELATION OF DENSITY WITH SOLAR FLUX

SUBARCTIC SPRING DIURNAL MEAN

SAME DAY--CROSSES PRECEEDING DAY--DOTS

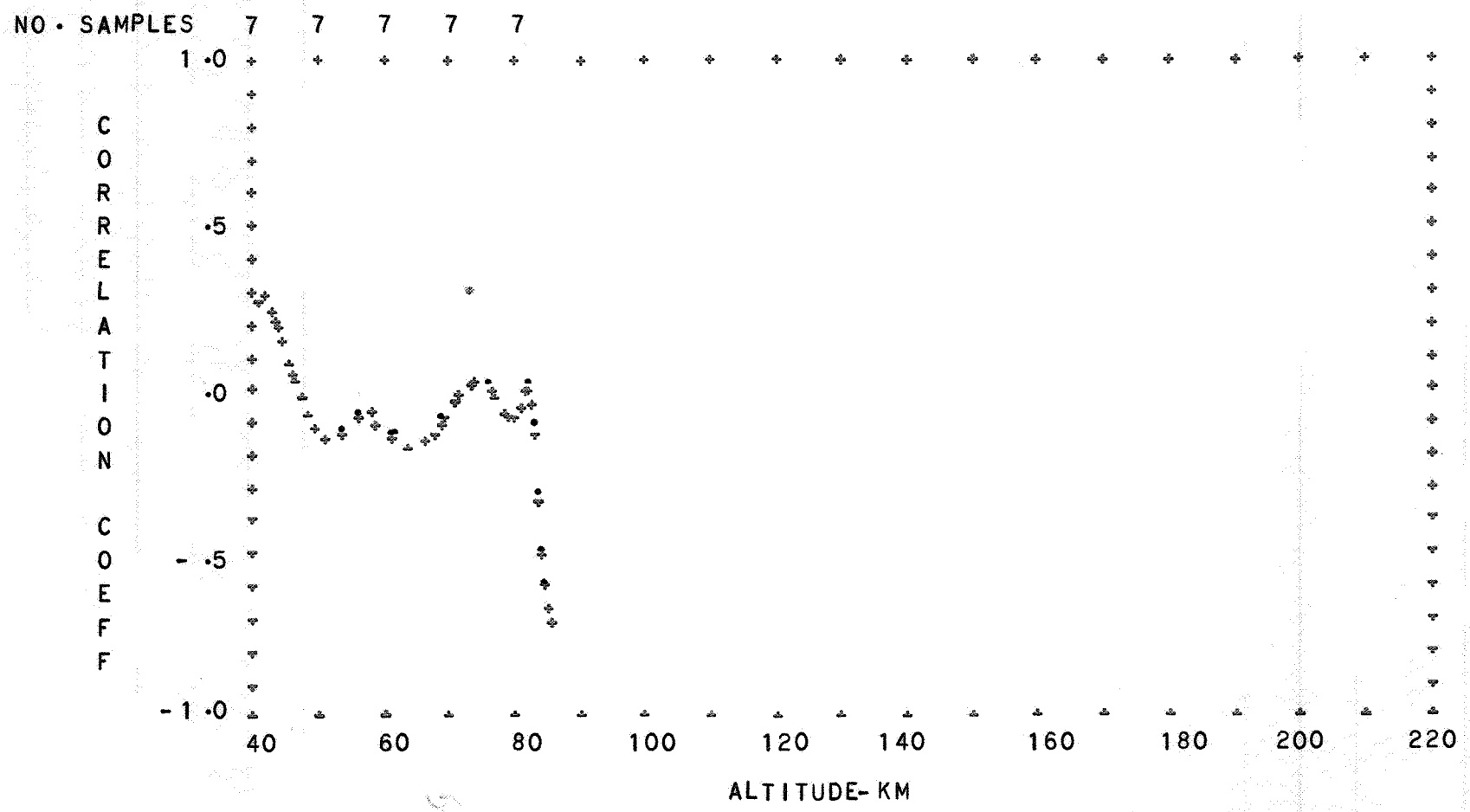

FIG. 53 CORRELATION OF DENSITY WITH SOLAR FLUX

SUBARCTIC SUMMER DIURNAL TRANSITION

SAME DAY--CROSSES PRECEEDING DAY--DOTS

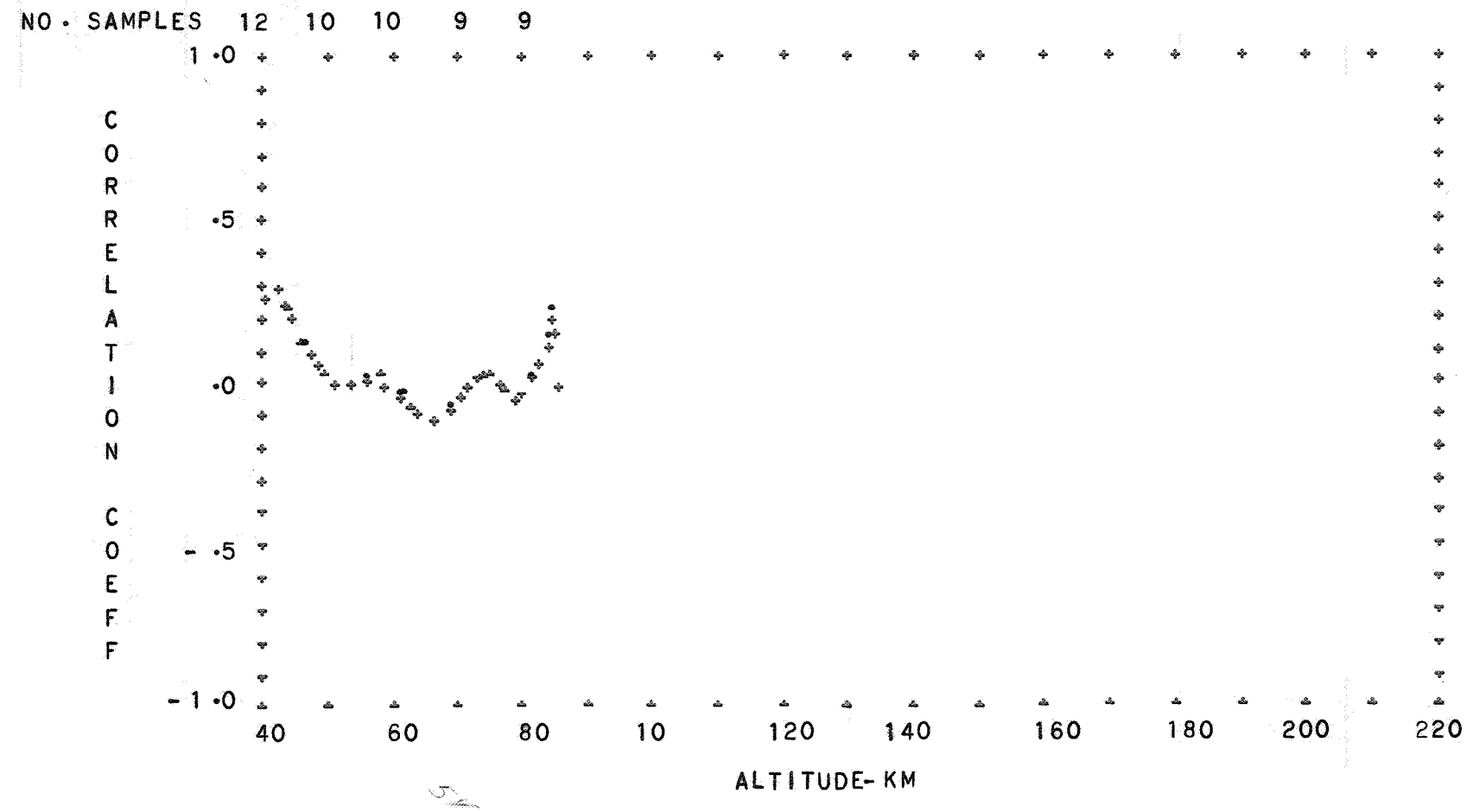

FIG. 54. CORRELATION OF DENSITY WITH SOLAR FLUX

SUBARCTIC SUMMER DIURNAL MEAN

SAME DAY--CROSSES PRECEEDING DAY--DOTS

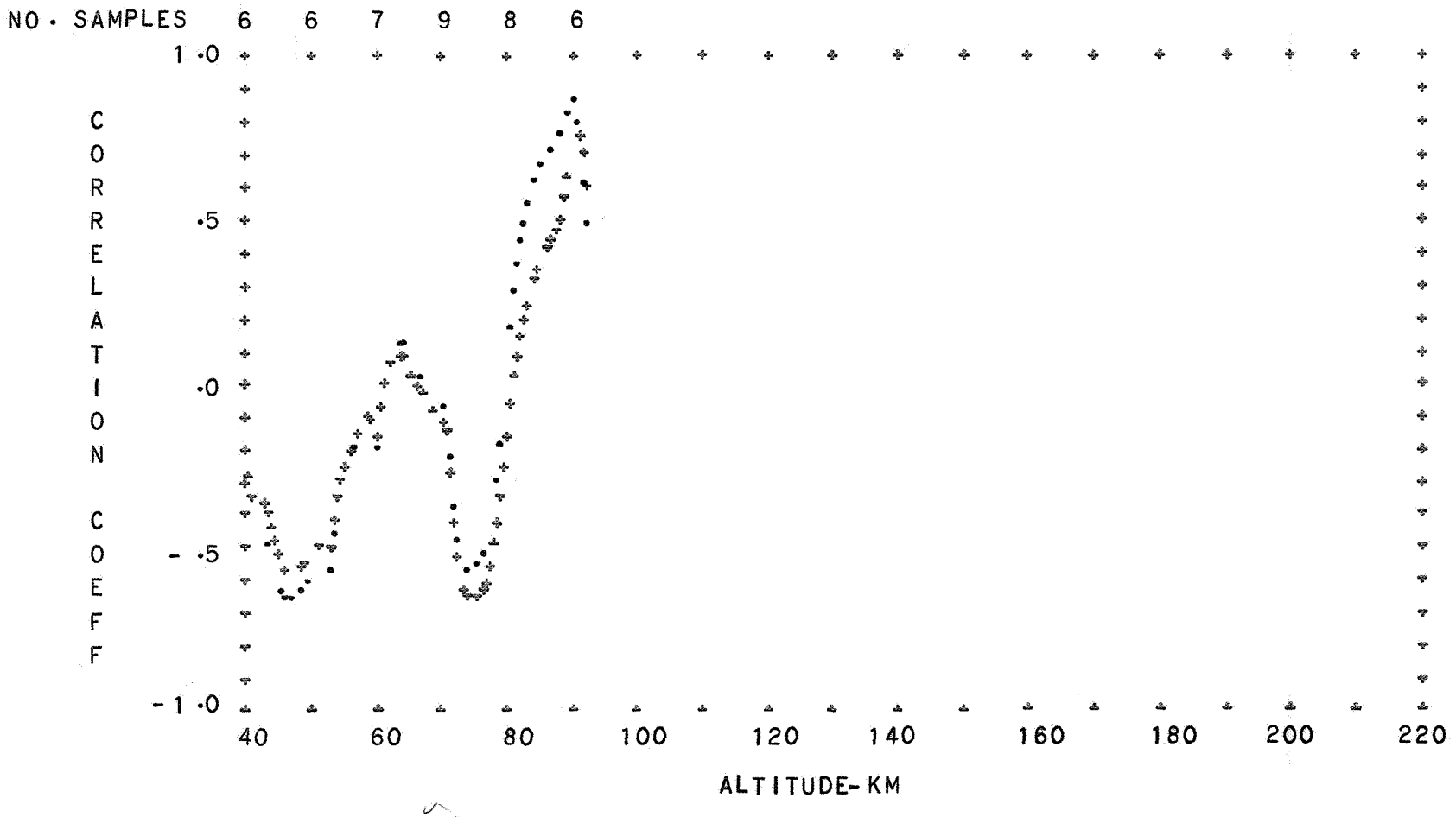

FIG. 55. CORRELATION OF DENSITY WITH SOLAR FLUX

SUBARCTIC AUTUMN DIURNAL TRANSITION

SAME DAY--CROSSES PRECEEDING DAY--DOTS

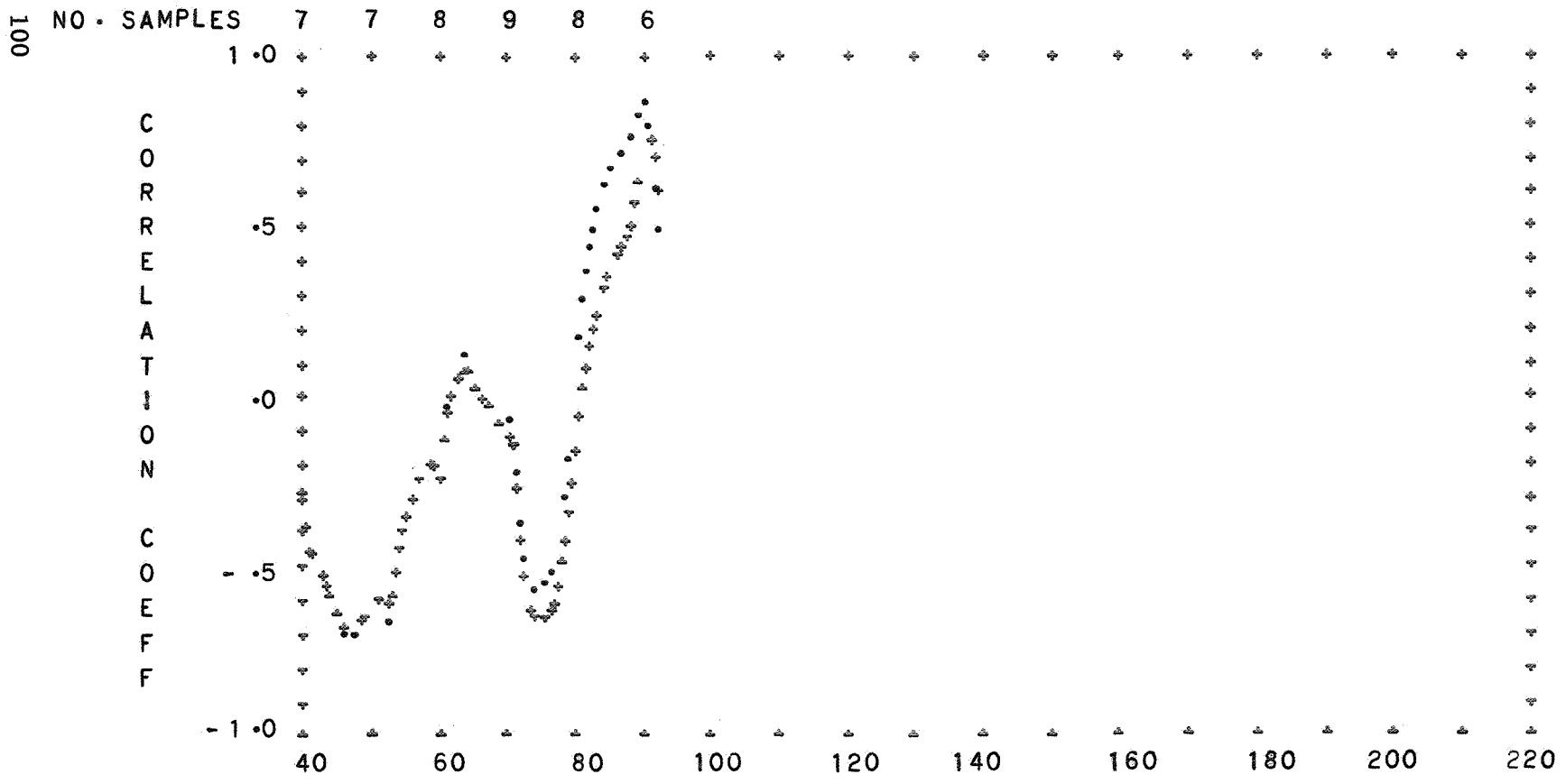

FIG. 56. CORRELATION OF DENSITY WITH SOLAR FLUX

SUBARCTIC AUTUMN DIURNAL MEAN

SAME DAY--CROSSES PRECEEDING DAY--DOTS

diurnal

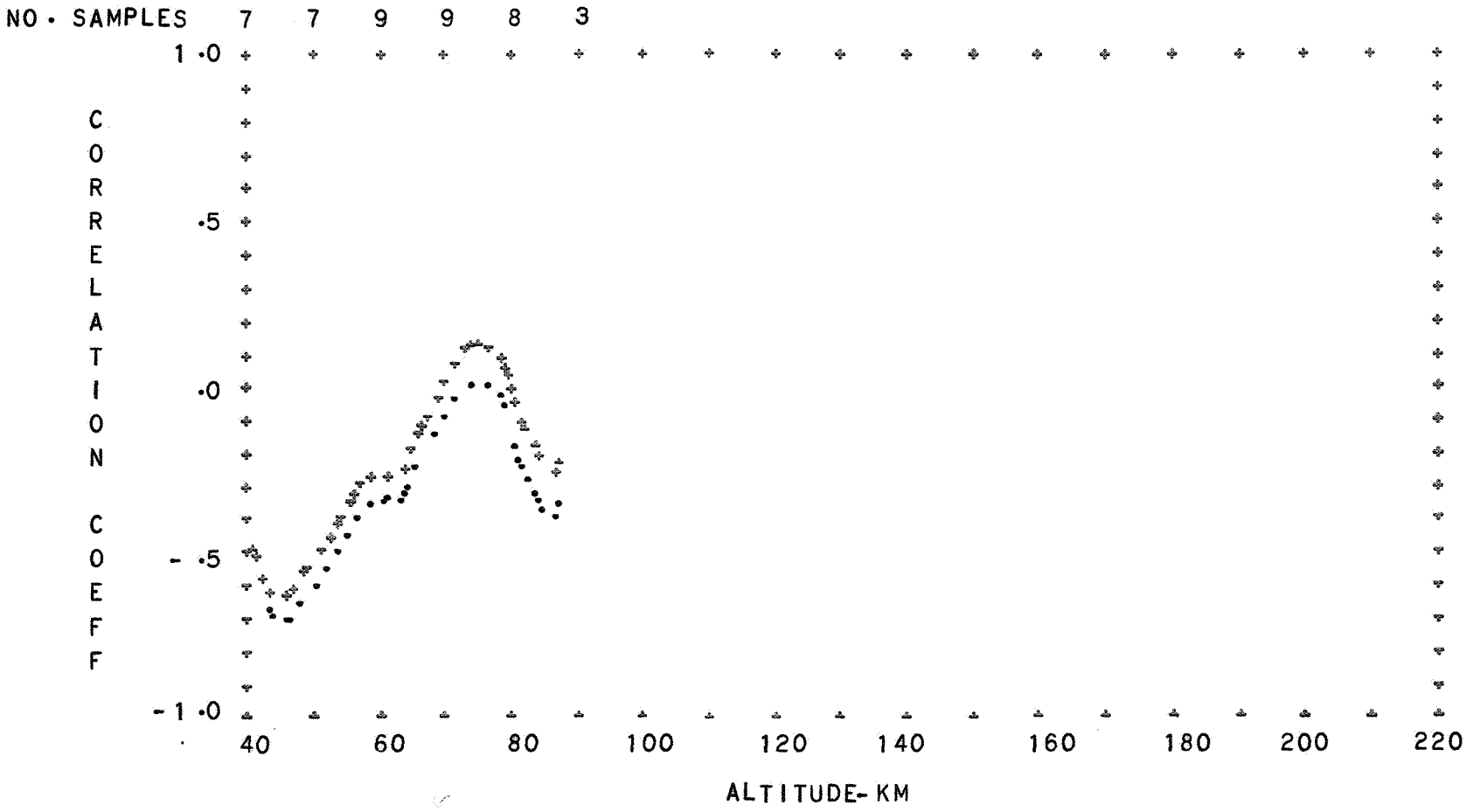

FIG. 57. CORRELATION OF DENSITY WITH SOLAR FLUX

SUBARCTIC WINTER DIURNAL TRANSITION

SAME DAY--CROSSES PRECEEDING DAY--DOTS

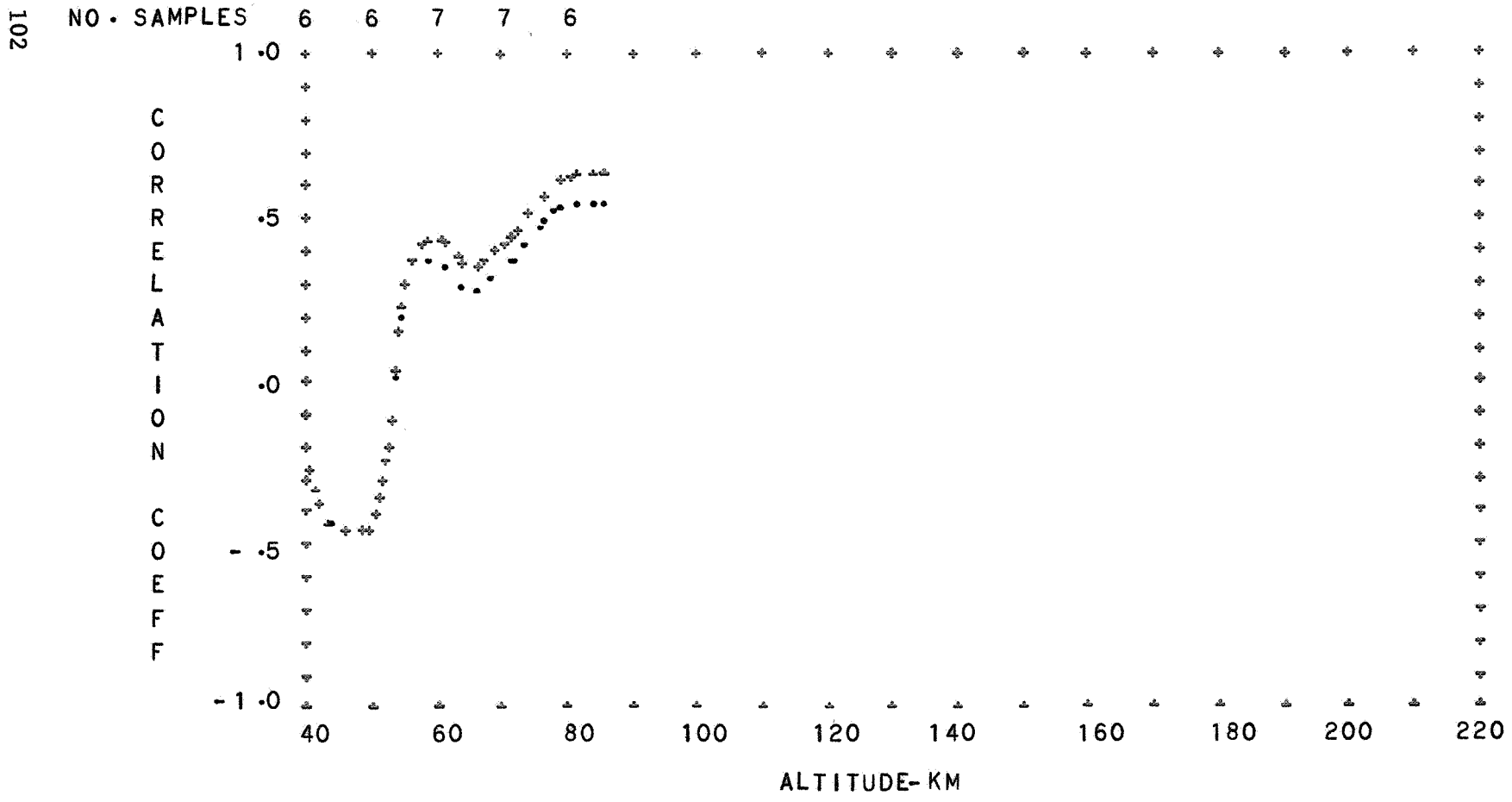

FIG. 58. CORRELATION OF DENSITY WITH SOLAR FLUX

SUBARCTIC WINTER NIGHTTIME

SAME DAY--CROSSES PRECEEDING DAY--DOTS

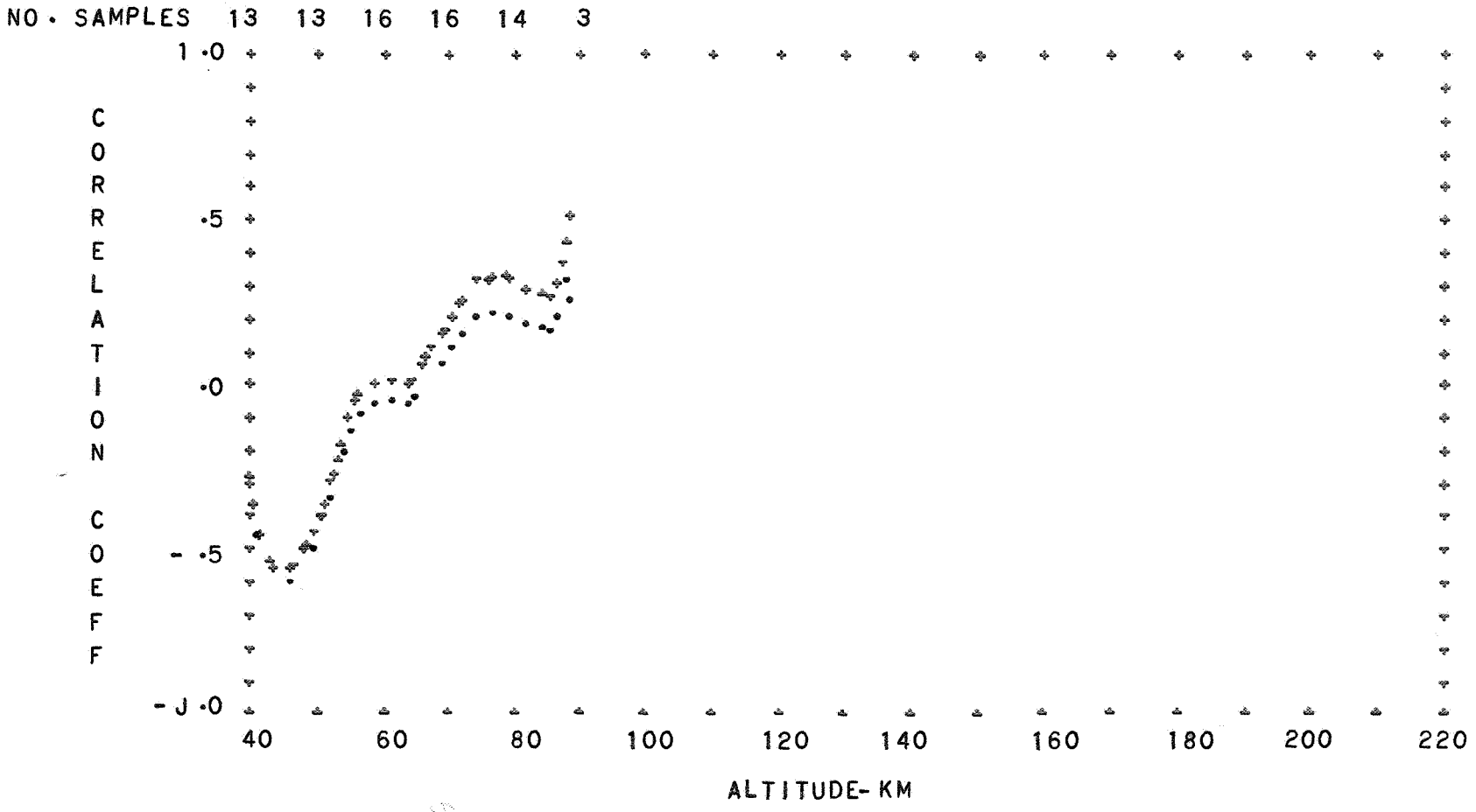

FIG. 59. CORRELATION OF DENSITY WITH SOLAR FLU

SUBARCTIC WINTER DIURNAL MEAN

SAME DAY--CROSSES PRECEEDING DAY--DOTS

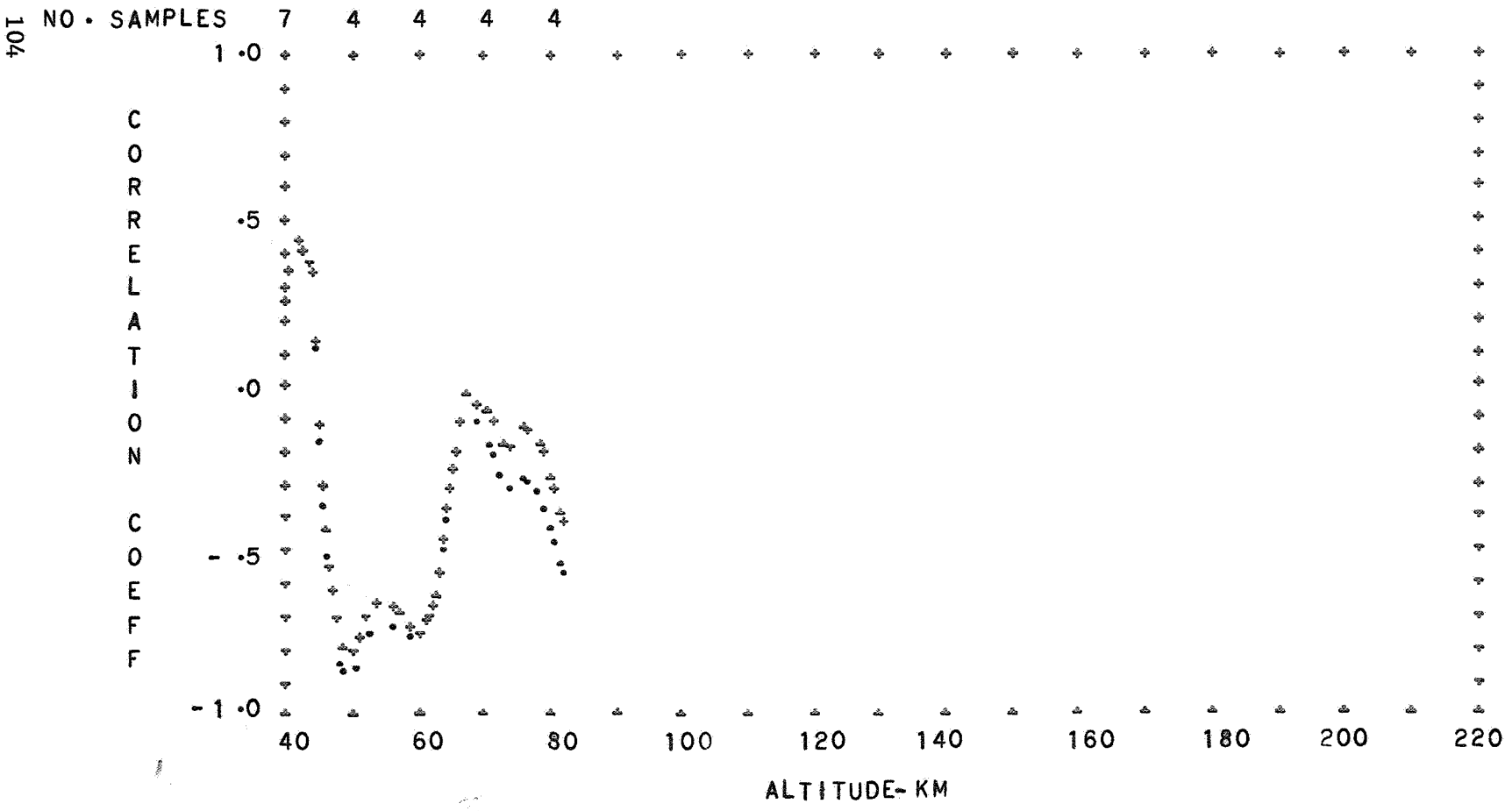

FIG. 60. CORRELATION OF DENSITY WITH SOLAR FLUX

SUBARCTIC SUMMER EXTREME DIURNAL MEAN

SAME DAY--CROSSES PRECEEDING DAY--DOTS

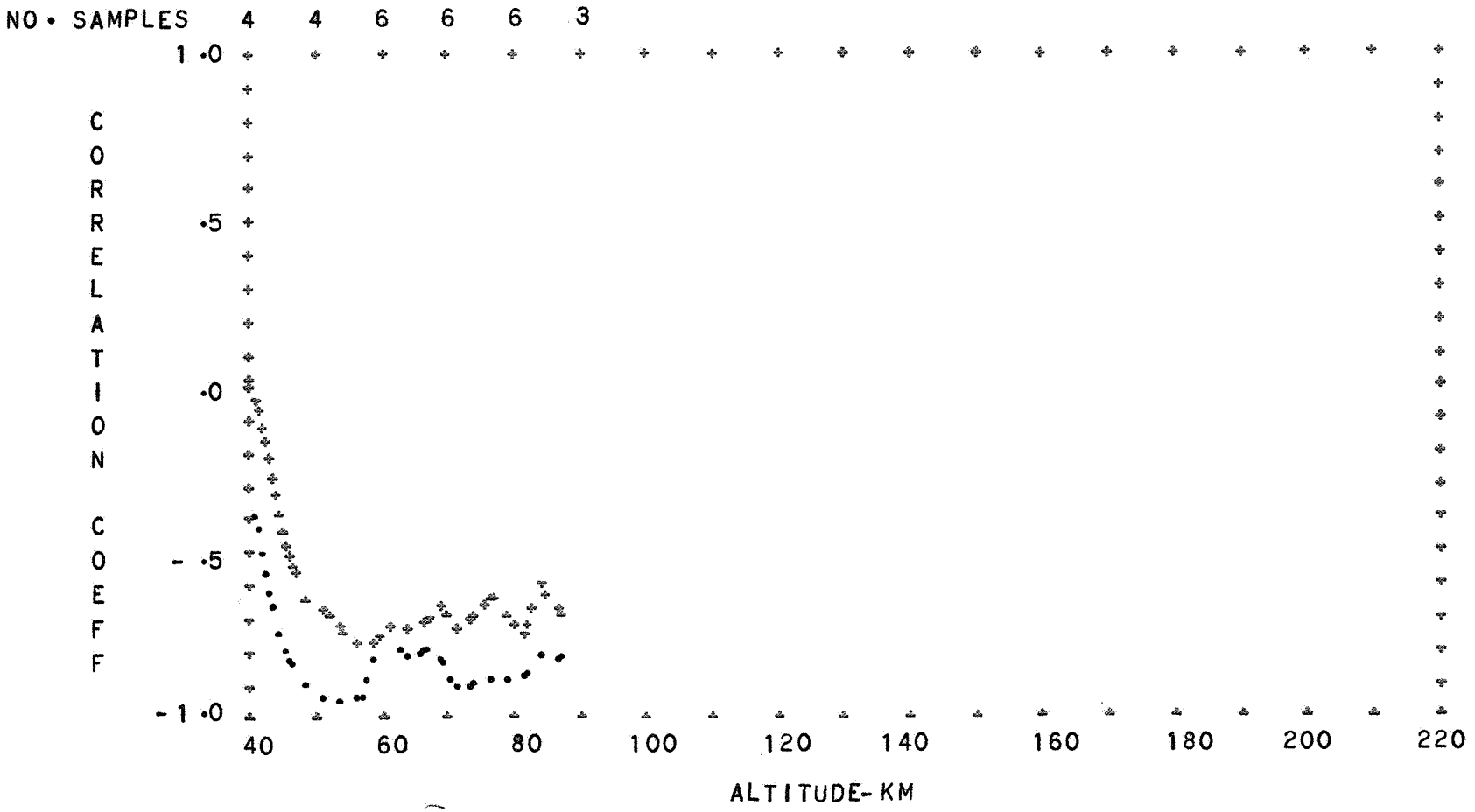

FIG. 61. CORRELATION OF DENSITY WITH SOLAR FLUX

SUBARCTIC WINTER EXTREME DIURNAL TRANSITION

SAME DAY--CROSSES PRECEEDING DAY--DOTS

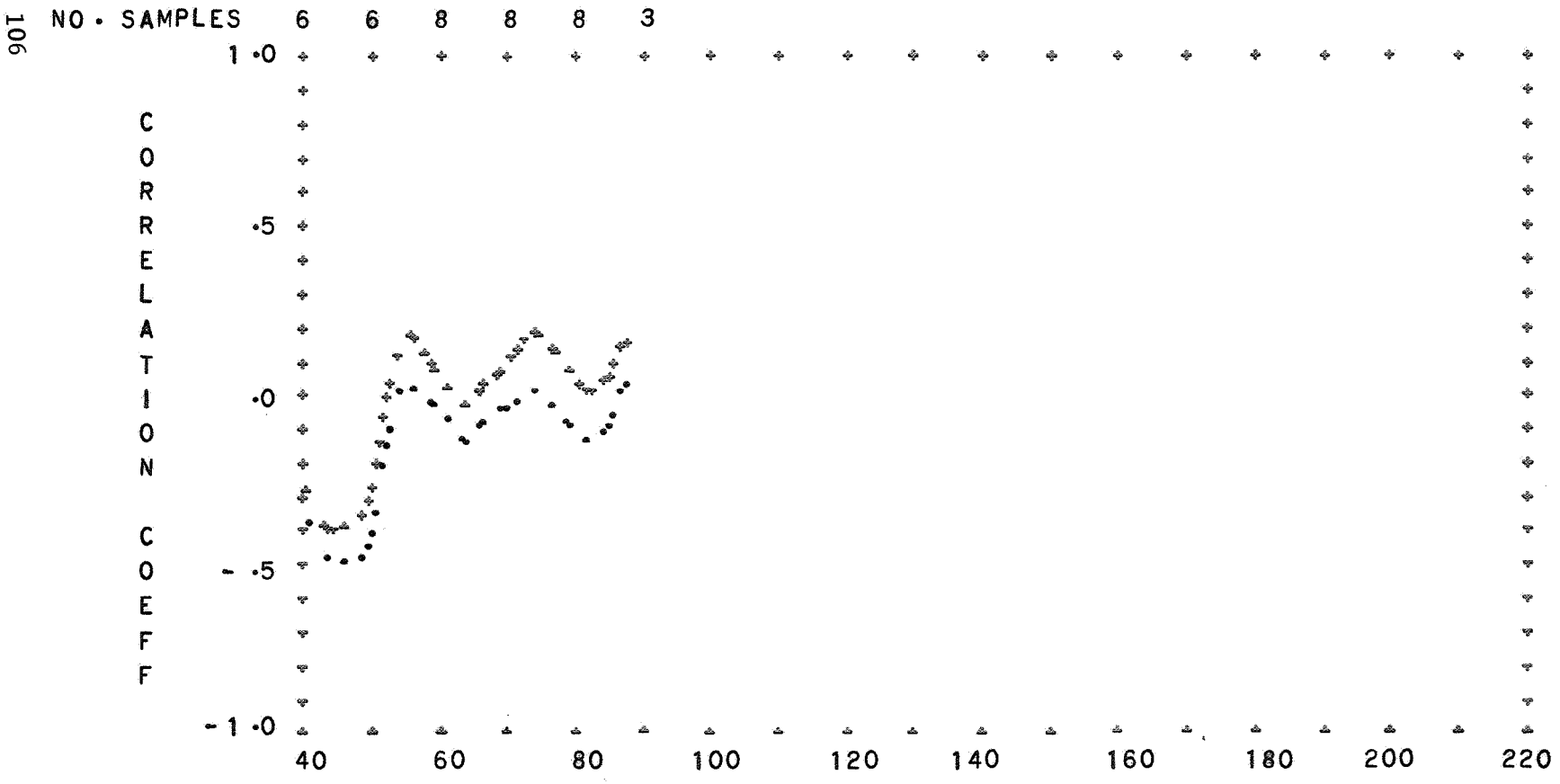

FIG. 62 CORRELATION OF DENSITY WITH SOLAR FLUX

SUBARCTIC WINTER EXTREME DIURNAL MEAN

SAME DAY--CROSSES PRECEEDING DAY--DOTS

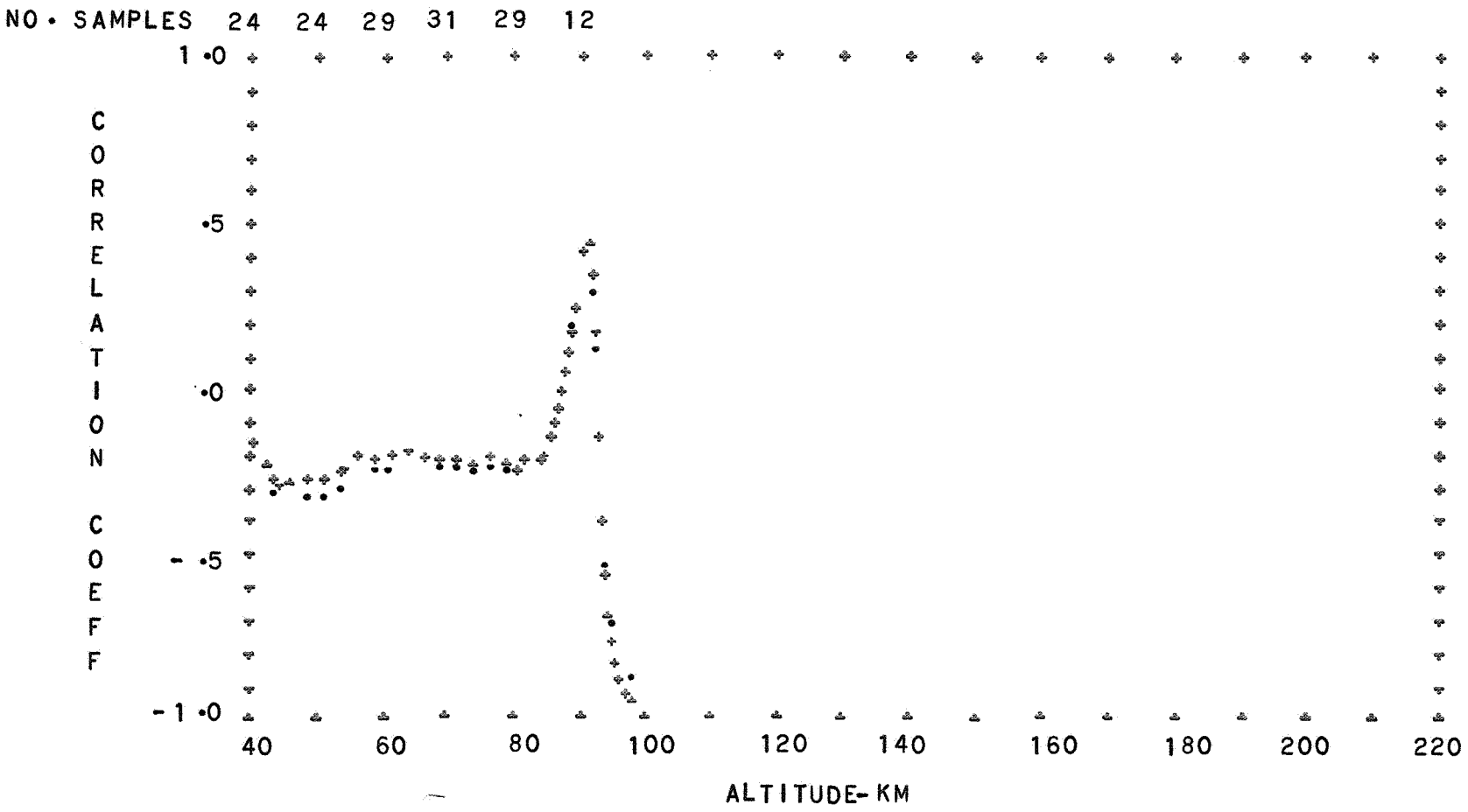

FIG. 63. CORRELATION OF DENSITY WITH SOLAR FLUX

SUBARCTIC ANNUAL MEAN DIURNAL TRANSITION

SAME DAY--CROSSES PRECEEDING DAY--DOTS

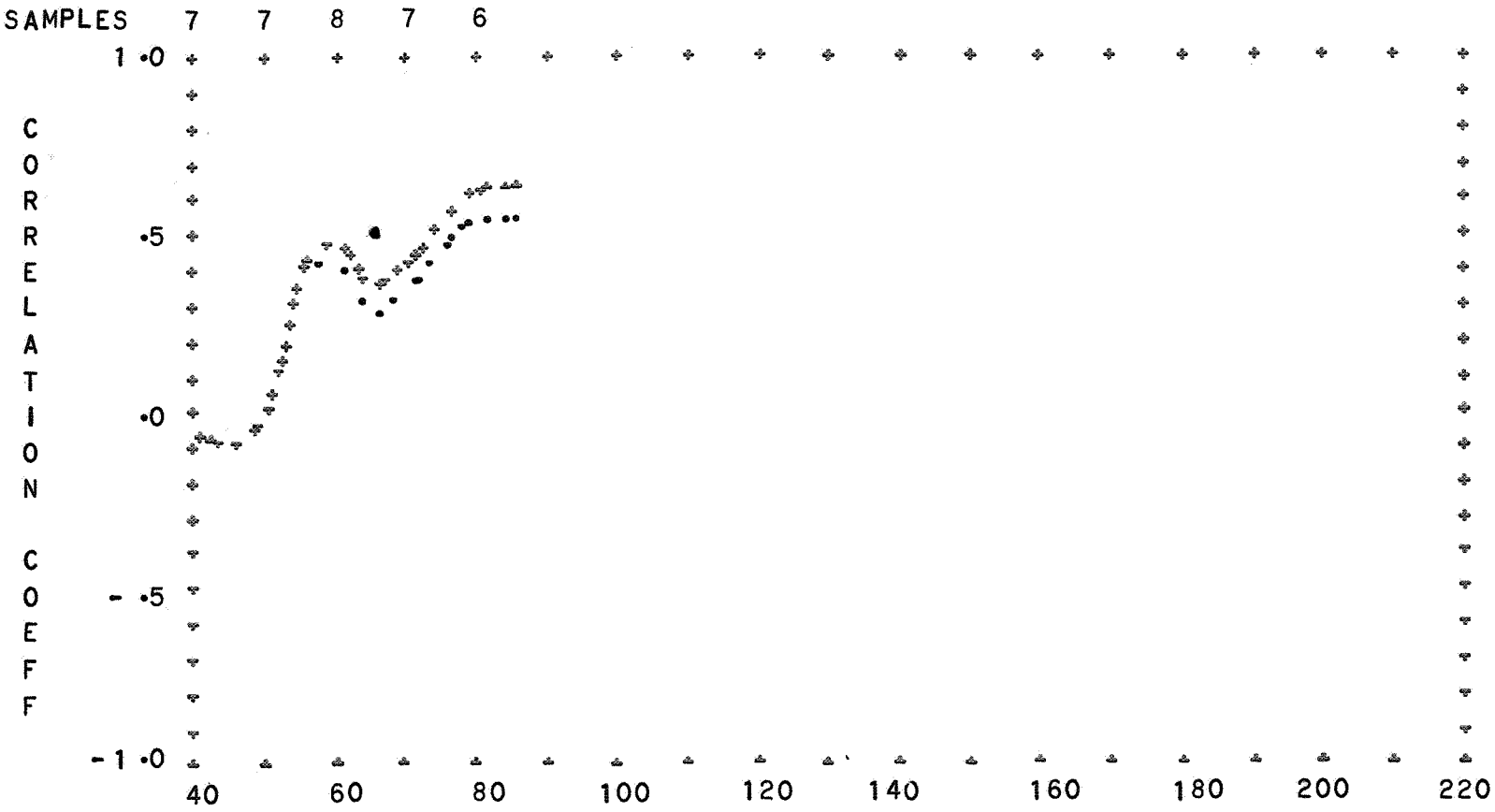

FIG. 64 CORRELATION OF DENSITY WITH SOLAR FLUX

SUBARCTIC ANNUAL MEAN NIGHTTIME

SAME DAY--CROSSES PRECEEDING DAY--DOTS

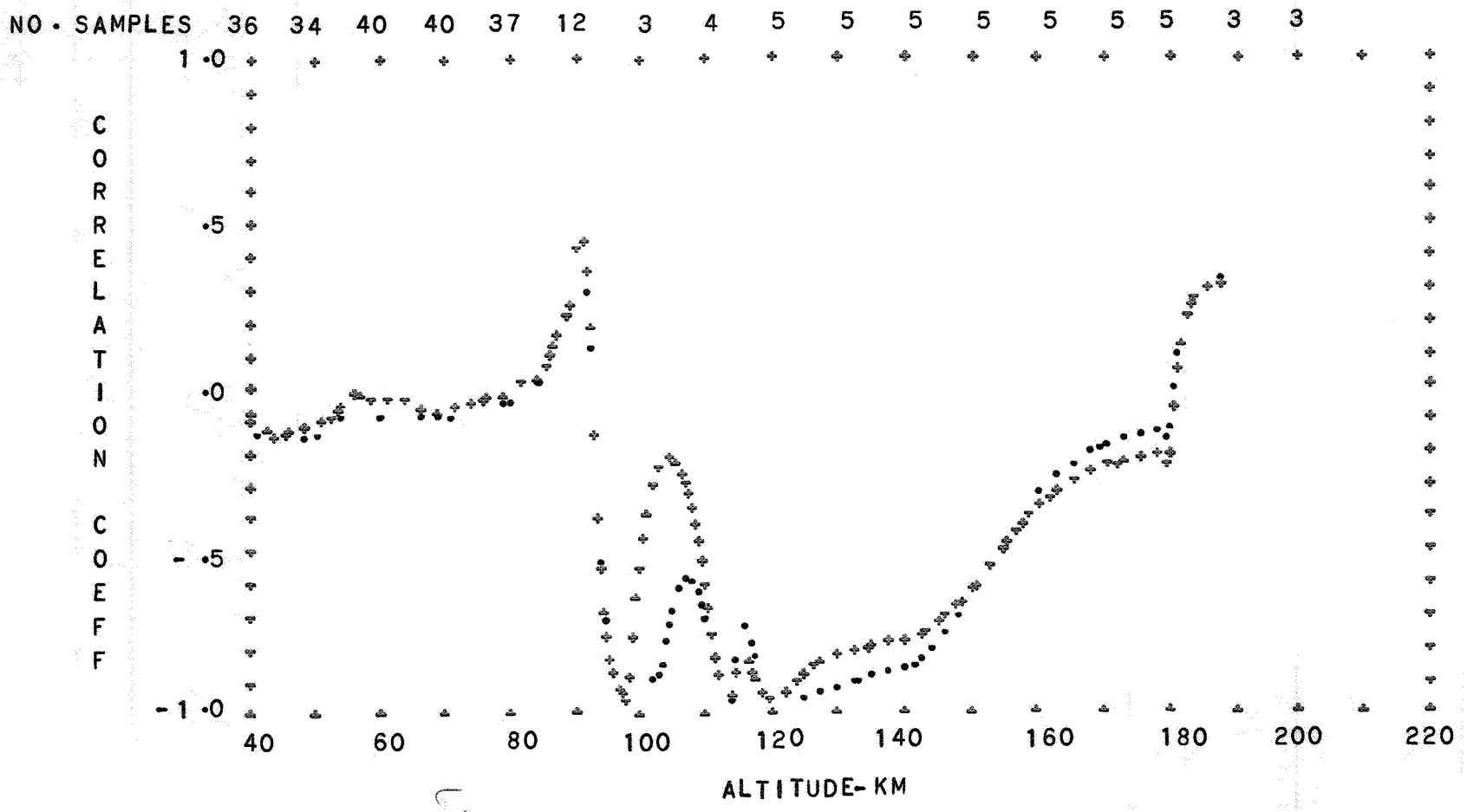

FIG. 65. CORRELATION OF DENSITY WITH SOLAR FLUX

SUBARCTIC ANNUAL MEAN DIURNAL MEAN

SAME DAY--CROSSES PRECEEDING DAY--DOTS

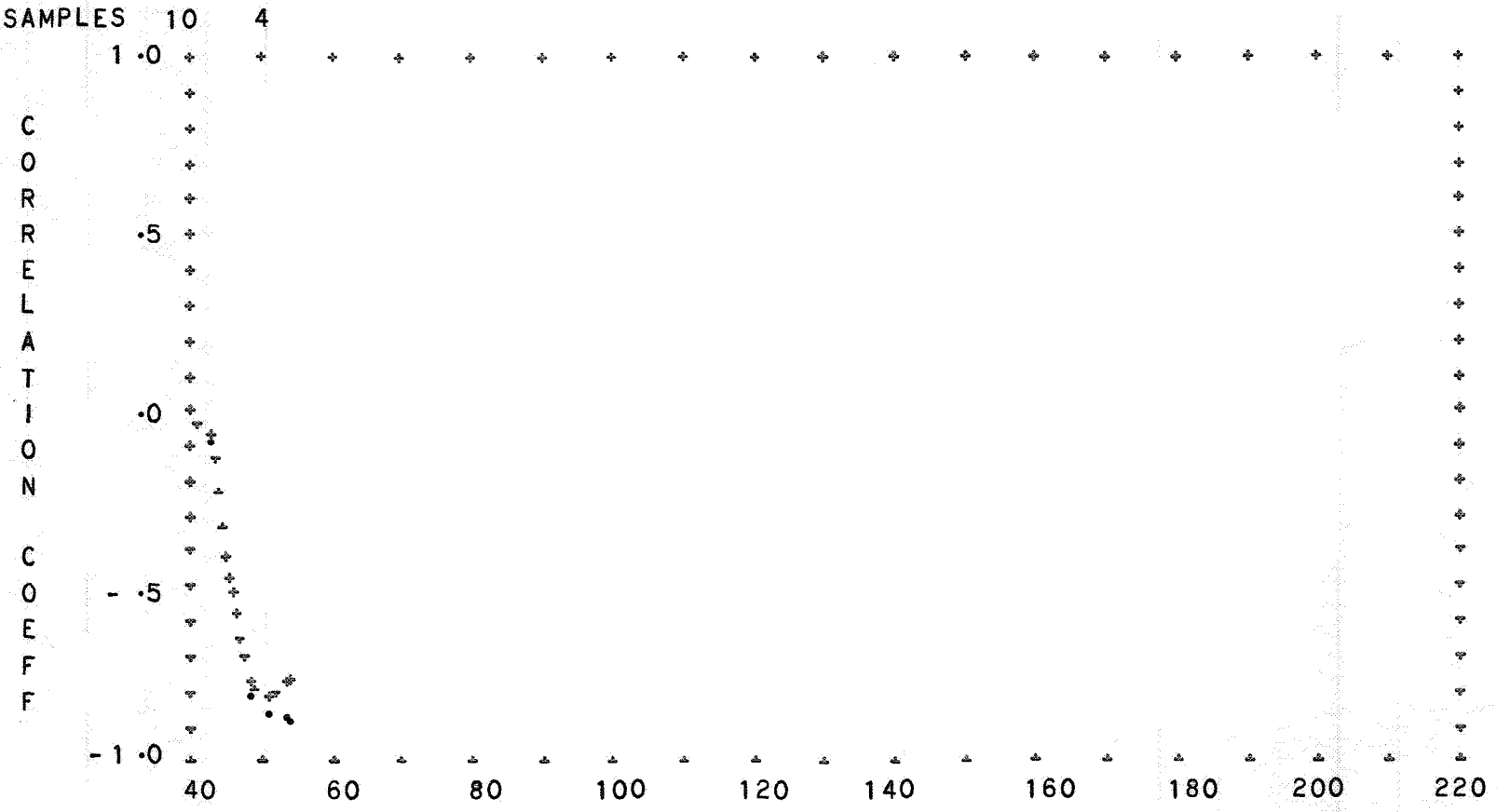

FIG. 66. CORRELATION OF DENSITY WITH SOLAR FLUX

ARCTIC SPRING DIURNAL TRANSITION

SAME DAY--CROSSES PRECEEDING DAY--DOTS

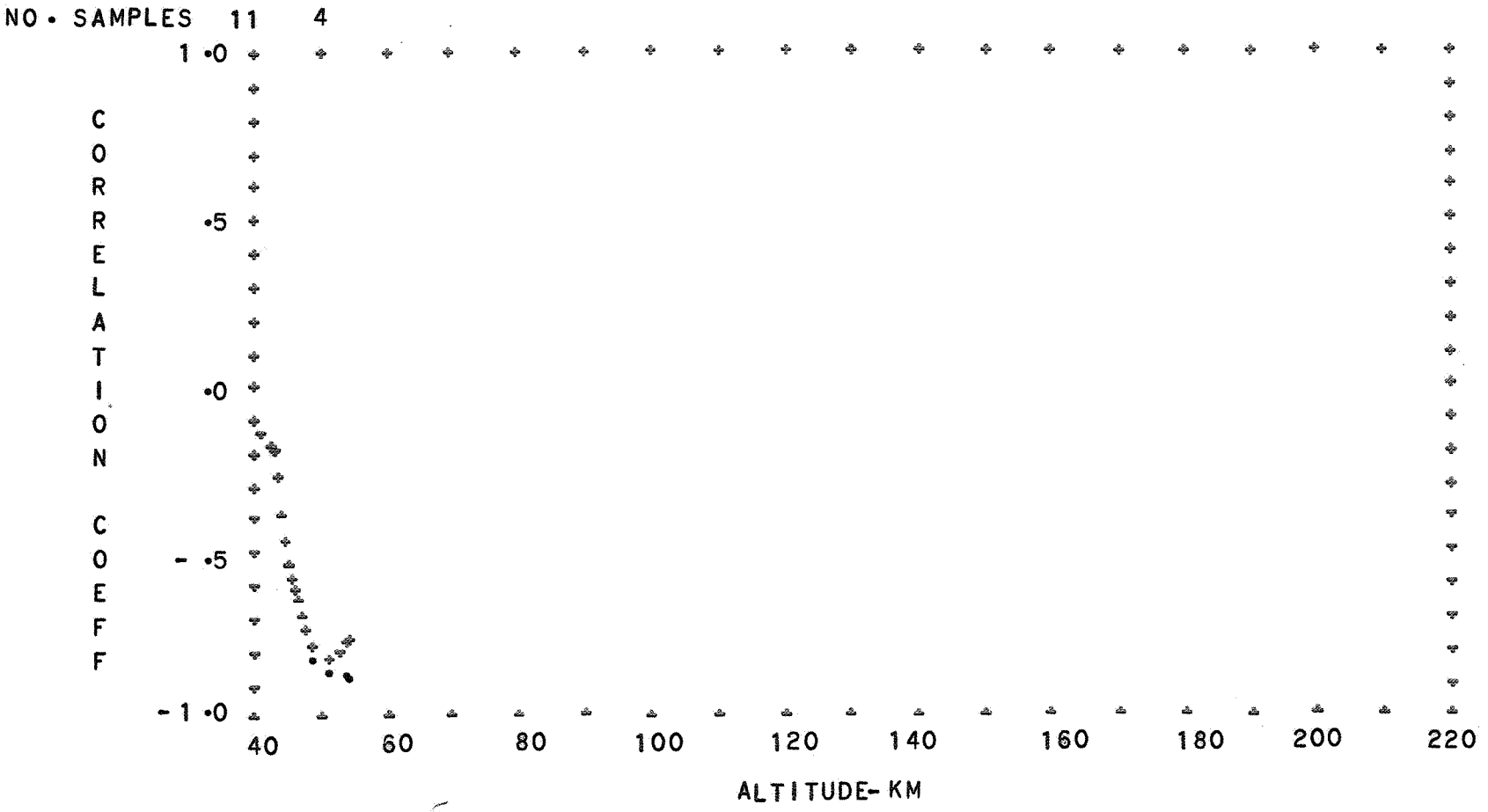

FIG. 67. CORRELATION OF DENSITY WITH SOLAR FLUX

ARCTIC SPRING DIURNAL MEAN

SAME DAY--CROSSES PRECEEDING DAY--DOTS

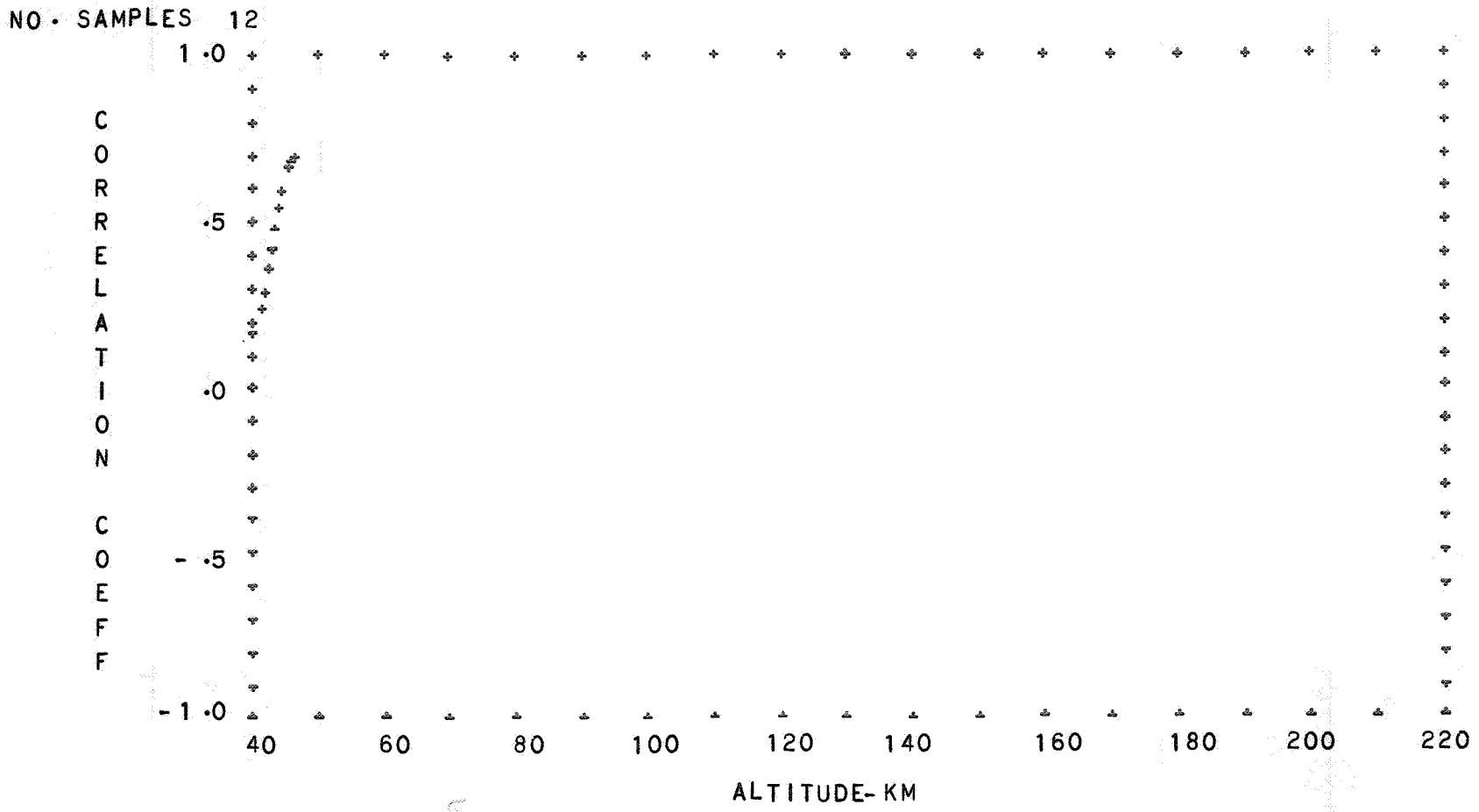

FIG. 68. CORRELATION OF DENSITY WITH SOLAR FLUX

ARCTIC SUMMER DIURNAL TRANSITION

SAME DAY--CROSSES PRECEEDING DAY--DOTS

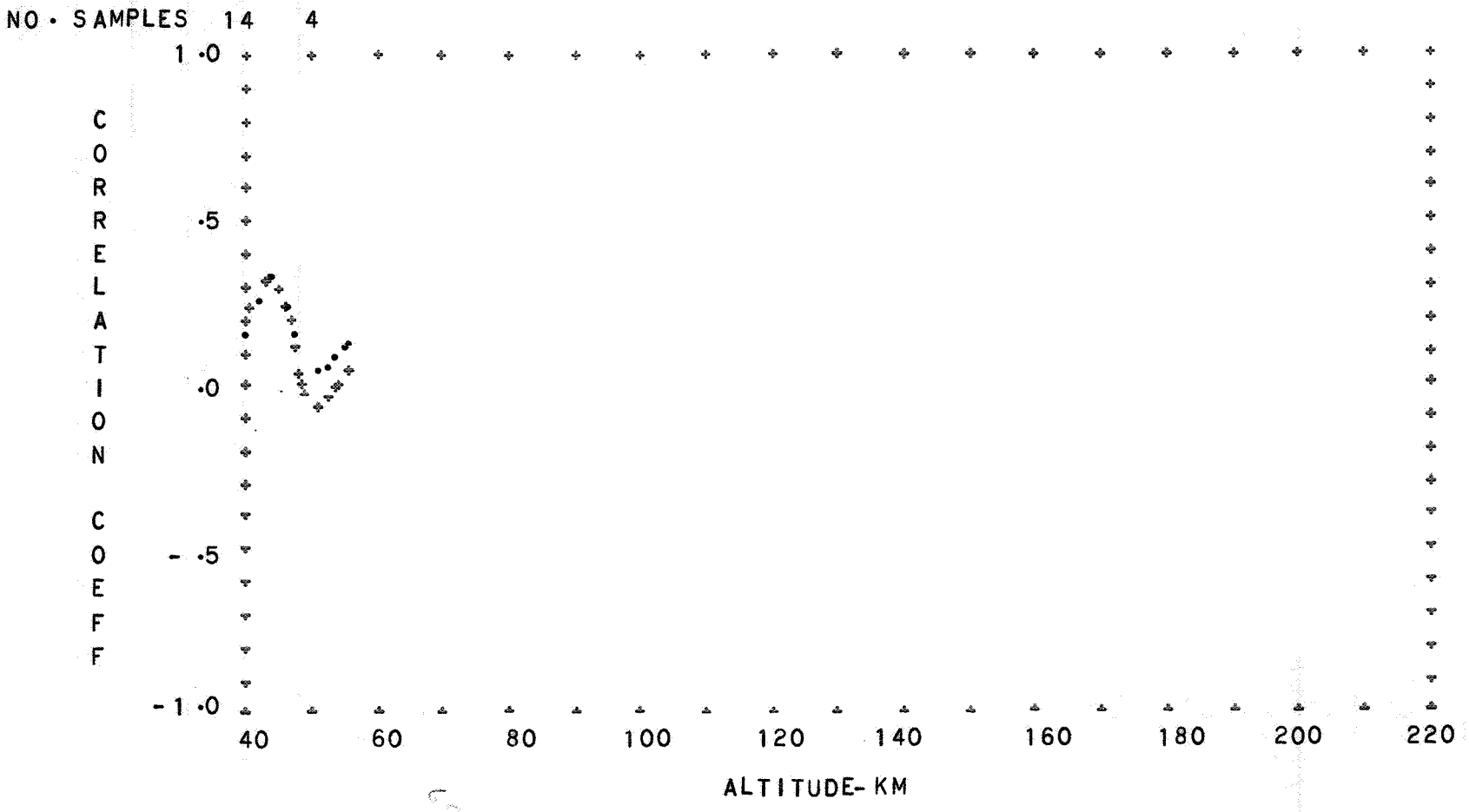

FIG. 69. CORRELATION OF DENSITY WITH SOLAR FLUX

ARCTIC WINTER HALF DIURNAL TRANSITION

SAME DAY--CROSSES PRECEEDING DAY--DOTS

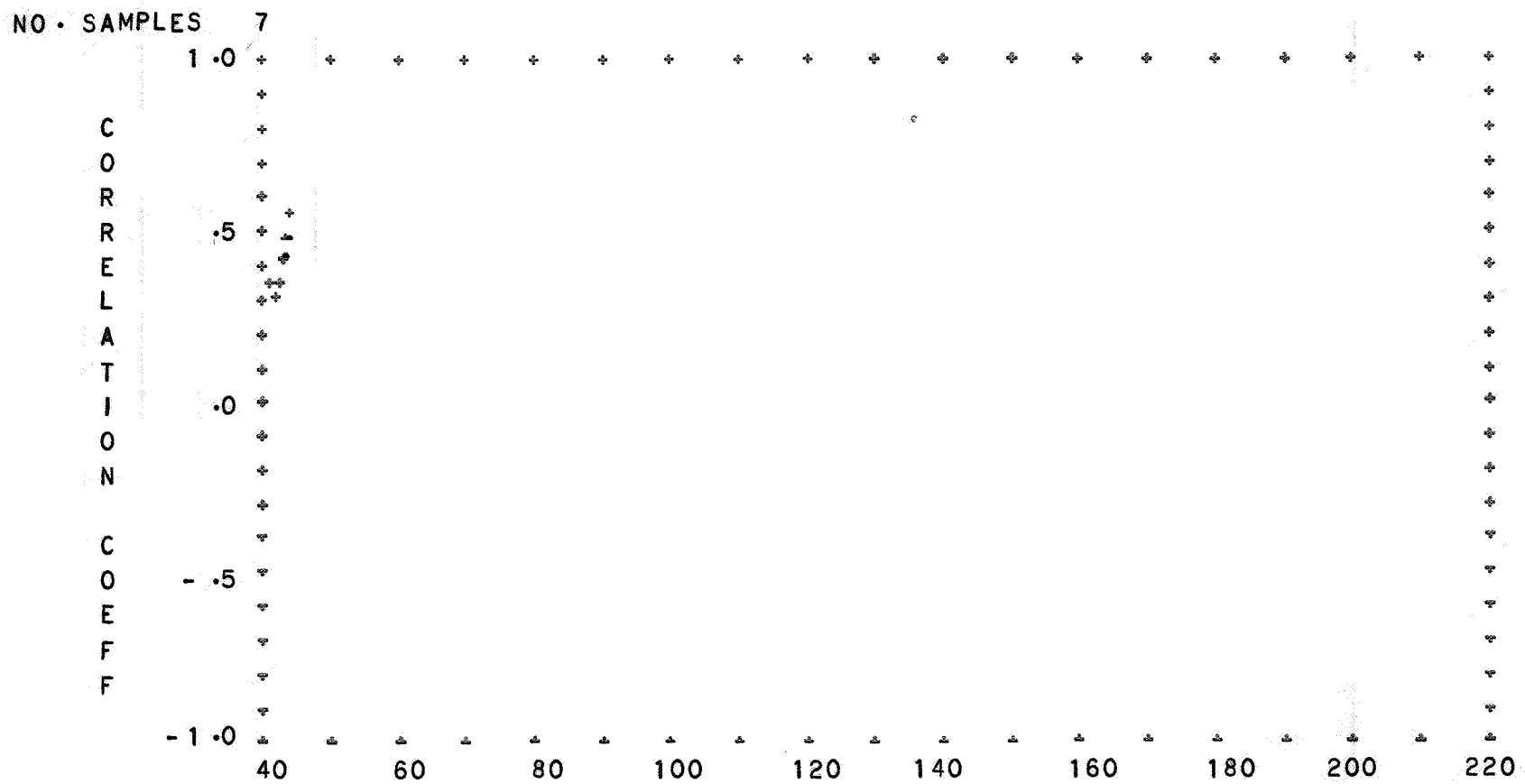

FIG. 70. CORRELATION OF DENSITY WITH SOLAR FLUX

ARCTIC WINTER HALF NIGHTTIME

SAME DAY--CROSSES PRECEEDING DAY--DOTS

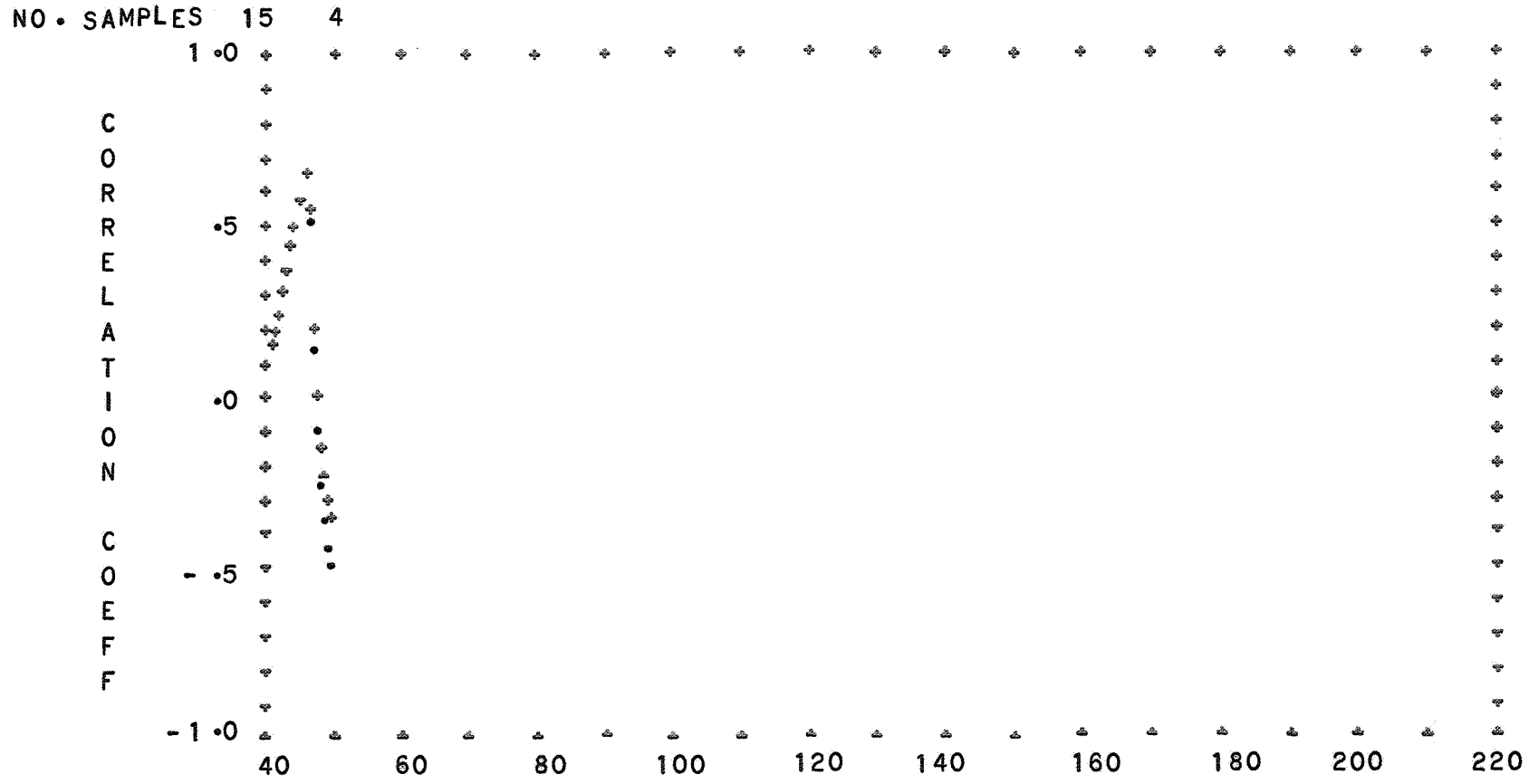

FIG. 71. CORRELATION OF DENSITY WITH SOLAR FLUX

ARCTIC SUMMER DIURNAL MEAN

SAME DAY--CROSSES PRECEEDING DAY--DOTS

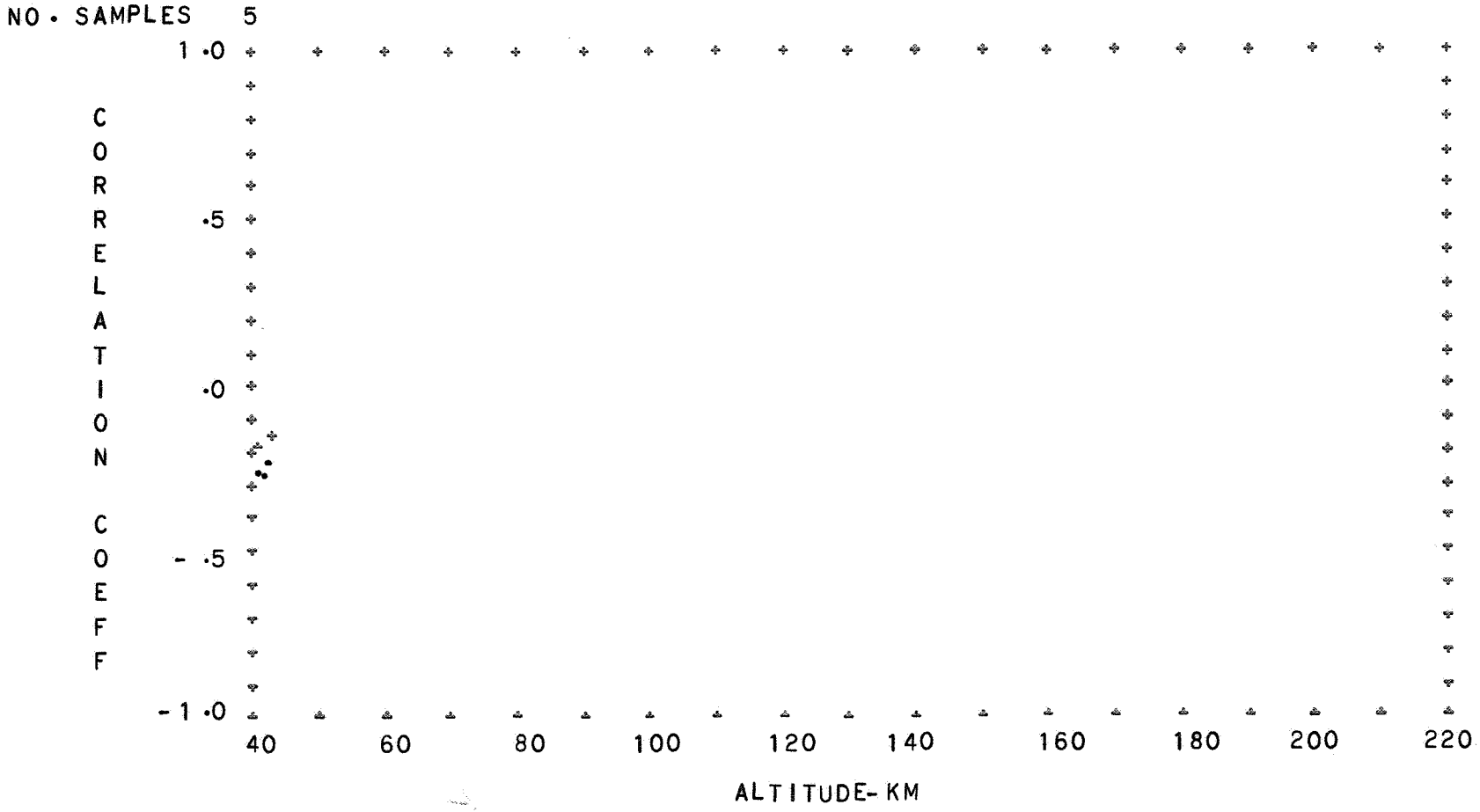

FIG. 72. CORRELATION OF DENSITY WITH SOLAR FLUX

ARCTIC AUTUMN DIURNAL TRANSITION

SAME DAY--CROSSES PRECEEDING DAY--DOTS

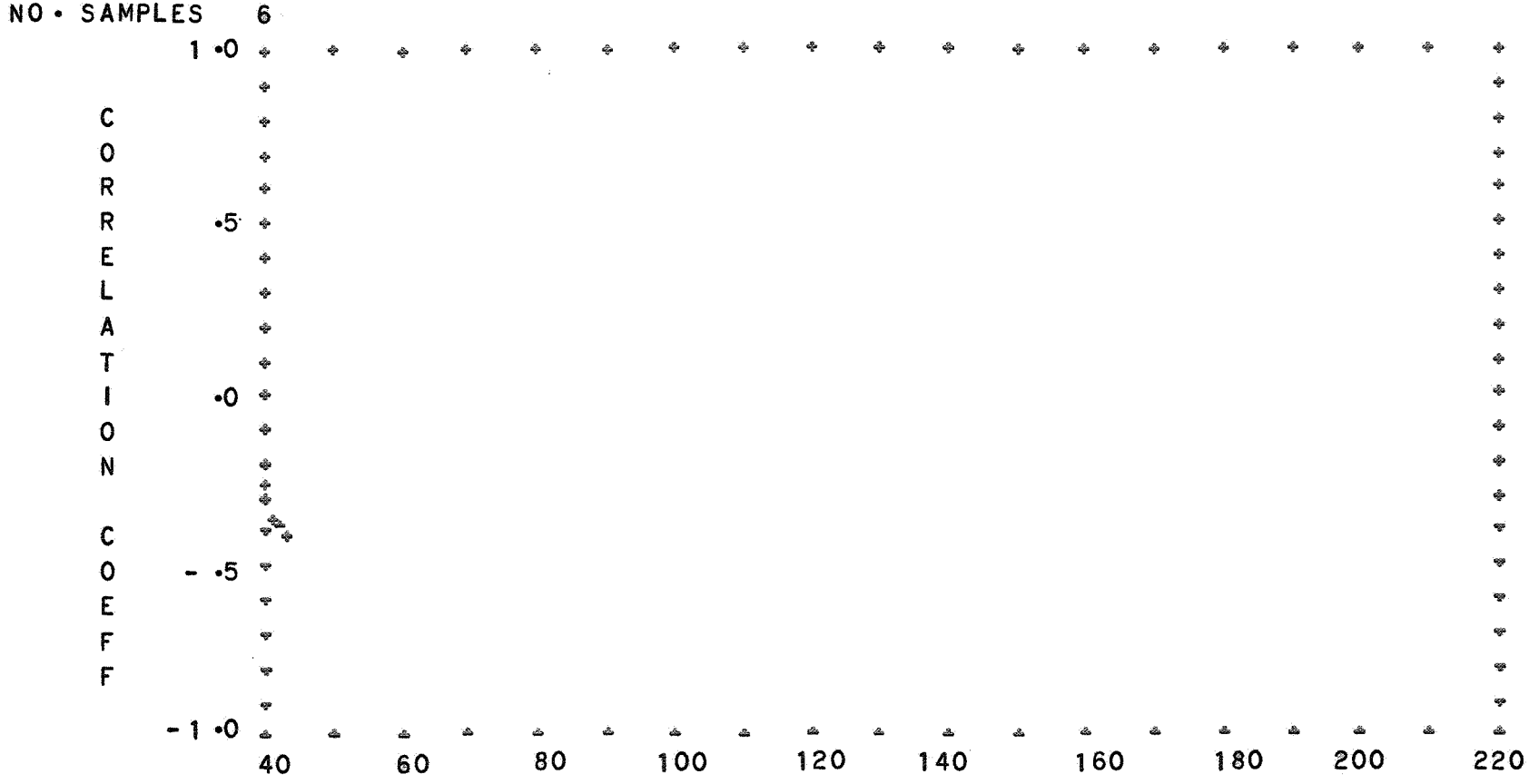

FIG. 73. CORRELATION OF DENSITY WITH SOLAR FLUX

ARCTIC AUTUMN DIURNAL MEAN

SAME DAY--CROSSES PRECEEDING DAY--DOTS

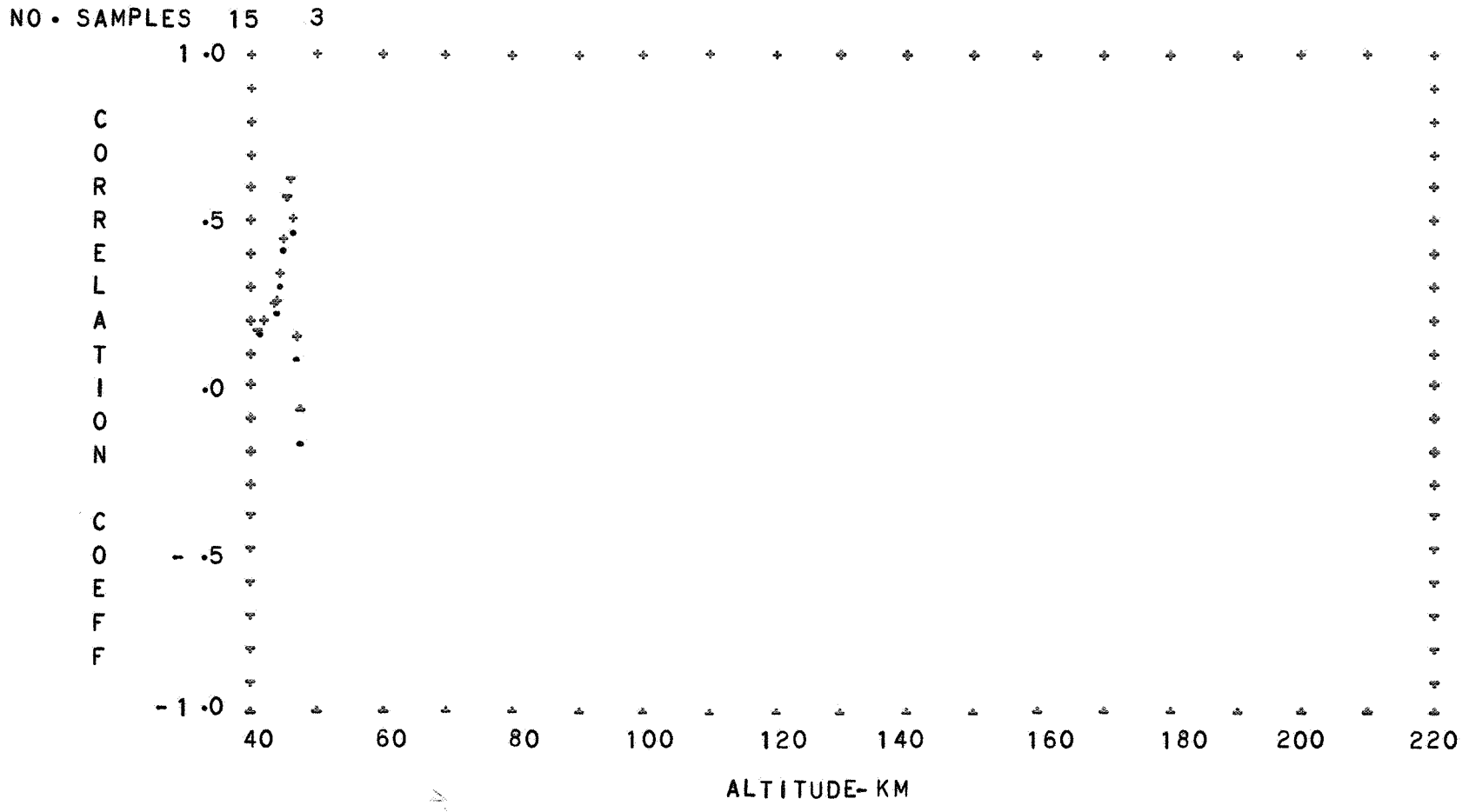

FIG. 74. CORRELATION OF DENSITY WITH SOLAR FLUX

ARCTIC SUMMER HALF DIURNAL TRANSITION

SAME DAY--CROSSES PRECEEDING DAY--DOTS

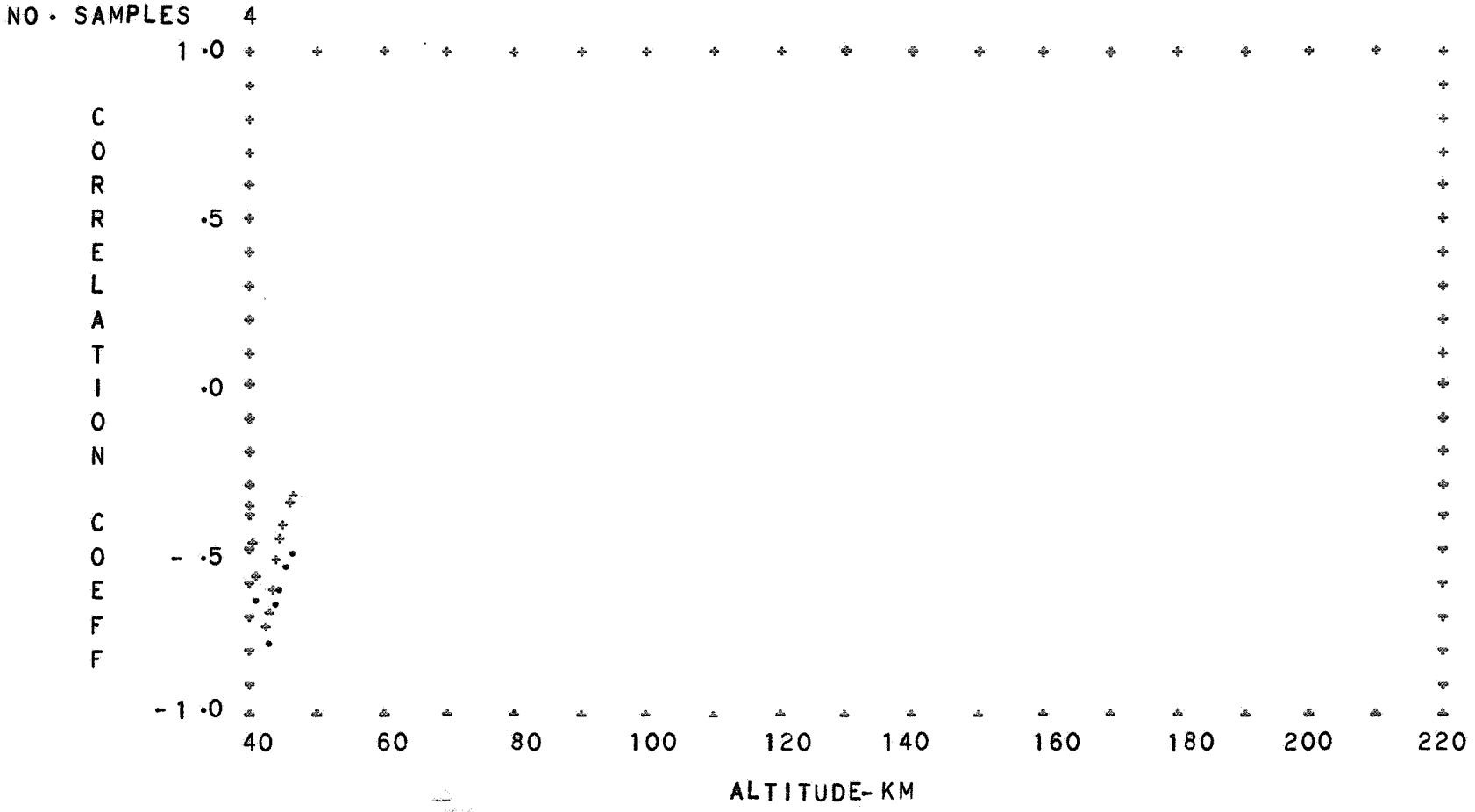

FIG. 75. CORRELATION OF DENSITY WITH SOLAR FLUX

ARCTIC SUMMER HALF DAYTIME

SAME DAY--CROSSES PRECEEDING DAY--DOTS

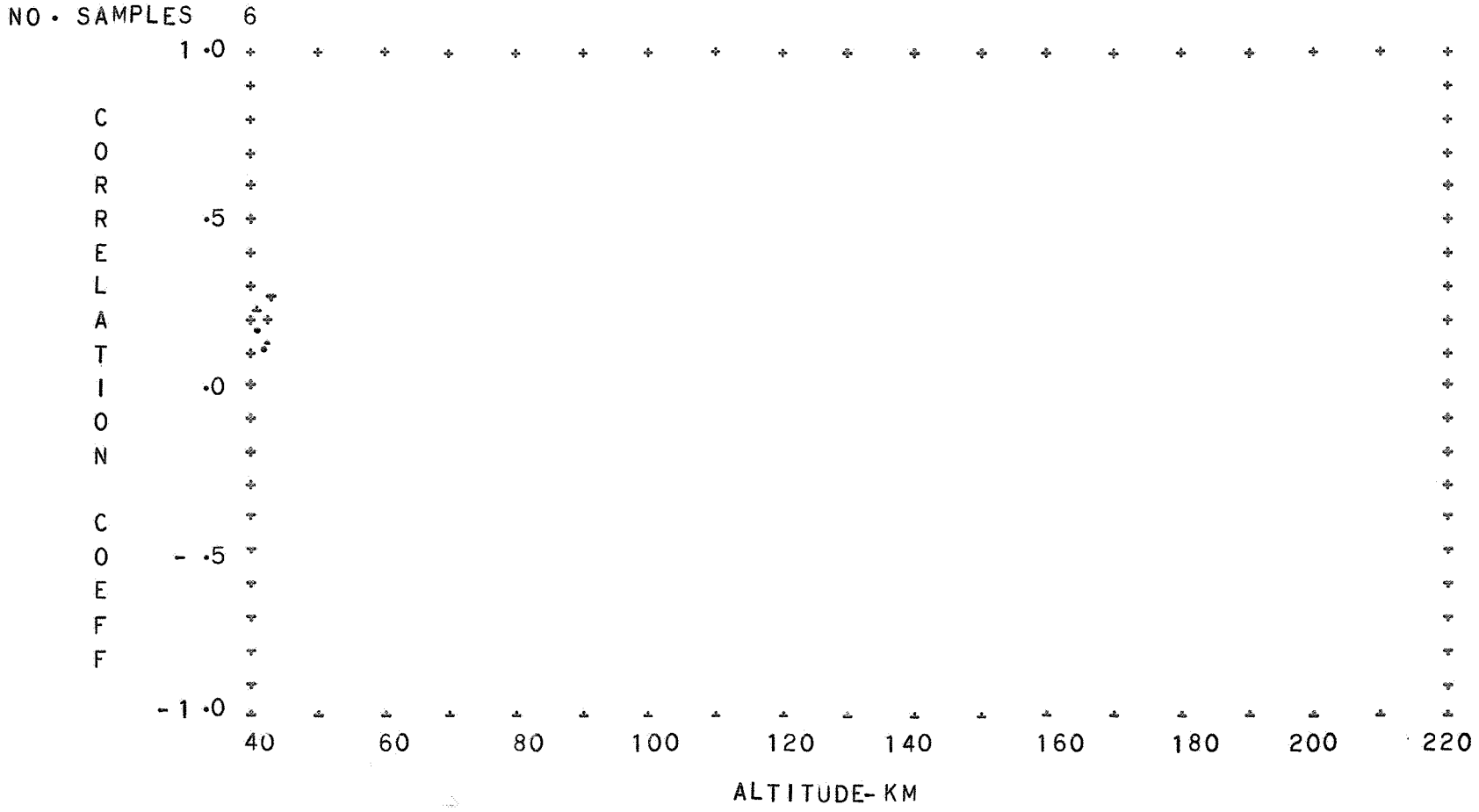

FIG. 76. CORRELATION OF DENSITY WITH SOLAR FLUX

ARCTIC WINTER NIGHTTIME

SAME DAY--CROSSES PRECEEDING DAY--DOTS

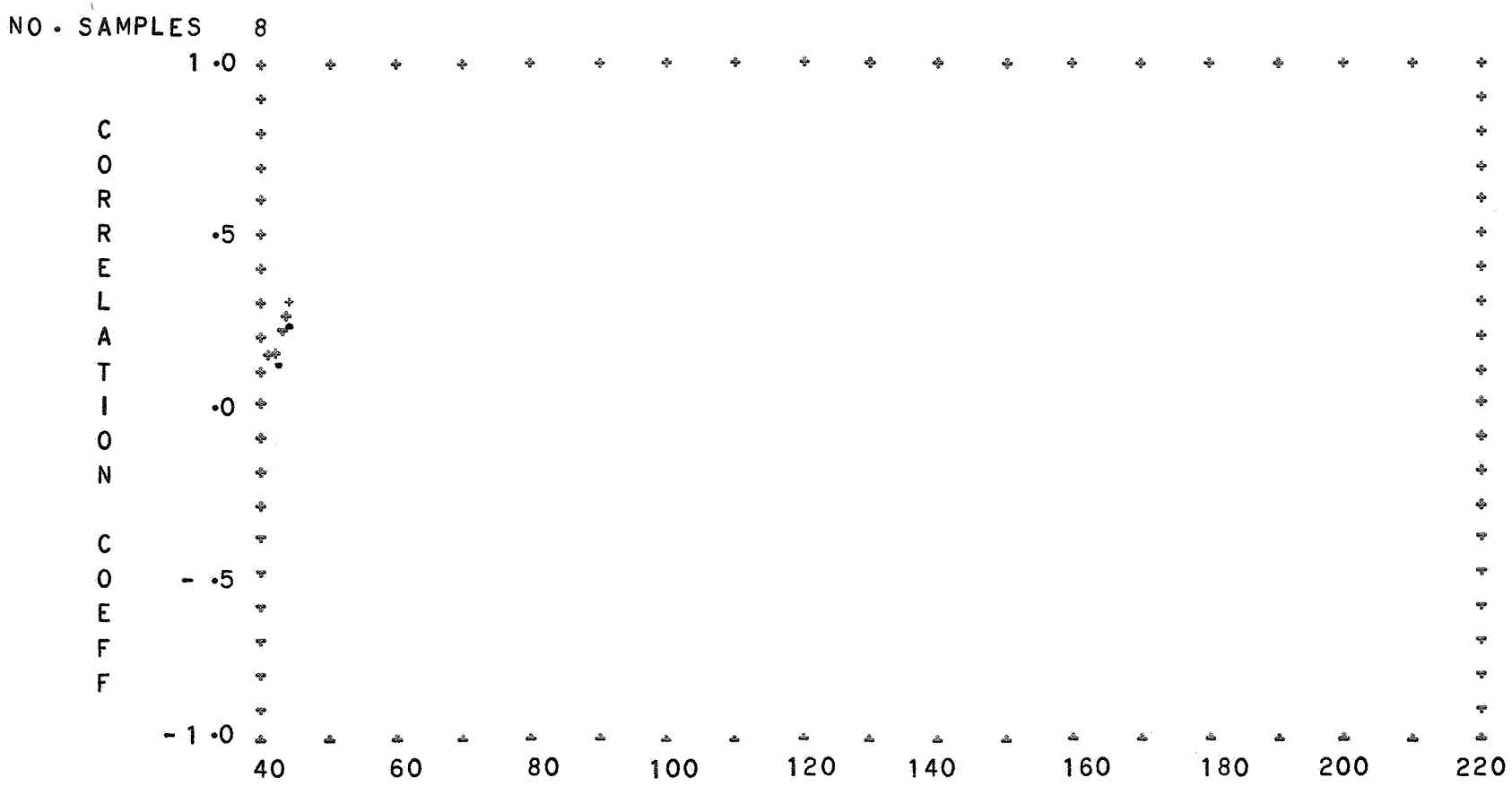

FIG. 77. CORRELATION OF DENSITY WITH SOLAR FLUX

ARCTIC WINTER DIURNAL MEAN

SAME DAY--CROSSES PRECEEDING DAY--DOTS

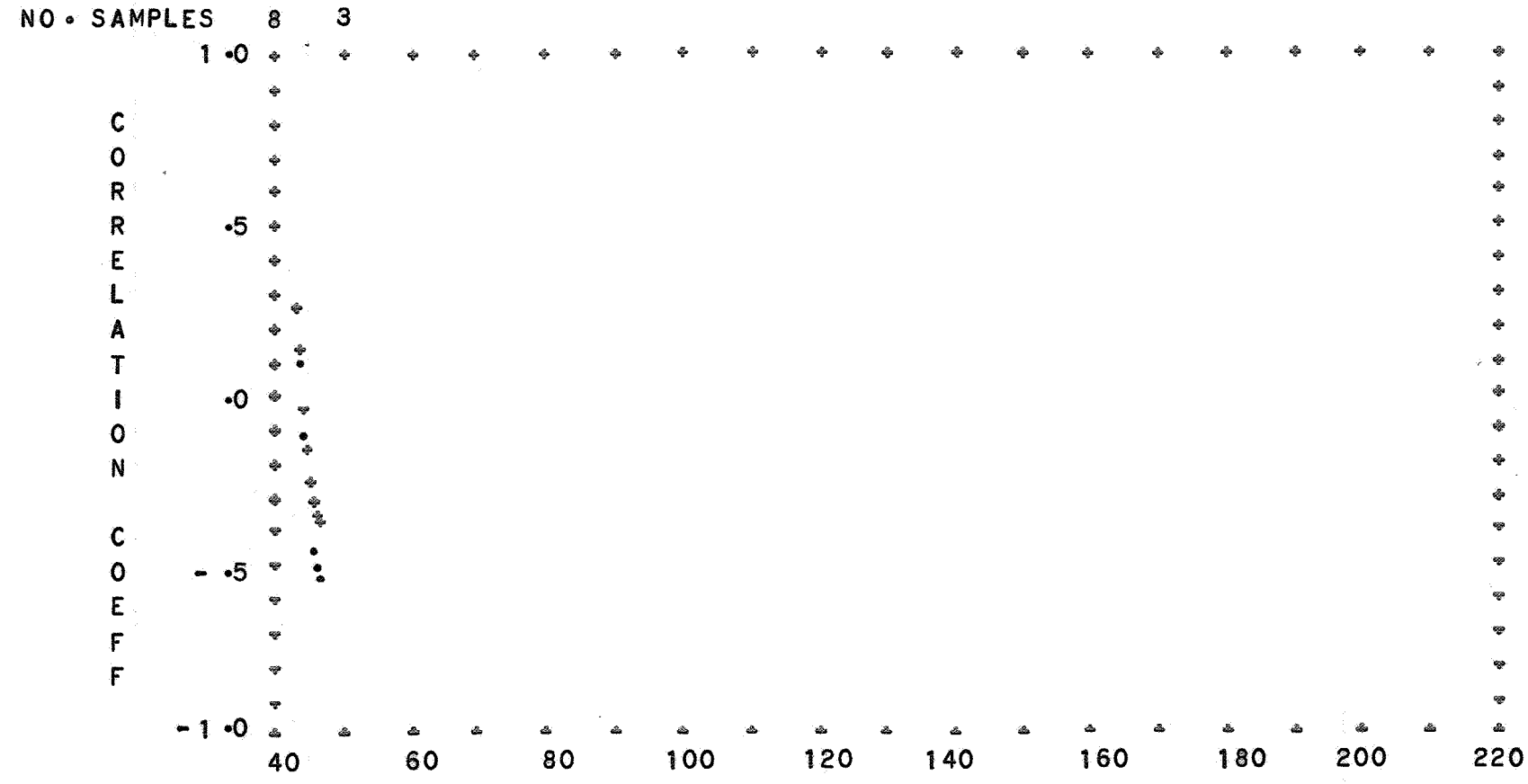

FIG. 78. CORRELATION OF DENSITY WITH SOLAR FLUX

ARCTIC SUMMER EXTREME DIURNAL MEAN

SAME DAY--CROSSES PRECEEDING DAY--DOTS

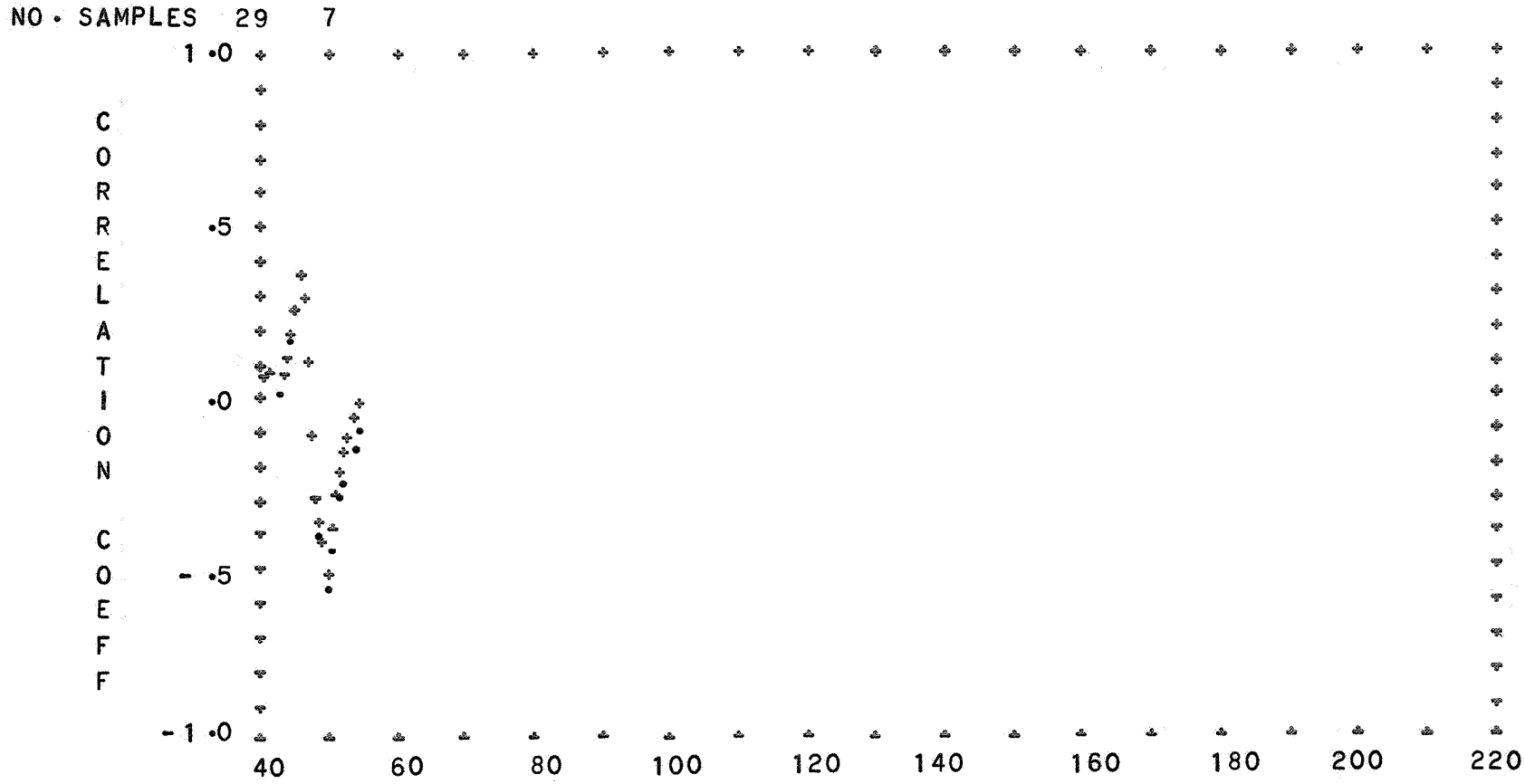

FIG. 79. CORRELATION OF DENSITY WITH SOLAR FLUX

ARCTIC ANNUAL MEAN DIURNAL TRANSITION

SAME DAY--CROSSES PRECEEDING DAY--DOTS

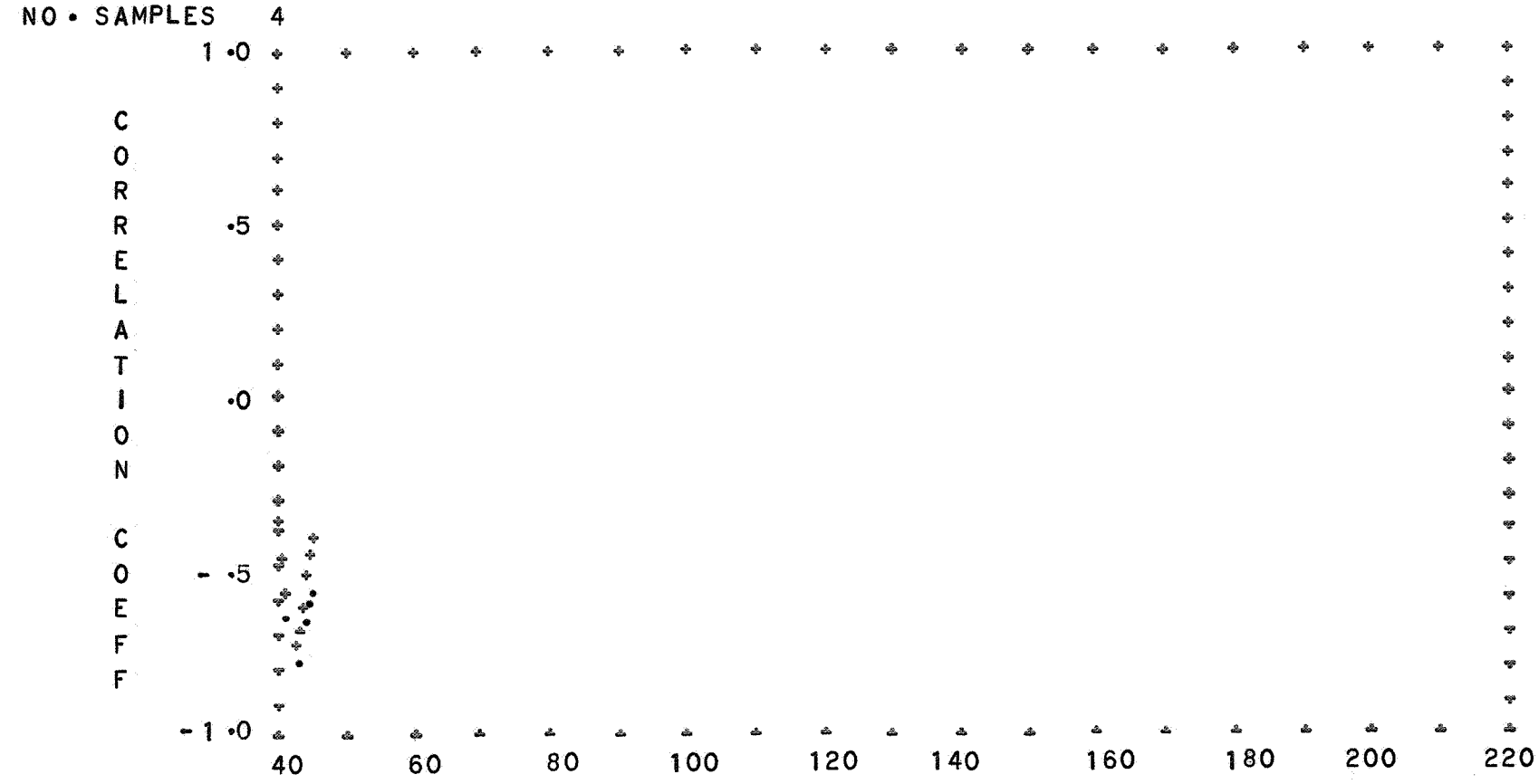

FIG. 80. CORRELATION OF DENSITY WITH SOLAR FLUX

ARCTIC ANNUAL MEAN DAYTIME

SAME DAY--CROSSES PRECEEDING DAY--DOTS

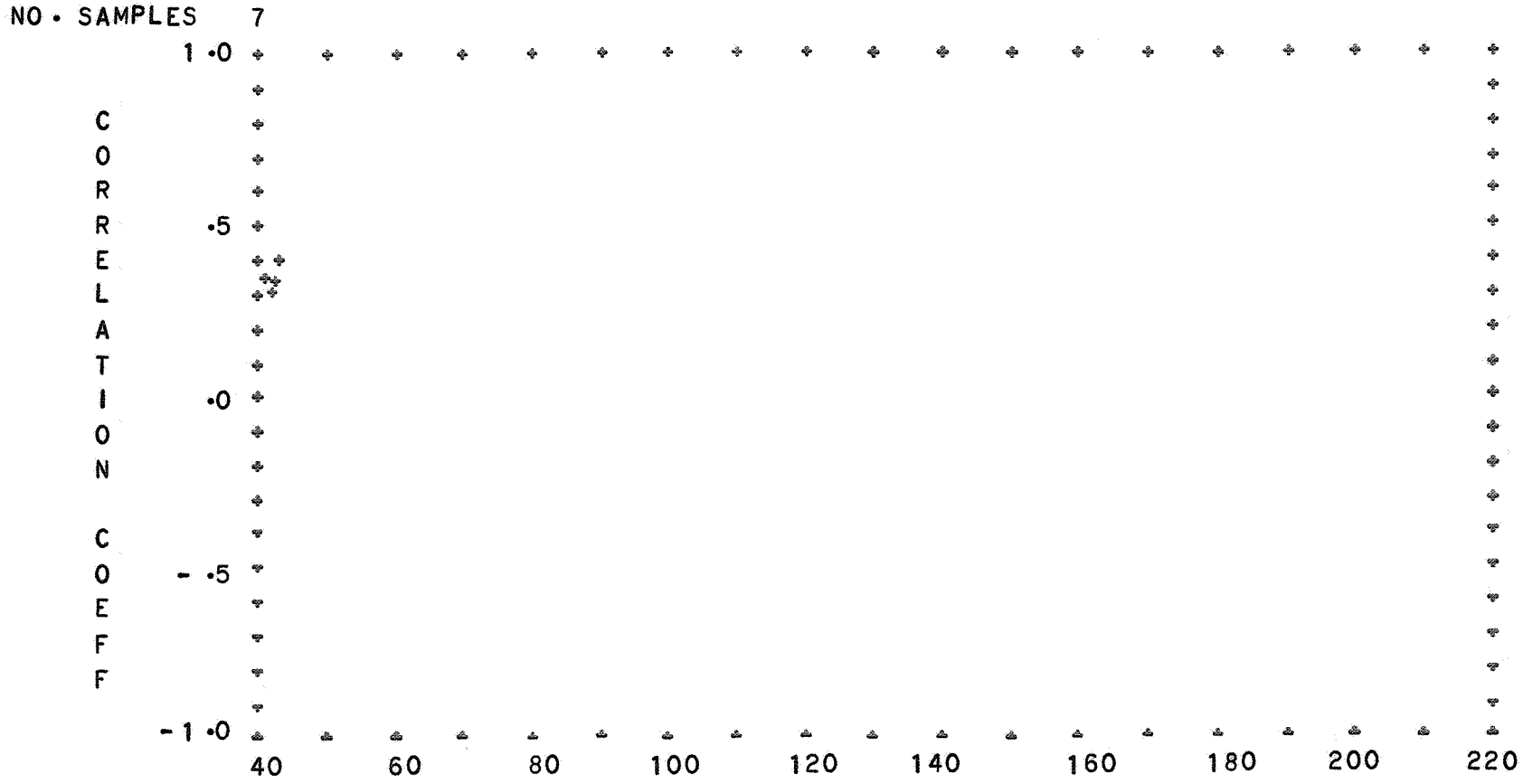

FIG. 81 CORRELATION OF DENSITY WITH SOLAR FLUX

ARCTIC ANNUAL MEAN NIGHTTIME

SAME DAY--CROSSES PRECEEDING DAY--DOTS

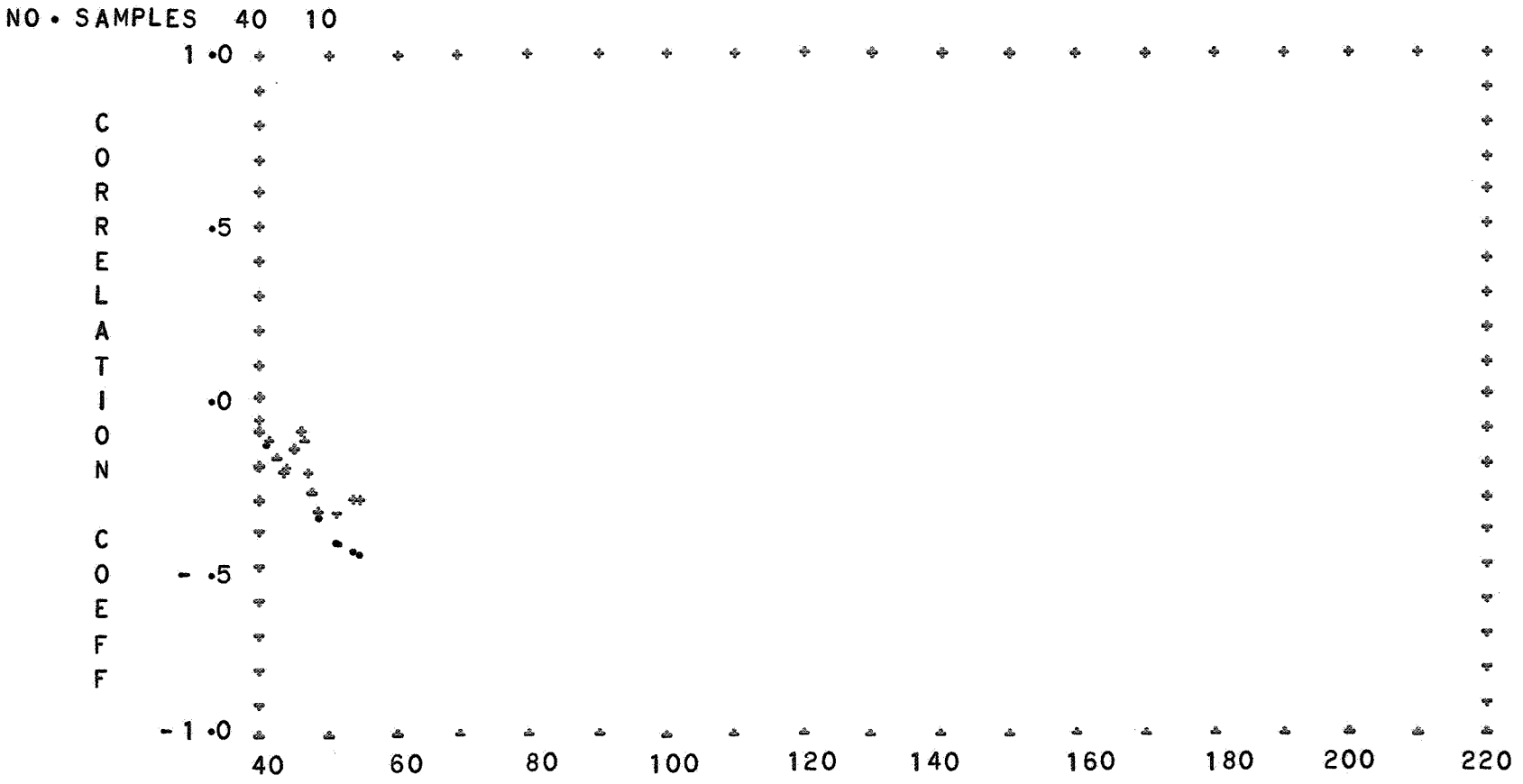

FIG. 82 CORRELATION OF DENSITY WITH SOLAR FLUX

ARCTIC ANNUAL MEAN DIURNAL MEAN

SAME DAY-- CROSSES PRECEEDING DAY-- DOTS

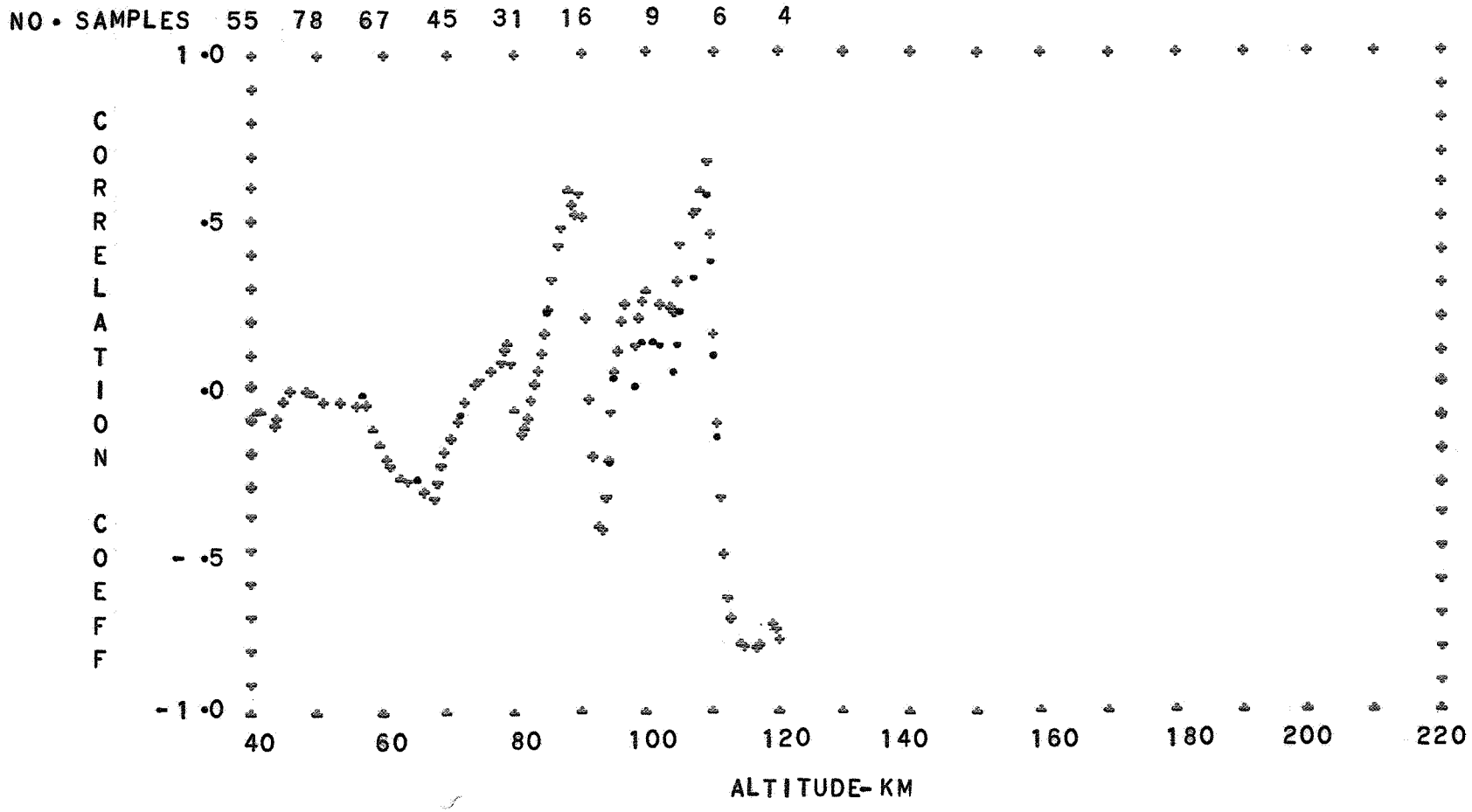

FIG. 83 CORRELATION OF DENSITY WITH SOLAR FLUX

HEMISPHERICAL MEAN SPRING DIURNAL MEAN

SAME DAY--CROSSES PRECEEDING DAY--DOTS

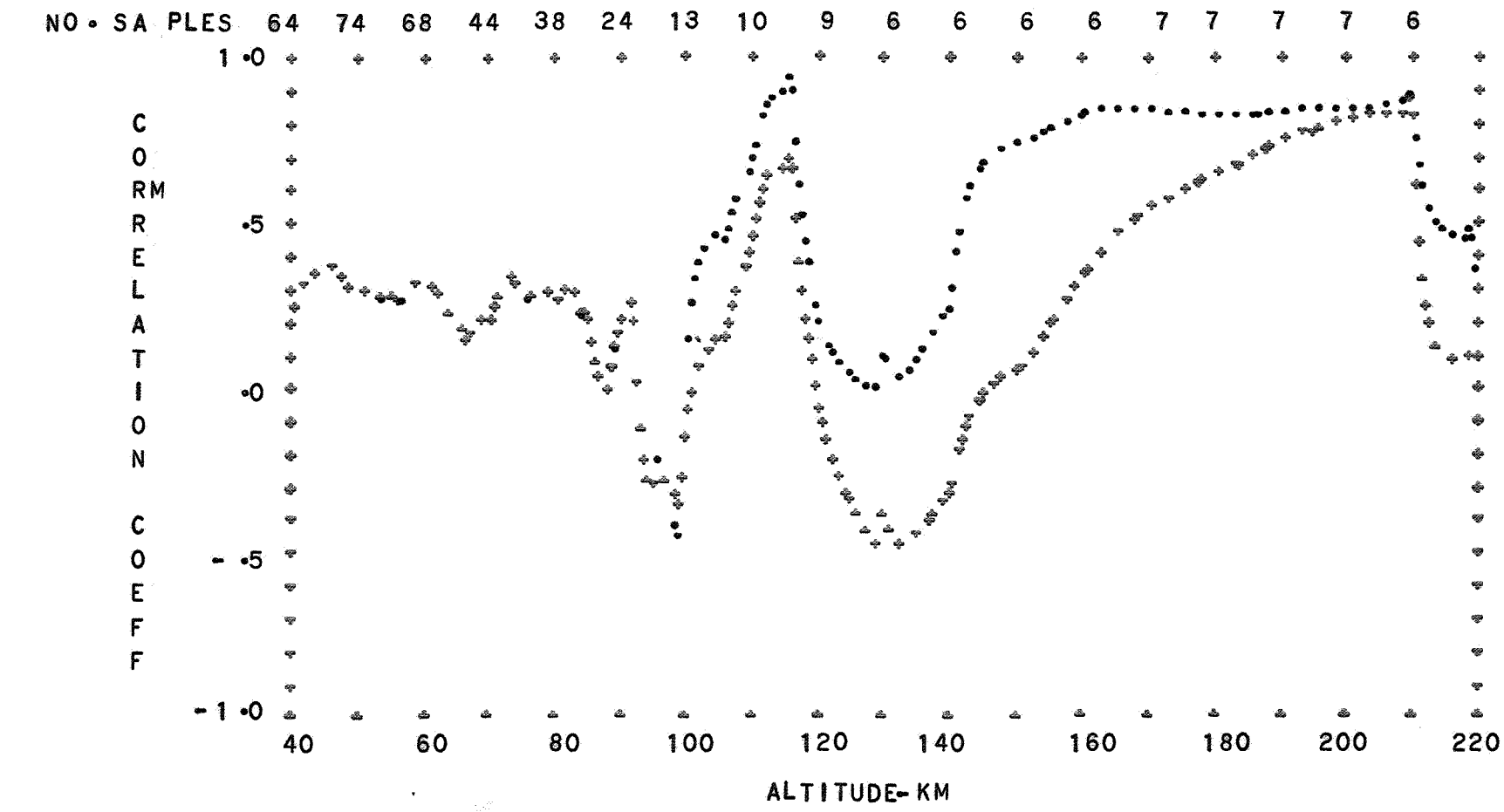

FIG. 84 CORRELATION OF DENSITY WITH SOLAR FLUX

HEMISPHERICAL MEAN SUMMER DIURNAL MEAN

SAME DAY--CROSSES PRECEEDING DAY--DOTS

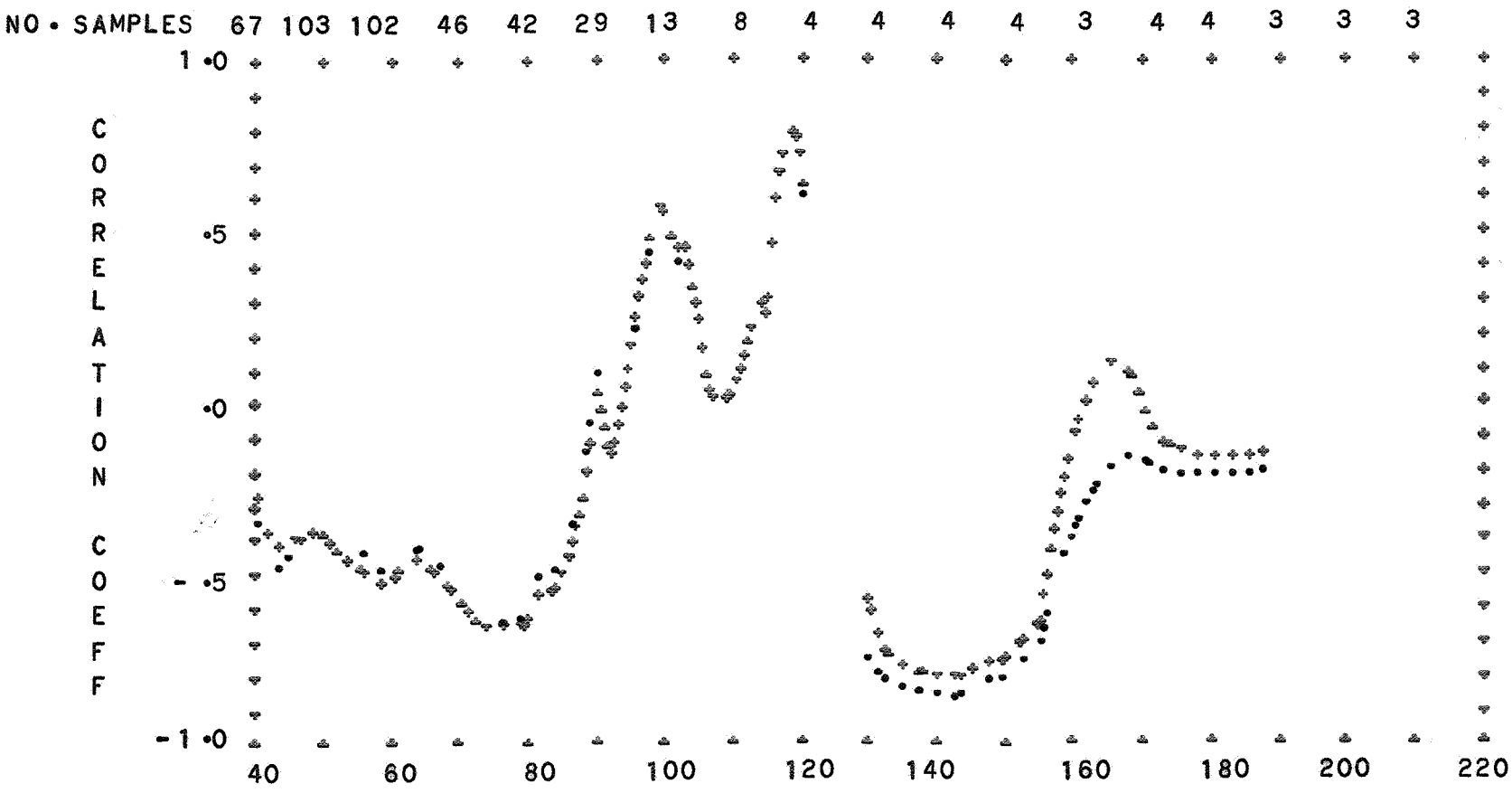

FIG. 85 CORRELATION OF DENSITY WITH SOLAR FLUX

HEMISPHERICAL MEAN AUTUMN DIURNAL MEAN

SAME DAY--CROSSES PRECEEDING DAY--DOTS

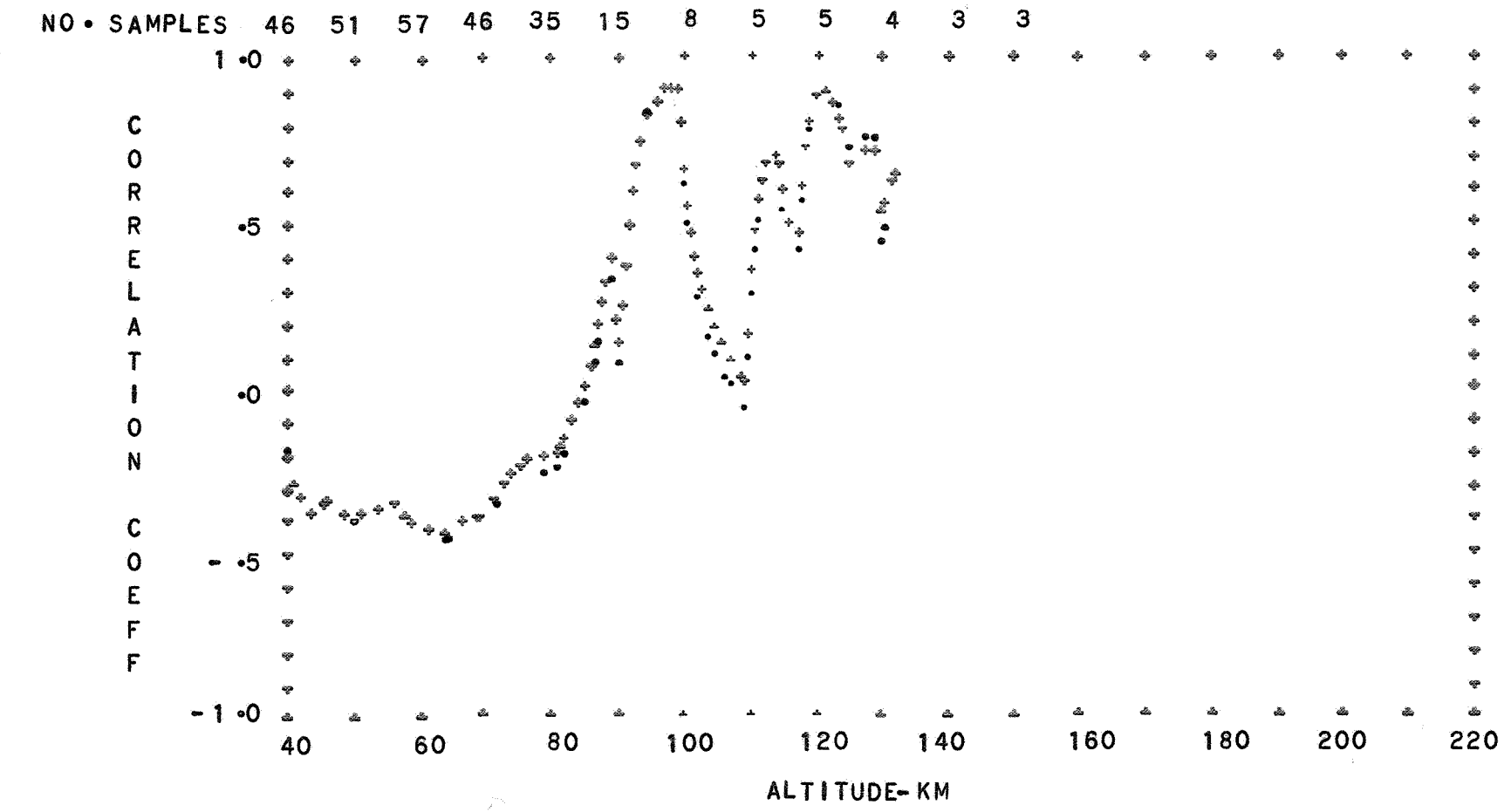

FIG. 86 CORRELATION OF DENSITY WITH SOLAR FLUX

HEMISPHERICAL MEAN WINTER DIURNAL MEAN

SAME DAY--CROSSES PRECEEDING DAY--DOTS

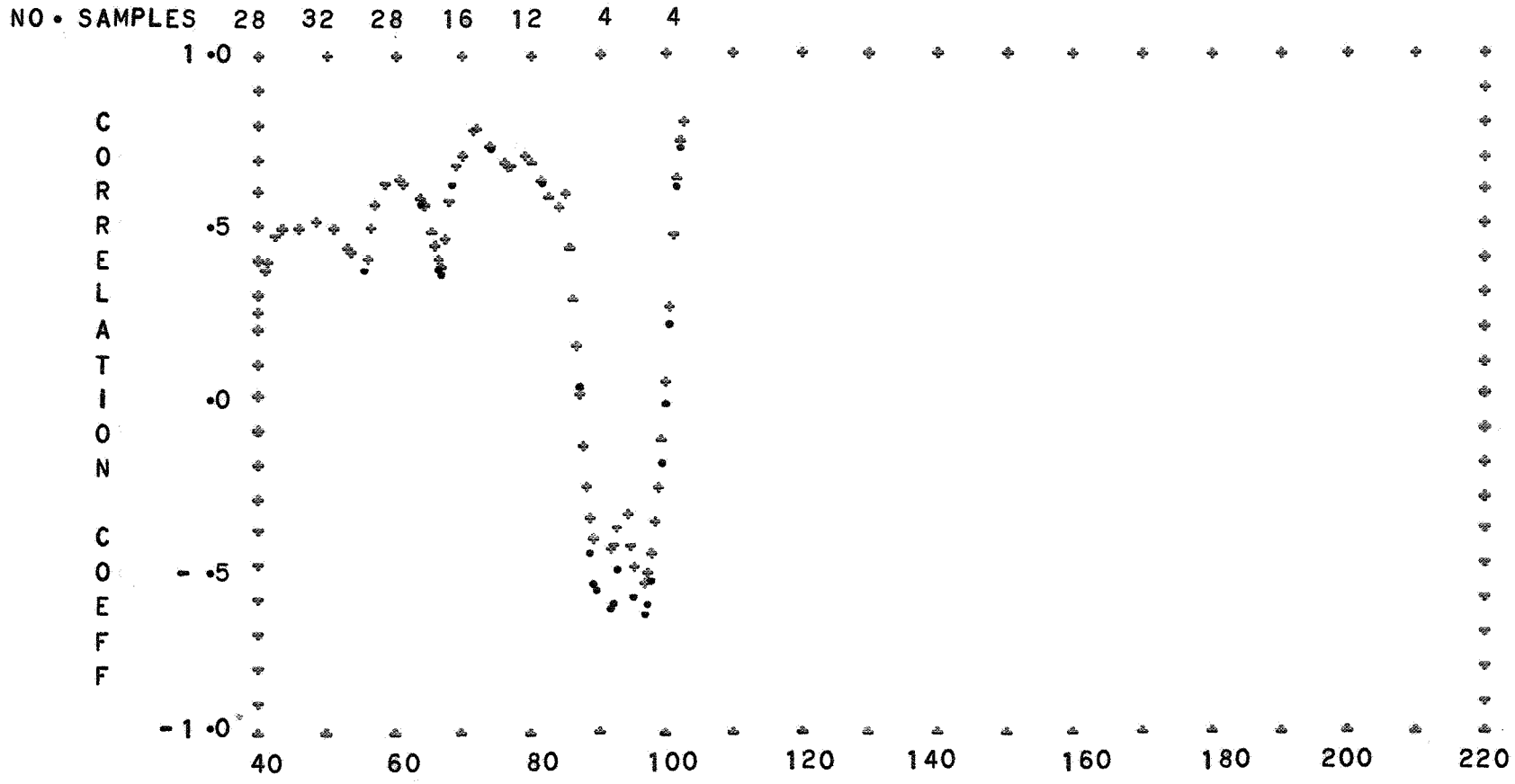

FIG. 87. CORRELATION OF DENSITY WITH SOLAR FLUX

HEMISPHERICAL MEAN SUMMER EXTREME DIURNAL MEAN

SAME DAY--CROSSES PRECEEDING DAY--DOTS

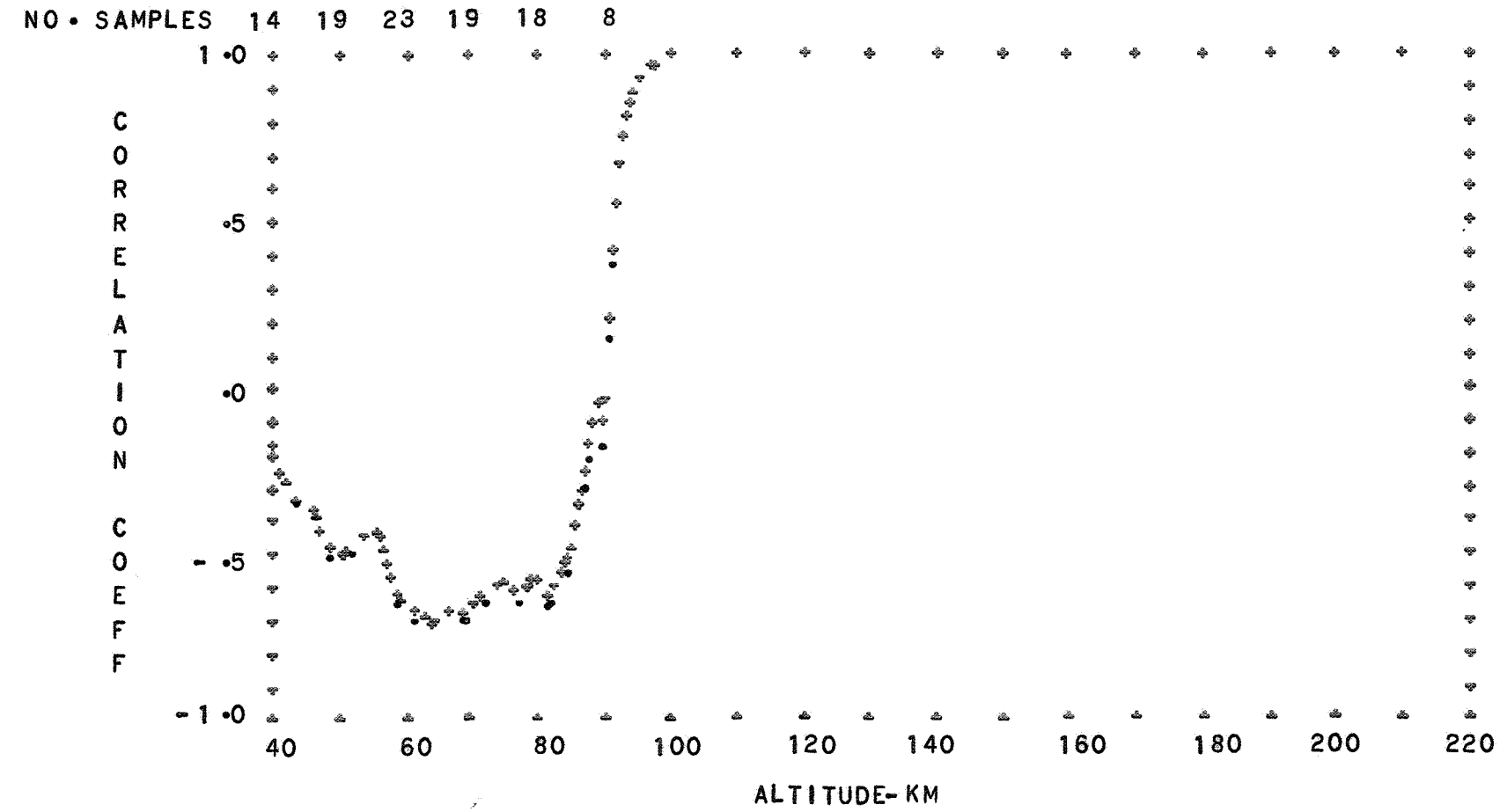

FIG. 88. CORRELATION OF DENSITY WITH SOLAR FLUX

HEMISPHERICAL MEAN WINTER EXTREME DIURNAL MEAN

SAME DAY--CROSSES PRECEEDING DAY--DOTS

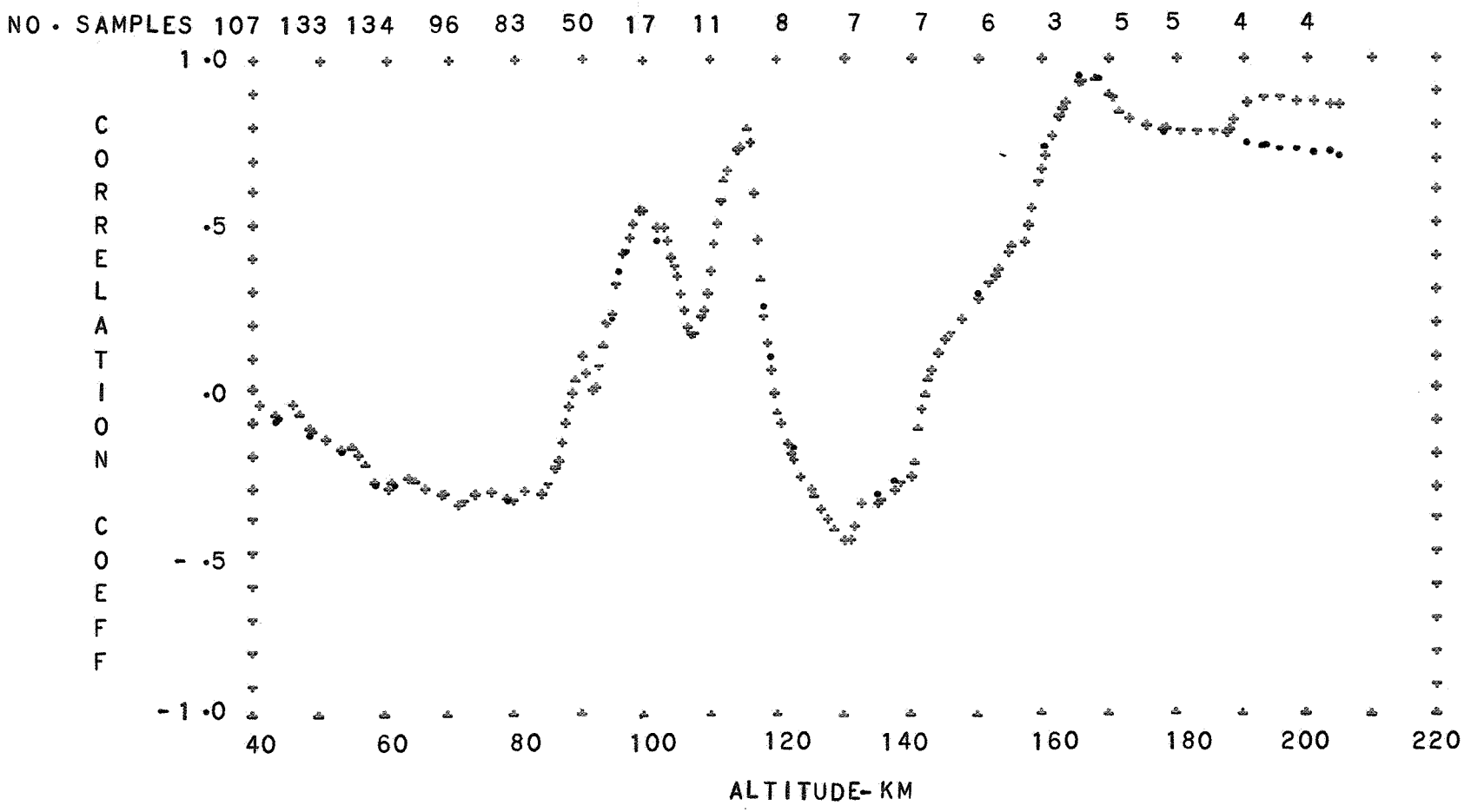

FIG. 89 CORRELATION OF DENSITY WITH SOLAR FLUX

HEMISPHERICAL MEAN ANNUAL MEAN DIURNAL TRANSITION

SAME DAY--CROSSES PRECEEDING DAY--DOTS

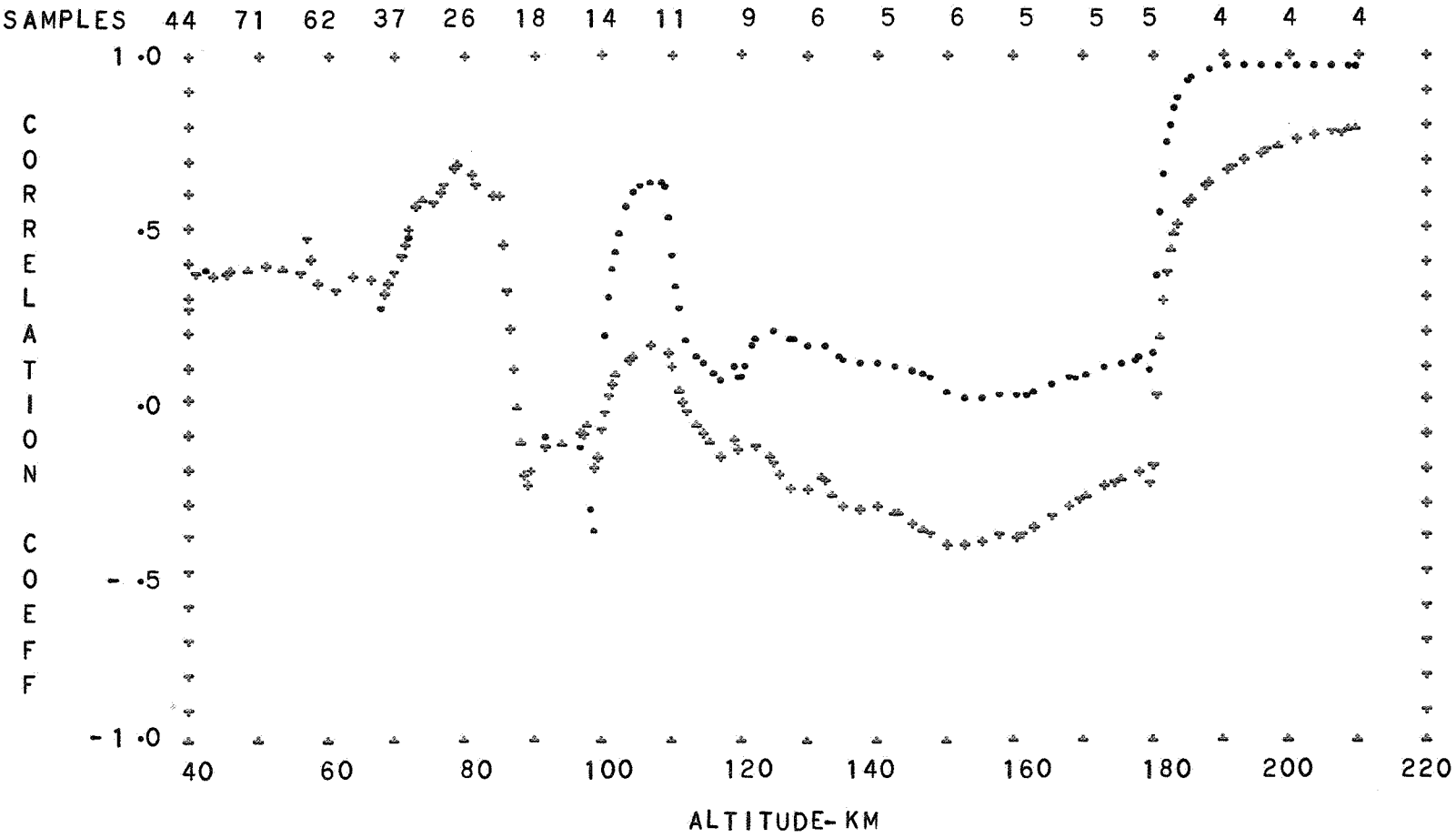

FIG. 90. CORRELATION OF DENSITY WITH SOLAR FLUX

HEMISPHERICAL MEAN ANNUAL MEAN DAYTIME

SAME DAY--CROSSES PRECEEDING DAY--DOTS

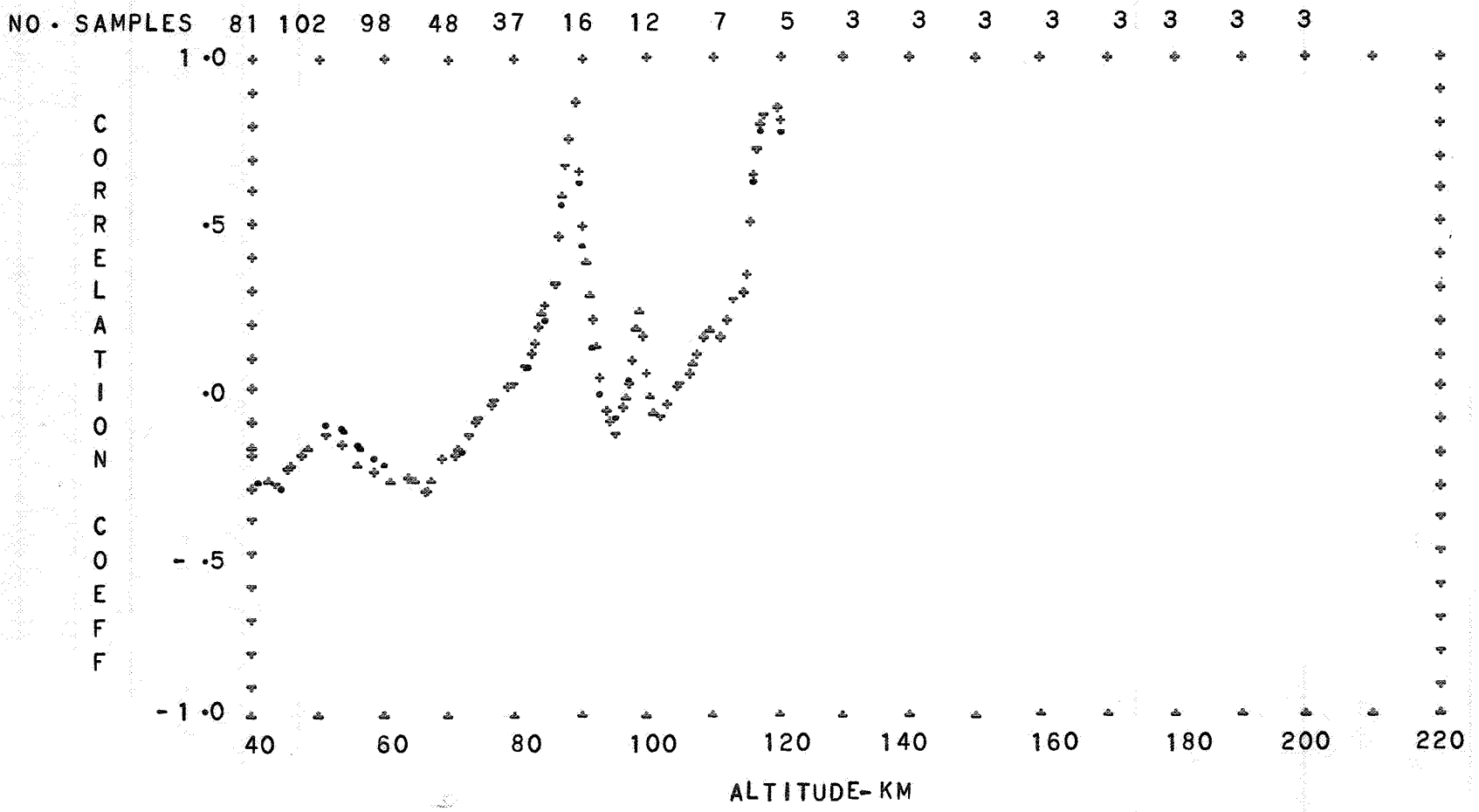

FIG. 91. CORRELATION OF DENSITY WITH SOLAR FLUX

HEMISPHERICAL MEAN ANNUAL MEAN NIGHTTIME

SAME DAY--CROSSES PRECEEDING DAY--DOTS

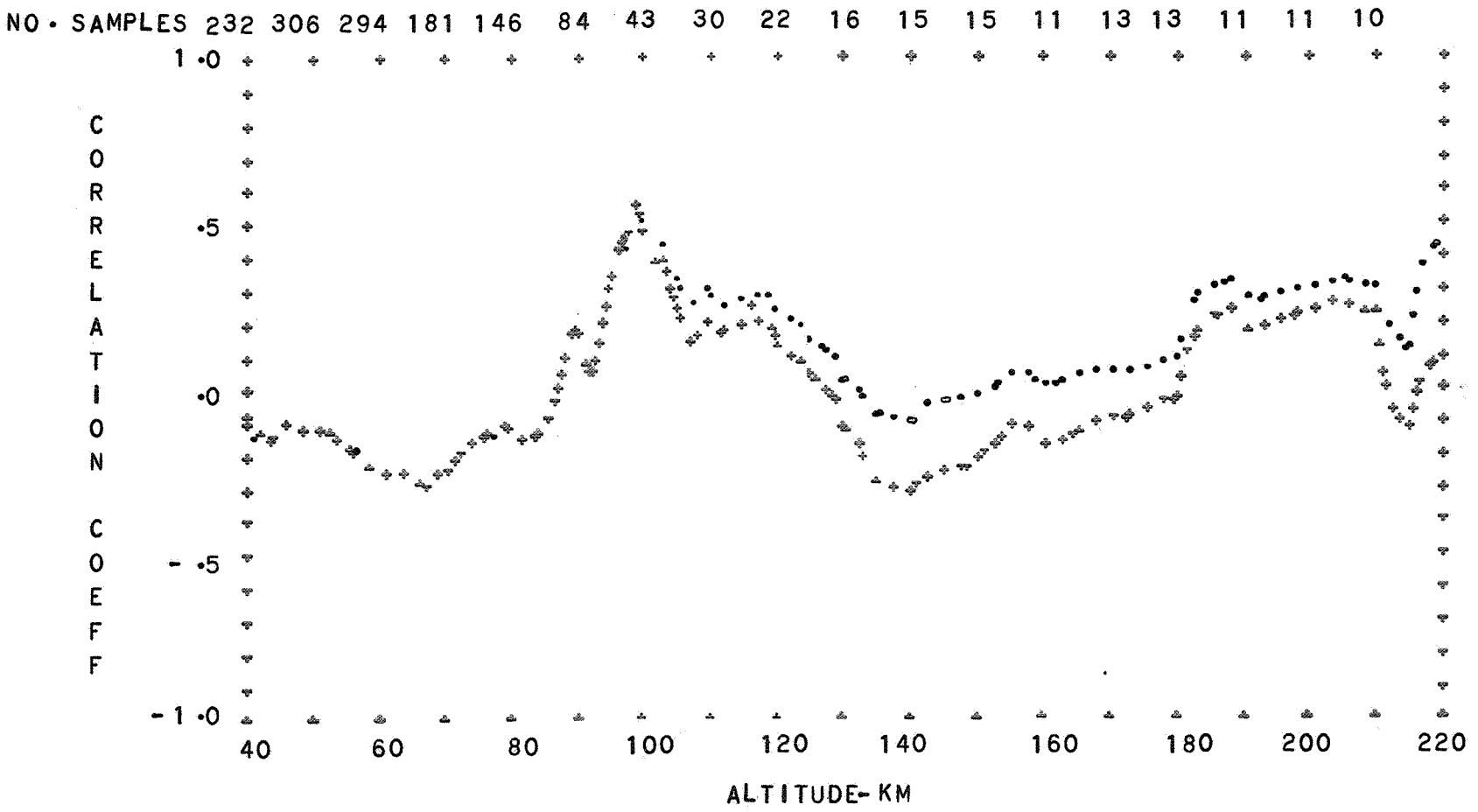

FIG. 92. CORRELATION OF DENSITY WITH SOLAR FLUX

HEMISPHERICAL MEAN ANNUAL MEAN DIURNAL MEAN

SAME DAY--CROSSES PRECEEDING DAY--DOTS

APPENDIX B

COMPUTER PROGRAMS

```
C      PROGRAM TO CORRELATE DENSITY WITH 10.7-CM SOLAR FLUX
C      COMBINES DATA INTO FOLLOWING TYPES OF CELLS) (5,1,3) (5,4,1)
C      (5,1,1) (1,1,3) (1,4,1) AND (1,1,1)
C      P. MORGENSTERN     6/29/67
C
       DIMENSION SD(10,6),SDD(10,6),SSOL(10,6),SSOLL(10,6),SFLUX(10,6)
       DIMENSION SFLXX(10,6),SDSOL(10,6),SDFLX(10,6),N(10,6)
       BEGIN TRACE
C                                  MINIMUM ALTITUDE
       IHT1=40
C
       EXECUTE PROCEDURE 2000
     4 READ 101,IHT2,D,SOL,FLUX,ILAT,ISEA2,ISEA3,IETR
   101 FORMAT(I4,E10.4,35X2F3.0,6XI1,6X2I1,9XI1)
       IF(IHT2-IHT1) 4,8,6
C                                  SQUARES AND CROSS-PRODUCTS
     8 SIGD=D*D
       SIGSL=SOL*SOL
       SIGFX=FLUX*FLUX
       COVDS=D*SOL
       COVFS=D*FLUX
C                                  STRATIFY DATA BY SEASON AND TIME OF DAY
       II=ISEA3
       IF(ILAT)30,30,31
    30 ILAT=ILAT+1
    31 JJ=ILAT
       EXECUTE PROCEDURE 10
       IF(ISEA2)20,20,11
    11 II=ISEA2
       EXECUTE PROCEDURE 10
    20 II=IETR+5
       EXECUTE PROCEDURE 10
       II=10
       EXECUTE PROCEDURE 10
       GO TO 4
C                                  SUMMATION,SUMMATION OF SQUARES, AND
C                                  SUMMATION OF CROSS-PRODUCTS
       BEGIN PROCEDURE 10
12     N(II,JJ)=N(II,JJ)+1
11     SD(II,JJ)=SD(II,JJ)+D
       SDD(II,JJ)=SDD(II,JJ)+SIGD
10     SSOL(II,JJ)=SSOL(II,JJ)+SOL
       SSOLL(II,JJ)=SSOLL(II,JJ)+SIGSL
9      SFLUX(II,JJ)=SFLUX(II,JJ)+FLUX
       SFLXX(II,JJ)=SFLXX(II,JJ)+SIGFX
8      SDSOL(II,JJ)=SDSOL(II,JJ)+COVDS
       SDFLX(II,JJ)=SDFLX(II,JJ)+COVFS
7      END PROCEDURE 10
C                                  COMPRESSION ACROSS LATITUDE BELTS
     6 DO 33 II=1,10
6      DO 33 JJ=1,5
       N(II, 6)=N(II, 6)+N(II,JJ)
5      SD(II, 6)=SD(II, 6)+SD(II,JJ)
       SDD(II, 6)=SDD(II, 6)+SDD(II,JJ)
4      SSOL(II, 6)=SSOL(II, 6)+SSOL(II,JJ)
       SSOLL(II, 6)=SSOLL(II, 6)+SSOLL(II,JJ)
3      SFLUX(II, 6)=SFLUX(II, 6)+SFLUX(II,JJ)
       SFLXX(II, 6)=SFLXX(II, 6)+SFLXX(II,JJ)
2
```

```
      SDSOL(II, 6)=SDSOL(II, 6)+SDSOL(II,JJ)
   33 SDFLX(II, 6)=SDFLX(II, 6)+SDFLX(II,JJ)
C
      DO 7II=1,10
      DO 7JJ=1,6
      L=JJ+1
C                                SAMPLE SIZE EQUAL TO OR GREATER THAN 3
      IF(N(II,JJ)-3)7,9,9
C                                CALCULATE CORRELATION COEFFICIENT
    9 EN=N(II,JJ)
      XSD=SD(II,JJ)
      XSSOL=SSOL(II,JJ)
      XFLUX=SFLUX(II,JJ)
      ENN=EN**2
      SIGD=SQRTF((EN*SDD(II,JJ)-XSD**2)/ENN)
      SIGSL=SQRTF((EN*SSOLL(II,JJ)-XSSOL**2)/ENN)
      SIGFX=SQRTF((EN*SFLXX(II,JJ)-XFLUX**2)/ENN)
      COVDS=(EN*SDSOL(II,JJ)-XSD*XSSOL)/ENN
      COVDF=(EN*SDFLX(II,JJ)-XSD*XFLUX)/ENN
      RHODS=COVDS/(SIGD*SIGSL)
      RHODF=COVDF/(SIGD*SIGFX)
C                                CALCULATE CELL CODE
   16 GO TO (21,21,21,21,22,22,22,21,21,23),II
   21 IJ=II
      JI=7
      LAT=JJ
      GO TO 14
   22 IJ=0
      JI=II-5
      LAT=JJ
      GO TO 14
   23 IJ=0
      JI=0
      LAT=-JJ
   14 GO TO (18,18,18,18,18,18,19),L
   19 LAT=(LAT*L)/JJ
C
   18 PUNCH 103,IHT1, LAT,IJ,JI,RHODS,RHODF,N(II,JJ)
  103 FORMAT(I4,3I2,2F6.3,I4)
    7 CONTINUE
   15 EXECUTE PROCEDURE 2000
      IHT1=IHT2
      END TRACE
      GO TO 8
C                                INITIALIZE CELL SUMMATIONS
      BEGIN PROCEDURE 2000
      DO 5II=1,10
      DO 5JJ=1,6
      N(II,JJ)=0
      SD(II,JJ)=0.0
      SDD(II,JJ)=0.0
      SSOL(II,JJ)=0.0
      SSOLL(II,JJ)=0.0
      SFLUX(II,JJ)=0.0
      SFLXX(II,JJ)=0.0
      SDSOL(II,JJ)=0.0
    5 SDFLX(II,JJ)=0.0
      END PROCEDURE 2000
C
  140 END
```

```
C      AUTOPLOT PROGRAM FOR CORRELATION COEFFICIENT BETWEEN ATMOSPHERIC
C      DENSITY AND 10.7 SOLAR FLUX
C      JEAN M. HARRISON
C
       DIMENSION ALT(90),SF1(90),SF2(90),NF(90)
       DIMENSION SEAS1(9),SEAS2(9),SEAS3(9)
       DIMENSION DIA1(3),DIA2(3),DIA3(3),DIA4(3)
       DIMENSION XL1(7),XL2(7),XL3(7),XL4(7)
       BEGIN TRACE
       DO 65 I=1,9
    65 READ 66,SEAS1(I),SEAS2(I),SEAS3(I)
    66 FORMAT(4A5)
       DO 67 I=1,3
    67 READ 66,DIA1(I),DIA2(I),DIA3(I),DIA4(I)
       DO 69 I=1,7
    69 READ 66,XL1(I),XL2(I),XL3(I),XL4(I)
   100 FORMAT(7I5)
     2 FORMAT(I1,F3.0,1XI1,2I2,2F6.3,I4)
    20 DX=2.54001*10./100.
       DY=.2*2.54001/100.
C                                  DATA EXPLAINING TITLES TO BE INSERTED
       NX=40./DX
       NY=-1./DY
       PUNCH 100,1,1100,900,225,300,NX,NY
       NSF1=0
       NSF2=0
       NLAT=0
       NSEA=0
       NDIA=0
       DO 38 J=1,2
    33 DO 21 I=1,90
       NLATO=NLAT
       NSEAO=NSEA+1
       NDIAO=NDIA+1
       READ 2,ID,ALT(I),NLAT,NSEA,NDIA,SF1(I),SF2(I),NF(I)
       IF(ALT(I)-40.) 32,21,21
    32 I=I-1
       IF(ID-1) 21,22,21
    21 CONTINUE
C                                  ID=1 SIGNIFIES THE END OF A DATA GROUP.
    22 PUNCH 100,2,41,10
C                                  PRECEEDING DAY SOLAR FLUX WILL BE IN BLACK
C                                  DOTS.
       I=I-1
       DO 23 K=1,I
       NALT=ALT(K)/DX
       ENSF1=NSF1
       ENSF1=ENSF1*DY
       NSF1=(SF1(K)/2.+ENSF1/2.)/DY
       IF(NF(K)-4)23,19,19
    19 PUNCH 100,3,NALT,NSF1
    23 CONTINUE
       PUNCH 100,2,41,01
C                                  SAME DAY SOLAR FLUX WILL BE IN RED CROSSES.
       DO 24 K=1,I
       NALT=ALT(K)/DX
       ENSF2=NSF2
       ENSF2=ENSF2*DY
```

```
      NSF2=(SF2(K)/2.+ENSF2/2.)/DY
      IF(NF(K)-4)24,18,18
   18 PUNCH 100,3,NALT,NSF2
   24 CONTINUE
C                                  THE FOLLOWING STATEMENTS THROUGH STATEMENT 30
C                                  PLACE THE FREQUENCY AT ALTITUDE INCREMENTS
C                                  OF 10 KM
      NY=1.1/DY
      DO 30 K=1,I
C                                  LOCATE ALTITUDE OF MULTIPLES OF TEN
      SAT=DRH(ALT(K)/10.)
      IF(ALT(K)/10.-SAT) 30,31,30
   31 NX=(ALT(K)-6.9)/DX
      PUNCH 100,4,NX,NY,00
      PUNCH 7,NF(K)
C                                  PUNCH FREQUENCY AT THAT ALTITUDE.
   30 CONTINUE
      IF(ID-1)38,17,38
   38 CONTINUE
C                                  THE FOLLOWING STATEMENTS TO STATEMENT 29
C                                  PLACES THE RED GRID AROUND THE GRAPH.
   17 PUNCH 100,2,01,01
      X=40.
      Y=-1.1
      DO 25 K=1,21
      Y=Y+.1
      NX=X/DX
      NY=Y/DY
   25 PUNCH 100,3,NX,NY
      DO 26 K=1,18
      X=X+10.
      NX=X/DX
      NZ=-1./DY
      PUNCH 100,3,NX,NY
   26 PUNCH 100,3,NX,NZ
      Y=-1.1
      DO 27 K=1,21
      Y=Y+.1
      NY=Y/DY
   27 PUNCH 100,3,NX,NY
C                                  LOCATE ABCISSA LABEL
      N=-1.25/DY
      NX=114./DX
      PUNCH 100,4,NX,N,00
C                                  ABCISSA LABEL
      PUNCH 3
    3 FORMAT(11HALTITUDE-KM)
C                                  LOCATE ORDINATE LABEL
      N=.8/DY
      NX=16./DX
      PUNCH 100,4,NX,N,10
C                                  ORDINATE LABEL
      PUNCH 4
    4 FORMAT(17HCORRELATION COEFF)
C                                  LOCATE FREQUENCY LABEL
      NY=1.10/DY
      NX= 5./DX
      PUNCH 100,4,NX,NY,00
C                                  FREQUENCY LABEL
  142 PUNCH 6
```

```
    6 FORMAT(11HNO. SAMPLES)
C                                   THE STATEMENTS UP TO 50 LOCATE AND LABEL THE
C                                   ABCISSA SCALE.
      X=16.
      NY=-1.1/DY
      DO 50 K=1,10
      X=X+20.
      IF(K-4) 34,35,36
   35 X=X-1.0
   36 IF(K-7) 34,37,34
   37 X=X+1.
   34 NX=X/DX
      PUNCH 100,4,NX,NY,00
      L=20*K+20
      PUNCH 7,L
    7 FORMAT(I4)
   50 CONTINUE
C                                   THE STATEMENTS FROM HERE TO STATEMENT 61
C                                   LOCATES AND LABELS ORDINATE SCALE.
      NX=28./DX
      Y=-1.5
      DO 61 K=1,5
      XK=K
      Y=Y+.5
      NY=Y/DY
      PUNCH 100,4,NX,NY,00
   52 FORMAT(F4.1)
      Y=-1.0+(XK-1.)*.5
   61 PUNCH 52,Y
C                                   THE REMAINING STATEMENTS LABEL THE GRAPH.
      NX=53./DX
      NY=-1.4/DY
      PUNCH 100,4,NX,NY,00
      PUNCH 40
   40 FORMAT(4HFIG.)
      NX=79./DX
      PUNCH 100,4,NX,NY,00
   62 FORMAT(38HCORRELATION OF DENSITY WITH SOLAR FLUX)
      PUNCH 62
      NX=53./DX
      NY=-1.55/DY
      PUNCH 100,4,NX,NY,00
      PUNCH 63,XL1(NLATO),XL2(NLATO),XL3(NLATO),XL4(NLATO),SEAS1(NSEAO),
     1SEAS2(NSEAO),SEAS3(NSEAO),DIA1(NDIAO),DIA2(NDIAO),DIA3(NDIAO),DIA4(NDIAO)
   63 FORMAT(4A5, 2X3A5,3X4A5)
      NY=-1.7/DY
      PUNCH 100,4,NX,NY,00
      PUNCH 64
   64 FORMAT(17HSAME DAY--CROSSES,23X20HPRECEEDING DAY--DOTS)
      PUNCH 100,6
      GO TO 20
      END TRACE
      END
```